OCT 08th, 2024

Ulrich L. Rohde[1]

Microwave Systems

Department of Technical Informatics

University of the Armed Forces, Munich, Germany

Brandenburgische Technische Universität Cottbus-Senftenberg

Rohde & Schwarz , Munich , Synergy Microwave , USA

1) https://orcid.org/0009-0009-2271-4438

A complete practical and mathematical treatment of Microwave LC Based 0scillators using Bipolar, MESFETs and CMOS Transistors

A potpourri of essential topics for this application

Copyright permission received 10/25/2024

As this article is also based on several books mentioned above, it is presented here as a potpourri and the sometimes refers to the figures and equations numbering as per the original books and are easy to find.

Ulrich L. Rohde
Ajay K. Podder
Matthias Rudolph

Transistor Applications from RF to Microwave Frequencies

Theory of SiGe HBTs and pHEMT and practical circuits up to Sub Terahertz frequencies
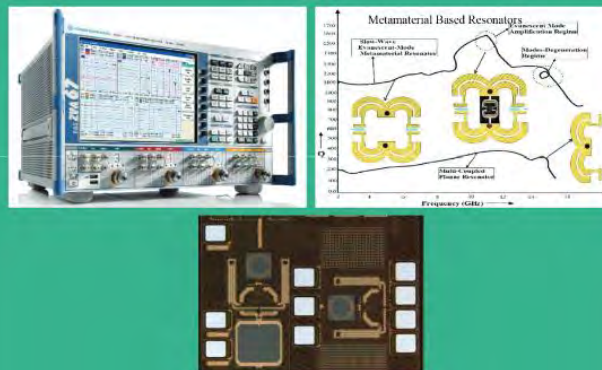
WILEY

The design of RF/microwave oscillators has been, and continues to be, the subject of many publications. Historically, oscillators have been designed largely based on past experience with mostly successful designs, and to a lesser degree on experimental data. Furthermore, high-resolution test equipment for validation of device phase noise has only become available in the last decade or so, and accurate measurement can still take hours. For a designer, however, it is preferable to start from a set of specifications and then apply a rigorous and advanced mathematics-based design procedure. In this talk, we will present linear data-based, measured large-signal-based, and non-linear Bessel function-based treatments of RF/microwave oscillators. The discussion will include LC-based oscillators, such as those using bipolar, MESFET, and CMOS transistors, as well as the design of high-performance, low-phase-noise oscillators, ranging from VHF crystal resonators to YIG oscillators, and their measured data.

Topics

- **Introduction**
- **What is an oscillator?**
- **Introduction to Microwave Oscillators and Their Mathematical Treatment**
- **Transistor models and Noise Contributions**
- **Transistor Types**
- **Linear Approach to the Calculation of Oscillator Phase Noise**
- **Typical Microwave Oscillator (Colpitts Oscillator)**
- **Designing an Oscillator**
- **Tuning Diode Noise Contribution**
- **Designing an Oscillator based on Linear S-Parameters**
- **Large signal Operation of Oscillators (Colpitts/YIG)**
- **Classical Linear Two-Port Oscillator Design**
- **Microwave Resonators**
- **A Novel Tunable Active Spiral Inductor**
- **The Active Inductor Using a Gyrator**
- **INTRODUCTION: Active Inductor Oscillator**
- **Synthesized Inductor Circuits**
- **Phase Noise Contribution of the Various Parts of the Oscillator Using an Active Inductor**
- **The Modern Time-Domain Behavior of an Oscillator**
- **Test Case: Design Example of a 100MHz crystal oscillator**
- **Phase Noise Analysis Based on the Negative Resistance Model**
- **Oscillator Phase Noise**

➤ Introduction

The following presentation will be a thorough practical and mathematical description of how to build optimized oscillators, mostly LC based, such as the one shown below, in Fig.1, but also with specific microwave resonators, crystals and other resonators.

The oscillator below is from the MIMIC Program

The acronym, "MIMIC" stood for Microwave/Millimeter-Wave Monolithic Integrated Circuits. The DARPA program manager was Dr. Eliot Cohen. In 2012 Eliot Cohen wrote an article on the MIMIC Program for IEEE MTT-S Microwave Magazine which is a good resource if you want to learn about this historic program. Here are the details:

Eliot Cohen, "The MIMIC Program - A Retrospective", *Microwave Magazine*, June 2012, pp. 77-88.

Printed   Resonator
for frequency tuning
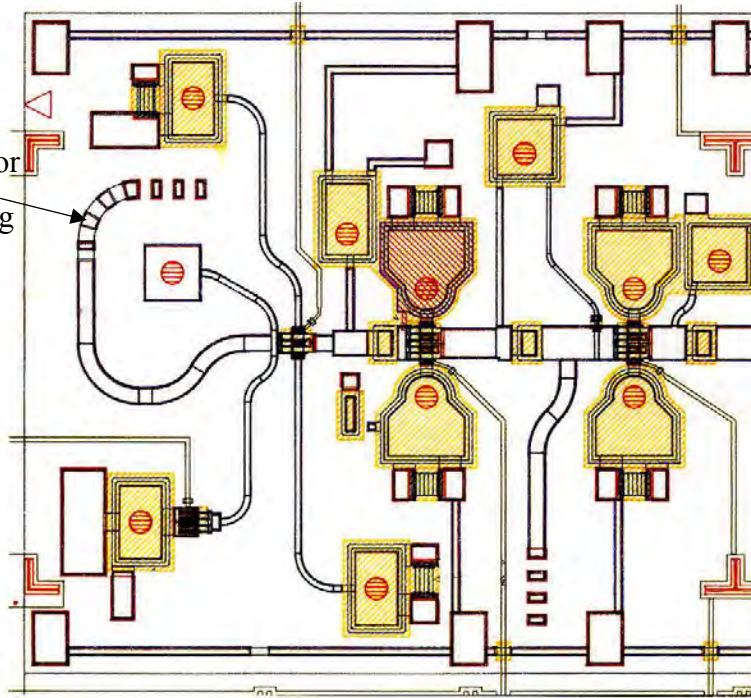
Figure 1:   *Two stage FET based Microwave tunable Oscillator Built on GaAs Substrate*

160 GHz Oscillator – Measured Phase Noise Plot

Typical sensitivity at 1 GHz input frequency with R&S®FSWP-B61 option (start offset 1 Hz)

	1 Hz	10 Hz	100 Hz	1 kHz	10 kHz	100 kHz	1 MHz	10 MHz
1 GHz	–84 dBc	–108 dBc	–127 dBc	–157 dBc	–174 dBc	–182 dBc	–185 dBc	–185 dBc

Typical sensitivity at various frequencies with R&S®FSWP-B61 option (start offset 1 Hz)

Rohde&Schwarz R&S®FSWP Phase Noise Analyzer and VCO Tester **7**

Figure 2:   *Typical Sensitivity at various frequencies with R&S FSWP-B61option (starts @1Hz offset)*

Figure 3:   *Measured Phase Noise of a PLL System at about 162 GHz using the R&S FSWP Signal Source Analyzer*

This CAD tool was developed under the MIMIC Program

Figure 4:   *Advertising for the Serenade Program developed under the MIMIC Program*

➢ WHAT IS AN OSCILLATOR

❖ An Oscillator is an Electronic Circuit that converts DC power to RF power, this can range from a few Hz to Tera Hz and higher

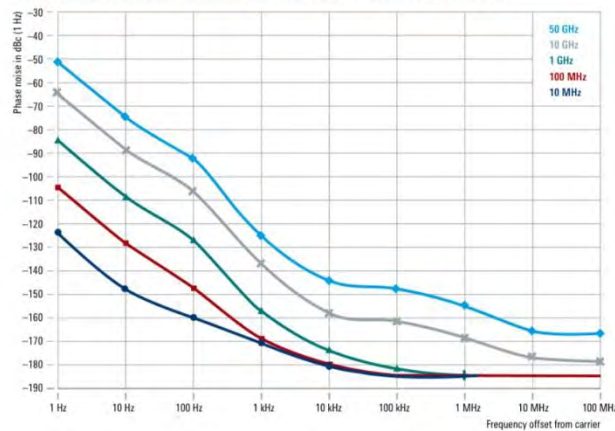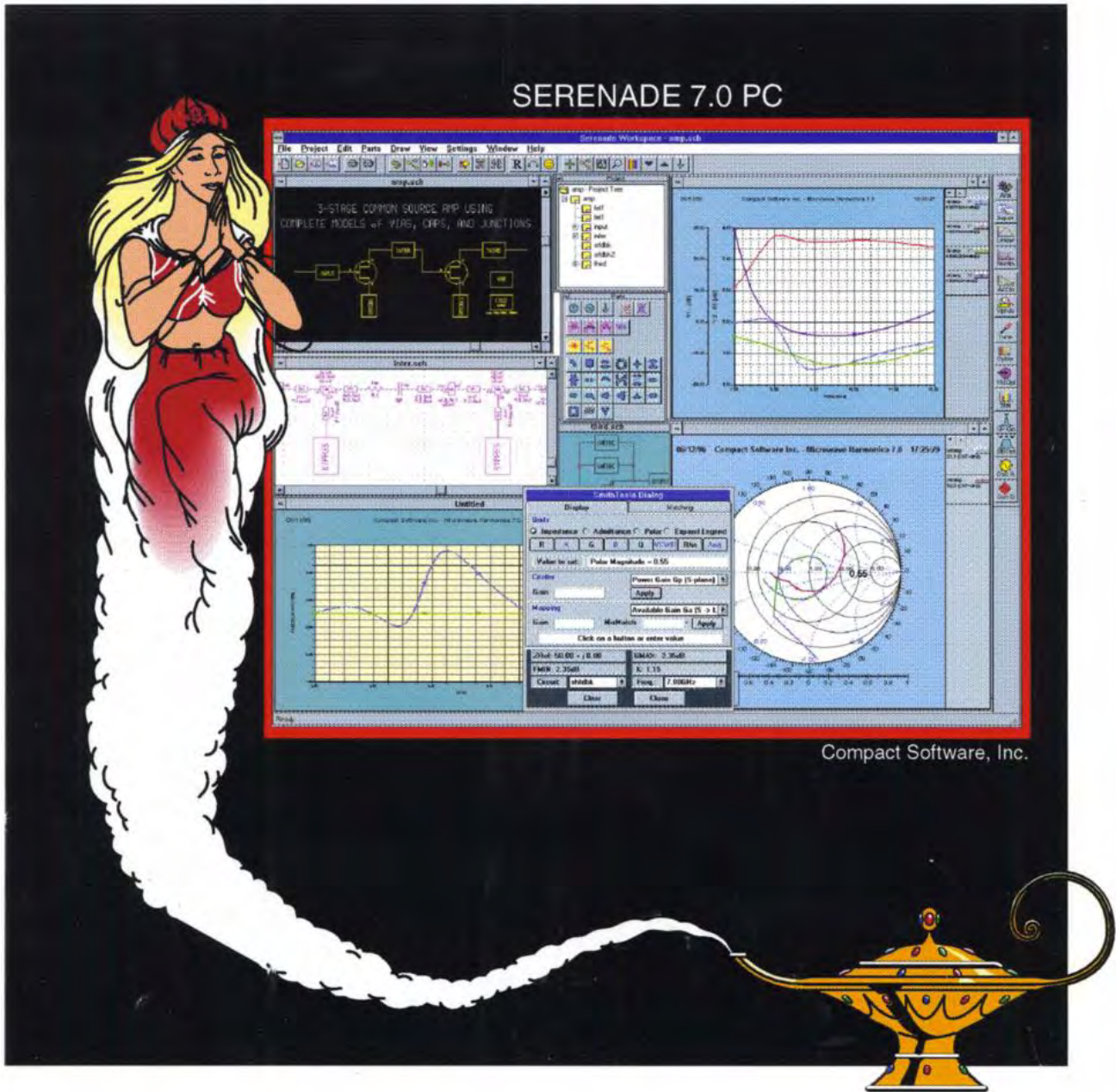❖ An oscillator consists of an active device acting as an amplifier, a resonator, and a feedback circuit

❖ A small amount of energy feedback is needed to sustained oscillation and the majority of available energy appears at the output terminals

❖ Resonators can be LC based circuits, transmission line based, crystal, ceramic, dielectric resonator, YIG (Yttrium Garnet) based, and others

For RF application, the most relevant features besides size are:

❖ Output power

❖ Harmonic content

❖ Phase Noise

❖ Power consumptions, to name a few

➢ Introduction to Microwave Oscillators and Their Mathematical Treatment:

The design of microwave oscillators has been and is the subject of many publications. To a certain degree, oscillators have been designed based on experimental data and experience, and the resulting performance has been measured and published. The designer, however, considers it important and useful to start from a set of specifications and then applies a synthesis procedure, which leads to a successful circuit. The following are popular transistor oscillator designs.

History

The first time an oscillator became important was when Maxwell's Equations were to be experimentally proven. Heinrich Hertz made the first known oscillator. He used a dipole as the resonator and a spark gap generator as the oscillator circuit as shown in Figure 1-1.
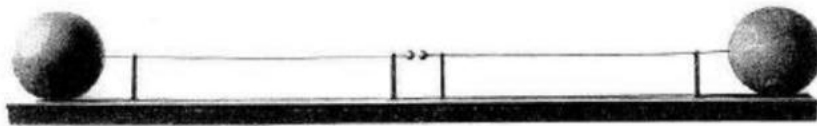

Figure 5:   *Figure 1-1 Original dipole made by Heinrich Hertz in 1887 using balls at the end to form a capacitive load (Deutsches Museum, Munich).*

Modern communications systems need oscillators as part of the design. In most cases these oscillators are part of a synthesizer and they are voltage-controlled, meaning that the frequency is determined by tuning diodes, frequently called varactors. The applied DC voltage varies the frequency. For high performance circuits the Colpitts oscillator is most frequently selected [1–30]. A large part of this work is taken from our book mentioned above and reproduced with permission.

The Colpitts oscillator comes in three flavors. Figure 1a, shows the conventional circuit configuration. This type of circuit is based on a design developed by Edwin Henry Colpitts, known for his invention of this oscillator and hence carries his name [1]. It uses a capacitive voltage divider and an inductor. In reality this simple circuit is not used but rather a derivation of this. This is shown in Figure 1b. The advantage of this circuit is that the values for C_1 and C_2 are fixed and the frequency change occurs by changing C_3. If the frequency of Figure 1a needs to be changed, a better choice is to vary the inductor L.

Colpitts colleague Ralph Hartley [2] invented an inductive coupling oscillator. The advantage of such an oscillator having capacitors C_1 and C_2 replaced with a tap of the inductor has been used together with helical resonators. The frequency tuning is achieved purely capacitively. To minimize loading, the transistor of choice here is a FET, which has very high input impedance and provides minimum loading to the circuit. The disadvantage is that this circuit, using junction FETs, is limited to about 400 MHz. The transition frequency f_T is about 500 MHz. FETs can also be used in the Colpitts oscillator as shown in Figure 1a, because of relatively lower loading than the bipolar transistor. The drawback of Figure 1a is the heavy loading of the tuned circuit by the transistor.

Important: These oscillators are called one port oscillators as the resonator losses are compensated with the negative but noisy Re(Z11) resistor compensated are! The Im(Z11) adds to the AM to PM conversion.

Figure 6: **Basic Oscillator Configurations**

➤ Transistor models and Noise Contributions

For the design of oscillators we are looking at members of bipolar and field-effect transistor families. In the case of the bipolar transistor, conventional microwave silicon transistors are manufactured with an f_T up to 25 GHz, while the more advanced SiGe transistors take over from this frequency range. Today, SiGe transistors are available up to 900 GHz and are used as part of an RFIC. Their cousins, the heterojunction bipolar transistors (HBTs), based on GaAs technology, can achieve similar cut-off frequencies, but this technology is much more expensive for medium to large integrated circuits. HBTs also have a higher flicker noise corner frequency. SiGe transistors have a much lower flicker noise corner frequency and lower breakdown voltages (typically 2-3V). However, because of the losses of the transmission line in practical circuits, there is not much difference between HBT and SiGe oscillator noise as f_T is the same.

There is a similar competing situation between Bi-CMOS transistors implemented in a 0.062 micron technology and with GaAs FETs, specifically p-HEMTs. The GaAs FETs have well-established performance with good models, and the Bi-CMOS transistors are currently being investigated as to what models are the best. Also, there is the $1/f$ noise problem, specifically, with GaAs FETs more than with MOS transistors. The 6 nm technology is somewhat impractical because of poor modeling. This means that many CAD predictions do not translate in a good design.

Noise in Semiconductors and Circuits

Microwave applications generally use bipolar transistors and following are their noise contributions

Johnson noise

The Johnson noise (thermal noise) is due to the movement of molecules in solid state devices called "Brown's molecular movements"

It is expressed as $v_n^2 = 4kT_0RB$ (emf) (volt ^{2}/Hz)

The power of thermal noise can thus be written as

$$\text{Noise Power} = \frac{v_n^2}{4R} = kT_0B(W/Hz)$$

It is most common to do noise evaluations using a noise power density, in Watts per Hz.

By setting $B = 1$ Hz we get:

For $B = 1$ Hz, Noise Power $= kT_0$

By Thevinin, Noise Power $= 1.38 \times 10^{-23} \times 290 = 4 \times 10^{-23}$ W

- Noise floor below the carrier for zero dBm output is given by:

$L(\omega) = 10log\left(\frac{v_n^2/R}{1mW}\right) = -173.97dBm \text{ or about } -174dBm$

- In order to reduce this noise, the only option is to lower the temperature, since noise power is directly proportional to temperature.

- The Johnson noise sets the theoretical noise floor.

- The available noise power does not depend on the value of resistor but it is a function of temperature T. The noise temperature can thus be used as a quantity to describe the noise behavior of a general lossy one-port network.

- For high frequencies and/or low temperature a quantum mechanical correction factor has to be incorporated for the validation of equation. This correction term results from Planck's radiation law, which applies to blackbody radiation.

$$P_{av} = kT.B \cdot p(f,T), \ with \ p(f,T) = \left[\frac{hf}{kT} \Big/ \left(e^{\left(\frac{hf}{kT}\right)} - 1\right)\right]$$

- where $h = 6.626.\,10^{-34} J - s$, Planck's Constant (**Planck's Radiation Noise**)

Schottky/Shot noise

The Schottky noise occurs in conducting PN junctions (semiconductor devices) where electrons are freely moving. The root mean square (RMS) noise current in 1 Hz bandwidth given by

$$\overline{i_n^2} = 2 \times q \times I_{dc} \ P = i_n^2 \times R_L$$

Where, q is the charge of the electron, P is the noise power, and I_{dc} is the dc bias current, R_L is the termination load (can be complex).

Since the origin of this noise generated is totally different, they are independent of each other.

Flicker noise

The electrical properties of surfaces or boundary layers are influenced energetically by states, which are subject to statistical fluctuations and therefore, lead to the flicker noise or $1/f$ noise for the current flow. $1/f$ noise is observable at low frequencies and generally decreases with increasing frequency f according to the $1/f$-law until it will be covered by frequency independent mechanism, like thermal noise or shot noise.

Example: The noise for a conducting diode is bias dependent and is expressed in terms of AF and KF.

Transit time and Recombination Noise

When the transit time of the carriers crossing the potential barrier is comparable to the periodic signal, some carriers diffuse back and this causes noise. This is really seen in the collector area of NPN transistor. The electron and hole movements are responsible for this noise. The physics for this noise has not been fully established.

Avalanche Noise

When a reverse bias is applied to semiconductor junction, the normally small depletion region expands rapidly.

The free holes and electrons then collide with the atoms in depletion region, thus ionizing them and produce spiked current called the avalanche current.

The spectral density of avalanche noise is mostly flat. At higher frequencies the junction capacitor with lead inductance acts as a low-pass filter.

Zener diodes are used as voltage reference sources and the avalanche noise needs to be reduced by big bypass capacitors.

$$\langle i_{Dn}^2 \rangle_{AC} = 2qI_{dc}B + Kf \frac{I_{DC}^{Af}}{f}B$$

Af Generally is in the range of 1 to 3 (dimensionless quantity) and is a bias dependent curve fitting term, typically 2.

The Kf value is ranging from $1E^{-12}$ to $1E^{-6}$, and defines the flicker corner frequency.

➢ Transistor Types

Bipolar Transistors

The bipolar transistor has been known and used for many decades. Many scientists have explained its behavior, and probably the best analysis in the DC/RF area is summarized in [29]. This summary is based largely on the Infineon transistor BFP520 as an example, but is applicable to other transistors also.
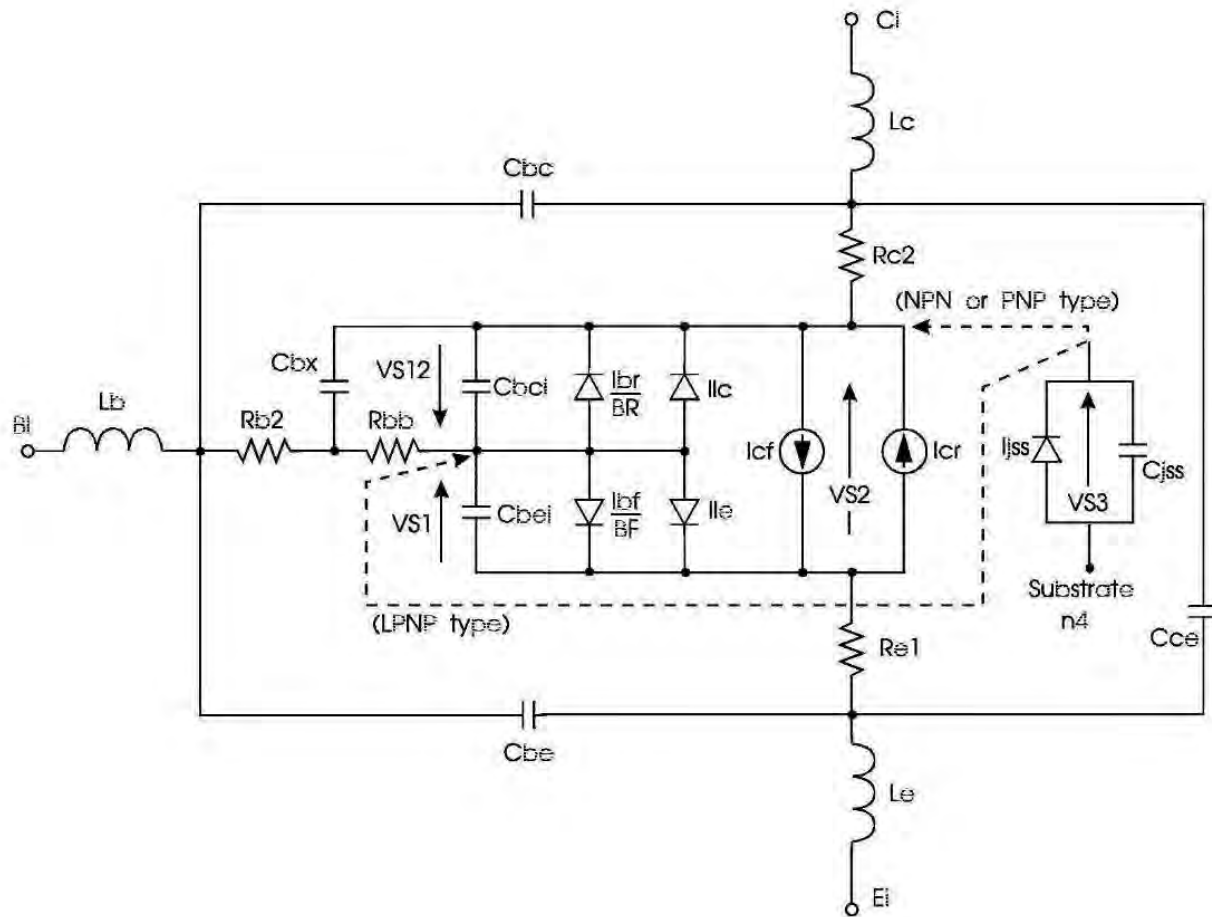
Figure 7: *Equivalent circuit for a microwave bipolar transistor. It deviates from the SPICE implementation by having two base-spreading resistors.*

The first thing we need to do is look at the model used to calculate the DC and RF performance of a microwave transistor. There are subtle differences between the standard SPICE implementation and the one suited for higher frequencies. Figure 7 shows a modification that was necessary for greater accuracy by introducing an additional base-spreading resistor, R_{b2}.

Let Δf be the bandwidth (usually normalized to a 1Hz bandwidth). The noise generators introduced in the intrinsic device are shown below, and have mean-square values of:

$$\left\langle i_{bn}^2 \right\rangle = 2qI_B \, \Delta f + \text{KF} \frac{I_B^{\text{AF}}}{f^{\text{FCP}}} \, \Delta f$$

$$\left\langle i_{cn}^2 \right\rangle = 2qI_C \, \Delta f$$

$$\left\langle i_{Rbb}^2 \right\rangle = \frac{4kT}{R_{bb}} \, \Delta f$$

$$\left\langle i_{Re1}^2 \right\rangle = \frac{4kT}{RE1} \, \Delta f$$

$$\left\langle i_{Rc2}^2 \right\rangle = \frac{4kT}{RC2} \, \Delta f$$

$$I_B = \frac{I_{bf}}{BF} + I_{le}$$

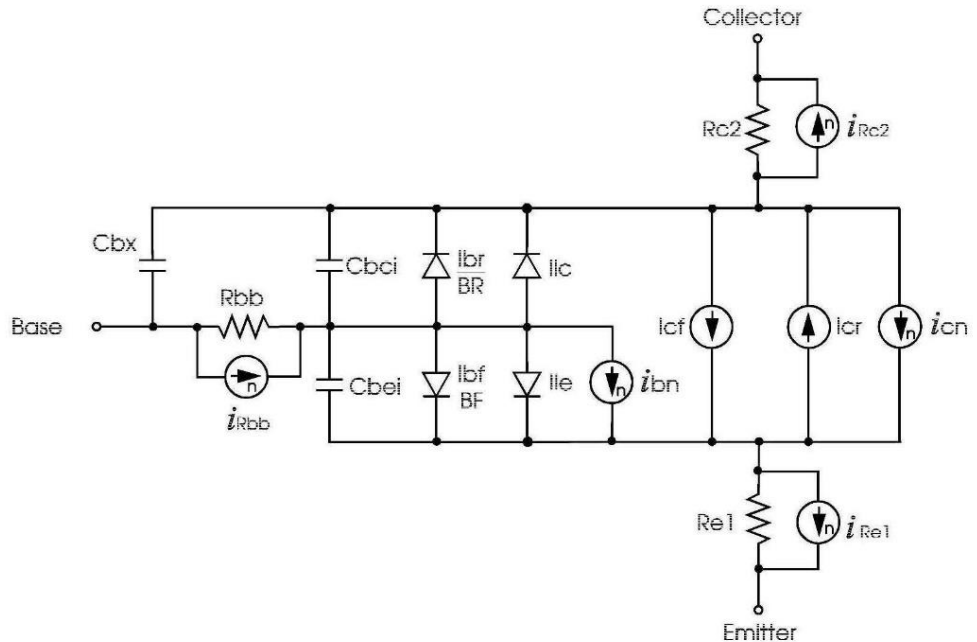$$I_C = I_{cf} - I_{cr}$$

Figure 8:   *Noise Model of a BJT*

Field-Effect Transistors

For RF applications, there are three types of transistors which can be used. The first is a junction FET, which have been shown to be useful up to 1 GHz at most. Their fairly high input capacitance of about 1pF and large feedback capacitance of about 0.1pF limits their use. They have been mentioned here only for completeness. The other two FETs of importance are members of the GaAs FET family and the BiCMOS transistors. Recent advances in technology have push the BiCMOS process close to 1009 GHz if the BiCMOS transistor is built on SiGe technology.
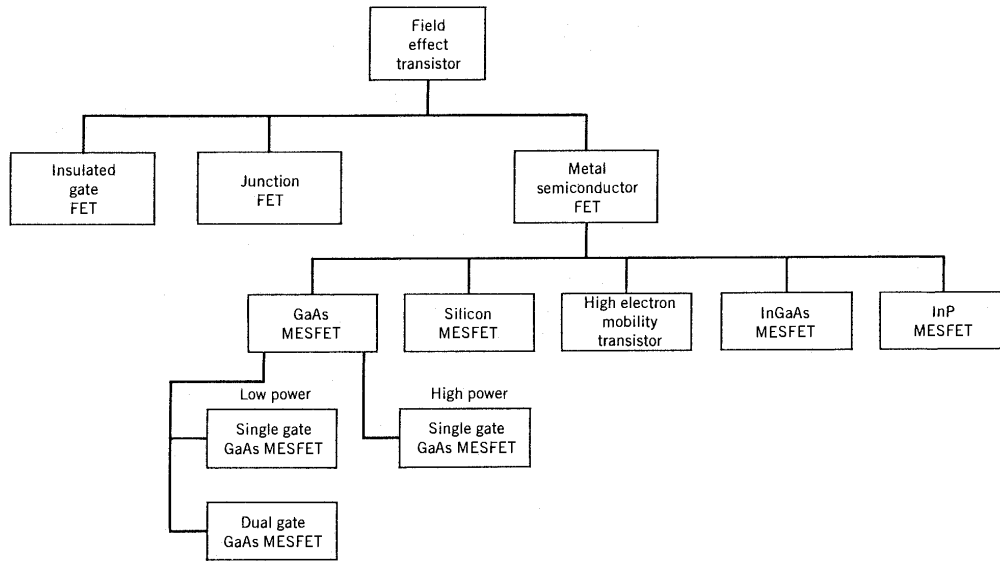
GaAs FETs (MESFET)

Figure 9: *RF-FET Family Tree*

For the purpose of modeling GaAs FETs, there is a large number of models available, and the list is longer if company or university internal models are added. The following models are popular with CAD tools.

- Chalmers (Angelov) Model

- Modified Materka-Kacprzak Model (low noise)

- Physics-Based MESFET Model

Their properties and different model equations can be found in the CAD user's manual. As an example, the Ansoft Designer's reference manual gives all the details and references on how the model was implemented. It is difficult to obtain a reliable parameter extractor for the models. Probably, the most popular model for commercial application is the Angelov model. The model for which good parameters can be extracted with reasonable effort is the Materka model. It requires a DC/IV curve tracer and a network analyzer which operates up to 84 GHz.
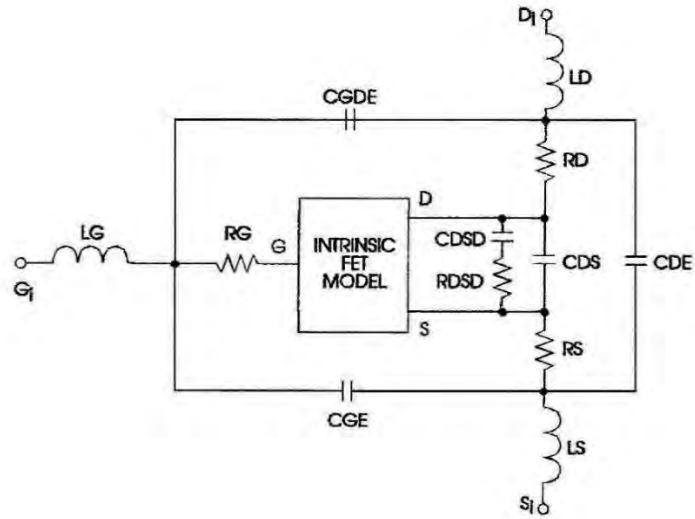
Figure 10: *Figure 3-11   Topology of the extrinsic model for all intrinsic models.*
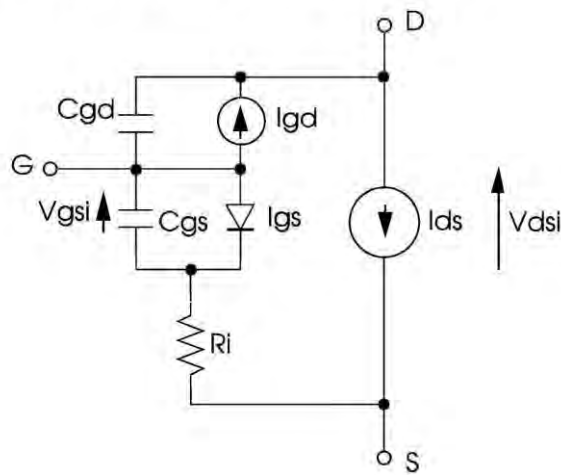
Materka-Kacprzak Intrinsic Model

Figure 11: *Figure 3-12   Topology of the intrinsic model.*

NMOS MOSFET

Figure 12: *Intrinsic model for an NMOS MOSFET.*

MOS Model Level 3 Example:

The following model shown in Figure 12 is the popular but simple MOSFET model and has been implemented in this configuration and in most of the simulators (ADS from Agilent, Designer from Ansoft, and Microwave Office from AWR to name a few). Addressing the model Level 3, here are the parameters extracted for the LDMOS device which works up to several GHz and was used for a 2 GHz oscillator.

L = 0.12um W = 0.15mm CBD = 0.863E-12 CGD0 = 166E-12 CGS0 = 246E-12 GAMA = 0.211 + IS = 6.53E-16 KAPA = 0.809 MJ = 0.536 NSUB = 1E15 PB = 0.71 PBSW = 0.71 + PHI = 0.579 RD = 39 RS = 0.1 THET = 0.588 TOX = 4E-8 U0 = 835 VMAX = 3.38E5 + VT0 = 2.78 XQC = 0.41

The data provided above was supplied for a LDMOS device.

Let Δf be the bandwidth (normalized to 1Hz). The noise generators introduced in the intrinsic device are shown below, and have mean-square values of:

$$\left\langle i_{dn}^2 \right\rangle = \frac{8kTg_m}{3}\Delta f + \text{KF}\ \frac{I_D^{\text{AF}}}{f^{\text{FCP}}}\Delta f$$

$$\left\langle i_{Rgn}^2 \right\rangle = 4\frac{kT}{R_g}\Delta f$$

$$\left\langle i_{Rdn}^2 \right\rangle = 4\frac{kT}{R_d}\Delta f$$

$$\left\langle i_{Rsn}^2 \right\rangle = 4\frac{kT}{R_s}\Delta f$$

$$\left\langle i_{Rbn}^2 \right\rangle = 4\frac{kT}{R_b}\Delta f$$
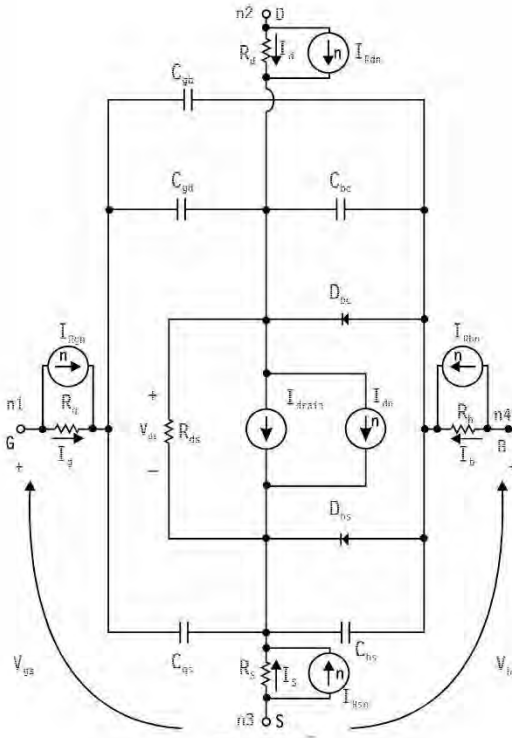

Figure 13: ***Noise model of the MOSFET transistor (not showing extrinsic parasitics). Current sources with "n" are noise sources.***

For the RFIC application, the BISIM Model 3V3 is the model of choice. Figures 13 and 14 show the MOSFET model representation.
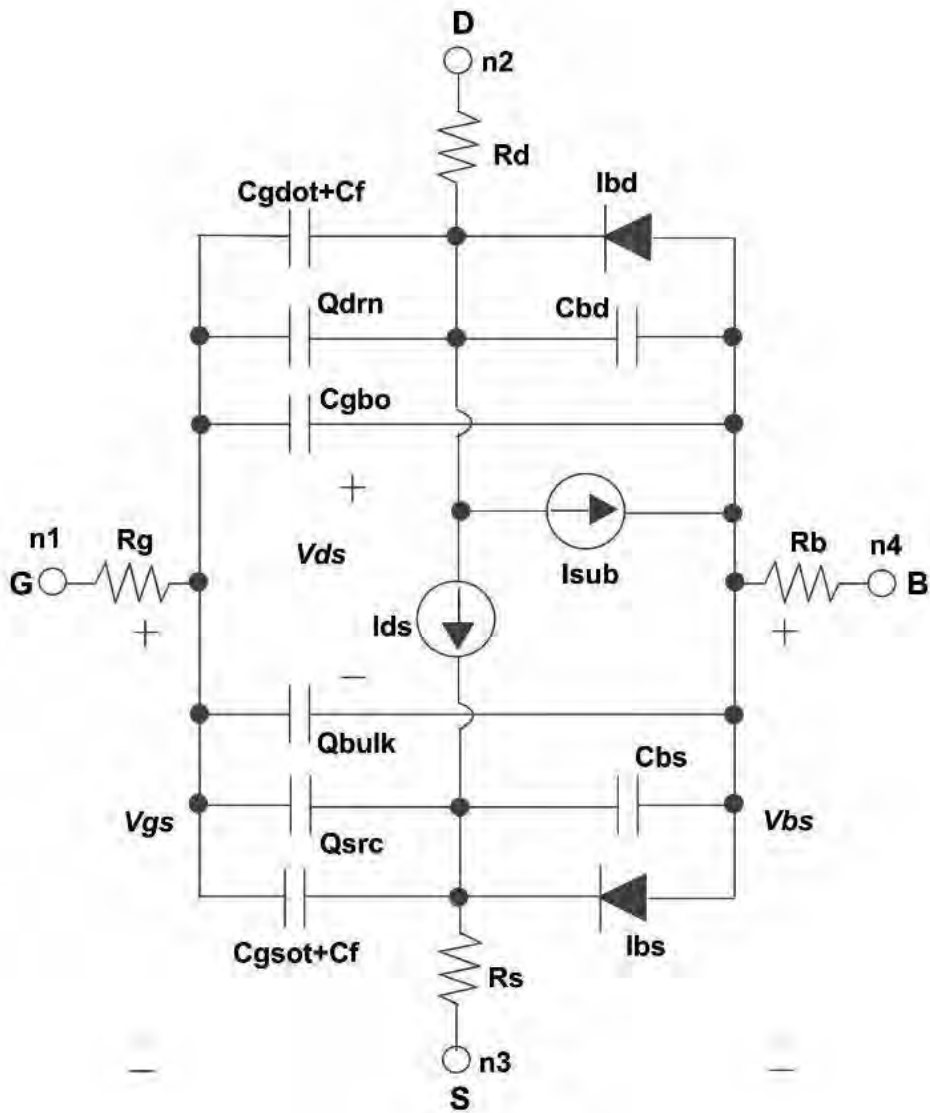
Figure 14: *FET-BSIM3V3 MOSFET model.*

While for the purpose of more insight this presentation uses detailed equivalent circuits and parameter the engineer in realty used either a characterized transistor or a foundry for the design.

While the transistor models are quite mature the real problem lies in the quality of the parameter extraction or likewise in the accuracy of the physics based models.

For the purpose of this presentation some easy to understand and simplified models are used, the refined models do not make the accuracy infinitely better.

Noise Model

Let Δf be the bandwidth (normalized to 1Hz). The noise generators introduced in the intrinsic device are shown below, and have mean-square values of:

$$\left\langle i_{dn}^2 \right\rangle = \left\langle i_{dn}^2 \right\rangle_f + \left\langle i_{dn}^2 \right\rangle_{th}$$

$$\left\langle i_{Rgn}^2 \right\rangle = 4\frac{kT}{R_g}\Delta f$$

$$\left\langle i_{Rdn}^2 \right\rangle = 4\frac{kT}{R_d}\Delta f$$

$$\left\langle i_{Rsn}^2 \right\rangle = 4\frac{kT}{R_s}\Delta f$$

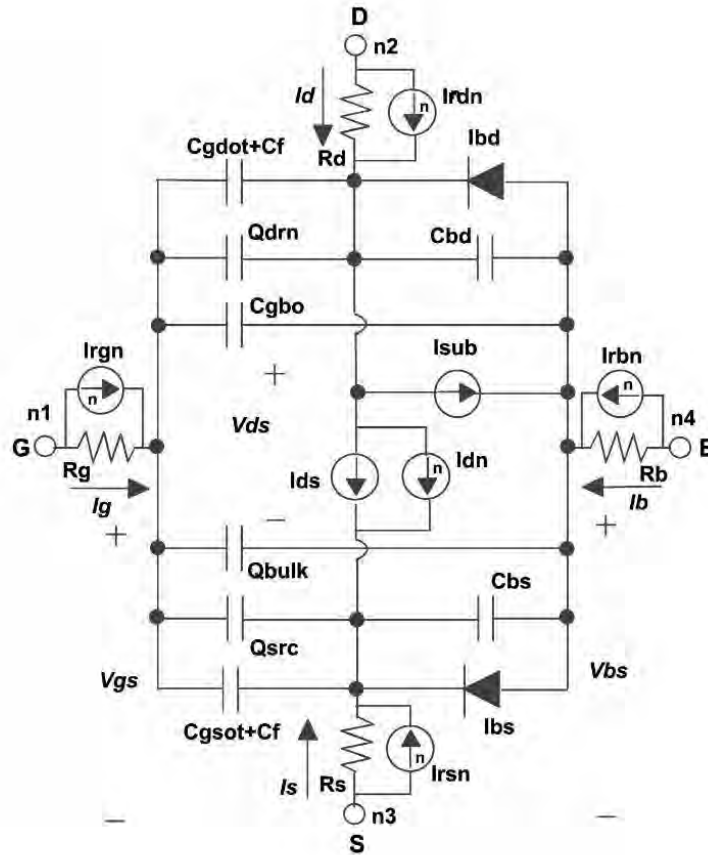$$\left\langle i_{Rbn}^2 \right\rangle = 4\frac{kT}{R_b}\Delta f$$

Figure 15: *Enhanced Noise Model of MOSFET*

➤ Linear Approach to the Calculation of Oscillator Phase Noise

In transmitters, oscillator noise can result in adjacent-channel interference and modulation errors; in receivers, oscillator noise can result in demodulation errors, and degraded sensitivity and dynamic range. The specification, calculation and reduction of oscillator noise is therefore of great importance in wireless system design.

See also: https://www.analog.com/en/resources/app-notes/an-1067.html

https://tf.nist.gov/general/tn1337/Tn190.pdf

The definition of phase noise was first given by E. J. Baghdady, R. N. Lincoln and B. D. Nelin, "Short-term Frequency Stability: Characterization Theory, and Measurement," in Short-Term Frequency Stability, NASA SP-80, 1965, pp. 65-87.
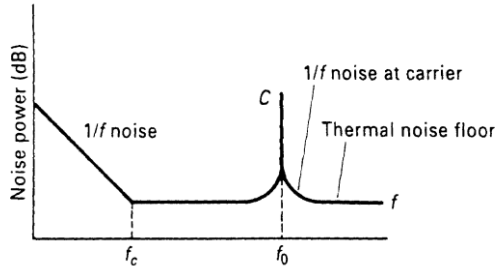

Figure 16: *Noise power versus frequency of a transistor amplifier with an input signal applied.*

Since an oscillator can be viewed as an amplifier with feedback (Figure 16), it is helpful to examine the phase noise added to an amplifier that has a noise figure F. With F defined as

$$F = \frac{(S/N)_{\text{in}}}{(S/N)_{\text{out}}} = \frac{N_{\text{out}}}{N_{\text{in}}\,G} = \frac{N_{\text{out}}}{GkTB} \tag{5-97}$$

$$N_{\text{out}} = FGkTB \tag{5-98}$$

$$N_{\text{in}} = kTB \tag{5-99}$$

where N_{in} is the total input noise power to a noise-free amplifier. The input phase noise in a 1-Hz bandwidth at any frequency $f_0 + f_m$ from the carrier produces a phase deviation given by (Figure 17)

$$\Delta\theta_{\text{peak}} = \frac{V_{\text{nRMS1}}}{V_{\text{avsRMS}}} = \sqrt{\frac{fKT}{P_{\text{avs}}}} \tag{5-100}$$

$$\Delta\theta_{\text{1RMS}} = \frac{1}{\sqrt{2}}\sqrt{\frac{FkT}{P_{\text{avs}}}} \tag{5-101}$$
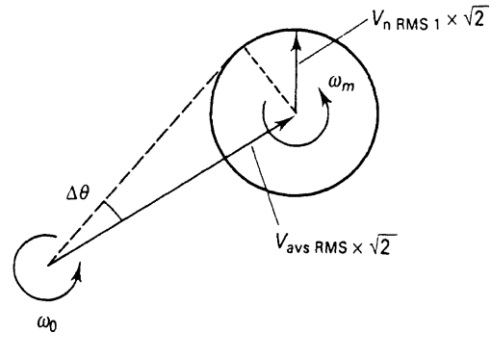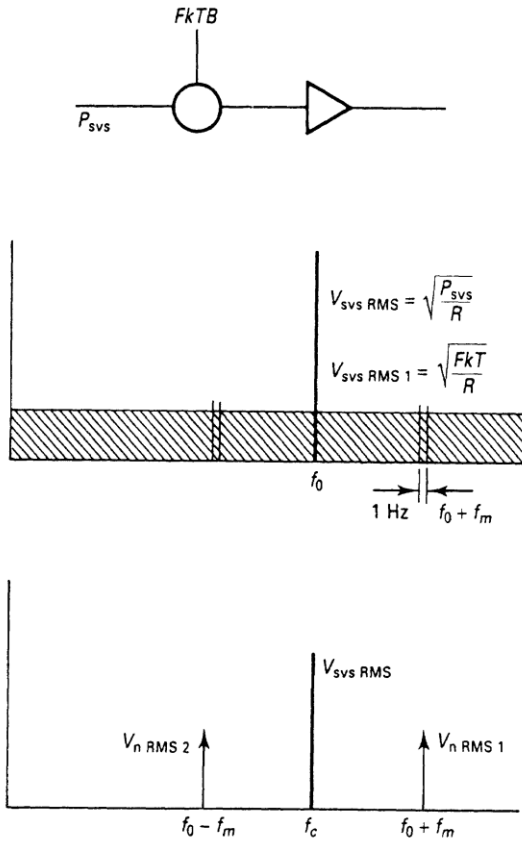
23

Figure 17: **Phase noise added to carrier**

Since a correlated random phase-noise relation exists at $f_0 - f_m$, the total phase deviation becomes

$$\Delta\theta_{\text{RMStotal}} = \sqrt{FkT / P_{\text{avs}}}$$

(5-102)

The spectral density of phase noise becomes

$$S_\theta\left(f_m\right) = \Delta\theta_{\text{RMS}}^2 = FkTB / P_{\text{avs}}$$

(5-103)

where $B = 1$ for a 1-Hz bandwidth. Using

24

$$kTB = -174 \, \text{dBm/Hz} \qquad (B = 1) \qquad\qquad\qquad \text{(5-104)}$$

allows a calculation of the spectral density of phase noise that is far removed from the carrier (that is, at large values of f_m). This noise is the theoretical noise floor of the amplifier. For example, an amplifier with +10 dBm power at the input and a noise figure of 6 dB gives

$$S_\theta(f_m > f_c) = -174 \, \text{dBm} + 6 \, \text{dB} - 10 \, \text{dBm} = -178 \, \text{dBm} \qquad \text{(5-105)}$$

Only if P_{OUT} is > 0 dBm can we expect $\mathcal{L}$ (signal-to-noise ratio) to be greater than 174 dBc/Hz (1-Hz bandwidth.) For a modulation frequency close to the carrier, S_θ (f_m) shows a flicker or $1/f$ component, which is empirically described by the corner frequency f_c. The phase noise can be modeled by a noise-free amplifier and a phase modulator at the input as shown in Figure 18.
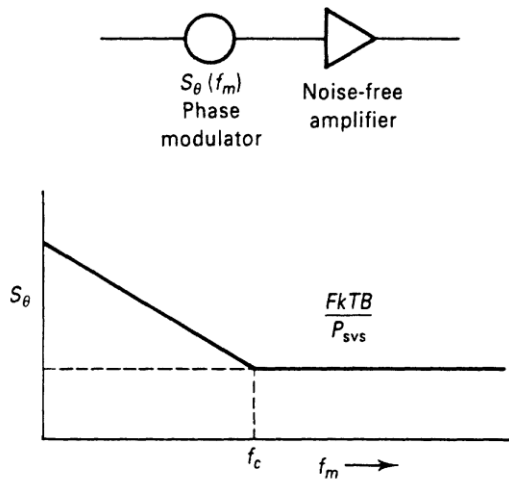

Figure 18: *Phase noise modeled by a noise-free amplifier and phase modulator*

The purity of the signal is degraded by the flicker noise at frequencies close to the carrier. The spectral phase noise can be described by

$$S_\theta(f_m) = \frac{FkTB}{P_{avs}}\left(1 + \frac{f_c}{f_m}\right) \qquad (B = 1) \qquad\qquad \text{(5-106)}$$

No AM-to-PM conversion is considered in this equation. The oscillator may be modeled as an amplifier with feedback as shown in Figure 19. The phase noise at the input of the amplifier is affected by the bandwidth of the resonator in the oscillator circuit in the following way. The tank circuit or bandpass resonator has a low-pass transfer function

$$L(\omega_m) = \frac{1}{1 + j(2Q_L \omega_m / \omega_0)}$$

(5-107)

where

$$\omega_0 / 2Q_L = B/2$$

(5-108)

is the half-bandwidth of the resonator. These equations describe the amplitude response of the bandpass resonator; the phase noise is transferred attenuated through the resonator up to the half-bandwidth.
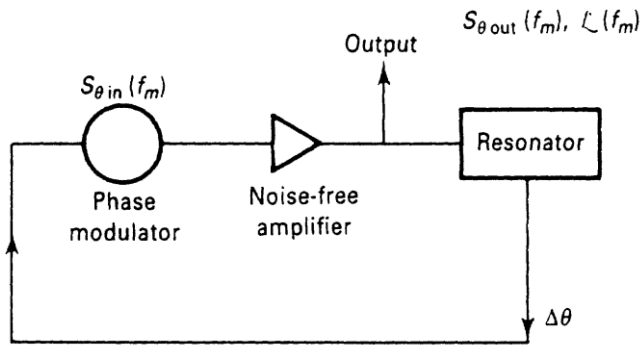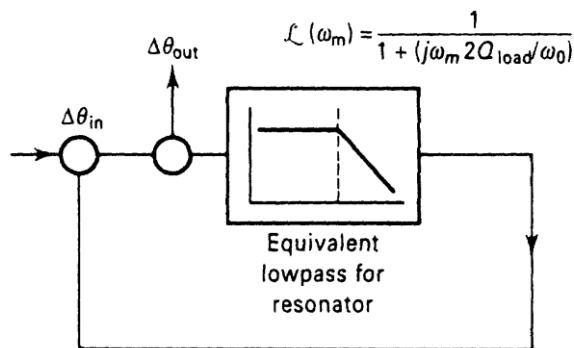

Figure 19: *Equivalent feedback models of oscillator phase noise.*

The closed-loop response of the phase feedback loop is given by

26

$$\Delta\theta_{out}(f_m) = \left(1 + \frac{\omega_0}{j2Q_L\omega_m}\right)\Delta\theta_{in}(f_m)$$

(5-109)

The power transfer becomes the phase spectral density is given by

$$S_{\theta out}(f_m) = \left[1 + \frac{1}{f_m^2}\left(\frac{f_0}{2Q_L}\right)^2\right]S_{\theta in}(f_m)$$

(5-110)

where $S_{\theta\,in}$ was given by Eq. (5-106). Finally, $\mathcal{L}(f_m)$ is

$$\mathcal{L}(f_m) = \frac{1}{2}\left[1 + \frac{1}{f_m^2}\left(\frac{f_0}{2Q_L}\right)^2\right]S_{\theta in}(f_m)$$

(5-111)

This equation describes the phase noise at the output of the amplifier (flicker corner frequency and AM-to-PM conversion are not considered). The phase perturbation $S_{\theta in}$ at the input of the amplifier is enhanced by the positive phase feedback within the half-bandwidth of the resonator, $f_0/2Q_L$.
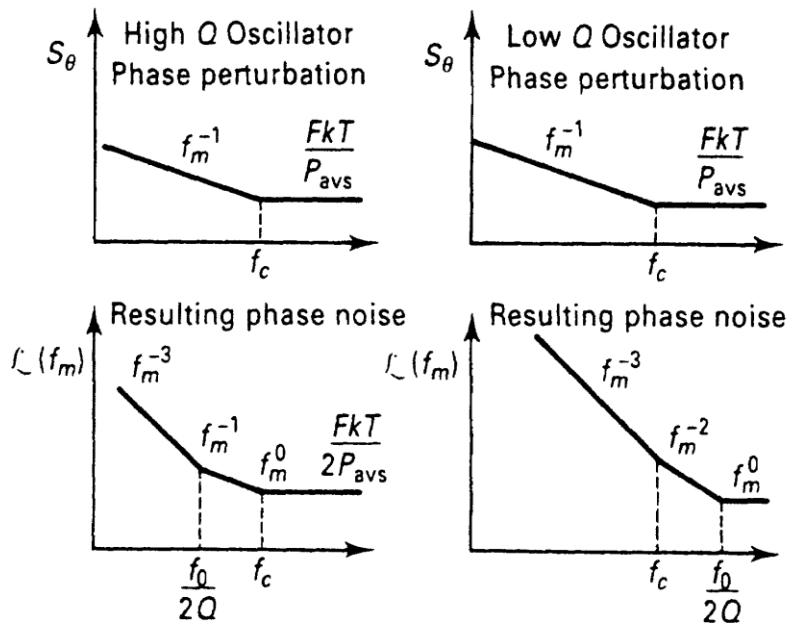

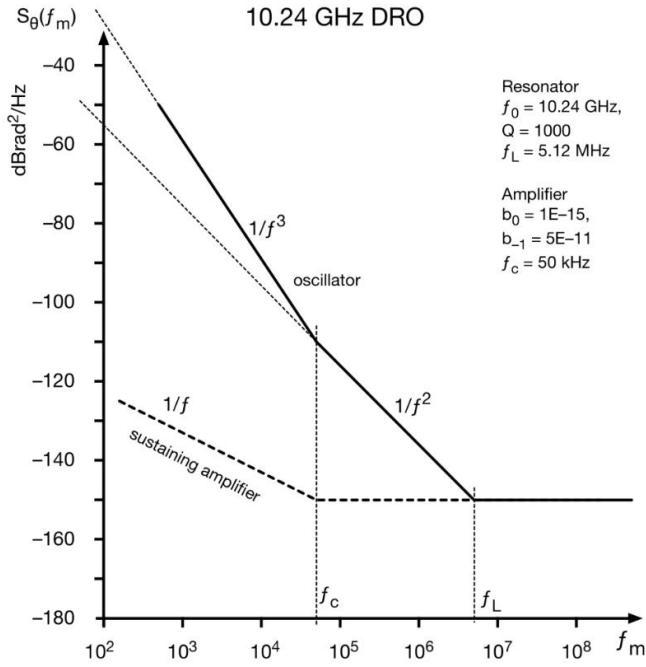Figure 20: *Equivalent feedback models of oscillator phase noise.*

27

Figure 21: *Figure 2-45: Phase Noise PSD of the 10.24 GHz DRO discussed in the example*

Depending on the relation between f_c and $f_0/2Q_L$, there are two cases of interest, as shown in Figure 20. For the low-Q case, the spectral phase noise is unaffected by the Q of the resonator, but the $\mathcal{L}(f_m)$ spectral density will show a $1/f^3$ and $1/f^2$ dependence close to the carrier. For the high-Q case, a region of $1/f^3$ and $1/f$ should be observed near the carrier. Substituting Eq. (5-106) in (5-111) gives an overall noise of

$$
\mathcal{L}(f_m) = \frac{1}{2}\left[1 + \frac{1}{f_m^2}\left(\frac{f}{2Q_L}\right)^2\right]\frac{FkT}{P_{\text{avs}}}\left(1 + \frac{f_c}{f_m}\right)
$$

$$
= \frac{FkTB}{2P_{\text{avs}}}\left[\frac{1}{f_m^3}\frac{f^2 f_c}{4Q_L^2} + \frac{1}{f_m^2}\left(\frac{f}{2Q_L}\right)^2 + \left(1 + \frac{f_c}{f_m}\right)\right] \text{ dBc/Hz}
$$

$$(5\text{-}112)$$

Examining Eq. (5-112) gives the four major causes of oscillator noise: the up-converted $1/f$ noise or flicker FM noise, the thermal FM noise, the flicker phase noise, and the thermal noise floor, respectively.

Q_L (loaded Q) can be expressed as

$$Q_L = \frac{\omega_o W_e}{P_{\text{diss, total}}} = \frac{\omega_o W_e}{P_{\text{in}} + P_{\text{res}} + P_{\text{sig}}} = \frac{\text{reactive power}}{\text{total dissipated power}} \tag{5-113}$$

where W_e is the reactive energy stored in L and C,

$$W_e = \tfrac{1}{2} C V^2 \tag{5-114}$$

$$P_{\text{res}} = \frac{\omega_o W_e}{Q_{\text{unl}}} \tag{5-115}$$

$$\mathcal{L}(f_m) = \frac{1}{2}\left[1 + \frac{\omega_o^2}{4\omega_m^2}\left(\frac{P_{\text{in}}}{\omega_o W_e} + \frac{1}{Q_{\text{unl}}} + \frac{P_{\text{sig}}}{\omega_o W_e} \right)^2 \right]\left(1 + \frac{\omega_c}{\omega_m} \right)\frac{FkT_o}{P_{\text{sav}}}$$

| input power over reactive power | | resonator Q | | signal power over reactive power | | flicker effect | | phase perturbation |

$$\tag{5-116}$$

The following examples refer to bipolar transistors ONLY

Typical oscillator
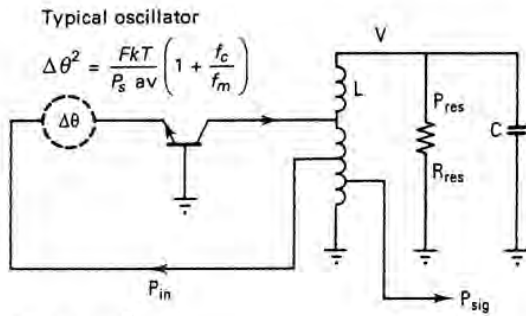
$$\Delta\theta^2 = \frac{FkT}{P_s\ \text{av}}\left(1 + \frac{f_c}{f_m}\right)$$

For $f_m < \dfrac{f_o}{2Q_{\text{load}}}$

$$\mathcal{L}(f_m) = \frac{1}{2}\frac{1}{\omega_m^2}\left(\frac{\omega_o}{2Q_{\text{load}}}\right)^2\frac{FkT}{P_s\ \text{av}}\left(1 + \frac{f_c}{f_m}\right)$$

$$Q_{\text{load}} = \frac{\omega_o W_e}{P_{\text{diss, total}}} = \frac{\omega_o W_e}{P_{\text{in}} + P_{\text{res}} + P_{\text{sig}}}$$

$$= \frac{\text{Reactive power}}{\text{Total dissipated power}}$$

Maximum energy in C or L : $W_e = \frac{1}{2}CV^2$

$$\mathcal{L}(\omega_m) = \frac{1}{8}\frac{FkT}{P_s\ \text{av}}\frac{\omega_o^2}{\omega_m^2}\left(\frac{P_{\text{in}}}{\omega_o W_e} + \frac{1}{Q_{\text{unl}}} + \frac{P_{\text{sig}}}{\omega_o W_e}\right)^2\left(1 + \frac{\omega_c}{\omega_m}\right)$$

Phase	Resonator Q	Flicker
Perturbation		Effect
	Input power	Signal power
	over	over

Figure 5-19--Diagram for a feedback oscillator illustrating the principles involved, and showing the key components considered in the phase noise calculation and its contribution.

Figure 22: *Example of a typical but simplified grounded base oscillator*

This equation is extremely significant because it covers most of the causes of phase noise in oscillators. [AM-to-PM conversion must be added; see (5-56).]

The basic equation (Scherer, Rohde's Modified Leeson's Equation) needed to calculate the phase noise is found in The Design of Modern Microwave Oscillators for Wireless Applications: Theory and Optimization [9].

$$\pounds(f_m) = 10\log\left\{\left[1 + \frac{f_0^2}{[2f_m Q_0 m(1-m)]^2}\right]\left(1 + \frac{f_c}{f_m}\right)\frac{FkT}{2P_0} + \frac{2kTRK_0^2}{f_m^2}\right\}$$

where $£(f_m), f_m, f_0, f_c, Q_L, Q_0, F, k, T, P_o, R, K_0$ and m are the ratio of the sideband power in a 1 Hz bandwidth at f_m to total power in dB , offset frequency, flicker corner frequency, loaded Q , unloaded Q, noise factor, Boltzmann's constant, temperature in degree Kelvin, average output power, equivalent noise resistance of tuning diode, voltage gain and ratio of the loaded and unloaded Q, respectively. From (1.1), the minimum phase noise can be found by differentiating Equation (1.1b) and equating to zero as $\frac{\partial}{\partial m}[£(f_m)]_{m=m_{\text{opt}}} = 0$

$$£(f_m) = \frac{d}{dm}\left\{10\log\left\{\left[1 + \frac{f_0^2}{[2f_m Q_0 m(1-m)]^2}\right]\left(1 + \frac{f_c}{f_m}\right)\frac{FkT}{2P_0} + \frac{2kTRK_0^2}{f_m^2}\right\}\right\}_{m\neq 1} = 0$$

$$\to m_{\text{opt}} \cong 0.5$$

Figure 23 shows the relative phase noise of the typical oscillator versus the ratio of loaded and unloaded Q of the resonator for noise factor F_1 and $F_2, (F_1 > F_2)$.
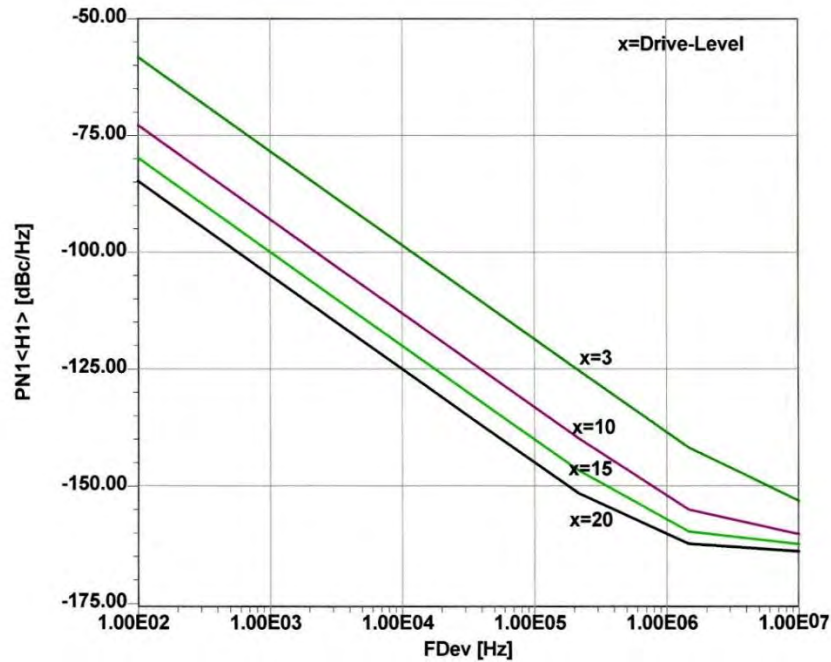
Figure 23: *Single sideband phase noise as a function of the normalized drive level x.*

The collector current plotted in Figure 20 becomes more narrow as the normalized drive level x moves towards x = 20. At the same time, the base-emitter voltage swing increases. This is plotted in Figure 6-21.

Figure 24: *Figure 6-20   shows the collector current pulses of the oscillator.*
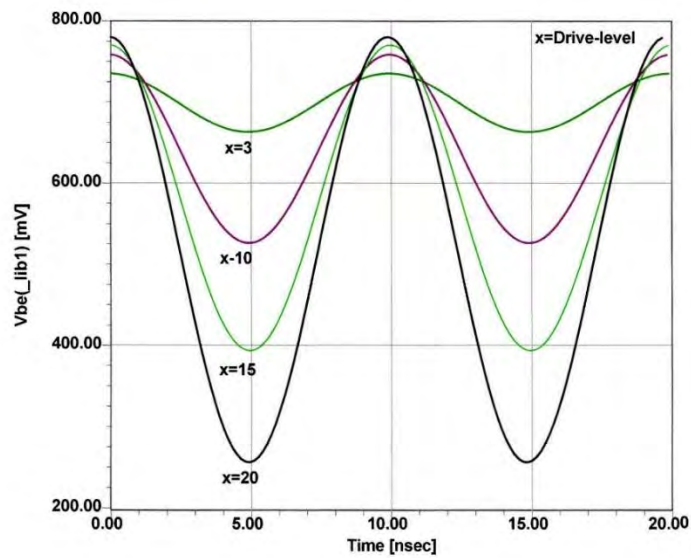
Figure 25: *Figure 6-21: RF voltage Vbe across the base-emitter junction as a function of the normalized drive level x.*

Here is a brief introduction to the definition of X, in a way the duty cycle. The voltage $v(t)$ across the base-emitter junction consists of a DC component and a driven signal voltage $V_1 \cos(wt)$. It can be expressed as

$$v(t) = V_{dc} + V_1 \cos(wt)$$

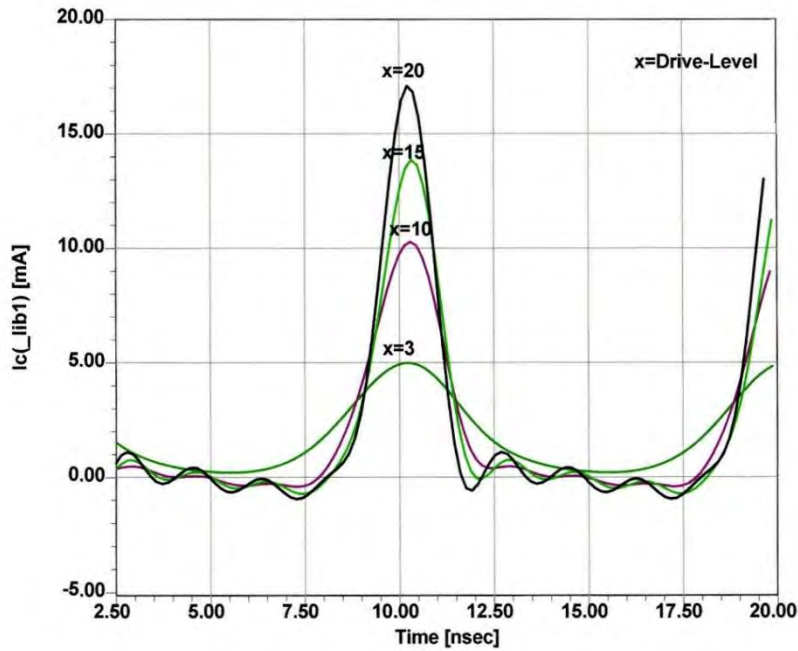As the driven voltage $V_1 \cos(wt)$ increases and develops enough amplitude across the base-emitter junction, the resulting current is a periodic series of pulses whose amplitude depends on the nonlinear characteristics of the device and is given as

$$i_e(t) = I_s e^{\frac{qv(t)}{kT}}$$

$$i_e(t) = I_s e^{\frac{qV_{dc}}{kT}} e^{\frac{qV_1 \cos(wt)}{kT}}$$

$$i_e(t) = I_s e^{\frac{qV_{dc}}{kT}} e^{x \cos(wt)}$$

assuming $I_c \approx I_e$ ($\beta > 10$)

$$x = \frac{V_1}{(kT/q)} = \frac{qV_1}{kT}$$

$i_e(t)$ is the emitter current and x is the drive level which is normalized to kT/q.
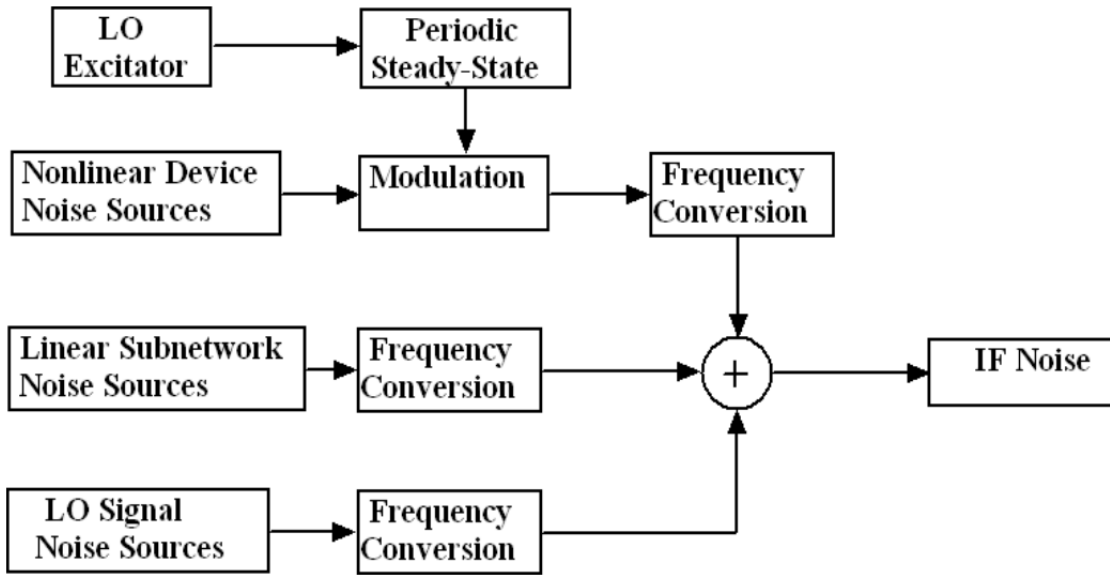
Figure 26: *Noise sources of oscillators being mixed on the carrier, amazing to see all the relevant contributions*

OSCILLATOR PHASE NOISE

Repeat: This equation does not take into consideration the conducting angle, because it is in the linear domain.

The Leeson phase noise equation is modified to accommodate the tuning diode noise contribution

$$\pounds(f_m) = 10\log\left\{\left[1 + \frac{f_0{}^2}{(2f_mQ_0)^2 m^2(1-m)^2}\right]\left(1 + \frac{f_c}{f_m}\right)\frac{FkT}{2P_0} + \frac{2kTRK_0^2}{f_m^2}\right\}$$

The Equation above explain the phase noise degradation (as compared to the fixed frequency LC oscillator due to the oscillator voltage gain K_0 associated with the tuning diode network as described by Rohde).

The reason for noise degradation is due to the increased tuning sensitivity of the varactor diode tuning network.
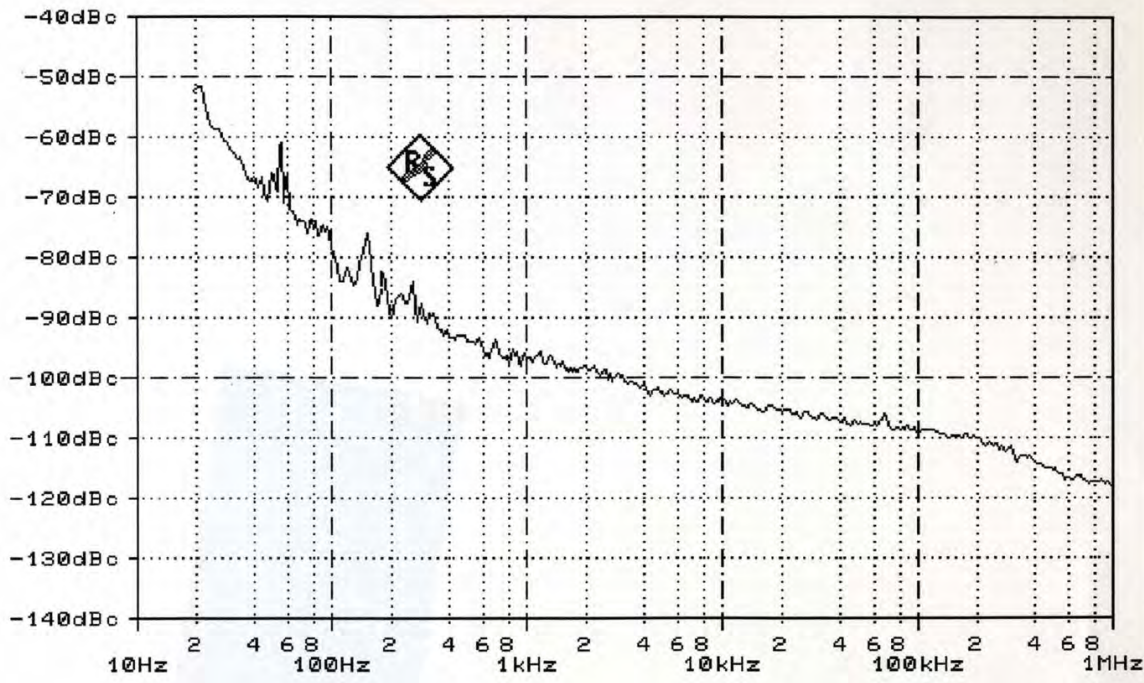
Figure 27: *Typical phase noise of a PLL 50 GHz PLL synthesizer*

https://www.researchgate.net/profile/Mehran-Mossammaparast/publication/4135164_A_review_of_sapphire_whispering_gallery-mode_oscillators_including_technical_progress_and_future_potential_of_the_technology/links/56187e1f08ae044edbad246c/A-review-of-sapphire-whispering-gallery-mode-oscillators-including-technical-progress-and-future-potential-of-the-technology.pdf

A REVIEW OF SAPPHIRE WHISPERING GALLERY-MODE OSCILLATORS INCLUDING TECHNICAL PROGRESS AND FUTURE POTENTIAL OF THE TECHNOLOGY

C. McNeilage, J. H. Searls, E. N. Ivanov*, P. R. Stockwell, D. M. Green, M. Mossammaparast

Poseidon Scientific Instruments Pty Ltd,

1/95 Queen Victoria St, Fremantle WA 6160, Australia

*School of Physics, The University of Western Australia, 35 Stirling Hwy, Crawley WA 6009, Australia

RECENT RESULTS AT PSI

The PSI 'SBO' series are compact, sapphire oscillators operating near room temperature, while the 'SLCO' is a 19" rack instrument. Since the first SLCOs were produced in 1996, the application-demanded requirements for temperature range, phase and amplitude noise performance, vibration sensitivity, and reliability have become more stringent.

Phase Noise Results

As mentioned above, the phase noise has shown steady improvement over the last few years, and Figure 12 shows the current level of performance.
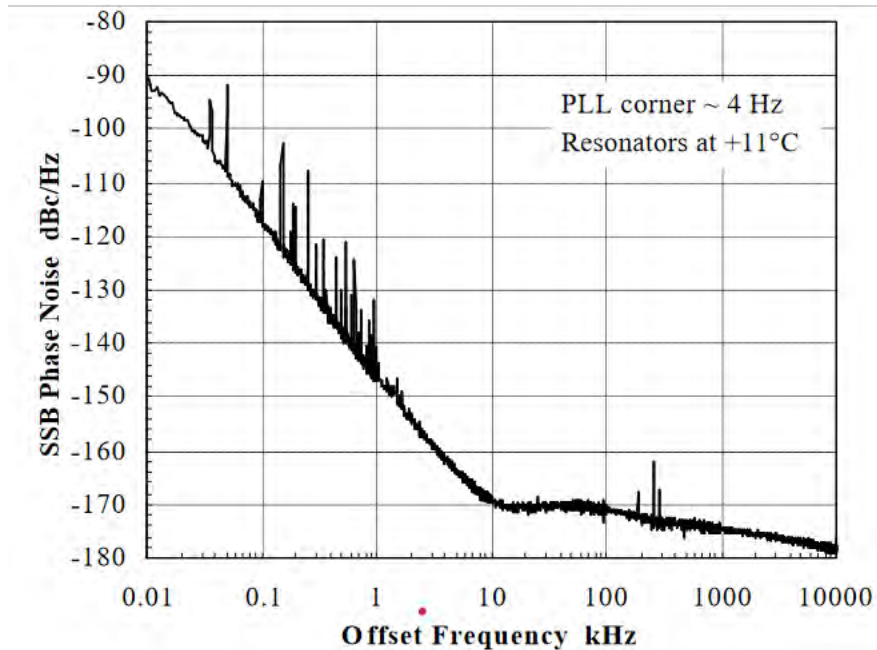
Figure 28: *Figure 12. Measured phase noise of PSI room temperature SLCO at 10.24 GHz (August 2003).*

Amplitude Noise Results

With phase noise at these low levels, amplitude (AM) noise can no longer be ignored. In fact, poor AM noise can readily degrade phase noise performance, particularly as temperature varies (an oscillator tuned for minimum AM-to-PM conversion at room temperature may well suffer at operating

36

temperature extremes). At PSI, we have tested various amplifier designs and developed low noise power supplies to minimize oscillator AM noise, and Figure 13 shows the current 'SBO' performance.
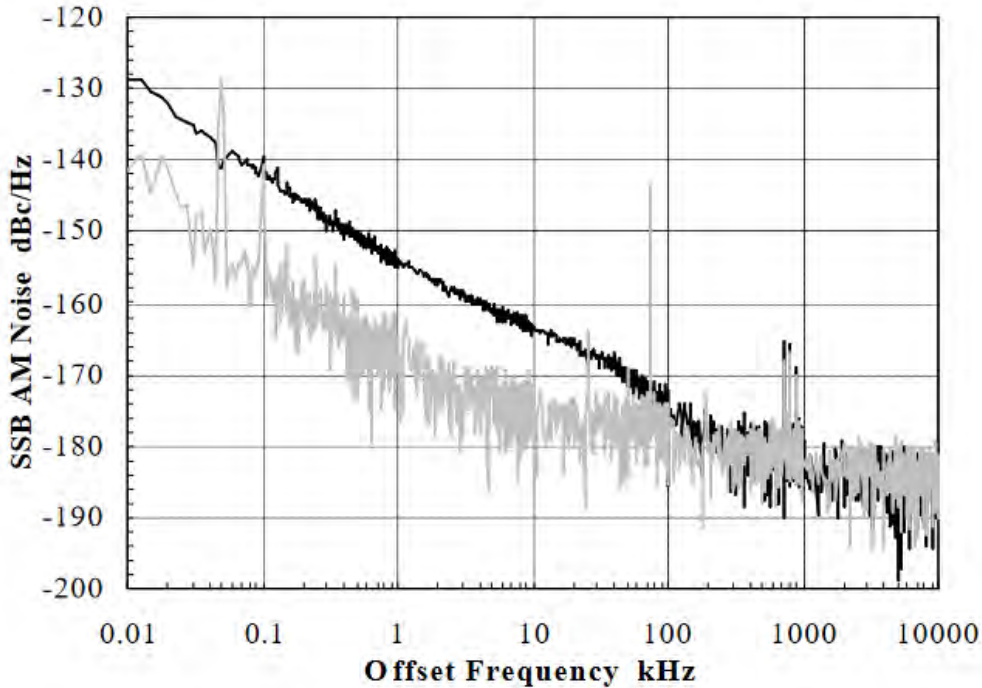
Figure 13. Measured amplitude noise of PSI room temperature SBO at 10.24 GHz (August 2004).

Figure 29:

AM noise is -154dBc/Hz at 1 kHz offset, with a 1/f characteristic through to 50 kHz, where the effect of resonator filtering is visible. The measurement was done using cross correlation of the signals from two AM-sensitive mixers, to achieve a low measurement noise floor. The apparent steps in the data are due to limited averaging in the cross-correlation method (a higher number of averages was taken at higher frequencies).

by Dieter Scherer (Hewlett Packard, about 1975).

Phase noise is a dimensionless number, and expressed in dBc/Hz, measured at an offset of Δf (f_m) from the carrier relative to the RF output power. At 0 dBm output, the ideal phase noise level far off the carrier is -174dB (T_0= 300 Kelvin)

➢ **Designing an Oscillator**

- Microwave oscillators are based on the negative resistance principle to compensate for the losses.

- Maximum frequency of oscillation can be determined from linear analysis for start-up conditions, but not necessarily for sustaining oscillation (large signal condition will reduce the gain and shift the frequency).

- Linear analysis is unreliable to determine resonance frequency and other dynamic parameters, beware of parasitics.
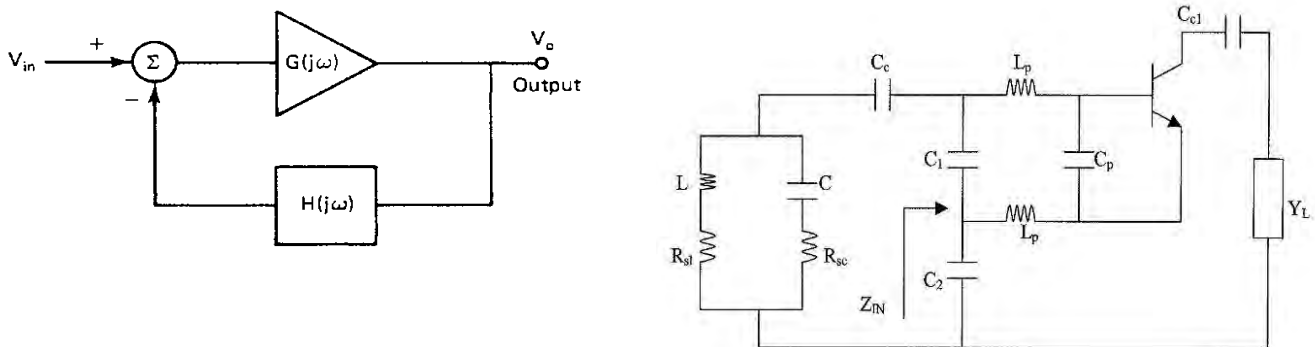
Figure 30: *Oscillator as a feedback model and as a*
one port producing a loss compensation with the electronically generated negative impedance.

$$Z_{IN}\big|_{pacakage} = -\left[\frac{Y_{21}^*}{\omega^2 (C_1 + C_p)C_2} \frac{1}{(1+\omega^2 Y_{21}^{*2} L_p^2)} \right] - j\left[\frac{(C_1 + C_P + C_2)}{\omega(C_1 + C_P)C_2} - \frac{\omega Y_{21}^* L_P}{(1+\omega^2 Y_{21}^{*2} L_p^2)} \frac{Y_{21}^*}{\omega(C_1 + C_P)C_2} \right]$$

Y^*_{21} = **Large signal value of g_m = Y21**

The Calculation of the Oscillating Condition Considering Parasitics of the Colpitts oscillator

In the practical case, the device parasitics and loss resistance of the resonator will play an important role in the oscillator design. Figure 6-2 incorporates the base lead-inductance Lp and the package-capacitance Cp.

It must be noted that part of the intrinsic transistor the Base-Collector capacitance is responsible for the Miller effect, and the Collector Emitter capacitance (Both are depletion capacitances), are non-linearly dependent on the collector voltage.
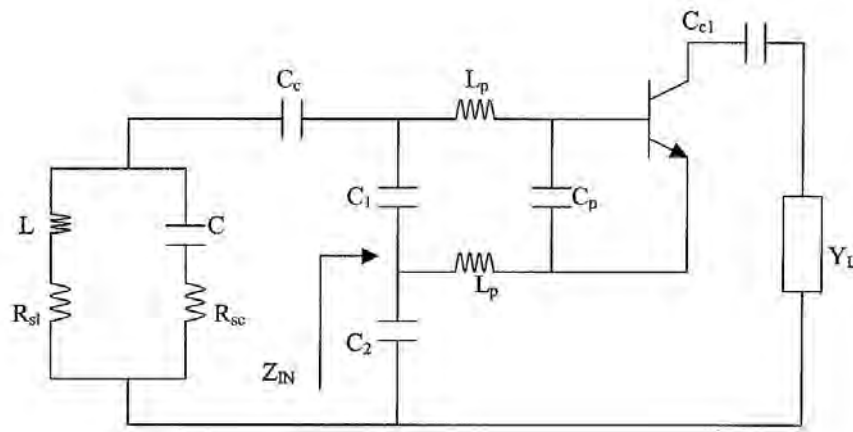
Figure 31: *Figure 6-2 Colpitts oscillator with base-lead inductances and package capacitance. Cc is neglected. The equivalent circuit of the intrinsic transistor is shown in Figure 8-12.*

The input impedance is

$$Z_{IN}\Big|_{pacakage} = -\left[\frac{Y_{21}}{\omega^2(C_1+C_p)C_2}\frac{1}{(1+\omega^2 Y_{21}^2 L_p^2)}\right] - j\left[\frac{(C_1+C_p+C_2)}{\omega(C_1+C_P)C_2} - \frac{\omega Y_{21}L_P}{(1+\omega^2 Y_{21}^2 L_p^2)}\frac{Y_{21}}{\omega(C_1+C_P)C_2}\right] \quad (6\text{-}1)$$

Because the real and imaginary part of Z11 contain Y21 which is both nonlinear and time dependent, The flicker and other noisy parts will be up converted to the carrier frequency, A high Q doesn't improve the noise unless the resonator also acts like a bandpass filter.

$$Z_{IN}\big|_{without-pacakage} = -\left[\frac{Y_{21}}{\omega^2 C_1 C_2}\right] - j\left[\frac{(C_1 + C_2)}{\omega C_1 C_2}\right] \qquad (6\text{-}2)$$

where L_p is the base-lead inductance of the bipolar transistor and C_p is base-emitter package capacitance. All further circuits are based on this model.

From the expression above, it is obvious that the base lead-inductance makes the input capacitance appear larger and the negative resistance appear smaller. The equivalent negative resistance and capacitance can be defined as

$$R_{NEQ} = \frac{R_N}{(1 + \omega^2 Y_{21}^2 L_p^2)} \qquad (6\text{-}3)$$

$$\frac{1}{C_{EQ}} = \left\{ \left| \frac{1}{\dfrac{(C_1 + C_P)C_2}{(C_1 + C_2 + C_P)}} \right| - \left[\frac{\omega^2 Y_{21} L_P}{(1 + \omega^2 Y_{21}^2 L_P^2)}\right]\left[\frac{Y_{21}}{\omega(C_1 + C_P)C_2}\right] \right\} \qquad (6\text{-}4)$$

$$R_N = -\frac{Y_{21}}{\omega^2 C_1 C_2} \qquad (6\text{-}5)$$

where

R_N :   Noisy negative resistance without lead inductance and package   capacitance.

R_{NEQ} : Negative resistance with base-lead inductance and package capacitance.

C_{EQ} :   Equivalent capacitance with base-lead inductance and package capacitance

At resonance:

$$j\left[\frac{\omega L}{1 - \omega^2 LC} - \frac{1}{\omega C_C}\right] - j\left|\frac{(C_1 + C_P + C_2)}{\omega(C_1 + C_P)C_2} - \frac{\omega Y_{21} L_P}{(1 + \omega^2 Y_{21}^2 L_p^2)}\frac{Y_{21}}{\omega(C_1 + C_P)C_2}\right| = 0 \qquad (6\text{-}6)$$

$$\Rightarrow \left[\frac{\omega L}{1-\omega^2 LC}-\frac{1}{wC_C}\right]=\left|\begin{array}{ccc}(C_1+C_P+C_2) & -\dfrac{Y_{21}}{\omega(C_1+C_P)C_2} & \dfrac{\omega Y_{21}L_P}{(1+\omega^2 Y_{21}^2 L_p^2)}\end{array}\right| \tag{6-7}$$

$$\Rightarrow \left[\frac{\omega^2 LC_C-(1-\omega^2 LC)}{\omega C_C(1-\omega^2 LC)}\right]=\left[\frac{(1+\omega^2 Y_{21}^2 L_p^2)(C_1+C_P+C_2)-\omega L_P Y_{21}^2}{\omega(C_1+C_P)C_2(1+\omega^2 Y_{21}^2 L_p^2)}\right] \tag{6-8}$$

The expression above can be rewritten in terms of a determinant as

$$\text{Det}\left|\begin{array}{cc}[\omega^2 LC_C-(1-\omega^2 LC] & [(1+\omega^2 Y_{21}^2 L_p^2)(C_1+C_P+C_2)-\omega L_P Y_{21}^2] \\ [\omega C_C(1-\omega^2 LC)] & [\omega(C_1+C_P)C_2(1+\omega^2 Y_{21}^2 L_p^2)]\end{array}\right|=0 \tag{6-9}$$

For $L_p \to 0$

$$\omega_0=\sqrt{\frac{[C_2 C_1+C_1 C_C+C_2 C_C]}{L[C_1 C_2 C_C+C_1 C_2 C+C_1 C C_C+C_2 C C_C]}} \tag{6-33}$$

$$\omega_0=\sqrt{\frac{1}{L\left[C+\dfrac{C_1 C_2 C_C}{C_1 C_2+C_1 C_C+C_2 C_C}\right]}} \tag{6-34}$$

C_C is a coupling capacitor used for separating the bias circuit, and its value is normally small, but similar to C_1 and C_2, typically 0.2pF to 2pF.

Rewriting the polynomial equation as ($C_C \to \infty$)

$$\omega_0 = \sqrt{\dfrac{1}{L\left[\dfrac{C_1 C_2}{C_1 + C_2} + C\right]}} \qquad (6\text{-}35)$$

For steady oscillation the following condition has to be satisfied:

$$R_{Loss} < G_i \left[\frac{(1 + \dfrac{Y_{21}}{G_i})}{\omega^2 C_1 C_2} - \frac{L_3}{C_1}\right]$$

Since $\dfrac{Y_{21}}{G_i}$ is the frequency dependent current gain β:

$$R_{Loss} < \left| real\left(Y_{11}\left[\frac{(1 + \beta)}{\omega^2 C_1 C_2} - \frac{L_3}{C_1}\right]\right)\right|$$

➢ Tuning Diode Noise Contribution

Now including a tuning diode and explaining and its noise contribution

(For the moment assuming it introduces no side effect).

The circuit assumes, C3>>C2. Both the Base Collector and the Collector to Emitter capacitance will act as a tuning diode.

This tuning diode itself generates a noise voltage and modulates its capacitance by a slight amount, and therefore modulates the frequency of the oscillator by minute amounts. The following calculates the phase noise generated from this mechanism, which needs to be added to the phase noise calculated above.

It is possible to define an equivalent noise R_{aeq} that, inserted in Nyquist's equation,

$$V_n = \sqrt{4kT_o R_{aeq} \Delta f} \qquad (7\text{-}21)$$

where $kT_o = 4.2 \times 10^{-21}$ at 300 K, R is the equivalent noise resistor, Δf is the bandwidth, and determines an open noise voltage across the tuning diode. Practical values of R_{aeq} for carefully selected tuning diodes

are in the vicinity of 100Ω, or higher. If we now determine the voltage $V_n = \sqrt{4 \times 4.2 \times 10^{-21} \times 100}$, the resulting voltage value is 1.265×10^{-9} V $\sqrt{\text{Hz}}$.

This noise voltage generated from the tuning diode is now multiplied with the VCO gain, resulting in the rms frequency deviation:

$$(\Delta f_{rms}) = K_o \times (1.265 \times 10^{-9} V) \text{ in 1 Hz bandwidth} \qquad (7\text{-}22)$$

In order to translate this into the equivalent peak phase deviation,

$$\theta_d = \frac{K_o \sqrt{2}}{f_m} (1.265 \times 10^{-9} \, rad) \text{ in 1 Hz bandwidth} \qquad (7\text{-}23)$$

or for a typical oscillator gain of 10 MHz/V,

$$\theta_d = \frac{0.00179}{f_m} \text{ rad in 1 Hz bandwidth} \qquad (7\text{-}24)$$

For f_m= 25 kHz (typical spacing for adjacent channel measurements for FM mobile radios), the θ_d = 7.17 × 10^{-8}. This can be converted into the SSB signal-to-noise ratio

$$\text{L}(f_m) = 20 \log_{10} \frac{\theta_c}{2}$$

(7-25)

$= -149$ dBc/Hz

Figure 32 shows a plot with an oscillator sensitivity of 10 kHz/V, 10 MHz/V, and 100 MHz/V. The center frequency is 2.4 GHz. The lowest curve is the contribution of the Leeson equation. The second curve shows the beginning of the noise contribution from the diode, and the third curve shows that at this tuning

sensitivity, the noise from the tuning diode by itself dominates as it modulates the VCO. This is valid regardless of the Q. This effect is called modulation noise (AM-to-PM conversion), while the Leeson equation deals with the conversion noise.
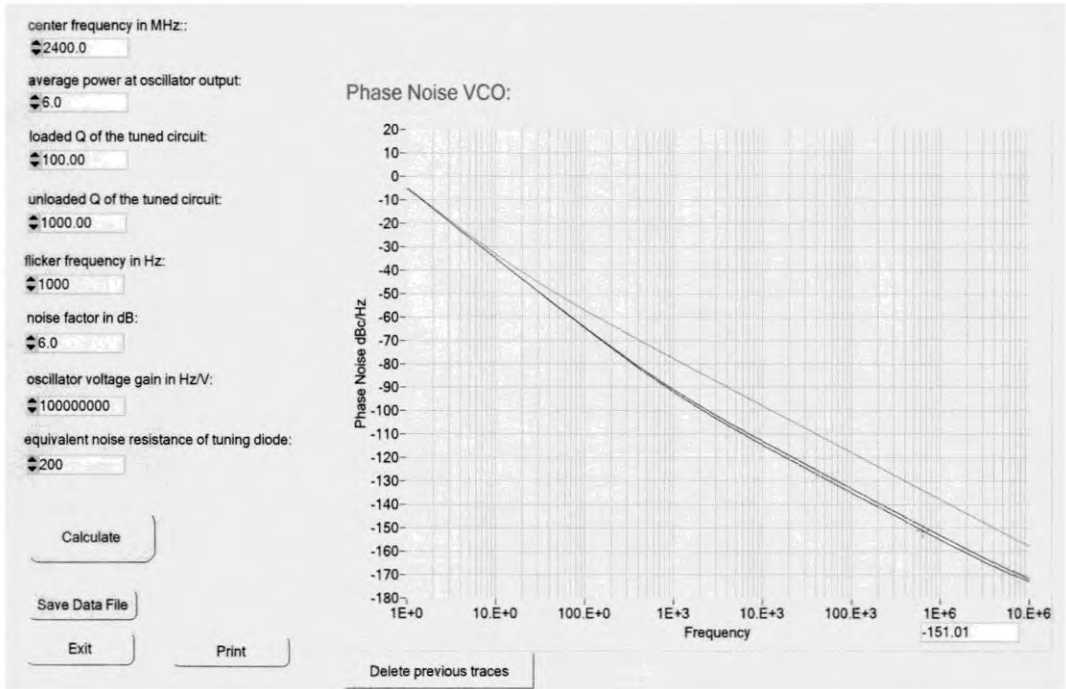
Figure 32: *Simulated phase noise following Equation (7-26).*

If we combine the Leeson formula with the tuning diode contribution, the following equation allows us to calculate the noise of the oscillator completely.

$$ L \ (f_m) = 10\log\left\{\left[1+\frac{f_0{}^2}{(2f_m Q_L)^2}\right]\left(1+\frac{f_c}{f_m}\right)\frac{FkT}{2P_{sav}}+\frac{2kTRK_0{}^2}{f_m{}^2}\right\} \qquad (7\text{-}26) $$

where

$L \ (f_m)$ = ratio of sideband power in a 1 Hz bandwidth at f_m to total power in dB

f_m = frequency offset

f_0 = center frequency

44

f_c = flicker frequency

Q_L = loaded Q of the tuned circuit

F = noise factor

$kT = 4.1 \times 10^{-21}$ at 300 K_0 (room temperature)

P_{sav} = average power at oscillator output

R = equivalent noise resistance of tuning diode (typically 50 Ω - 10 kΩ)

K_o = oscillator voltage gain

The limitation of this equation is that the loaded Q in most cases has to be estimated and the same applies to the noise factor. The microwave harmonic-balance simulator, which is based on the noise modulation theory (published by Rizzoli), automatically calculates the loaded Q and the resulting noise figure as well as the output power [73]. The following equations, based on this equivalent circuit, are the exact values for P_{sav}, Q_L, and F which are needed for the Leeson equation. This approach shown here is novel. It calculates the output power based on the Equations (8-66 to 8-76). The factor of 1000 is needed since the result is expressed in dBm and a function of n and C_1.

As a reminder this figure is repeated: The output coupling of the energy is done at the tapped inductor. As the inductor is part of the tuned circuit, the selectivity of the tuned circuit reduces the far out noise. This type of circuit has much better phase noise, than the output at the collector of a semi-isolated Colpitts circuit.

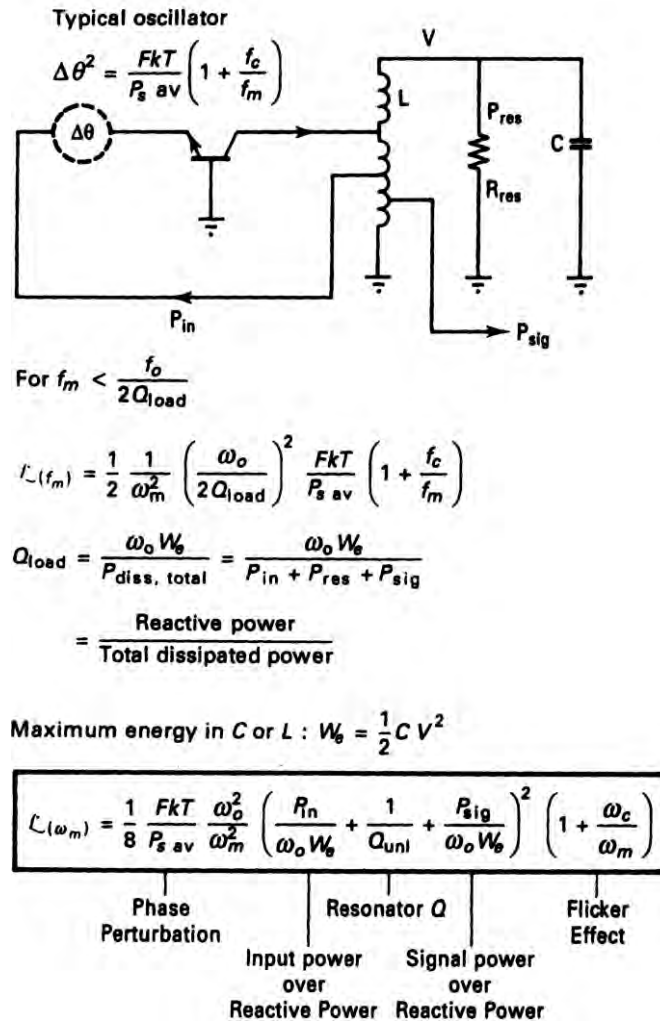Figure 33: **_Figure 4-16 Diagram for a feedback oscillator illustrating the principles involved and showing the key components considered in the phase noise calculation and its contribution._**

In frequency synthesizers, we have no use for *LC* oscillators without a tuning diode, but it may still be of interest to analyze the low-noise fixed-tuned *LC* oscillator first and later make both elements, inductor and capacitor, variable.

$$[P_o(n,C_1)]_{dBm} = 10Log\left\{\left[\frac{(V_{ce}=-0.7)^2}{4(\omega_0 L)^2}\right]\left[\frac{Q_L^2\left[C_1^2\left(\dfrac{C_1}{n-1}\right)^2\omega_0^4 L^2\right]}{Q_L^2\left(C_1+\dfrac{C_1}{n-1}\right)^2+\omega_0^4 L^2 C_1^2\left(\dfrac{C_1}{n-1}\right)^2}\right]R_L*1000\right\} \qquad (7\text{-}27)$$

0.7 = high current saturation voltage, V_{ce} collector emitter voltage $<V_{cc}$

To calculate the loaded Q_L, we have to consider the unloaded Q_0 and the loading effect of the transistor. There we have to consider the influence of Y_{21}^+. The inverse of this is responsible for the loading and reduction of the Q.

$$-Q_L = \frac{Q_0 \times Q^*}{Q_0 + Q^*}; \; Q^* = \frac{\omega_0 \times \left|\dfrac{1}{Y_{21}^+}\right|(C_1+C_2)}{1-\omega_0^2 C_1 L(Q=Q_0)} \qquad (7\text{-}28)$$

Based on Figure 8-7, which also shows the transformation of the loading of the differential emitter impedance (resistance), we can also calculate the noise factor of the transistor under large-signal conditions. Considering Y_{21}^+, this noise calculation, while itself uses a totally new approach, is based on the general noise calculations such as the one shown by Hawkins [117] and Hsu and Snapp [118]. An equivalent procedure can be found for FET's rather than bipolar transistors.

➢ Designing an Oscillator based on Linear S-Parameters

It may be interesting for readers to see how an oscillator can be analyzed using S-parameters. It should be noted that this method is based on linear approximations and works for practically all microwave oscillator designs [6, 28, pg. 741]. The equivalent criteria of the negative resistance can be calculated in the form of S-parameters. The detailed definitions of S-parameters can be found in [31]. This negative resistance will cause oscillations if the following conditions are satisfied. Assume that the oscillation condition is satisfied at port 1 and is given by

$$\frac{1}{S_{11}} = \Gamma_G \qquad (6)$$

Thus

$$S'_{11} = S_{11} + \frac{S_{12}S_{21}\Gamma_L}{1-S_{22}\Gamma_L} = \frac{S_{11}-D\Gamma_L}{1-S_{22}\Gamma_L} \qquad (7)$$

$$\frac{1}{S'_{11}} = \frac{1-S_{22}\Gamma_L}{S_{11}-D\Gamma_L} = \Gamma_G \qquad (8)$$

From expanding (7) we get

$$\Gamma_G S_{11} - D\Gamma_L\Gamma_G = 1 - S_{22}\Gamma_L \qquad (9)$$

$$\Gamma_L\left(S_{22} - D\Gamma_G\right) = 1 - S_{11}\Gamma_G \qquad (10)$$

$$\Gamma_L = \frac{1-S_{11}\Gamma_G}{S_{22}-D\Gamma_G} \qquad (11)$$

$$S'_{22} = S_{22} + \frac{S_{12}S_{21}\Gamma_G}{1-S_{11}\Gamma_G} = \frac{S_{22}-D\Gamma_G}{1-S_{11}\Gamma_G} \qquad (12)$$

$$\frac{1}{S'_{22}} = \frac{1-S_{11}\Gamma_G}{S_{22}-D\Gamma_G} \qquad (13)$$

Comparing equations (9) and (12), we find that

$$\frac{1}{S'_{22}} = \Gamma_G \qquad (14)$$

where, S_{11} and S_{22} are the input and output reflection coefficients, respectively

The discussion above means that the oscillation condition is also satisfied at port 2; which proves the simultaneous oscillation condition at both ports. Thus, if either port is oscillating the other port must be oscillating as well. A load may appear at either or both ports, but normally the load is in Γ_L, the output termination.

It is helpful to use the common-source based amplifier to compute the oscillator output power. For oscillators, the objective is to maximize $\left(P_{out} - P_{in}\right)$ of the amplifier, which is the useful power to the load. An empirical expression for the common-source amplifier output power found by Johnson [29] is

$$P_{out} = P_{sat}\left(1-\exp\frac{-GP_{in}}{P_{sat}}\right) \qquad (15)$$

where P_{sat} is the saturated output power of the amplifier and G is the tuned small-signal common-source transducer gain of the amplifier, which is identical to $|S_{21}|^2$. Since the objective is to maximize $(P_{out} - P_{in})$, where P_{out} and P_{in} are the output and input power of the amplifier,

$$d(P_{out} - P_{in}) = 0 \qquad (16)$$

$$\frac{\partial P_{out}}{\partial P_{in}} = 1 \qquad (17)$$

$$\frac{\partial P_{out}}{\partial P_{in}} = G_{exp} - \frac{GP_{in}}{P_{sat}} = 1 \qquad (18)$$

$$\exp\frac{GP_{in}}{P_{sat}} = G \qquad (19)$$

$$\frac{P_{in}}{P_{sat}} = \frac{\ln G}{G} \qquad (20)$$

At the maximum value of $(P_{out} - P_{in})$, the amplifier output is

$$P_{out} = P_{sat}\left(1 - \frac{1}{G}\right) \qquad (21)$$

and the maximum oscillator output power is

$$P_{osc} = (P_{out} - P_{in}) \qquad (22)$$

$$= P_{sat}\left(1 - \frac{1}{G} - \frac{\ln G}{G}\right) \qquad (23)$$

Thus, the maximum oscillator output power can be predicted from the common-source amplifier saturated output power and the small signal common source transducer gain G. For high oscillator output power, high (loop) gain is of importance. Another definition of gain that is useful for large-signal amplifier or oscillator design is the *maximum efficient gain*, defined by

$$G_{ME} = \frac{P_{out} - P_{in}}{P_{in}} \qquad (24)$$

For maximum oscillator power the maximum efficient gain from (20) and (21) is

$$G_{\text{MEmax}} = \frac{G-1}{\ln G}$$ (25) The RF gain G_{MEmax} is a considerably smaller value compared to G, the small-signal gain [7-12].

Designing oscillators based on S-parameters in a linear mode has been quoted by many authors using first approximation for large signals, as shown in [8]. The problem with this published approach is that it uses a GaAs FET, where only the transconductance g_m has a major influence. S_{11} changes very little under large signal conditions, as does S_{22}. Reliable large signal S-parameters for bipolar transistors and FETs are difficult to get. Under steady state condition Y21* is approximately Re(Y21)/π.
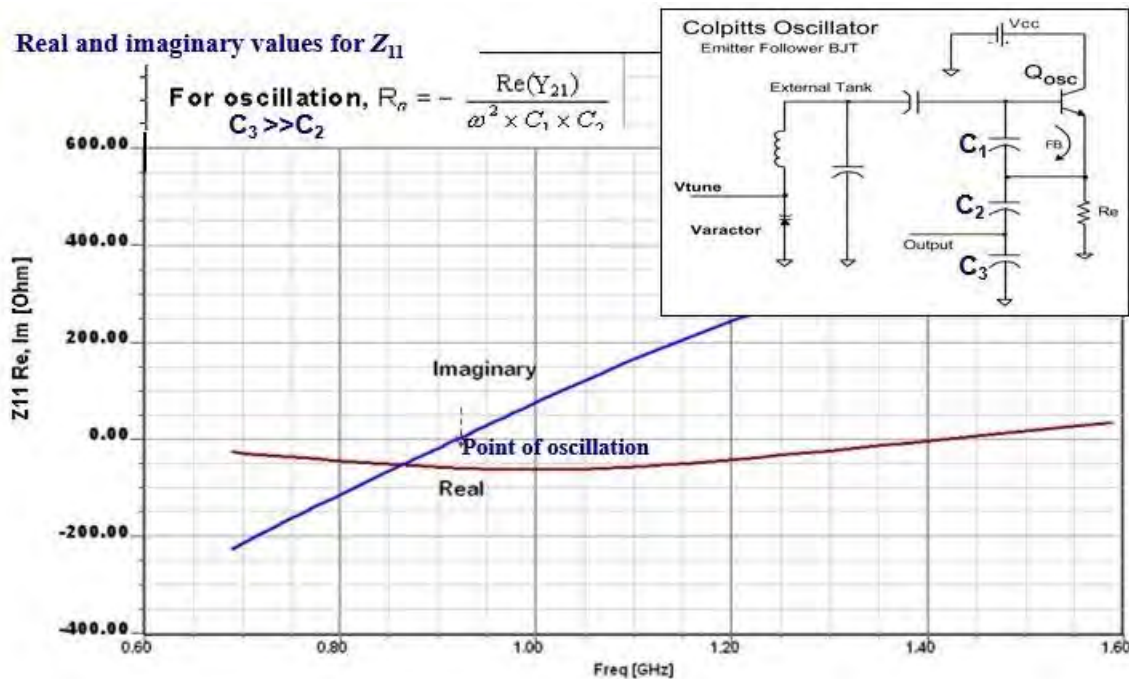
CONDITIONS FOR OSCILLATIONS

Figure 34: *Point of Oscillation as shown by the Zero reactance and negative resistance*

Real (Z_{11}) must be slightly more negative than the loss resistance in the circuit for oscillation to start. The resulting dc shift in the transistor will then provide the amplitude stabilization as g_m will be reduced.

Next we need to look at the large signal condition which will affect Y11 and Y21.The best way to get the data is to measure the parameters. At microwave frequencies it is convenient to do so in a 50 Ohm system and then convert them to Y parameter

➢ Large signal Operation of Oscillators

- Definition: RF voltages/currents are of similar magnitude as the DC values.

- Test points were V_c = 2V, I_c = 20mA.

- The transistor behaves differently under large signal conditions.

- Large signal parameters can be obtained from simulation using SPICE parameters, calculating the Bessel functions of the currents of the intrinsic transistor and adding the parasitics and measurements.

This Figure shows the R&S VNA and the test fixture for the transistor of choice
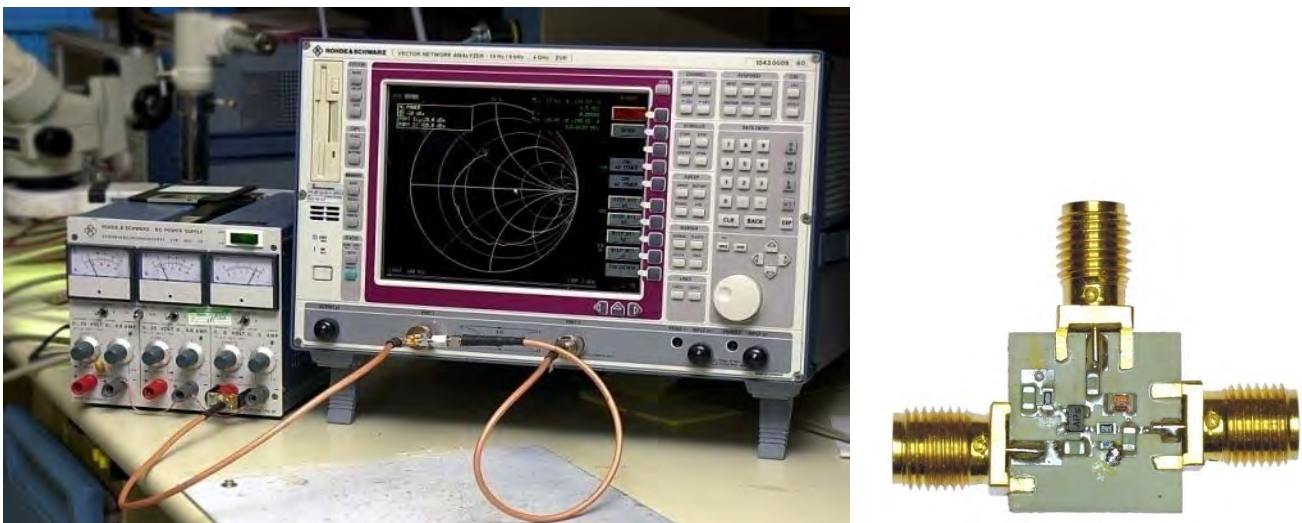
Figure 35: *Typical measurement setup for evaluation of large signal parameters*

Typical measurement setup for evaluation of large signal parameters (R&S vector analyzer and the test fixture for the transistor of choice), Agilent now calls this X Parameters

The bias, drive level, and frequency dependent S parameters are then obtained for practical use

Measured large-signal S_{11} of the BFP520
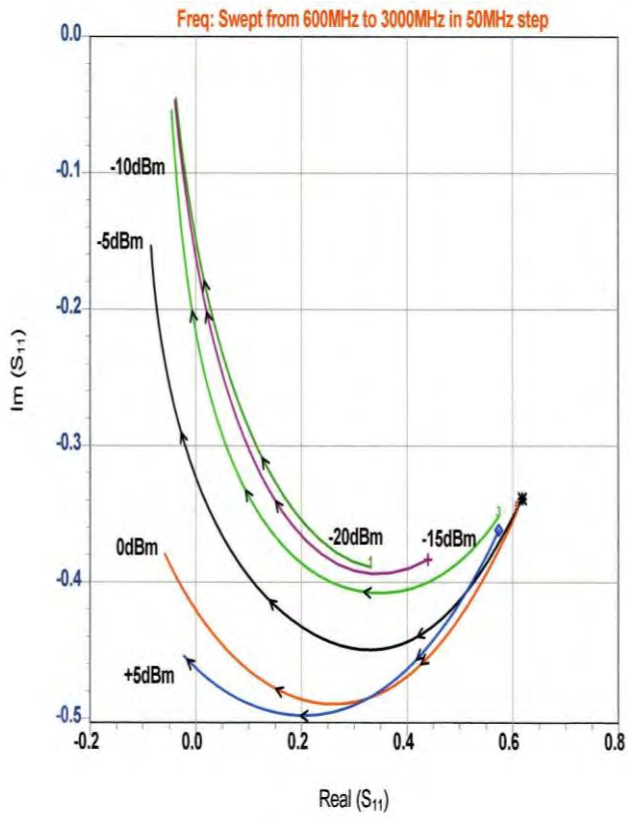
Measured large-signal S_{12} of the BFP520
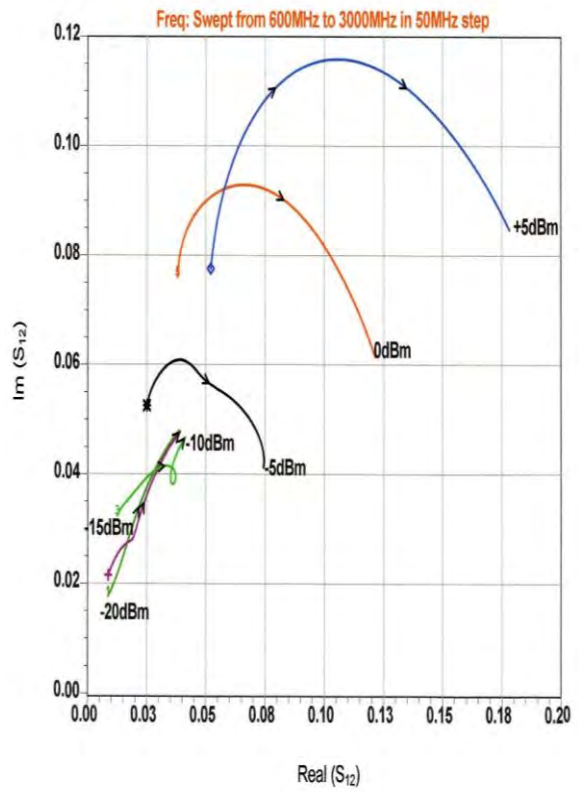
Measured large-signal S_{21} of the BFP520
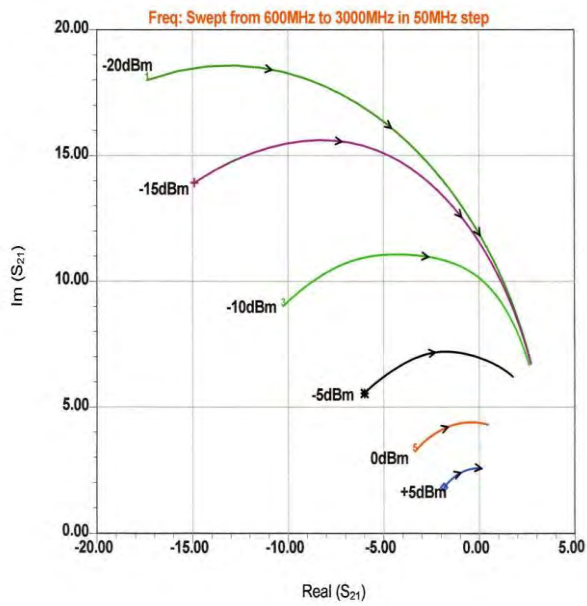
Measured large-signal S_{22} of the BFP520
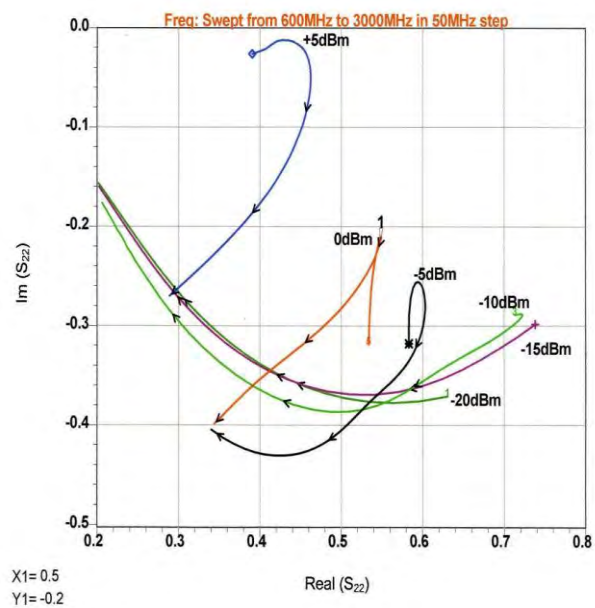
Figure 36: *Measured Large-signal S-parameters of the BFP520*

52

Oscillator Design Based on the Measured Large-Signal S-parameters

   A) Parallel Resonant (Colpitts Oscillator)

Figure 1 shows the standard Colpitts oscillator using large-signal *S*-parameters. This example is of particular interest because it requires an inductor instead of the familiar capacitor, C_2, between base and emitter.
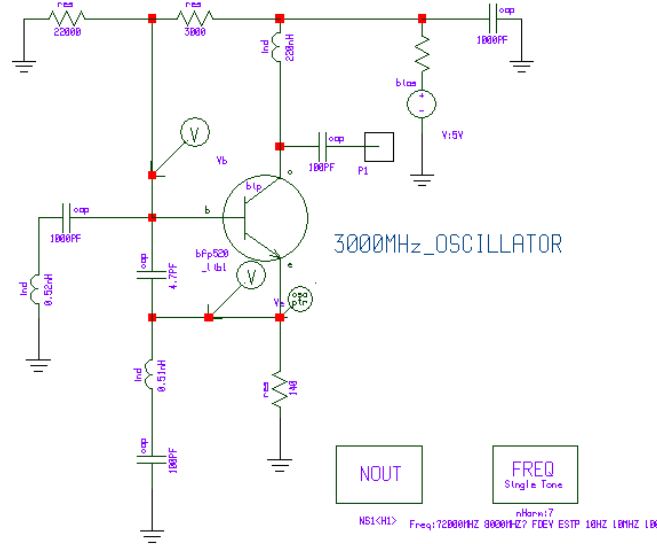
Figure 37: *Figure A-1   A 3000 MHz oscillator using a BFP520 transistor operating at 2V and 20mA.*

In this case, the capacitor C_2 needs to be replaced by an inductor L_3 which tunes out the collector emitter capacitance to achieve the optimum value. The 1nF on the left is a DC separation capacitor. This case is optimized for output power.

The measured large-signal *Y*-parameter data (I_c=20mA, V_{ce}=2V), see above, @ 3000MHz are:

$$Y_{11} = G_{11} + jB_{11} = (11.42 + j8.96)\ mS \tag{A-1}$$

$$Y_{21} = G_{21} + jB_{21} = (4.35 - j196.64)\ mS \tag{A-2}$$

$$Y_{12} = G_{12} + jB_{12} = (-433.09 - j1.5643\ mS \tag{A-3}$$

53

$$Y_{22} = G_{22} + jB_{22} = (4.41 + j9.10) \; mS \tag{A-4}$$

The optimum values of feedback element are calculated from the given expression of B_1^* and B_2^* are

$$B_1^* = -\left\{ B_{11} + \left[\frac{B_{12} + B_{21}}{2} \right] + \left[\frac{G_{21} - G_{12}}{B_{21} - B_{12}} \right]\left[\frac{G_{12} + G_{21}}{2} + G_{11} \right] \right\} \tag{A-5}$$

$$jB_1^* = 89.8E - 3 \tag{A-6}$$

$$jB_1^* = j\omega C_1 \tag{A-7}$$

$$C_1 = \frac{89.8E - 3}{2\pi f} = 4.77 \, pF \tag{A-8}$$

$$B_2^* = \left[\frac{B_{12} + B_{21}}{2} \right] + \left[\frac{(G_{12} + G_{21})(G_{21} - G_{12})}{2(B_{21} - B_{12})} \right] \tag{A-9}$$

$$jB_2^* = -103.5E - 3 \tag{A-10}$$

$$jB_2^* = \frac{1}{j\omega L_2} \tag{A-11}$$

$$L_2 = \frac{1}{(2\pi f) \times 103.5E - 3 L_2} 0.515nH \tag{A-12}$$

The optimum values of the real and imaginary part of the output admittance are

$$Y_{out}^* = [G_{out}^* + jB_{out}^*] \qquad\qquad\qquad \text{(A-13)}$$

where G_{out}^* and B_{out}^* is given as

$$G_{out}^* = G_{22} - \left[\frac{(G_{12} + G_{21})^2 (B_{21} - B_{12})^2}{4G_{11}} \right] \qquad \text{(A-14)}$$

$$G_{out}^* = -823.53E - 3 \qquad\qquad\qquad \text{(A-15)}$$

$$B_{out}^* = B_{22} + \left[\frac{G_{21} - G_{12}}{B_{21} - B_{12}} \right] - \left[\frac{(G_{12} + G_{21})}{2} + G_{22} - G_{out}^* \right] + \left[\frac{B_{21} + B_{12}}{2} \right] \qquad \text{(A-16)}$$

$$B_{out}^* = -105.63E - 3 \qquad\qquad\qquad \text{(A-17)}$$

$$jB_{out}^* = \frac{1}{j\omega L_3} \qquad\qquad\qquad \text{(A-18)}$$

$$L_3 = 0.502nH \qquad\qquad\qquad \text{(A-19)}$$
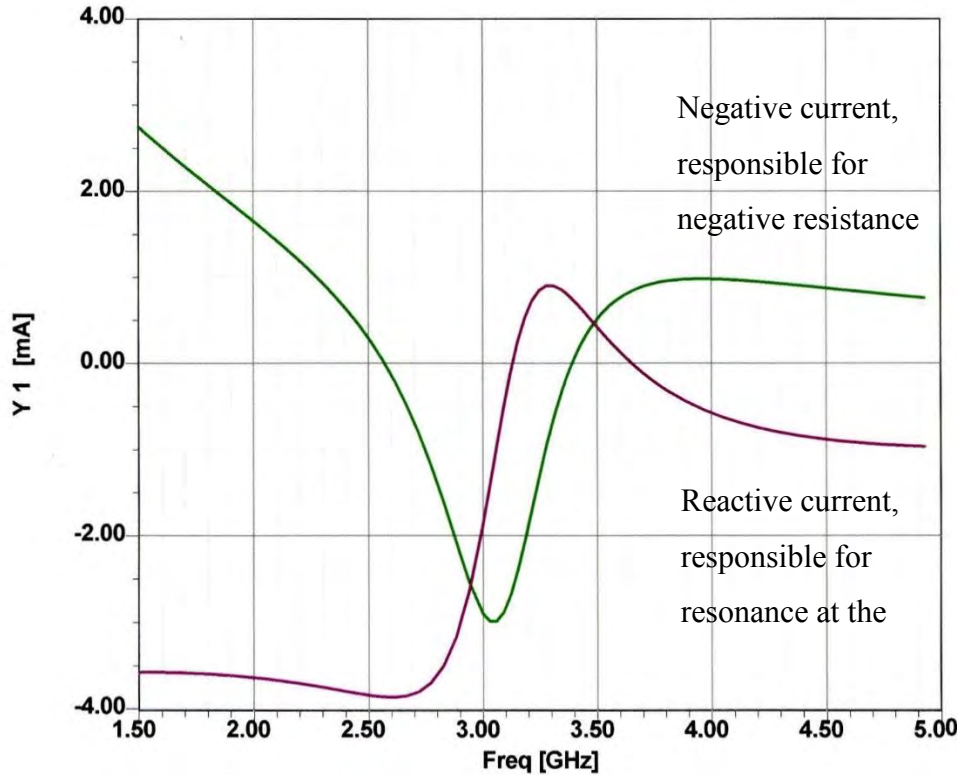
Figure 38: *Figure A-2   Shows the real and imaginary currents for oscillation. The reactive current crosses the zero line at 3120 MHz. This is close, but not exactly at the point of most negative resistance current. The reason for the shift of 120 MHz is due to the use of small-signal analysis rather than the large-signal analysis.*

Figure A-2 shows the simulated response of the oscillator circuit having resonance at 3120 MHz or 5% error. The little variation in resonant frequency may be due to the frequency dependent packaged parameters, but it is a good starting value for tuning and optimization for the best phase noise and output power. The best phase noise at a given power output is basically dependent upon the ratio and absolute value of the feedback capacitors, which in turn depends upon the optimum drive-level.

$$Z_{out}(I,\omega)+Z_L(\omega)=0 \qquad\qquad\qquad \text{(A-20)}$$

$$Z_L(\omega)\rightarrow Z_3(\omega) \qquad\qquad\qquad \text{(A-21)}$$

Where *I* is the load current amplitude and *w* is the resonance frequency. Z_{out} is current and frequency dependent output impedance, whereas Z_L is only function of frequency.

Now the evaluation

The bias condition of the transistor is

Voltage	Current
Vp(Vb) = 3.9442 V	Ip(Vb) = 0 A
Vp(Ve) = 3.01649 V	Ip(Ve) = 0 A
Vp() = 3.01649 V	Ip() = 0 A
Vbe(_lib1) = 0.912885 V	Ib(_lib1) = 0.172653 mA
Vce(_lib1) = 1.80815 V	Ic(_lib1) = 21.3737 mA

X1= 6.87GHz
Y1= -13.11
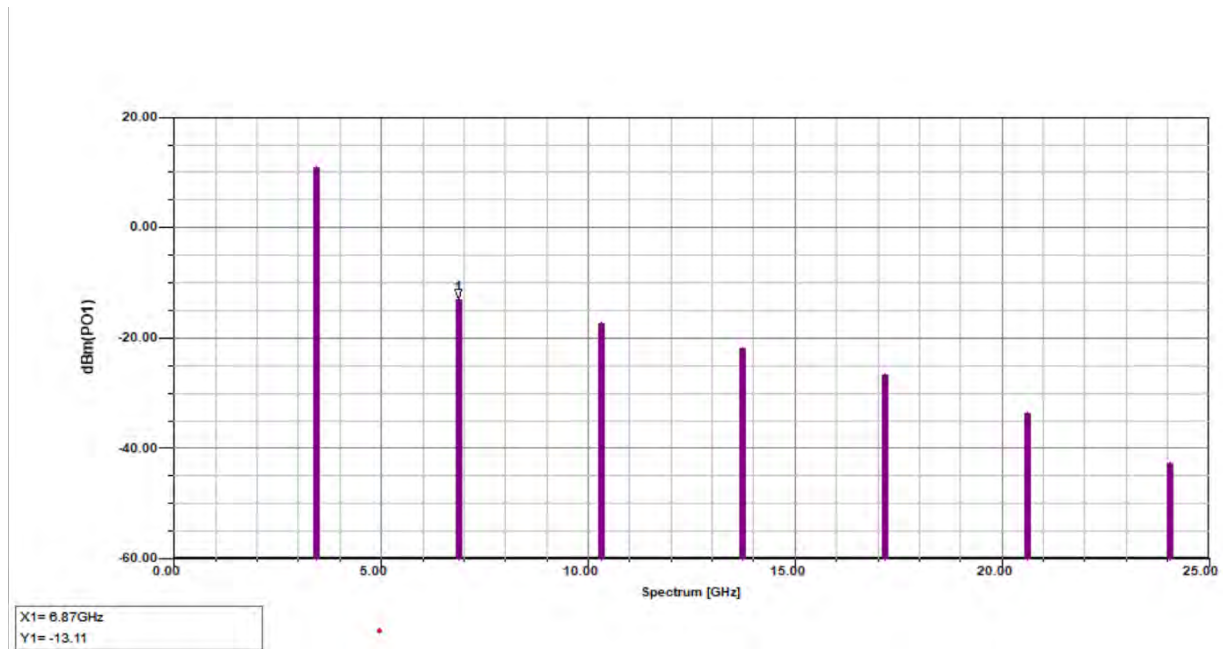
Figure 39: *Simulated Output power of the 3000 MHz oscillator using a BFP520 transistor*

Good news, the calculated feedback circuit makes the oscillator to oscillate,
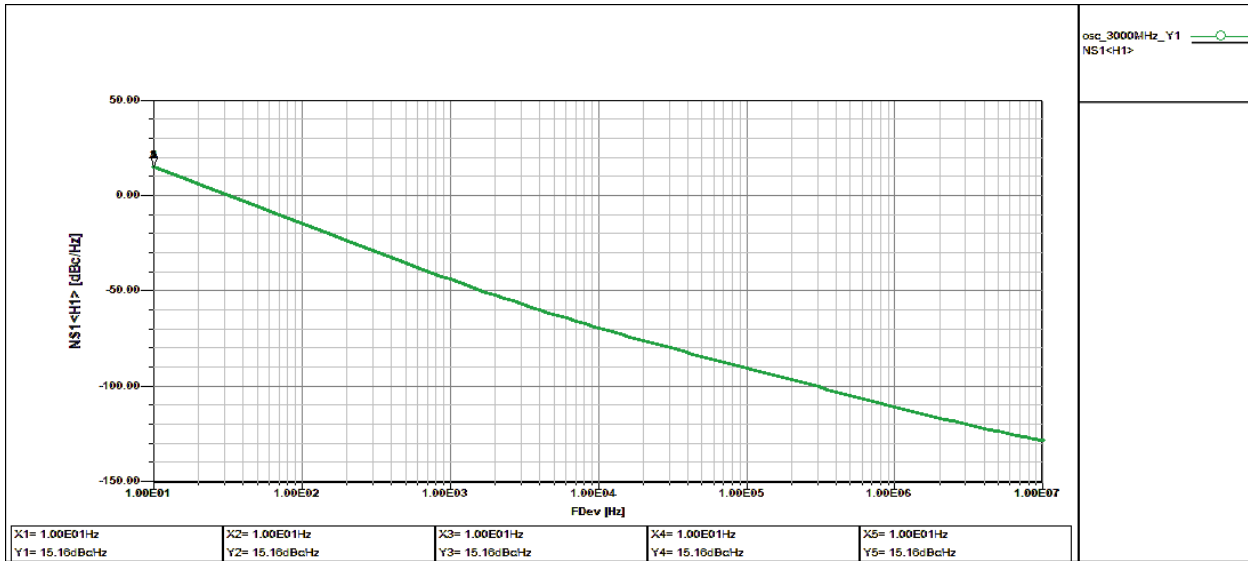
Figure 40: *Simulated Phase Noise of the 3000 MHz oscillator using a BFP520 transistor*

The loaded Q of the printed resonator was 200. Now evaluating the influence of the values of the feedback capacitors gives an interesting result.
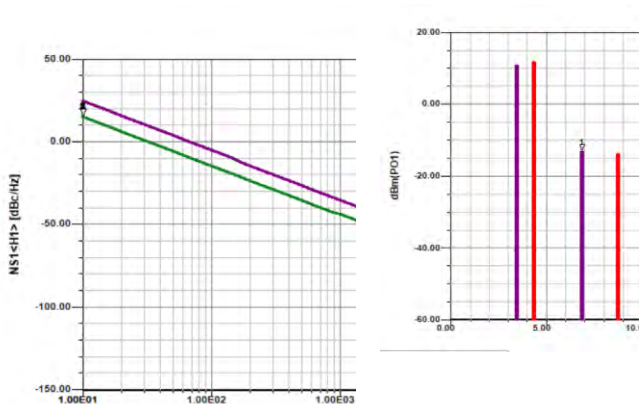
Figure 41: *Increasing the output power strongly reduces the phase noise*

Increasing the output power strongly reduces the phase noise!

The important message that can be derived from this calculation is the fact that the parasitics now dominate the design. The negative resistance which used to be proportional to $1/\omega^2$ now is $1/\omega^4$. The rule of thumb is to use a large device for lower frequencies and operate it at medium DC currents. This in the millimeter wave area would be fatal. The large device would have excessive parasitic elements such as inductors

58

and capacitors and the optimum design is no longer possible since the parasitics would be larger than the values required for optimum performance. These parasitics are the major reason why at millimeter wave and wide tuning ranges the phase noise is not as good as what a narrowband Colpitts oscillator would provide.

The oscillator operates in a reasonable linear mode so the load line has a minimum surface area

Modeling the actual complex layout is much more relevant than a standard circuit diagram

B)   Series Feedback Oscillator: Applicable to YIG Oscillators

The steady-state oscillation condition for series feedback configuration can be expressed as

$$Z_{out}(I,\omega) + Z_L(\omega) = 0 \qquad\qquad \text{(A-20)}$$

$$Z_L(\omega) \rightarrow Z_3(\omega) \qquad\qquad \text{(A-21)}$$

where I is the load current amplitude and w is the resonance frequency. Z_{out} is current and frequency dependent output impedance, where as Z_L is only function of frequency.

$$Z_{out}(I,\omega) = R_{out}(I,\omega) + jX_{out}(I,\omega) \qquad\qquad \text{(A-22)}$$

$$Z_L(\omega) = R_L(\omega) + jX_L(\omega) \qquad\qquad \text{(A-23)}$$

The expression of output impedance, Z_{out} can be written as

$$Z_{out} = -Z_3 \Rightarrow [Z_{22} + Z_2] - \frac{[Z_{12} + Z_2][Z_{21} + Z_2]}{[Z_{11} + Z_1 + Z_2]} \qquad \text{(A-24)}$$

where Z_{ij} (i,j=1,2) is Z-parameters of hybrid transistor model and can be written as

$$Z_{i,j} = [R_{ij} + jX_{ij}]_{i,j=1,2} \qquad \text{(A-25)}$$

According to optimum criterion, the negative real part of the output impedance Z_{out} has to be maximized and the possible optimal values of feedback reactance under which the negative value R_{out} is maximized by setting

$$\frac{\partial \operatorname{Re}[Z_{out}]}{\partial X_1} = 0 \ and \ \frac{\partial \operatorname{Re}[Z_{out}]}{\partial X_2} = 0 \qquad \text{(A-26)}$$

$$\Rightarrow \frac{\partial [R_{out}]}{\partial X_1} = 0 \ and \ \frac{\partial [R_{out}]}{\partial X_2} = 0 \qquad \text{(A-27)}$$

The optimal values X_1^* and X_2^*, based on above condition, can be expressed in terms of a 2-port parameter of the active device (BJT/FET) as [177, 178]:

$$X_1^* = -X_{11} + \left[\frac{X_{12} + X_{21}}{2} \right] + \left[\frac{R_{21} - R_{12}}{X_{21} - X_{12}} \right] \left[\frac{R_{12} + R_{21}}{2} - R_{11} - R_1 \right] \qquad \text{(A-28)}$$

$$X_2^* = -\left[\frac{X_{12} + X_{21}}{2} \right] - \left[\frac{(R_{21} - R_{12})(2R_2 + R_{12} + R_{21})}{2(X_{21} - X_{12})} \right] \qquad \text{(A-29)}$$

By substituting values of X_1^* and X_2^* into above equation, the optimal real and imaginary parts of the output impedance Z_{out}^* can be expressed as

$$Z_{out}^* = R_{out}^* + X_{out}^* \qquad \text{(A-30)}$$

$$R_{out}^* = R_2 + R_{22} - \left[\frac{(2R_2 + R_{21} + R_{12})^2 + (X_{21} - X_{12})^2}{4(R_{11} + R_2 + R_1)} \right] \qquad \text{(A-31)}$$

$$X_{out}^* = X_2^* + X_{22} - \left[\frac{R_{21} - R_{12}}{X_{21} - X_{12}} \right] \left[R_{out}^* - R_2 - R_{22} \right] \qquad \text{(A-32)}$$

where

$$X_2^* = -\left[\frac{X_{12} + X_{21}}{2} \right] - \left[\frac{(R_{21} - R_{12})(2R_2 + R_{12} + R_{21})}{2(X_{21} - X_{12})} \right] \qquad \text{(A-33)}$$

thus, in the steady-state operation mode of the oscillator, amplitude and phase balance conditions can be written as

$$R_{out}^* + R_L = 0 \qquad \text{(A-34)}$$

$$X_{out}^* + X_L^* = 0 \qquad \text{(A-35)}$$

The output power of the oscillator can be expressed in terms of load current and load impedance as

$$P_{out} = \frac{1}{2} I^2 \operatorname{Re}[Z_L]$$ (A-36)

where I and V is the corresponding load current and voltage across the output.

$$I = \left[\frac{Z_{11} + Z_1 + Z_2}{Z_{22}(Z_{11} + Z_1 + Z_2) - Z_{21}(Z_{12} + Z_2)} \right] V$$ (A-37)

The expression of the phase noise for the series feedback oscillator, following the approach for the Colpitts oscillator, is

$$\left| \overline{L} \right|_{SSB} = \left[4KTR + \frac{4qI_c g_m^2(t)}{\omega_0^4 \beta^2 C_{ce}^2 (C_2 + C_{be} - L_1 C_2 C_{be} \omega_0^2)^2 + g_m^2 \omega_0^2 (C_2 + C_{be} - L_1 C_2 C_{be} \omega_0^2)^2} \right] *$$

$$\left[\frac{\omega_0^2}{4(\Delta\omega)^2 V_{cc}^2} \right] \left[\frac{1}{Q_L^2} + \left(1 - \left(\frac{1}{\omega_0^2 L_1} \right) \left(\frac{[(C_2 + C_{be} - L_1 C_2 C_{be} \omega_0^2) + C_{ce}]}{C_{ce}[(C_2 + C_{be} - L_1 C_2 C_{be} \omega_0^2)]} \right) \right)^2 \right]$$ (A-38)

For large value of Q_l,

$$\left| \overline{L} \right|_{SSB} = \left[4KTR + \frac{4qI_c g_m^2(t)}{\omega_0^4 \beta^2 C_{ce}^2 (C_2 + C_{be} - L_1 C_2 C_{be} \omega_0^2)^2 + g_m^2 \omega_0^2 (C_2 + C_{be} - L_1 C_2 C_{be} \omega_0^2)^2} \right] *$$

$$\left[\frac{\omega_0^2}{4(\omega)^2 V_{cc}^2} \right] \frac{1}{\omega_0^4 L_1^2} \left(\frac{[(C_2 + C_{be} - L_1 C_2 C_{be} \omega_0^2) + C_{ce}]}{C_{ce}[(C_2 + C_{be} - L_1 C_2 C_{be} \omega_0^2)]} \right)$$ (A-39)

The important message that can be derived from this calculation is the fact that the parasitics now dominate the design. The negative resistance which used to be proportional to $1/\omega^2$ now is $1/\omega^4$. The rule of thumb

is to use a large device for lower frequencies and operate it at medium DC currents. This in the millimeterwave area would be fatal. The large device would have excessive parasitic elements such as inductors and capacitors and the optimum design is no longer possible since the parasitics would be larger than the values required for optimum performance. These parasitics are the major reason why at millimeterwave and wide tuning ranges the phase noise is not as good as what a narrowband Colpitts oscillator would provide.

Example: 3000 MHz YIG Oscillator

A 3000MHz oscillator is designed based on the above shown analytical series feedback approach and is also validated with the simulated results. Figure A-3 shows the series feedback oscillator.
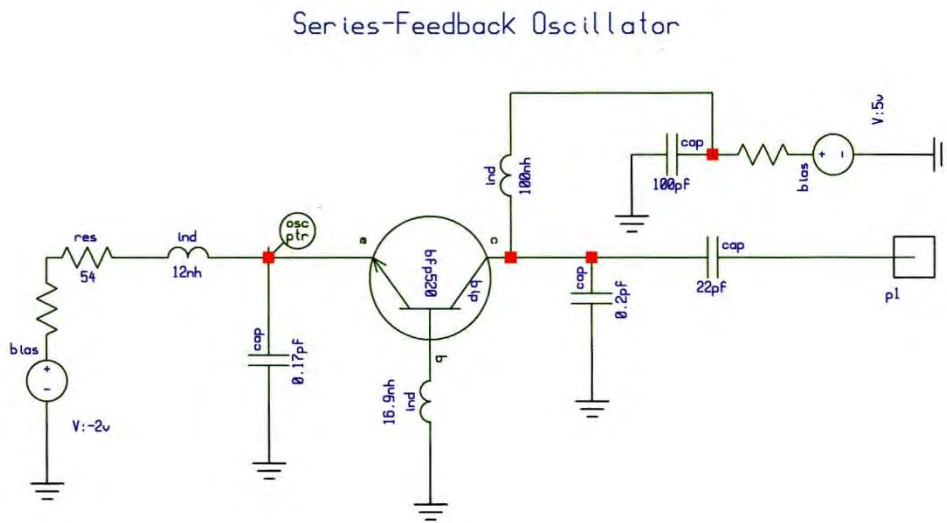
Figure 42: *Figure A-3 Shows a series feedback oscillator. For oscillation condition, the base to ground inductance and the emitter to ground capacitance is required. The 12nH inductor acts a choke. The output is tuned and terminated into 50Ω.*

Large signal Z-parameters measured data (I_c=20mA, V_{ce}=2V) @ 3000 MHz are given as

$$Z_{11} = R_{11} + jX_{11} = (22.96 + j27.30)\Omega \tag{A-40}$$

$$Z_{21} = R_{21} + jX_{21} = (140 + j670)\Omega \tag{A-41}$$

63

$$Z_{12} = R_{12} + jX_{12} = (2.72 + j4.99)\Omega \qquad \text{(A-42)}$$

$$Z_{22} = R_{22} + jX_{22} = (46.04 + j21.45)\Omega \qquad \text{(A-43)}$$

$$X_1^* = -X_{11} + \left[\frac{X_{12} + X_{21}}{2}\right] + \left[\frac{R_{21} - R_{12}}{X_{21} - X_{12}}\right]\left[\frac{R_{12} + R_{21}}{2} - R_{11} - R_1\right] \qquad \text{(A-44)}$$

$$X_1^* = 319.9654\Omega \Rightarrow L_1 = 16.9nH \qquad \text{(A-45)}$$

$$X_2^* = -\left[\frac{X_{12} + X_{21}}{2}\right] - \left[\frac{(R_{21} - R_{12})(2R_2 + R_{12} + R_{21})}{2(X_{21} - X_{12})}\right] \qquad \text{(A-46)}$$

$$X_2^* = -311.67084 \Rightarrow C_2 = 0.17pF \qquad \text{(A-47)}$$

$$X_{out}^* = X_2^* + X_{22} - \left[\frac{R_{21} - R_{12}}{X_{21} - X_{12}}\right]\left[R_{out}^* - R_2 - R_{22}\right] \qquad \text{(A-48)}$$

$$X_{out}^* = -259.31176 \Rightarrow C_3 = 0.2pF \qquad \text{(A-49)}$$

The simulated response of the oscillator circuit, having resonance at 2980MHz or 1% error, is a good starting value for tuning and optimization for optimum phase noise and output power. The best phase noise at a given power output is basically dependent upon the ratio and absolute value of the feedback capacitor, which in turn depends upon the optimum drive-level. The detailed analysis for designing the best phase noise, based on a unified approach, is discussed in the next section. Figure A-4 shows the real and imaginary currents for oscillating conditions for optimum output power. In this case, the operating Q

is very low, as can be seen from the shallow curve at which the imaginary current crosses the zero line, while the real current is still negative. To optimize this circuit for phase noise, the imaginary curve should go through the zero line at the point of steepest ascent, while maintaining a negative real current. The low Q resonator guarantees that the most output power is available, and the resonator is heavily loaded.
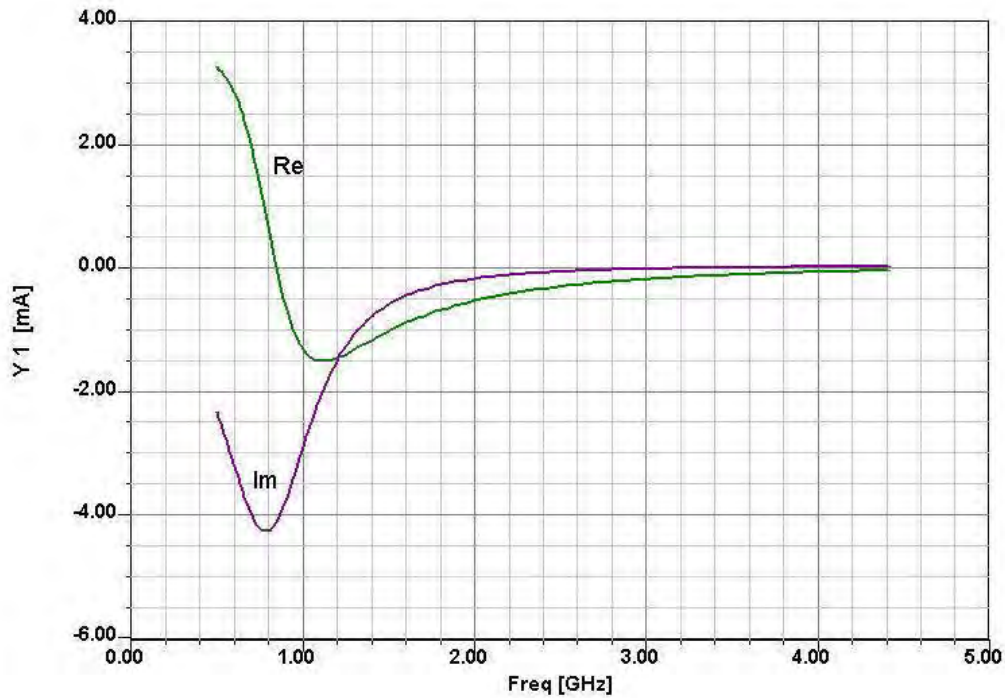
Figure 43: *Figure A-4   Shows the real and imaginary currents of the 3 GHz series-type oscillator. The very shallow curve should be noted.*

➢ Classical Linear Two-Port Oscillator Design

In many cases in old publications and even today a first approximation is made for two port oscillators using the published small signal S parameters. This may be good for getting oscillation started but may not be correct for predicting sustaining oscillation

This older, unreliable but frequently common method for designing oscillators is to resonate the input port with a passive high-Q circuit at the desired frequency of resonance. This only works if the transistor has access gain! It will be shown that if this is achieved with a load connected on the output port, the transistor is oscillating at both ports and is thus delivering power to the load port. The oscillator may be considered

65

a two-port structure, where M_3 is the lossless resonating port and M_4 provides lossless matching such that all of the external RF power is delivered to the load. The resonating network has been described. Nominally, only parasitic resistance is present at the resonating port, since a high-Q resonance is desirable for minimizing oscillator noise. It is possible to have loads at both the input and the output ports if such an application occurs, since the oscillator is oscillating at both ports simultaneously.

Note: Using the hopefully high Q tuned circuit also as a filter gives better far out phase noise than the more common method taking like the energy from the collector if the circuit is based on the Colpitts design.

The simultaneous oscillation condition is proved as follows. Assume that the oscillation condition is satisfied at port 1:

$$1/S_{11}' = \Gamma_G \tag{4-218}$$

Thus,

$$S_{11}' = S_{11} + \frac{S_{12}S_{21}\Gamma_L}{1-S_{22}\Gamma_L} = \frac{S_{11}-D\Gamma_L}{1-S_{22}\Gamma_L} \tag{4-219}$$

$$\frac{1}{S_{11}'} = \frac{1-S_{22}\Gamma_L}{S_{11}-D\Gamma_L} = \Gamma_G \tag{4-220}$$

By expanding Eq. (4-220), we find

$$\begin{aligned}
\Gamma_G S_{11} - D\Gamma_L \Gamma_G &= 1 - S_{22}\Gamma_L \\
\Gamma_L \left(S_{22} - D\Gamma_G \right) &= 1 - S_{11}\Gamma_G \\
\Gamma_L &= \frac{1-S_{11}\Gamma_G}{S_{22}-D\Gamma_G}
\end{aligned} \tag{4-221}$$

Thus,

$$S_{22}' = S_{22} + \frac{S_{12}S_{21}\Gamma_G}{1-S_{11}\Gamma_\Gamma} = \frac{S_{22}-D\Gamma_G}{1-S_{11}\Gamma_G} \tag{4-222}$$

$$\frac{1}{S_{22}'} = \frac{1-S_{11}\Gamma_G}{S_{22}-D\Gamma_G} \tag{4-223}$$

Comparing Eqs. (4-221) and (4-223), we find

$$1/S_{22}' = \Gamma_L \tag{4-224}$$

which means that the oscillation condition is also satisfied at port 2; this completes the proof. Thus, if either port is oscillating, the other port must be oscillating as well. A load may appear at either or both ports, but normally the load is in Γ_L, the output termination. This result can be generalized to an n-port oscillator by showing that the oscillator is simultaneously oscillating at each port:

$$\Gamma_1 S_{11}' = \Gamma_2 S_{22}' = \Gamma_3 S_{33}' = \cdots = \Gamma_n S_{nn}' \tag{4-225}$$

Before concluding this section on two-port oscillator design, the buffered oscillator shown in Figure 4-166 must be considered. This design approach is used to provide the following:

A reduction in loading-pulling, which is the change in oscillator frequency when the load reflection coefficient changes.

A load impedance that is more suitable to wideband applications, Eq. (4-198).

A higher output power from a working design, although the higher output power can also be achieved by using a larger oscillator transistor.

Buffered oscillator designs are quite common in wideband YIG applications, where changes in the load impedance must not change the generator frequency.
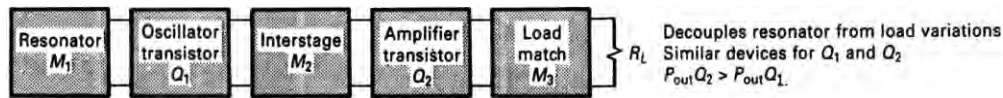
Figure 44: *Figure 4-166 Buffered oscillator design.*

Two-port oscillator design may be summarized as follows:

Select a transistor with sufficient gain and output power capability for the frequency of operation. This may be based on oscillator data sheets, amplifier performance, or S-parameter calculation.

Select a topology that gives $k < 1$ at the operating frequency. Add feedback if $k < 1$ has not been achieved.

Select an output load matching circuit that gives $|S_{11}'| > 1$ over the desired frequency range. In the simplest case this could be a 50-Ω load.

Resonate the input port with a lossless termination so that $\Gamma_G S_{11}' = 1$. The value of S_{22}' greater than unity with the input properly resonated.

In all cases, the transistor delivers power to a load and the input of the transistor. Practical considerations of readability and dc biasing will determine the best design.

For both bipolar and FET oscillators, a common topology is common-base or common-gate, since a common-lead inductance can be used to raise S_{22} to a large value, usually greater than unity even with a 50-Ω generator resistor. However, it is not necessary for the transistor S_{22} to be greater than unity, since the 50-Ω generator is not present in the oscillator design. The requirement for oscillation is $k < 1$; then resonating the input with a lossless termination will provide that $\left| S_{11}' \right| > 1$.

A simple example will clarify the design procedure. A common-base bipolar transistor (HP2001) was selected to design a fixed-tuned oscillator at 2 GHz. The common-base S parameters and stability factor are given in Table 4-16. Using the load circuit in Figure 4-167, we see that the reflection coefficients are

$$\Gamma_L = 0.62 \underline{|30°}$$
$$S_{11}' = 1.18 \underline{|173°}$$

Thus, a resonating capacitance of $G = 20$ pF resonates the input port. In a YIG-tuned oscillator, this reactive element could be provided by the high-Q YIG element. For a dielectric resonator oscillator (DRO), the puck would be placed to give $\Gamma_G \approx 1.0 \underline{|-173°}$.

Table 4-16 HP2001 bipolar chip common base $\left(V_{CE} = 15\,\text{V},\ l_c = 25\,\text{mA} \right)$

$L_B = 0$	$L_B = 0.5\,\text{nH}$
$S_{11} = 0.94 \underline{|174°}$	$1.04 \underline{|173°}$
$S_{21} = 1.90 \underline{|-28°}$	$2.00 \underline{|-30°}$
$S_{12} = 0.013 \underline{|98°}$	$0.043 \underline{|153°}$
$S_{22} = 1.01 \underline{|-17°}$	$1.05 \underline{|-18°}$
$k = -0.09$	-0.83
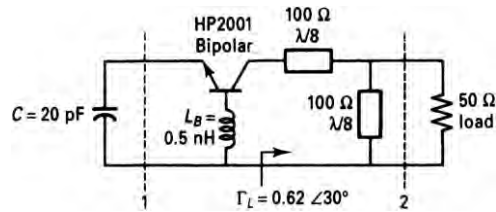
Figure 45: *Figure 4-167 Oscillator example at 2 GHz.*

Another two-port design procedure is to resonate the Γ_G port and calculate S'_{22}, until $\left| S'_{22} \right| > 1$, than design the load port to satisfy. This design procedure is summarized in Figure 4-168.

Figure 46: *Figure 4-168 Oscillator design flowchart.*

One word of caution:

At these high frequencies a good modeling is necessary, meaning that where possible the lumped elements have to be replaced by distributed elements. Here is an example:
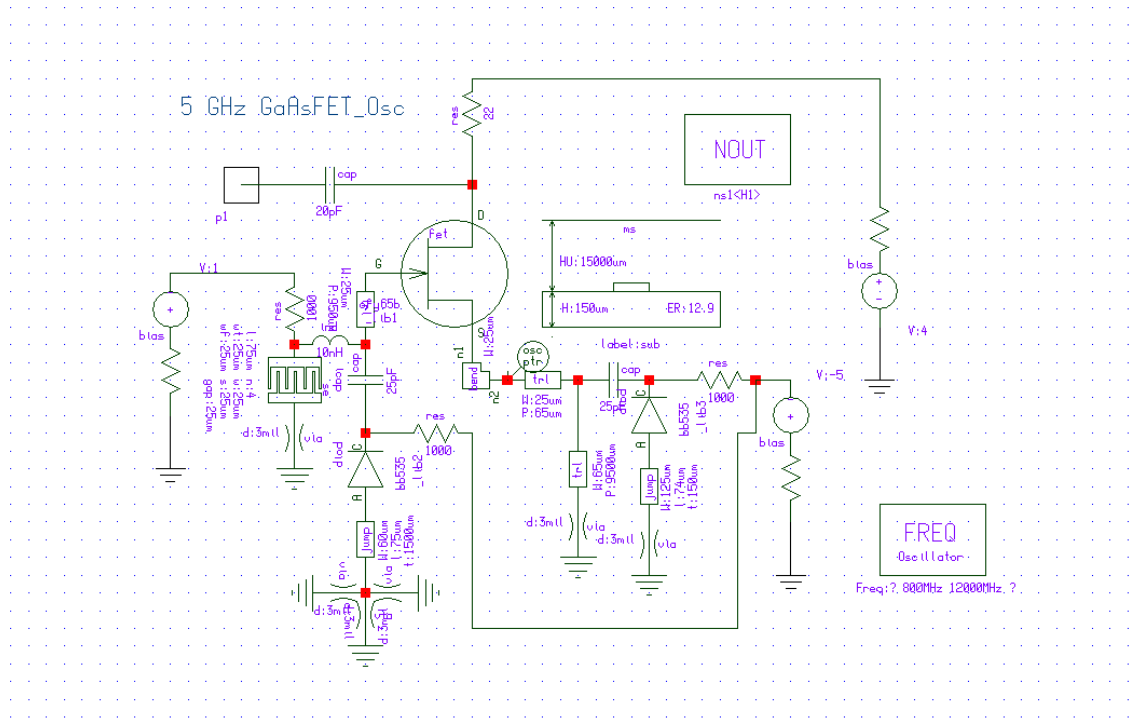
Figure 47: *Example of the modeling details required for a 5GHz Microwave Oscillator*
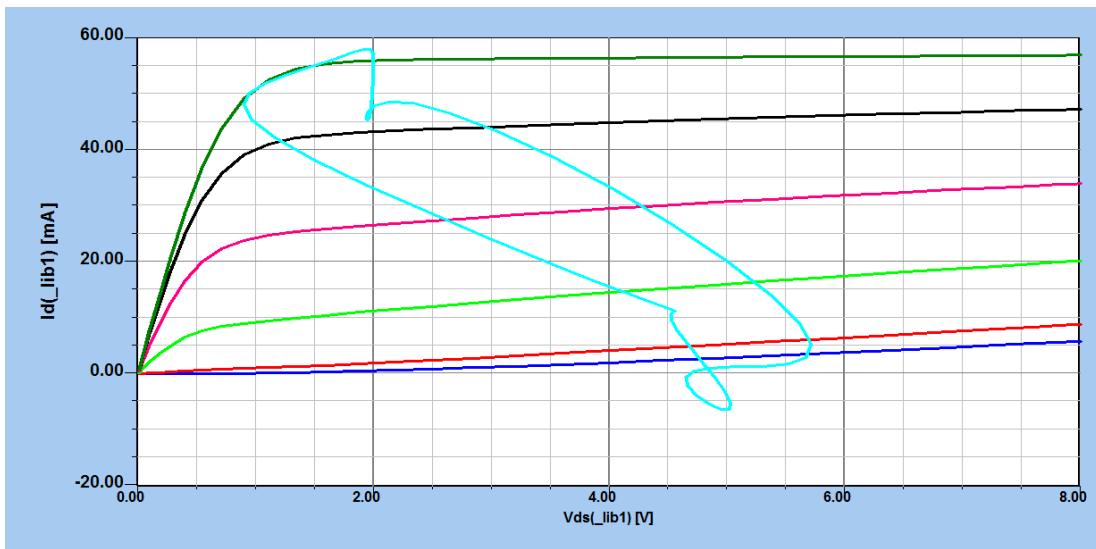
Figure 48: *DC-IV Output Curves of the 5GHz microwave oscillator*
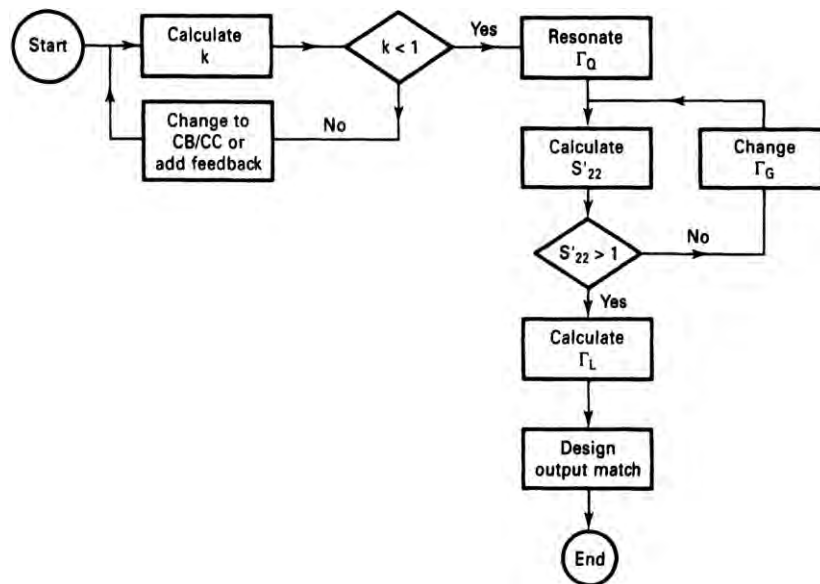
70
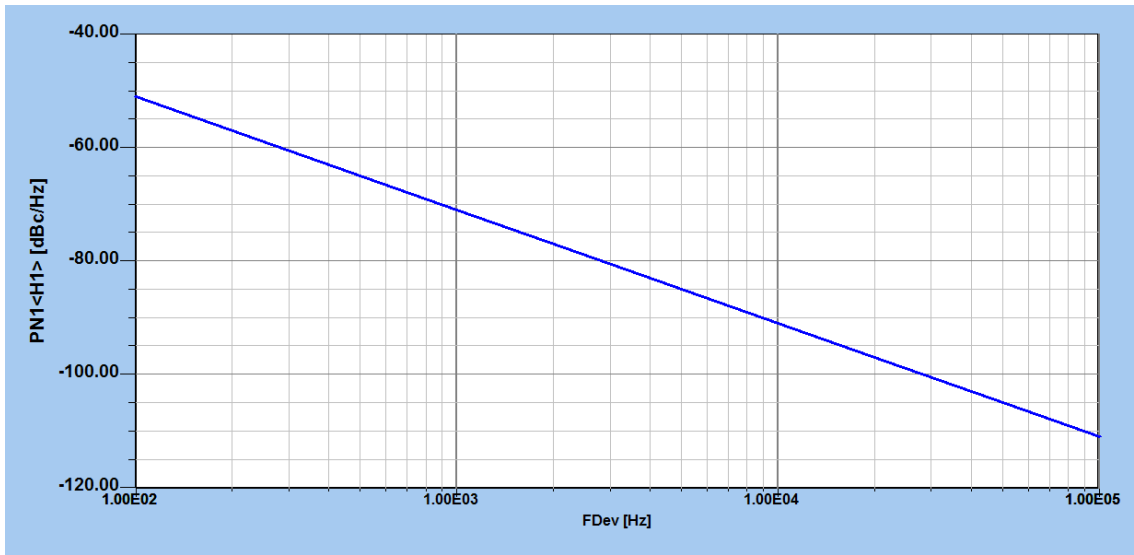
Figure 49: *Simulated Phase Noise of the 5GHz microwave oscillator*
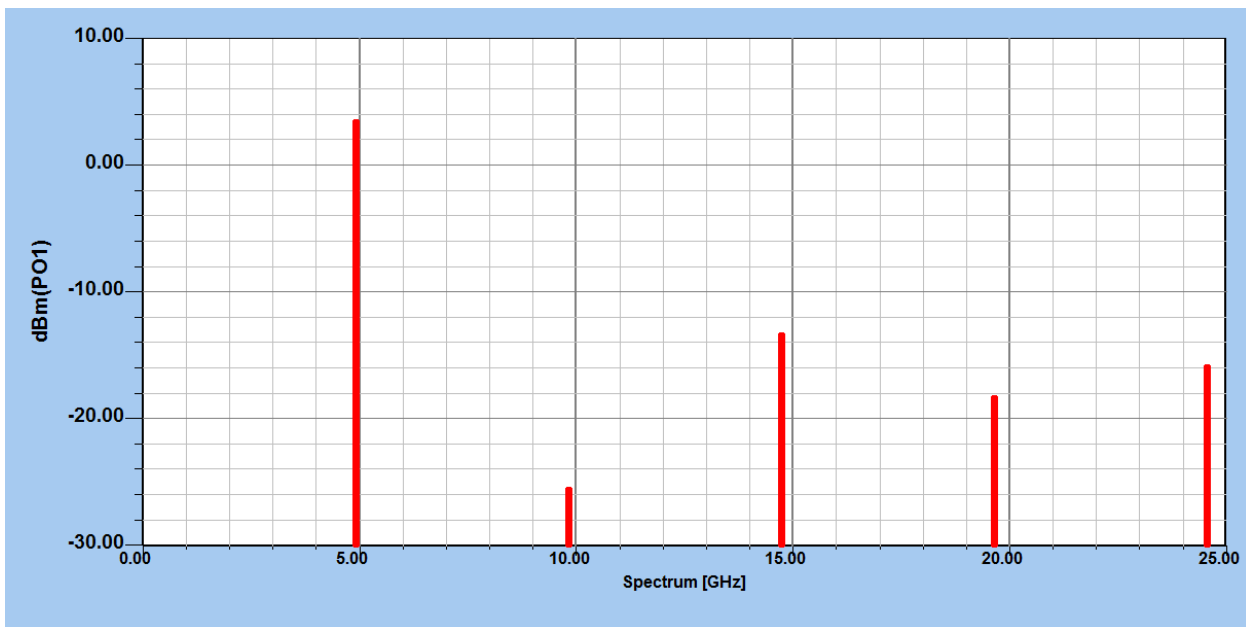
Figure 50: *Simulated Output power in dBm of the 5GHz microwave oscillator*

An example using this procedure at 4 GHz is given in Figure 4-169 using an AT 41400 silicon bipolar chip in the common-base configuration with a convenient value of base and emitter inductance of 0.5 nH. The feedback parameter is the base inductance, which can be varied if needed.

71
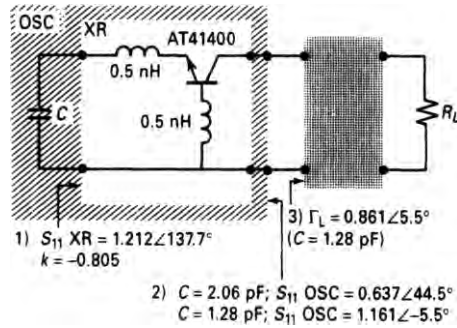
Figure 51: *Figure 4-169 A 4-GHz lumped resonator oscillator using AT41400.*

The two-port common-base *S*-parameters were used to give

$k = -0.805$

$S_{11}' = 1.212 \underline{|137.7°}$

Since a lossless capacitor at 4 GHz of 2.06 pF gives $\Gamma_G = 1 - 0 \underline{|-137.7°}$, this input termination is used to

calculate S_{22}', giving $S_{22}' = 0.637 \underline{|44.5°}$. This circuit will not oscillate into any passive load. Varying the

emitter capacitor about 20° on the Smith chart to 1.28 pF gives $S_{22}' = 1.16 \underline{|-5.5°}$, which will oscillate into

a load of $\Gamma_L = 0.861 \underline{|5.5°}$. The completed lumped element design is given in Figure 4-170.
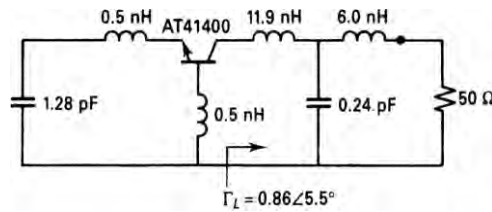
Figure 52: *Figure 4-170 Completed lumped resonator oscillator (LRO).*
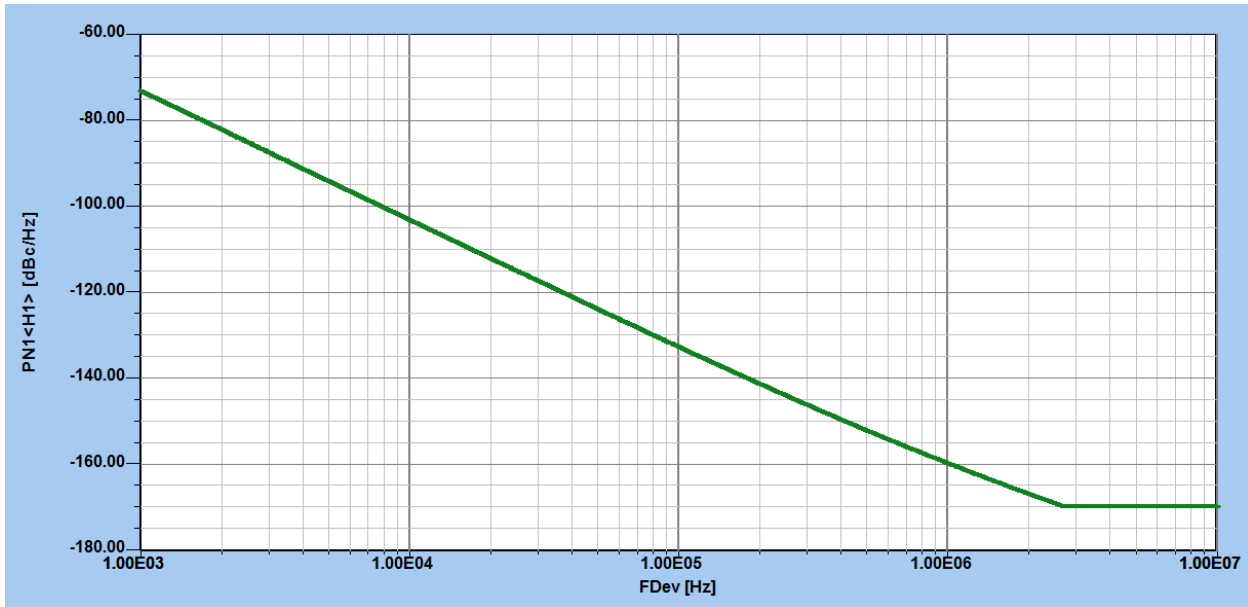
Figure 53: *Simulated Phase noise of the 4-GHz lumped resonator oscillator*
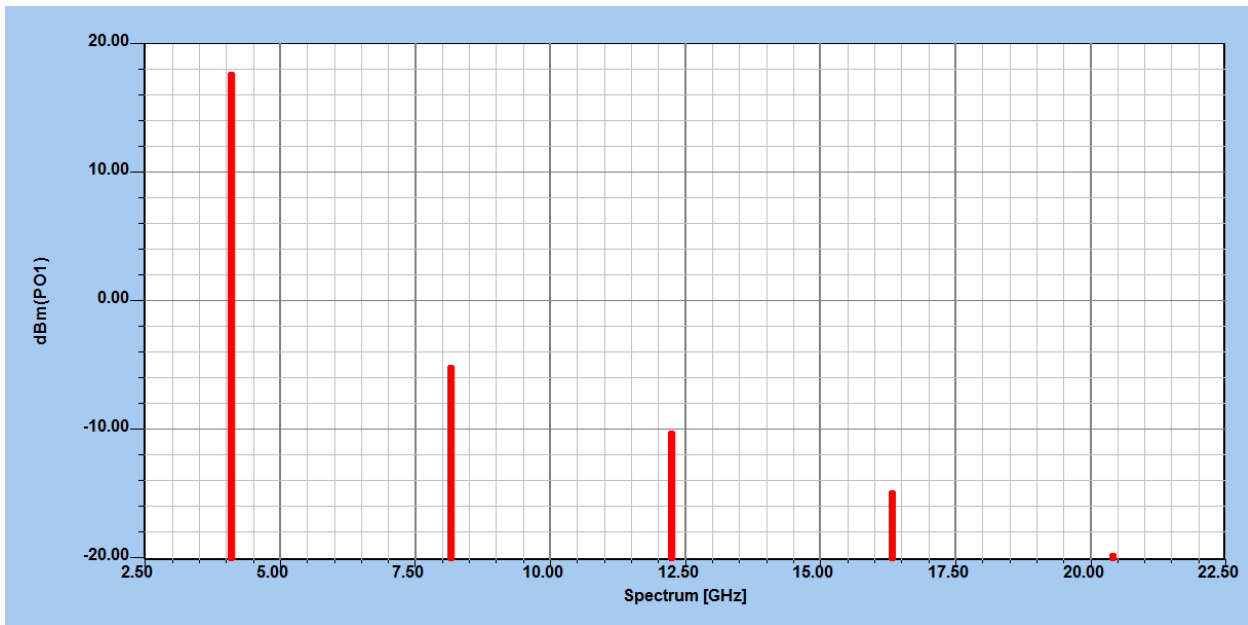
Figure 54: *Simulated output power in dBm of the 4-GHz lumped resonator oscillator*
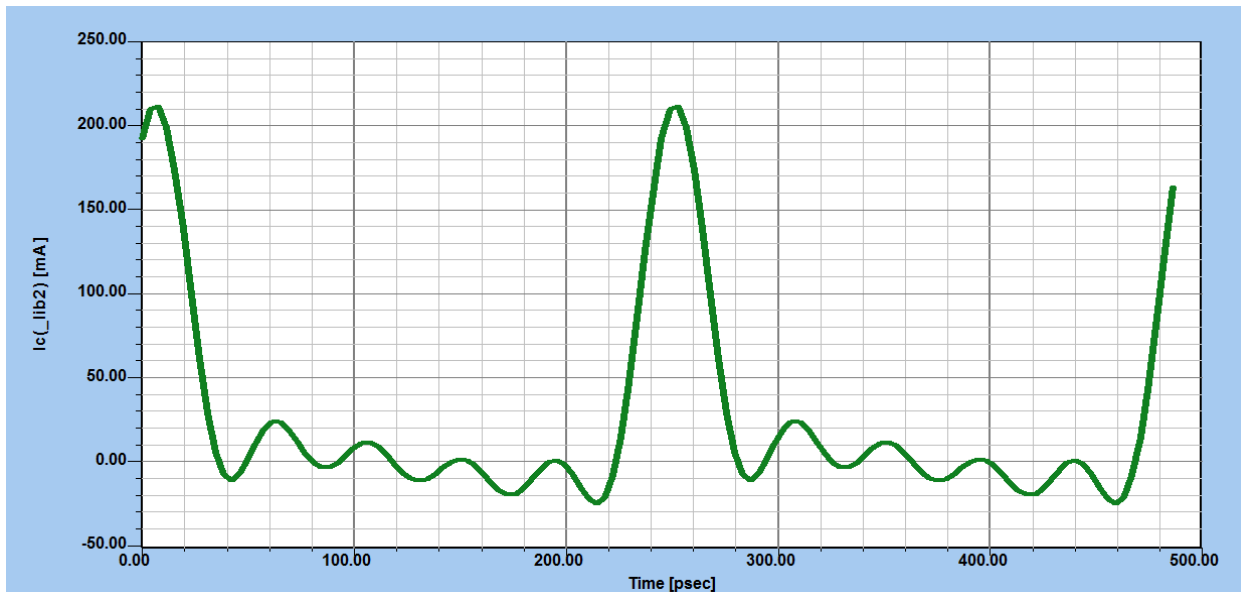
Figure 55: *Collector current duty cycle of the 4-GHz lumped resonator oscillator*

We now switch from the lumped design to a microstrip design that incorporates a dielectric resonator. This oscillator circuit is given in Figure 4-171, where the dielectric resonator (DR) will serve the function of the emitter capacitor. This element is usually coupled to the 50-Ω microstripline to present about 1000 Ω of loading $(\beta = 20)$ at f_0, the lowest resonant frequency of the dielectric puck, at the correct position on the line. The load circuit will be simplified to $50\ \Omega(\Gamma_L = 0)$, so the oscillator must have an output reflection coefficient of greater than 100, thus presenting a negative resistance between -49 and -50Ω. The computer file for analyzing this design is given in Table 4-17, where the variables are the puck resistance, the $-50\ \Omega$ microstripline length, and the base feedback inductance. The final design is given in Figure 4-172, where the 10-μH coils are present for the dc bias connections that need to be added to the design. It is important to check the stability of this circuit with the DR removed. The input $-50\ \Omega$ termination will usually guarantee unconditional stability at all frequencies. The phase noise of this oscillator is very low at -117 dBc/Hz at 10-kHz frequency offset.
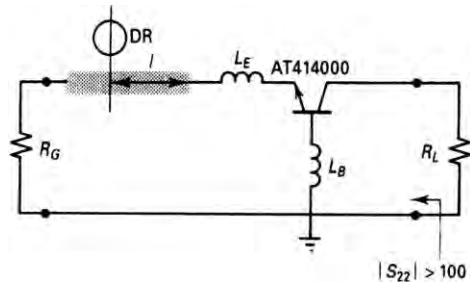
Figure 56: *Figure 4-171 Transmission line oscillator with dielectric resonator.*

Variables: *R* (coupling of puck) = 955 Ω
I (placement of puck) = 224.2 mils
(ϵ_L = 10, *h* = 25 mils)
L_B (base inductance) = 0.34 nH
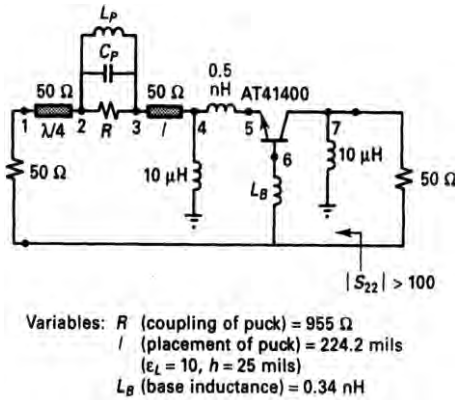
Figure 57: *Figure 4-172 Equivalent circuit for dielectric resonator oscillator (DRO).*

Figure 58: *Table 4-17 Super-compact file for DRO design in Figure 4-172*

```
*
-
* AT41400 AT 7.5V, 30 mA IN DRO
* OSCILLATOR By Vendelin et a I. Microwave Journal June 1986 pp. 151-152
BLK
 TRL 1 2 Z=50 P=250MIL K=6.6
 RES 2 3 R=?955.06?
 TRL 3 4 Z=50 P=?224.16MIL? K=6.6
 IND 4 0 L=1E4NH
 IND 4 5 L=.5NH
 TWO 6 7 5 Q1
 IND 6 0 L = ?.33843NH?
 IND 7 0 L=1E4NH
 0SC:2P0R 1 7
END
*
FREQ
 4GHZ
END
OUT
 PRI OSC S
END
OPT
 OSC
```

```
  MS22 = 100 GT
END
DATA
 Q1 : S
 4 . 8057–176.14 2.5990 74.77.0316 56.54 .4306 –22.94
END
```

For simple oscillators with no isolating stage, one can expect a certain amount of pulling. Figure 4-173 shows the tuning parameters as the load varies from 50 Ω. The load $C_L = R + jX$ influences the required input capacitance C_E and the base inductor L_B. The numbers in the graph are the resonant portion of the load impedance and the ratio X/R determines the Q line. It is obvious that such a circuit is quite interactive. As to the model for the dielectric resonator, the valid relationship is shown in Figure 4-174.
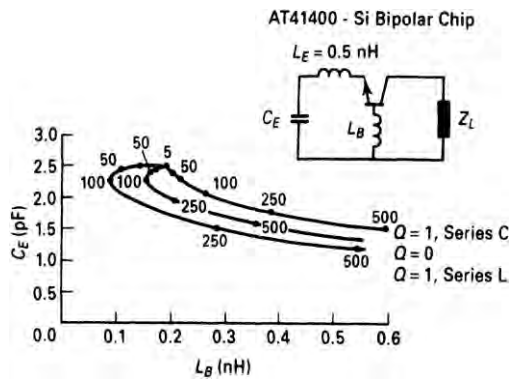
Figure 59: *Figure 4-173 Tuning parameters for a 4-GHz oscillator versus load impedance as the load varies from 50 H.*
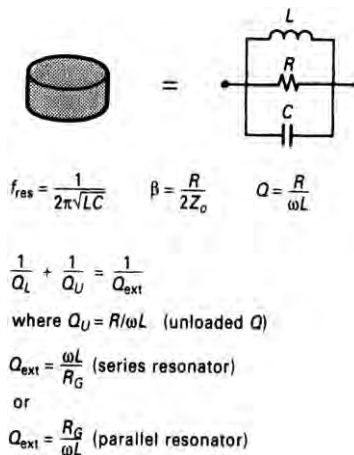
Figure 60: *Figure 4-174 Simple equivalent circuit for the dielectric resonator.*

In Section 4-9 on microwave resonators, we will look at a more physical model.

Finally, Table 4-18 describes the same DRO in the familiar Spice format. This particular Compact Software Inc. Spice model uses transmission elements Tl and T2 and the resonant frequency of the oscillator is determined by both the dielectric resonator and its position relative to the transmission line. In the equivalent circuit of the transistor, no values for a base-spreading resistor have been assumed. This modeling is done for demonstration purposes and does not relate to an actual transistor. A more practical circuit will follow.

Figure 61: *Table 4-18 Spice format*

```
Compact Software - SUPER-SPICE 1.1 08/09/95 13:38:56
File: C:\SPICE\CIR\DR0.cir
Dielectric Resonator Oscillator with a BJT
Q1 1 2 3 Q2NXXXX
C1 2 4 100pf
L1 4 0 0.3384nh
L2 1 100 1uh
L3 3 6 0.5nh
lb1 6 0 1uh
T1 6 0 7 0 Z0=50 TD=5.4378e–11
cdro 7 8 .0397p
Idro 7 8 40nh
rdro 7 8 955
T2 8 0 9 0 Z0=50 TD=4.876e–11
R1 9 0 50
C4 1 10 100pf
P1 10 0 PNR=1 ZL=50
*Biasing
R3 100 2 3.6k
R4 2 0 1.2k
V1 100 0 7.5V
● model Q2NXXXX NPN(Is=1-65e-18 Vaf=20 Bf=50 Nf=1.03
+ Ise=5f lkf=.1 Xtb=1.818 Br=5 cjc=.75p
+ Fc=.5 Cje=.75p Mje=.6 Vje=1.01 xcjc=.5
+ Tf=14p Itf=.3 Vtf=6 Xtf=4 Ptf=35)
● IC V(2)=.001
● TRAN 2N 500N
● AC LIN 500 3GHZ 5GMZ
● opt i 115 = 0
● PROBE
● END
```

➢ Microwave Resonators

For microwave applications, one is rapidly moving away from lumped to distributed elements. In the previous section, we looked at the case of a transmission line-based oscillator, which by itself has a low Q and was shown only for descriptive and design purposes. In similar fashion, we looked at the simplified description of a dielectric resonator-based oscillator.

From a practical design point of view, most relevant applications are SAW resonators, dielectric resonators, and YIG oscillators. These are the three types of resonators we will cover in this section.

SAW Oscillators

The SAW oscillator has an equivalent circuit similar to a crystal but should be enhanced by adding the appropriate capacitance to ground. Figure 4-175 shows this. SAW oscillators are frequently used in synthesizers and provide a low phase noise, highly stable source, as can be seen in Figure 4-175. The SAW oscillator comes as either a one-port or two-port device.
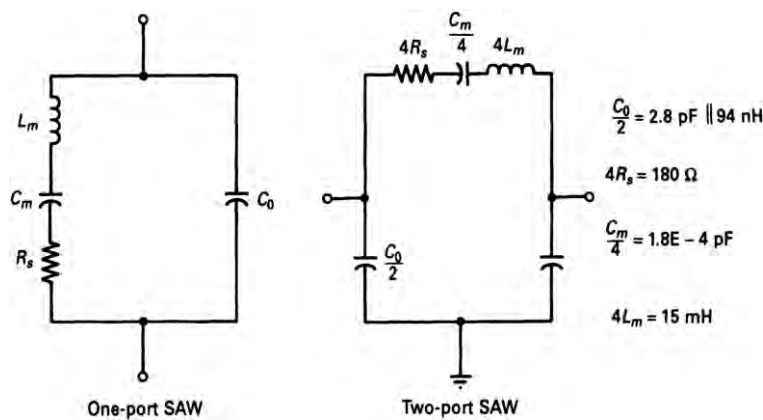
Figure 62: *Figure 4-175: Appropriate capacitance to ground for the SAW resonator*
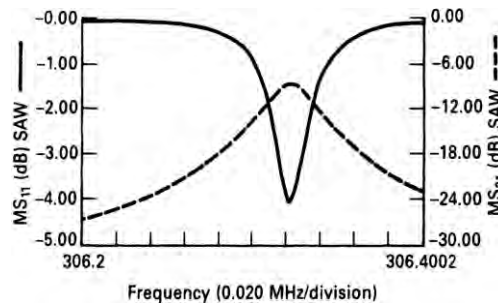
Figure 63: *Figure 4-176 Frequency response of a SAW oscillator.*

The SAW resonator has fairly high insertion loss, as can be seen from Figure 4-176. The actual circuit of a high-performance SAW oscillator, as shown in Figure 4-177, consists of a bipolar transistor with a dc stabilizing circuit, SAW oscillator, and a feedback loop, which allows the phase to be adjusted. The SAW oscillator provides very good phase noise. The measured phase noise of such an oscillator is shown in Figure 4-178. The actual measured phase noise agrees quite well with this prediction

78
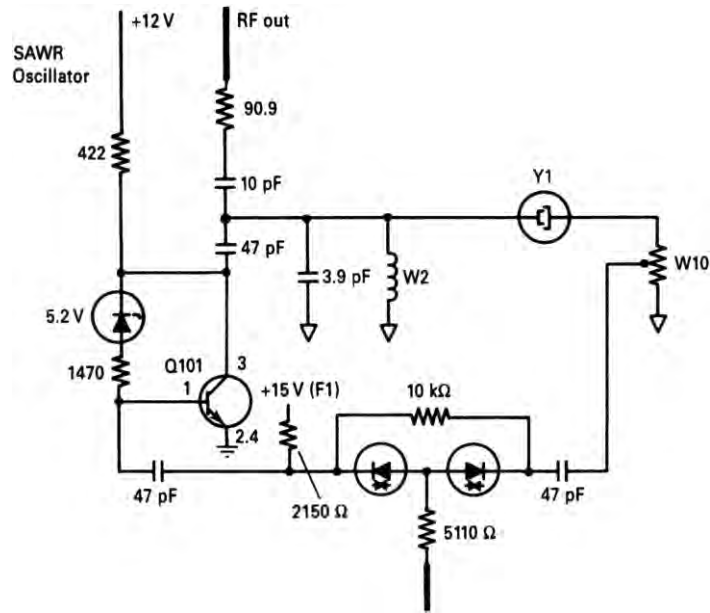
Figure 64: *Figure 4-177 Schematic of a SAW oscillator.*
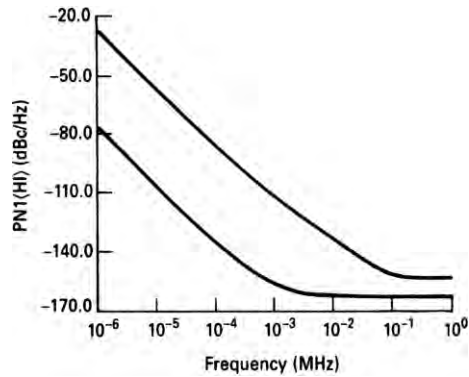
Figure 65: *Figure 4-178 Phase noise as determined by the initial start-up values and after optimization.*

Dielectric Resonators

In designing dielectric resonator-based oscillators, several methods of frequency stabilization are available that have been proposed by various authors. Figure 4-179 shows some recommended methods of frequency stabilization for dielectric resonator oscillators. The dielectric resonator consists of some high dielectric material coupled to a transmission line or microstrip structure.
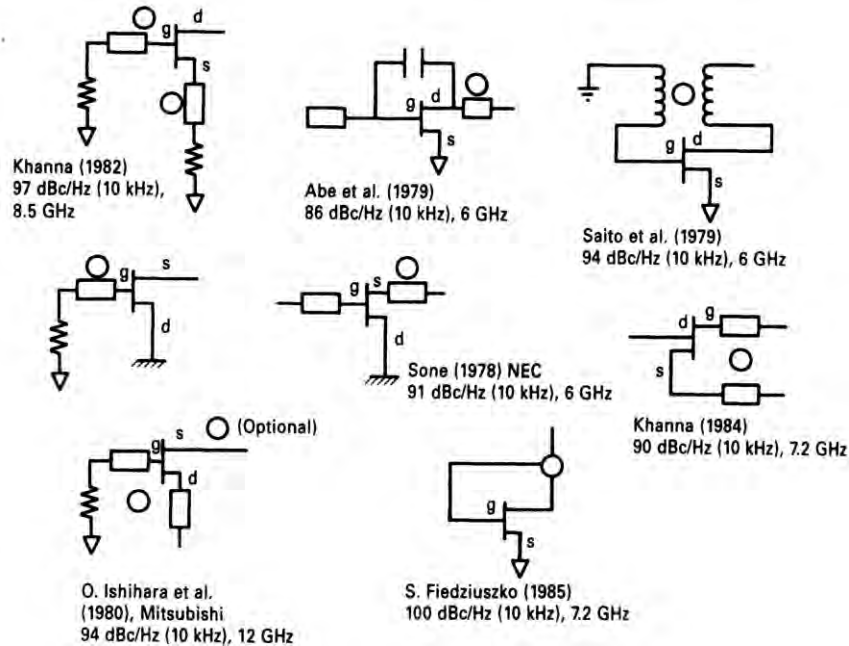
Figure 66: *Figure 4-179: Recommended methods of frequency stabilization for DROs.*

Figure 4-180 shows the field distribution and interaction between the microstrip and the dielectric resonator. The two resulting applications, BandStop and BandPass filters, are displayed. Modeling this type of resonator is done by describing the resonator in the form of its physical dimensions.

Table 4-19 shows the physical dimensions of the dielectric resonator in Super-Compact/Microwave Harmonica format.

Figure 67: *Table 4-19 Physical dimensions of DR*

BLK

DRM 1 2   D=6.12e-3 HD-2.45e-3 ER=38 HT=1.5e-3 S=.5e-3; + W=1.1e-3 L = 4e-3
           SRD=1e-4 BPF SUB;
           trf 2 0 0 3 N = 1
           pug: 2P0R 1 3

END

DATA

           SUB: MS er=2.4 h=0.380e-3 met1=cu 3.175e-6 and=0.0001

END

A practical example of a 6-GHz dielectric resonator-based oscillator is shown in Figure 4-181 and its predicted phase noise is shown in Figure 4-182.

For calibration purposes, it may be useful to plot the phase noise of different oscillators, including YIG oscillators, as shown in Figure 4-183, but normalized to a center frequency of 6 GHz. Another way of plotting this is to show the phase noise of silicon bipolar transistors versus FETs at 10 kHz offset from the carrier, as shown in Figure 4-184. This plot does not incorporate for heterojunction bipolar transistors because they are not yet readily or commercially available.
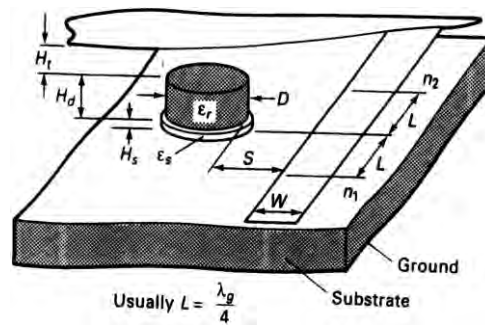
Figure 68: *Figure 4-180a DRO on microstrip as BandStop filter.*
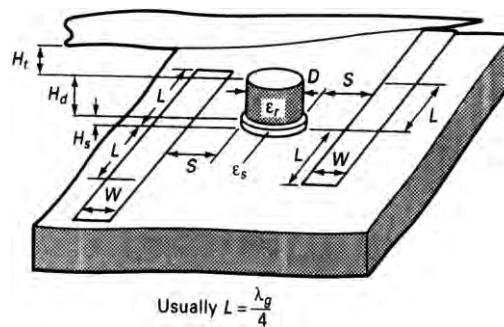
Figure 69: *Figure 4-180b DRO on microstrip as BandPass filter.*
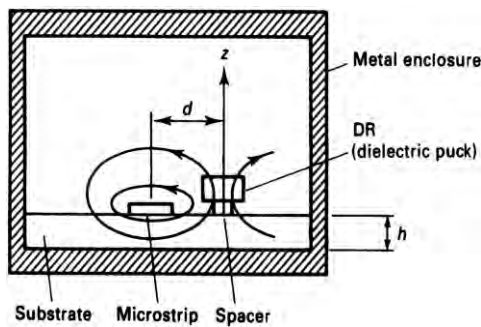
Figure 70: *Figure 4-180c Field distribution and interaction between the microstrip and the DRO.*
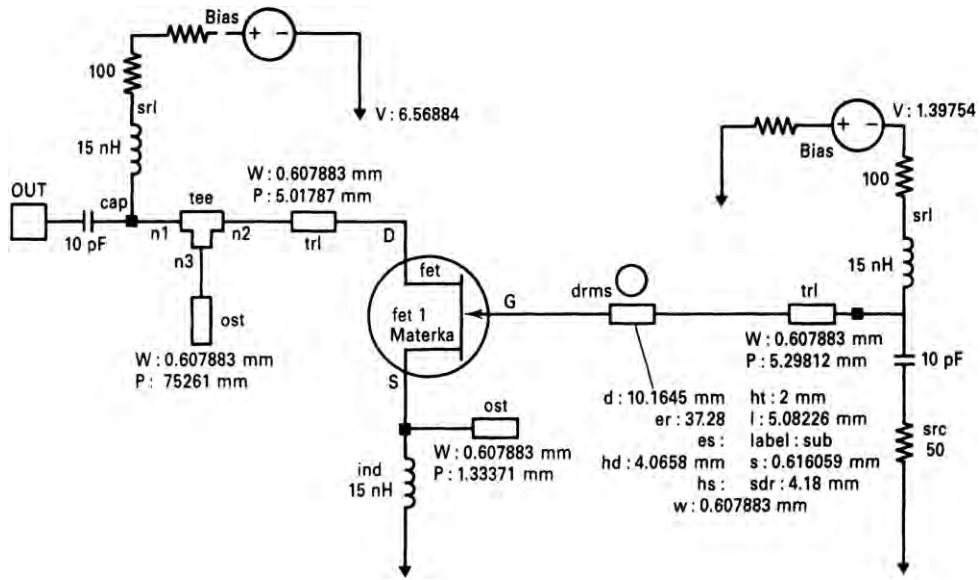
Figure 71: *Figure 4-181 Schematic of 6-GHz DRO.*
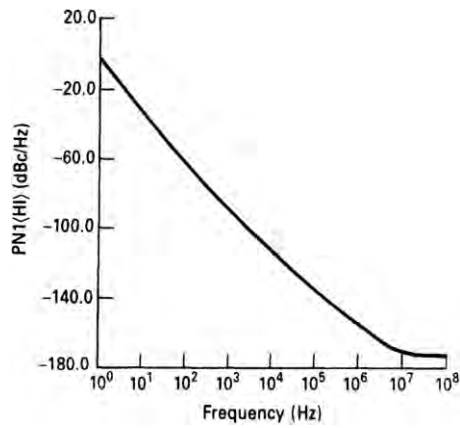
Figure 72: *Figure 4-182 Predicted phase noise of the 6-GHz DRO pictured in Figure 4-181.*
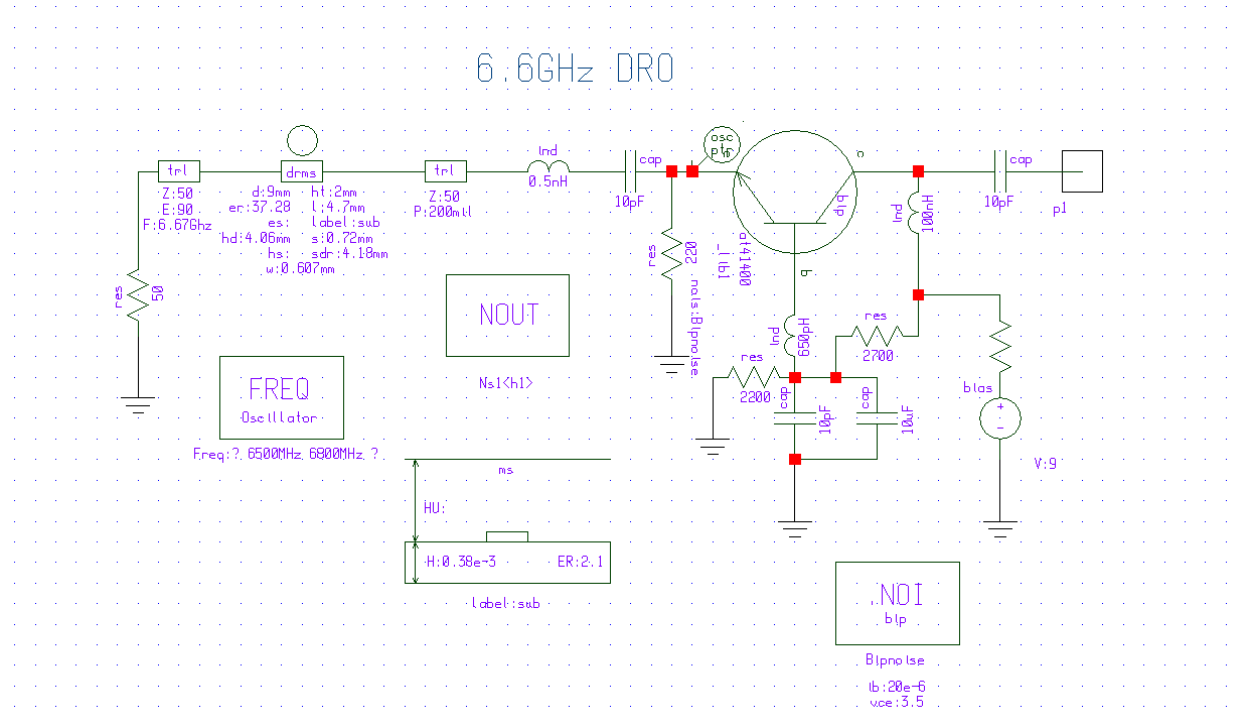
Figure 73: *Detailed Circuit schematic of a 6.6GHz DRO*
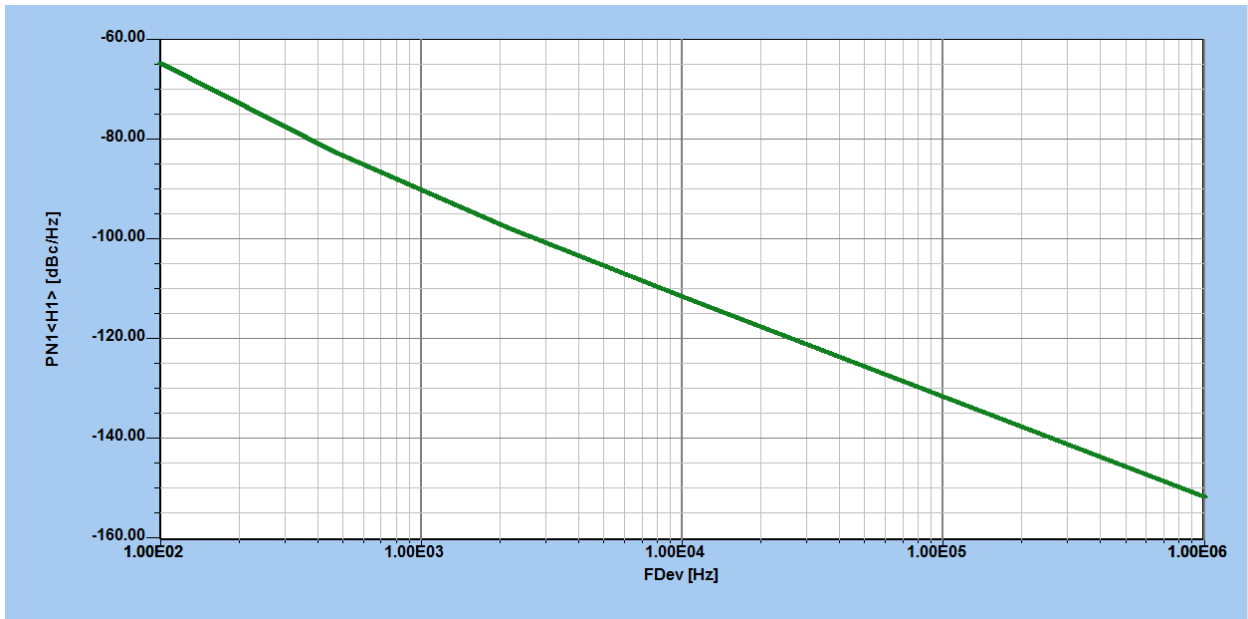
Figure 74: *Simulated Phase Noise of the 6.6GHz DRO*

83
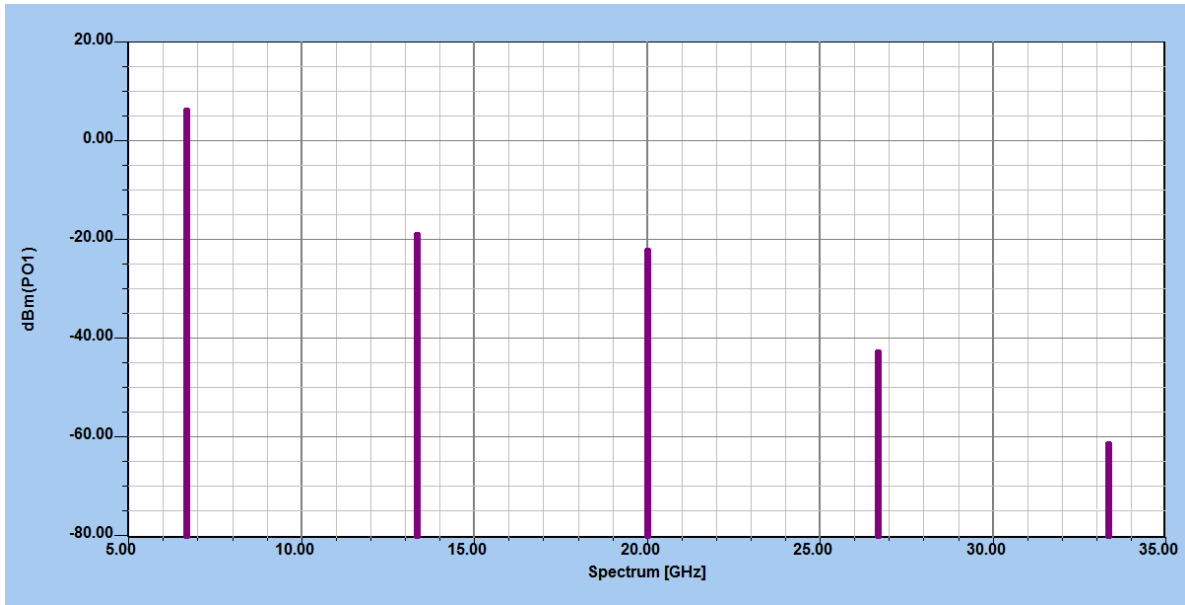
Figure 75: *Simulated output power in dBm of the 6.6GHz DRO*
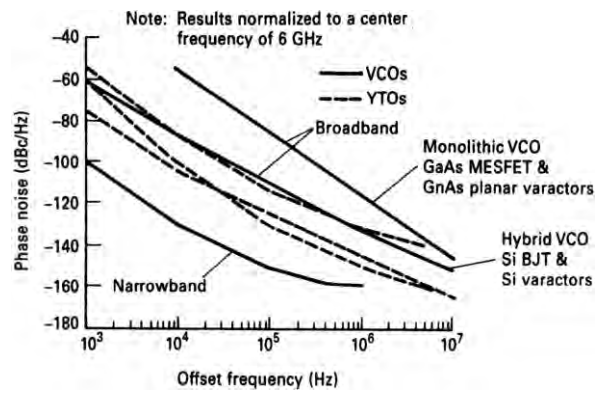
Figure 76: *Figure 4-183 Phase noise comparison of different YIG and varactor tuned oscillators*
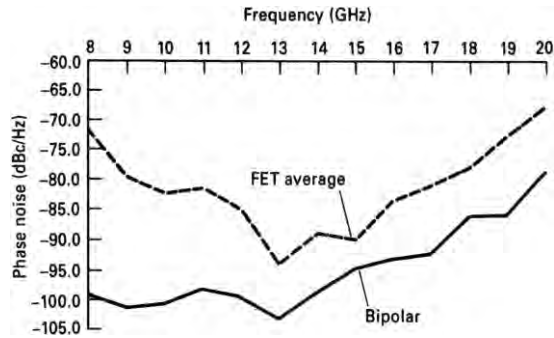
Figure 77: *Figure 4-184 Phase noise at 10 kHz off the carrier of silicon bipolar transistors versus FETs*

For more detailed information on DROs please refer to Appendix E.

YIG Oscillators

For wideband electrically tunable oscillators, we use either a YIG or a varactor resonator. The YIG resonator is a high-Q, ferrite sphere of yttrium ion garnet, $Y_2Fe_2 (FeO_4)_3$, that can be tuned over a wide band by varying the biasing dc magnetic field. Its high performance and convenient size for applications in microwave integrated circuits make it an excellent choice in a large number of applications, such as filters, multipliers, discriminators, limiters, and oscillators. A YIG resonator makes use of the ferrimagnetic resonance, which, depending on the material composition, size, and applied field, can be achieved from 500 MHz to 50 GHz. An unloaded Q greater than 1000 is usually achieved with typical YIG material.

Figure 4-185 shows the mechanical drawing of a YIG oscillator assembly. The drawing is somewhat simplified and the actual construction is actually more difficult to do. Its actual circuit diagram is shown in Figure 4-186.
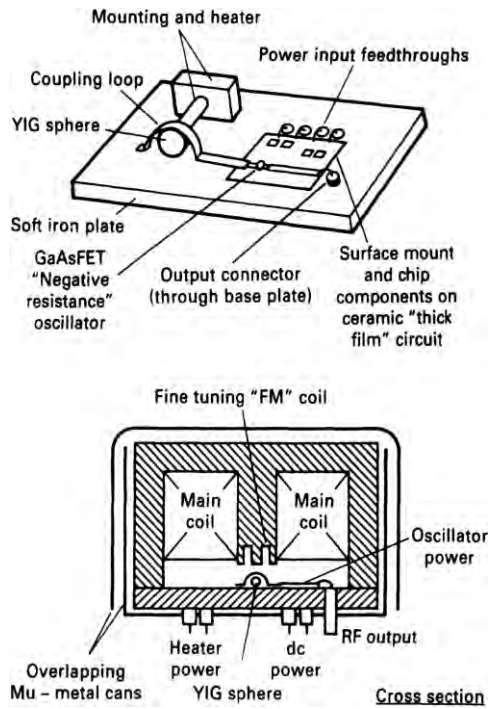
Figure 78: *Figure 4-185: The yttrium–iron–garnet (YIG) sphere serves as the resonator in the sweep oscillators used in many spectrum analyzers.*
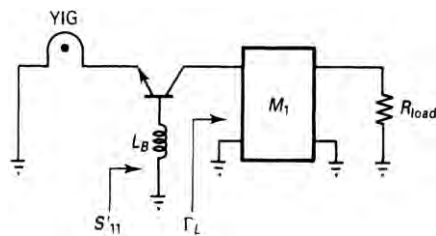
Figure 79: *Figure 4-186: Actual circuit diagram for YIG-tuned oscillator depicted in Figure 4-185.*

Figure 80: *10GHz YIG based oscillator with base-inductor feedback*

Figure 81: *Colpitts YIG oscillator*
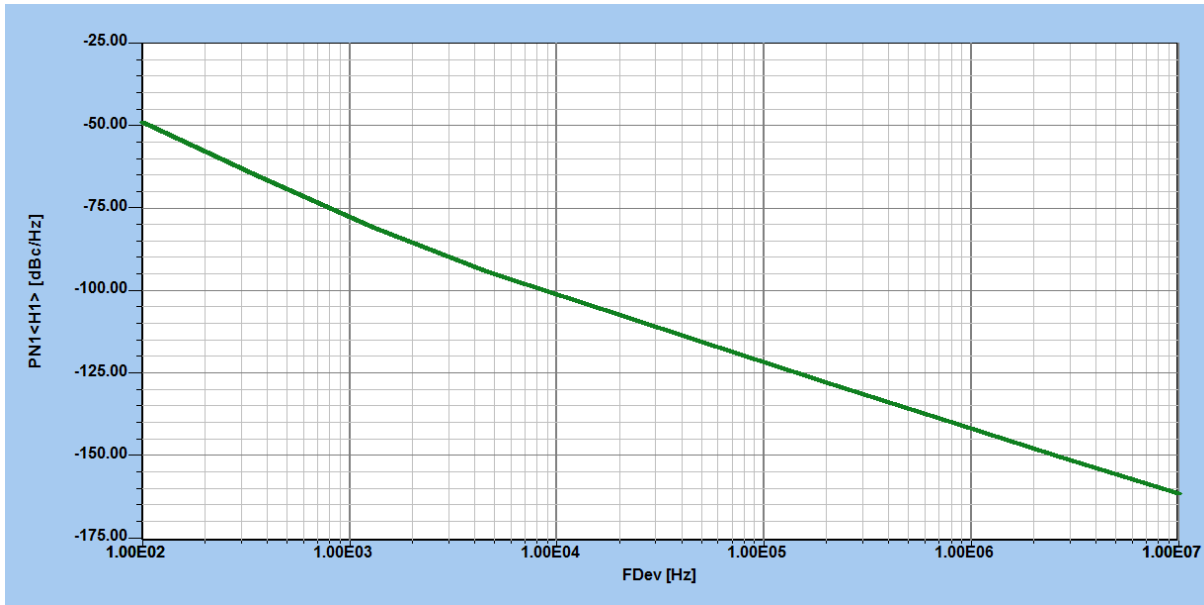
Figure 82: *YIG Oscillator Phase noise with base coil feedback*

In fig. 83, the first two traces (red and light blue) are for Flicker Corner Frequency 1 KHz and the green and dark blue are 1Hz Flicker corner frequency. The bottom red trace is the AM noise which dominates above 20 kHz offset.
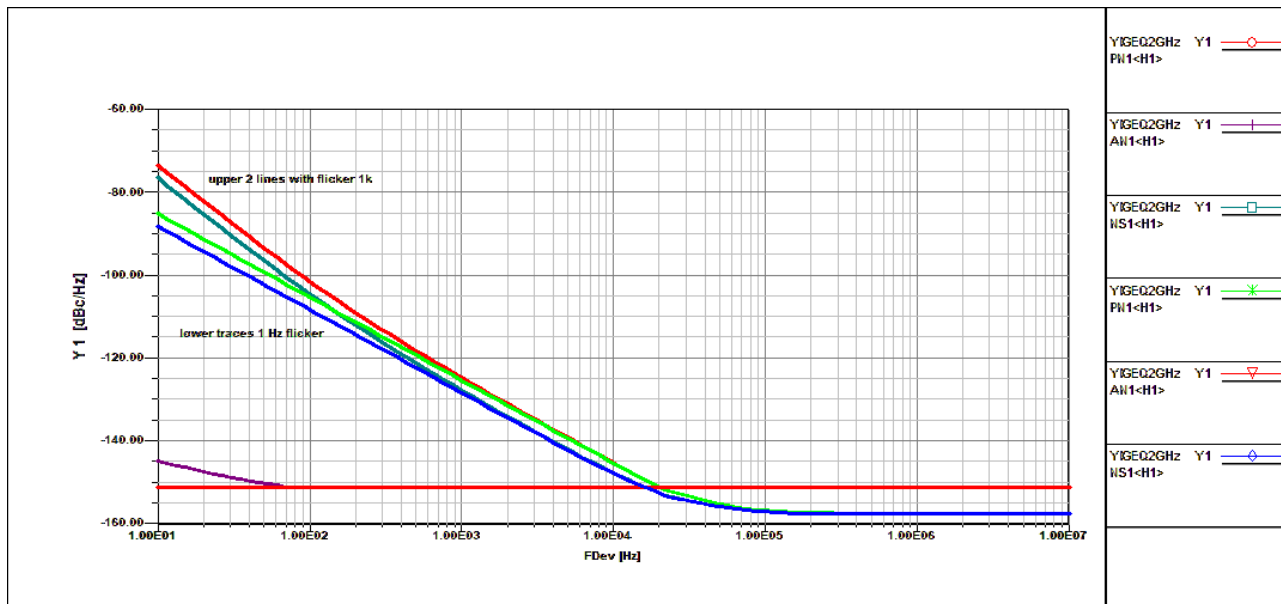
Figure 83: *Colpitts version of the Oscillator optimized - Red curve is Phase Noise dBc/Hz, dark green NS1 (Spectral Density dBc/Hz and the red one is AM Noise, also in dBc/Hz, Flicker noise set to zero*
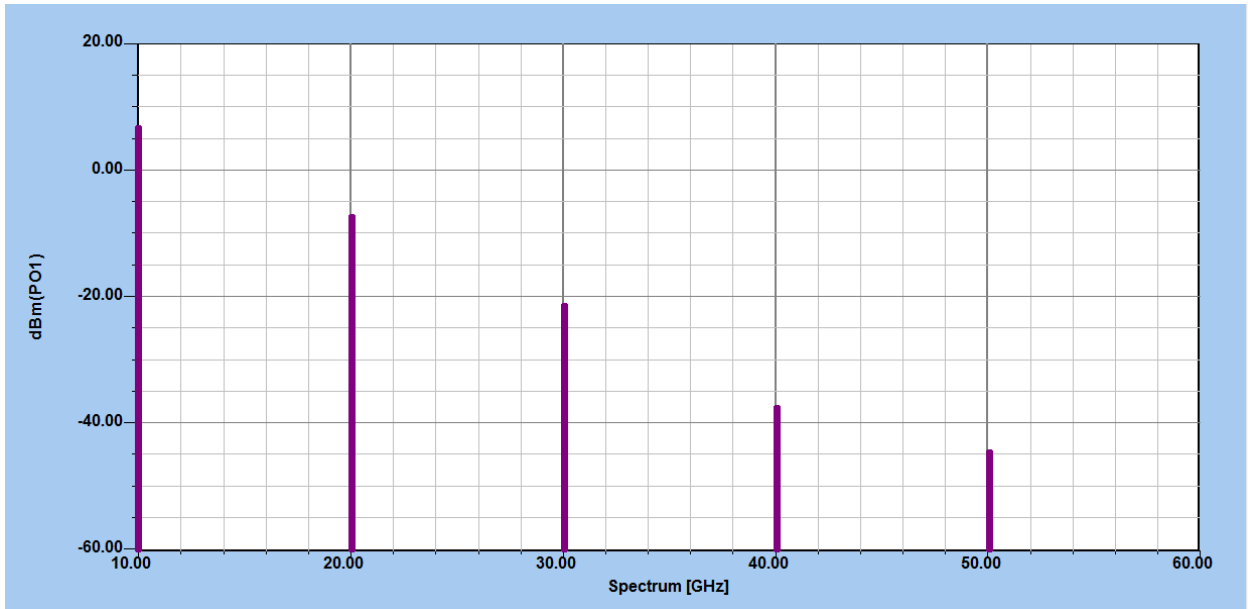
Figure 84: *Simulated Output power of the YIG oscillator base feedback design*
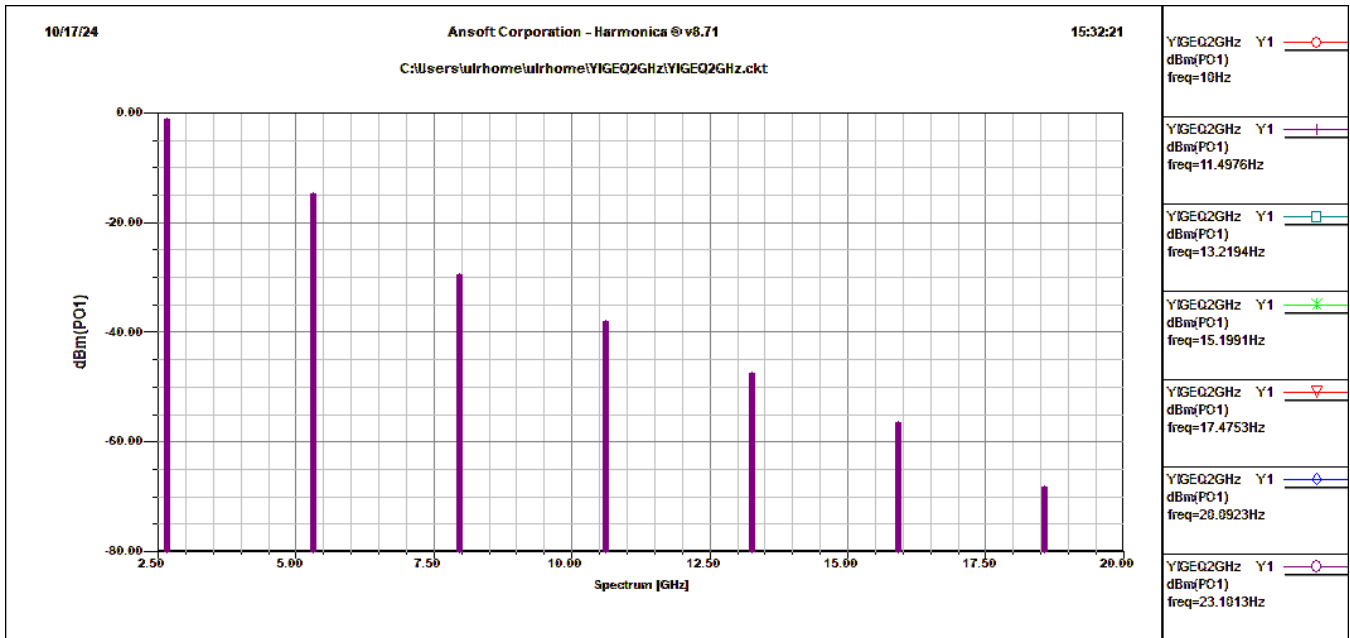
Figure 85: *Simulated output power of the Colpitts based oscillator*

➢ **Tuning Diode based Resonators**

The dual of the current-tuned YIG resonator is the voltage-tuned varactor, which is a variable reactance achieved from a low-loss, reverse-biased semiconductor PN junction. These diodes are designed to have

very low loss and therefore high Q. The silicon varactors have the fastest settling time in fast-tuning applications, but the gallium arsenide varactors have higher Q values. The cutoff frequency of the varactor is defined as the frequency where $Q_v = 1$. For a simple series RC equivalent circuit, we have

$$Q_v = \frac{1}{\omega R C_v}$$

(4-226)

$$f_{c0} = \frac{1}{2\pi R C_v}$$

(4-227)

The tuning range of the varactor will be determined by the capacitance ratio C_{max}/C_{min}, which can be 12 or higher for hyper-abrupt varactors. Since R is a function of bias, the maximum cutoff frequency occurs at a bias near breakdown, where both R and C_v have minimum values. Tuning diodes or GaAs varactors for microwave and millimeter-wave applications are frequently obtained by using a GaAs FET and connecting source and drain together. Figure 4-187 shows the dynamic capacitance and dynamic resistors as a function of tuning voltage. In using a transistor instead of a diode, the parameters become more complicated. Figure 4-188 shows the capacitance, equivalent resistor, and Q, as well as the magnitude of S_{11}, as a function of reverse voltage. This is due to the breakdown effects of the GaAs FET.
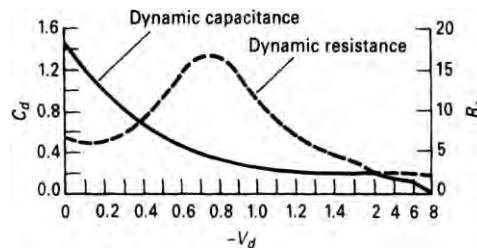
Figure 86: *Figure 4-187 Dynamic capacitance and dynamic resistors as a function of tuning voltage for GaAs varactor.*
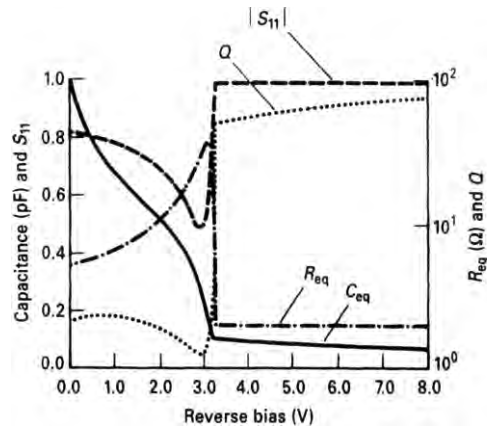
Figure 87: *Figure 4-188 Varactor parameters: capacitance, equivalent resistor, and Q, as well as the magnitude of S_{11}, as a function of reverse voltage.*

Previously, we had discussed in great detail the tuning diode applications. The major differences between these applications and microwave applications have to do with the resulting low Q and different technology. This is the reason why discussions of both applications were separated.
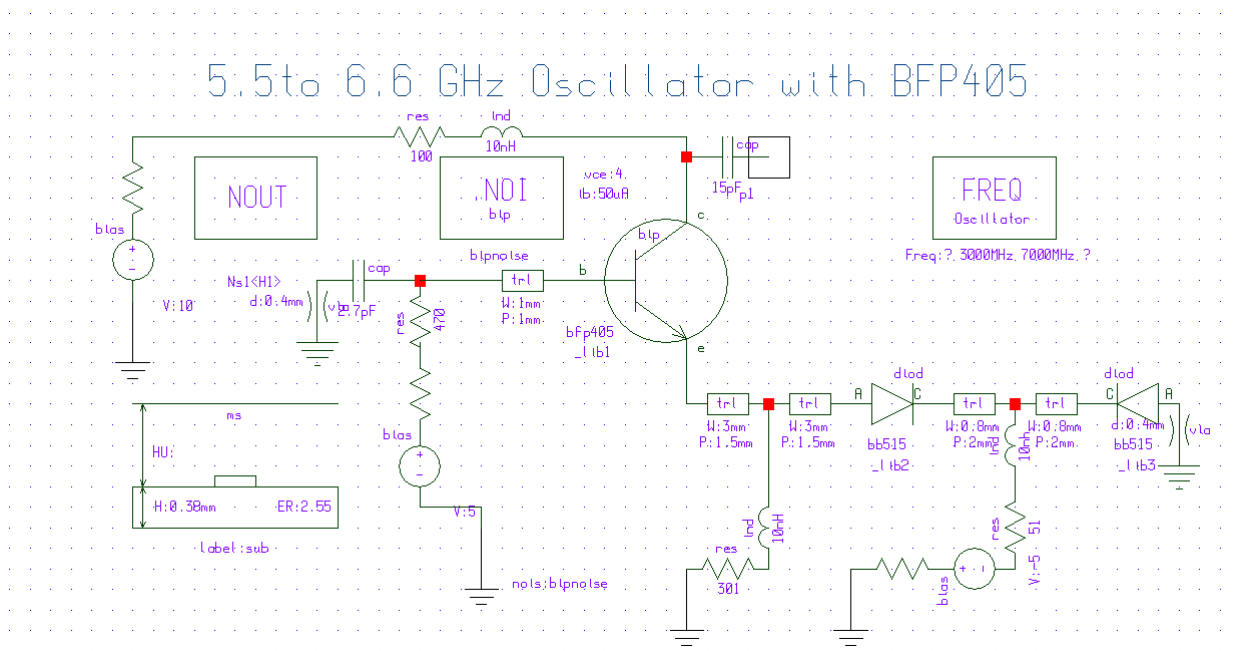
Figure 88: *Schematic of a 5.5 to 6.6 GHz VCO using BFP 405*
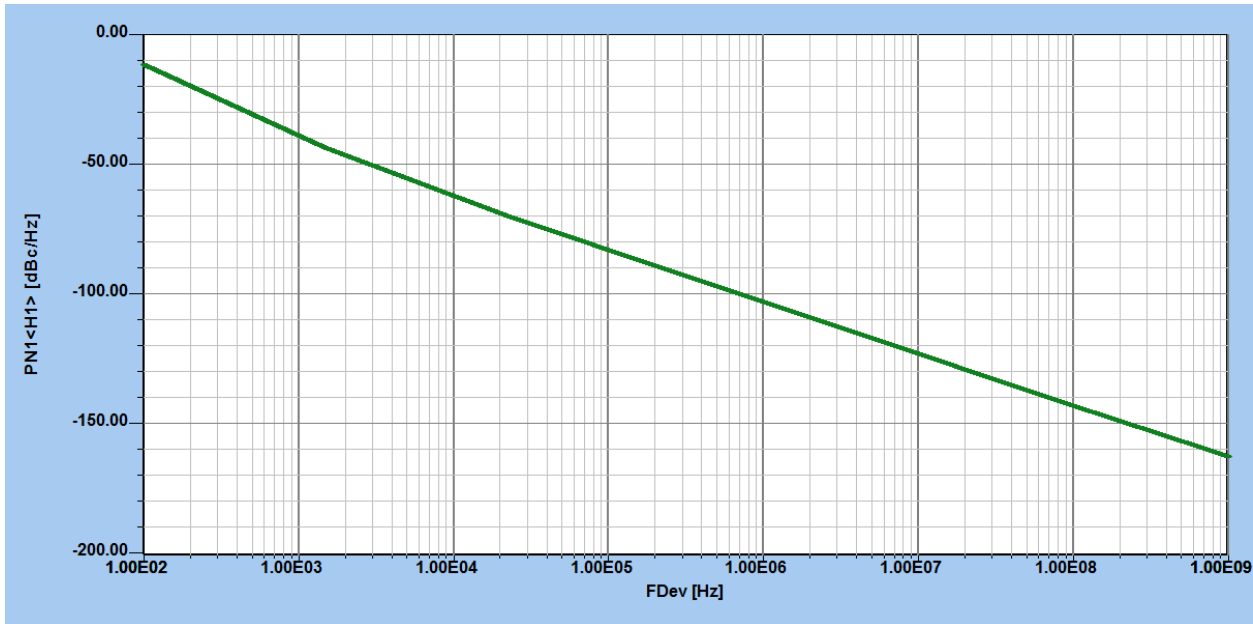
Figure 89: *Simulated Phase noise of a 5.5 to 6.6 GHz VCO using BFP 405*

➤ Ceramic Resonators

An important application for a new class of resonators called ceramic resonators (CRs) has emerged for wireless applications. The CRs are similar to shielded coaxial cable, where the center controller is connected at the end to the outside of the cable. These resonators are generally operating in quarter-wavelength mode and their characteristic impedance is approximately 10 Ω. Because their coaxial assemblies are made for a high-ε low-loss material with good silver plating throughout, the electromagnetic field is internally contained and therefore provides very little radiation. These resonators are therefore ideally suited for high-Q, high-density oscillators. The typical application for this resonator is VCOs ranging from not much more than 200 MHz up to about 3 or 4 GHz. At these high frequencies, the mechanical dimensions of the resonator become too tiny to offer any advantage. One of the principal requirements is that the physical length is considerably larger than the diameter. If the frequency increases, this can no longer be maintained.

Calculation of an Equivalent Circuit of the ceramic resonator

The equivalent parallel-resonant circuit has a resistance at resonant frequency of

92

$$R_p = \frac{2(Z_0)^2}{R^* l}$$

where Z_0 = characteristic impedance of the resonator

l = mechanical length of the resonator

R^* = equivalent resistor due to metalization and other losses

As an example, one can calculate

$$C^* = \frac{2\pi\varepsilon_0\varepsilon_r}{\log_e(D/d)} = 55.61\times 10^{-12}\frac{\varepsilon_r}{\log_e(D/d)} \tag{4-228}$$

and

$$L^* = \frac{\mu_r\mu_0}{2\pi} = \log_e\left(\frac{D}{d}\right) = 2\times 10^{-7}\log_e\left(\frac{D}{d}\right) \tag{4-229}$$

$$Z_0 = 60\,\Omega\frac{1}{\sqrt{\varepsilon_r}}\log_e\left(\frac{D}{d}\right) \tag{4-230}$$

A practical example for $\varepsilon_r = 88$ and 450 MHz is

$$C_p = \frac{C^* l}{2} = 49.7\text{ pF} \tag{4-231}$$

$$L_p = 8L^* l = 2.52\text{ nH} \tag{4-232}$$

$$R_p = 2.5\text{ k}\Omega \tag{4-233}$$

Manufacturers supply these resonators on a prefabricated basis. Figure 4-189 shows the standard round/square packaging available and the typical dimensions for a ceramic resonator.
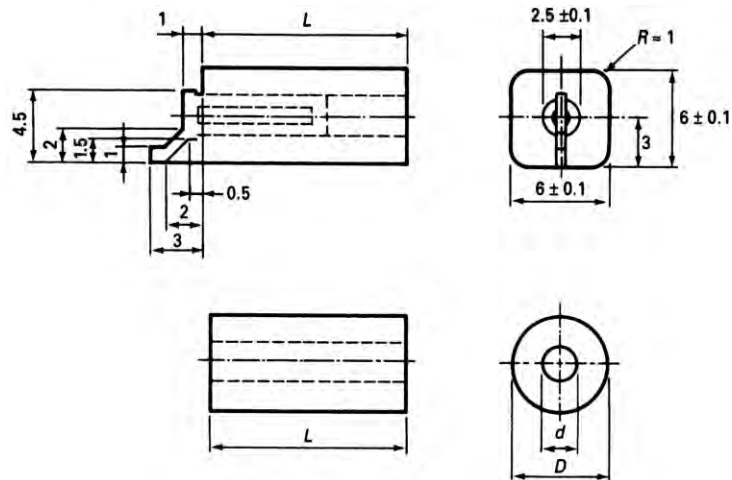
Figure 90: *Figure 4-189 Standard round/square packaging.*

The available material has a dielectric constant of 88 and is recommended for use in the 400- to 1500-MHz range. The next higher frequency range (800 MHz to 2.5 GHz) uses ε of 38, while the top range (1 to 4.5 GHz) uses ε of 21. Given the fact that ceramic resonators are prefabricated and have standard outside dimensions, the following quick calculation applies:

Relative dielectric constant of resonator material	$\varepsilon_r = 21$	$\varepsilon_r = 38$	$\varepsilon_r = 88$
Resonator length in millimeters	$l = \dfrac{16.6}{f}$	$l = \dfrac{12.6}{f}$	$l = \dfrac{8.2}{f}$
Temperature coefficient (ppm/°C)	10	6.5	8.5
Available temperature coefficients	−3 to +12	−3 to +12	−3 to +12
Typical resonator Q	800	500	400

Figure 4-190 shows the schematic of such an oscillator. Figures 4-191 and 4-192 show the simulated and measured phase noise of the ceramic-resonator-based oscillator.
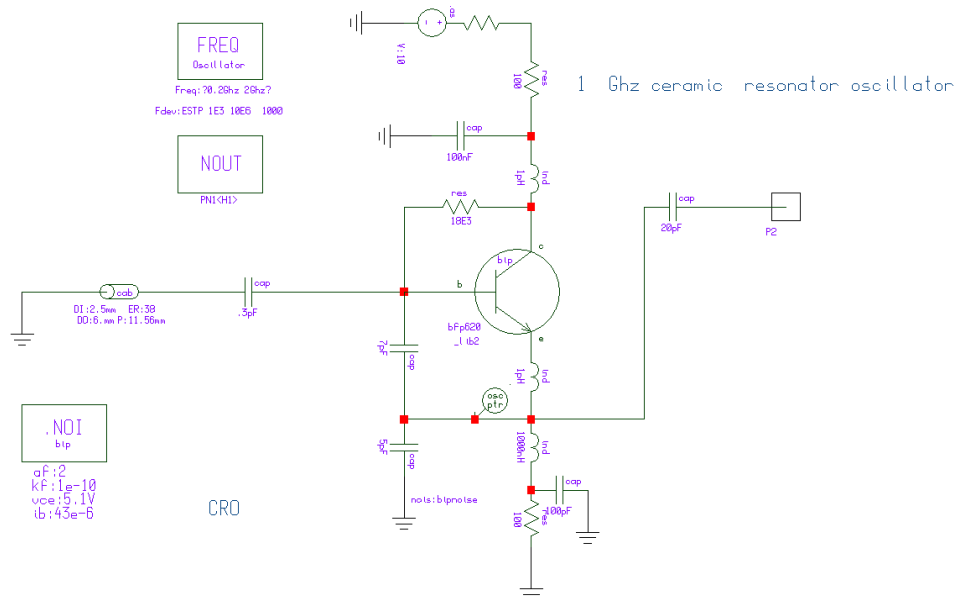
Figure 91: *Figure 4-190 Schematic of the ceramic resonator-based oscillator.*
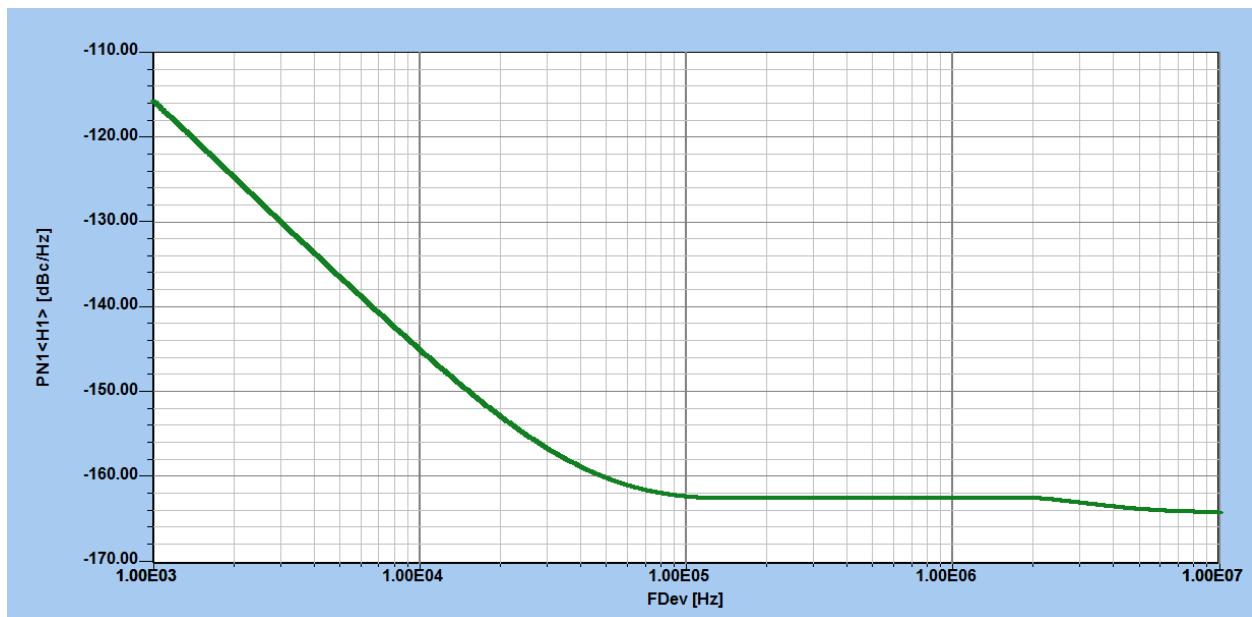
Figure 92: *Figure 4-191: Simulated phase noise of an NPN bipolar 1-GHz ceramic resonator-based oscillator.*
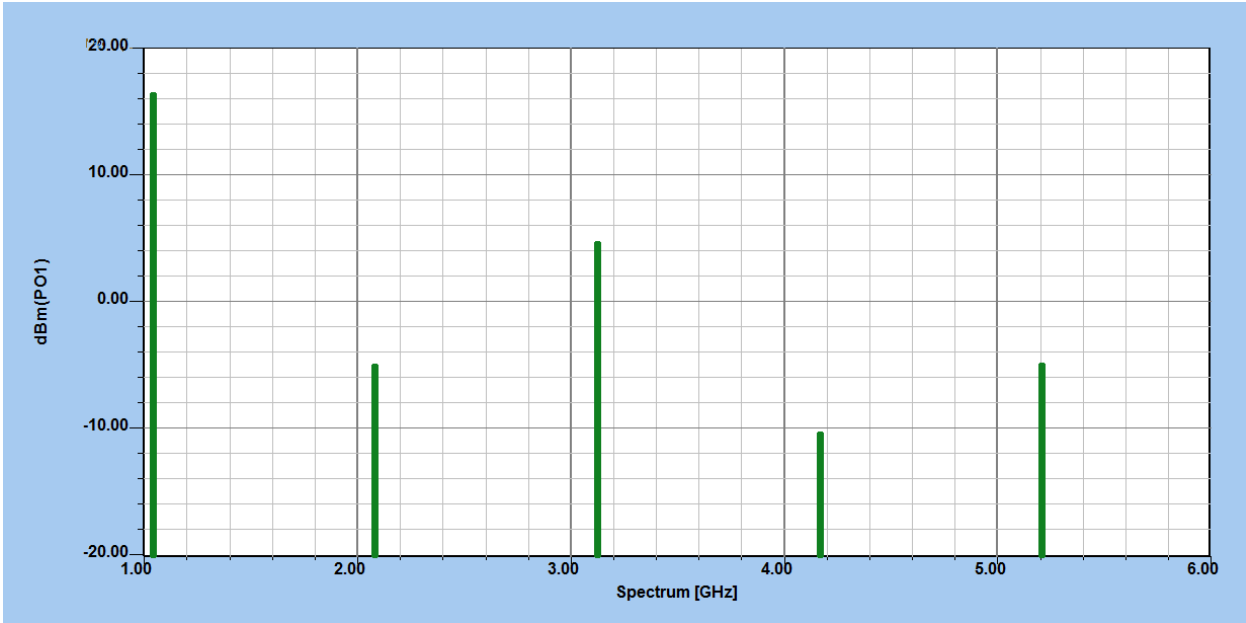
Figure 93: *Simulated output power of an NPN bipolar 1-GHz ceramic resonator-based oscillator*
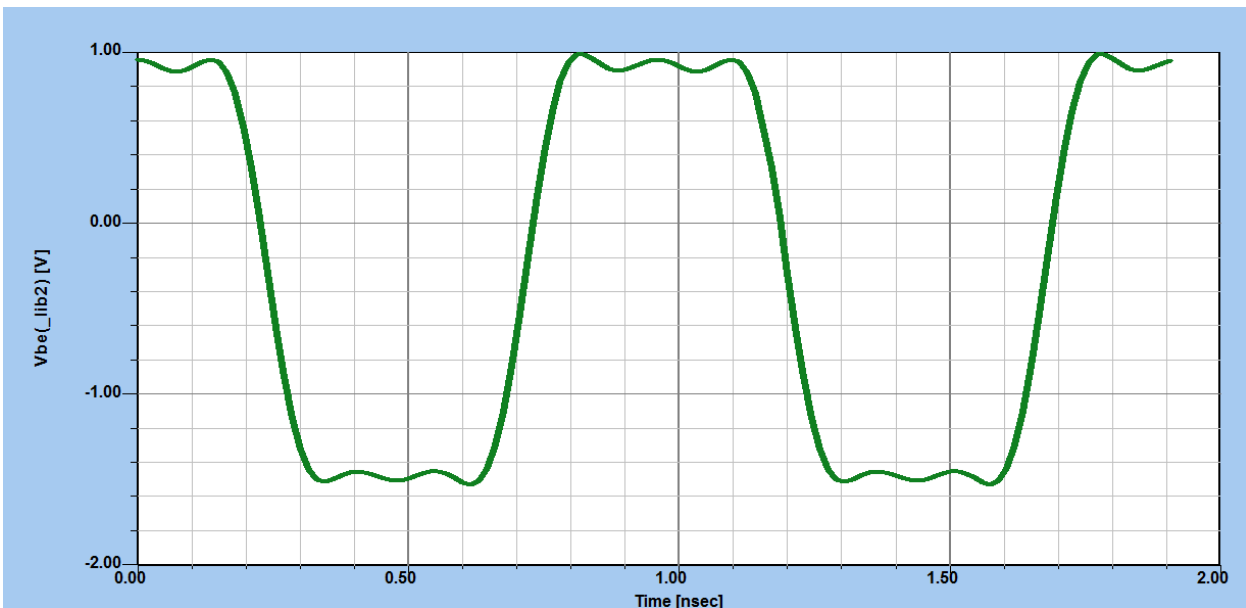
Figure 94: *Figure 4-192: Simulated Vbe voltage of the ceramic resonator-based oscillator.*

By using ceramic-resonator-based oscillators in conjunction with miniature synthesizer chips, it is possible to build extremely small phase-locked loop systems for cellular telephone operation. Figure 4-193 shows one of the smallest available PLL-based synthesizers manufactured by Synergy Microwave Corporation. Because of the high-Q resonator, these types of oscillators exhibit extremely low phase noise. Values of

96

better than 150 dB/Hz, 1 MHz off the carrier, are achievable. The ceramic resonator reduces the sensitivity toward microphonic effects and proximity effects caused by other components.
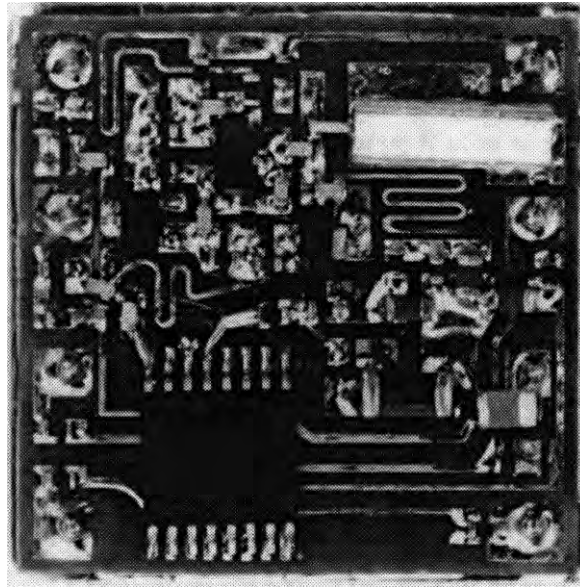
Figure 95: *Looking at the resonator of the oscillator*

➢ **A Novel Tunable Active Spiral Inductor**

All oscillators including the Colpitts Oscillator need both capacitor and inductor and they need to be in resonance at the desired frequency. So far we have made no comments about the inductor, but showed some resonators like the ceramic resonators (quarter wave resonator) or DRO (dielectric resonator based oscillator) but in most cases the inductor is a discrete element. For the use on printed circuits or in integrated circuits, the inductors are typically rectangular wound devices, as shown in the figure below:
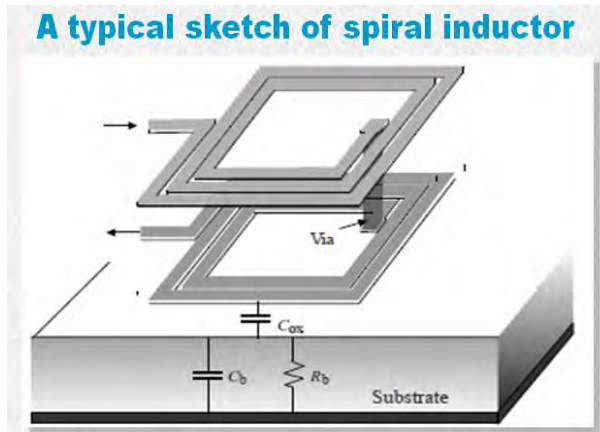
Figure 96: *A Typical Sketch of a Spiral Inductor*

The sketch of the spiral inductor shows the mechanical assembly. One of the tricks is to connect the input and output of the inductor, for the inner connection, an air-bridge is not uncommon. Of course it adds to the inductor value. The real electrical values depend upon the substrate and other manufacturing methods. The following is a detailed lumped model of a spiral inductor.
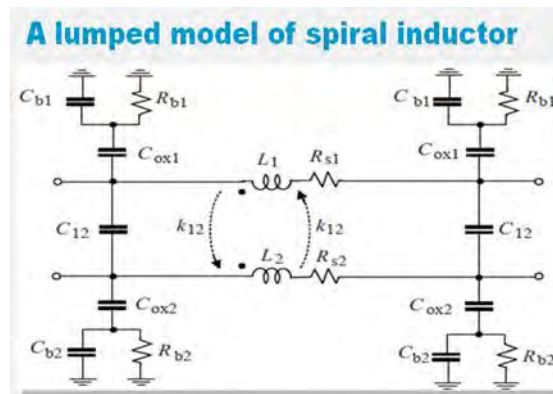
Figure 97: *A Lumped Model of Spiral Inductor*

With today's electromagnetic tools like ANSYS HFSS, or CST Software, a more exact value can be determined. The electromagnetic simulation would look like this fig (xx) shown below:

PASSIVE SPIRAL INDUCTOR BEHAVIOUR
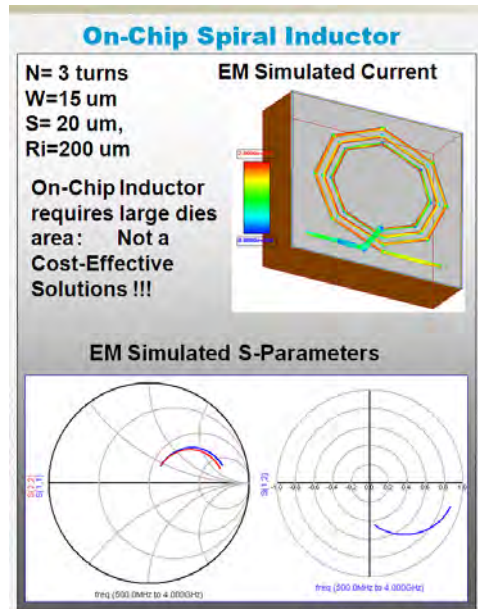
Figure 98: *On Chip Spiral Inductor*

The agreement between the measured S-parameter based and EM-Simulated values is extremely good. However, the physical size of the chip inductor requires a large die area, thus not a cost-effective solution.

➢ INTRODUCING THE GYRATOR:

B. D. H. Tellegen of Philips Research Laboratory proposed a new 2-port network element, a Gyrator in 1948, which exhibits an immittance conversion property, needed to generate a synthesized active inductor using transistors.

$$\begin{bmatrix} i_1 \\ i_2 \end{bmatrix} = \begin{bmatrix} 0 & g \\ -g & 0 \end{bmatrix} \begin{bmatrix} v_1 \\ v_2 \end{bmatrix}$$ Where 'g' is called gyration capacitance.
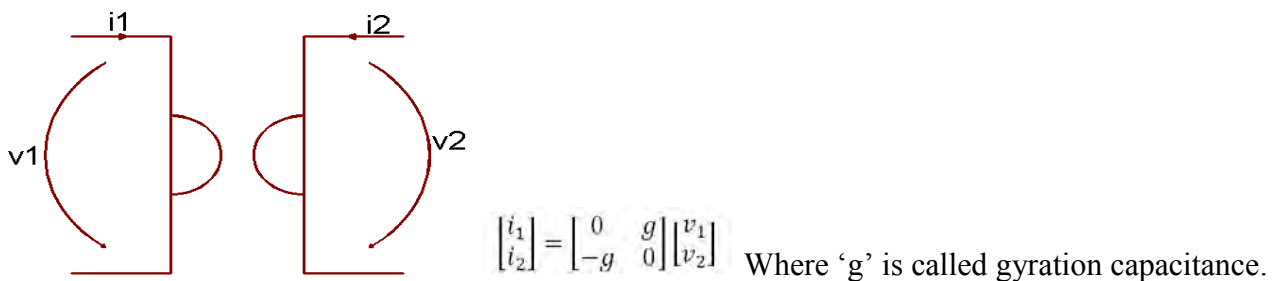
Figure 99: *Explanation of the Gyrator*

An admittance Y connected to the secondary terminals is converted to its dual g^2/Y, this phenomena is called immittance conversion, C transforms into L, parallel tuned circuit into series tuned circuit

We have just seen that the inductor requires a lot of space and is difficult to build. So if we resort to the gyrator, invented by a researcher of Phillips Research Lab, in 1948, we can electronically transform a capacitor into an inductor.

However, we need to ask the question immediately, how about the dynamic range under large signal conditions, the noise contribution of the active circuit and the required DC power? We will get to this soon.

➢ The Active Inductor Using a Gyrator

Tunable Active Inductor (TAI)

- ✓ Integrable and Compact
- ✓ Cost-Effective
- ✓ Power-Efficient Solutions

TAI: Design Challenges

- ✓ High Power Consumption
- ✓ Noise Figure & Instability
- ✓ Low Dynamic Ranges
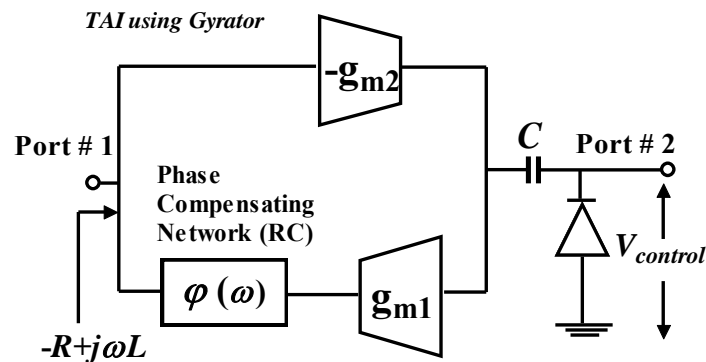
Figure 100: *Tunable Active Inductor (TAI) using Gyrator*

Phase shift network $\varphi(\omega)$ is required in TAI topology for suppressing the higher order modes and self-oscillation

SYNTHESIZED INDUCTOR BEHAVIOUR
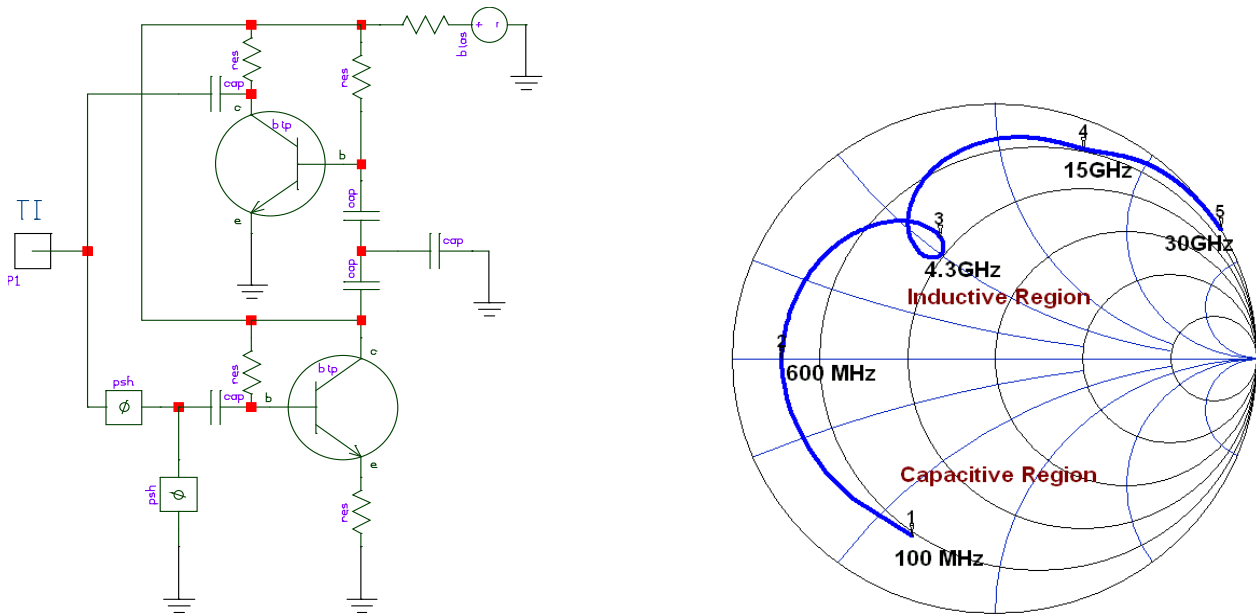
Figure 101: *Typical Schematic of a Synthesized Inductor and Impedance Plot*

Impedance plot reveals the inductive behavior of the circuit from 600MHz (#2) to 30GHz (#5). Care must be taken to avoid the encircling and crossing at 4.3GHz (#3), which limits the applications.

In the case of a mathematics based time domain related prediction in the nonlinear oscillator system the use of Bessel function is helpful.

➢ LAYOUT OF OSCILLATOR UISNG SPIRAL INDUCTOR

➢ **Why use an Active Inductor instead of a Spiral Inductor?**
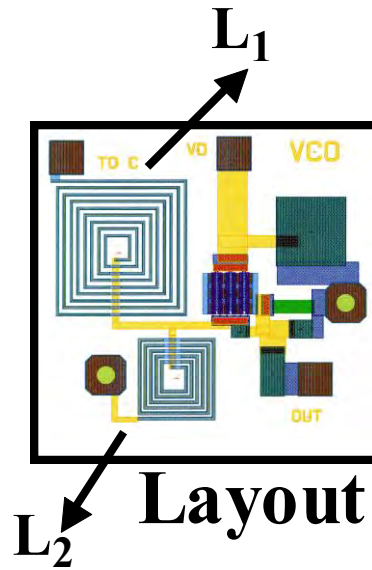
Figure 102: *Layout of a microwave oscillator*
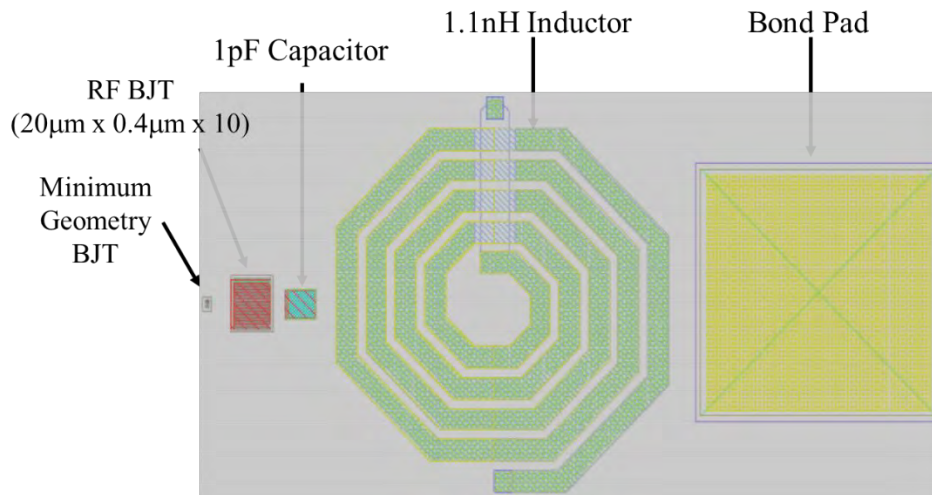
Figure 103: *Physical size of spiral inductor: Drawn to scale - Why we avoid the use of on-chip inductors!*

Passive and Active Inductors

Performances	Passive Inductor (Spiral)	Active Inductor (Simulated: Active Device
Q-factor	Low Q: Q-factor can be improved by differential method but added cost	High Q: active inductor offers higher Q than the passive spiral inductor
Tunability	Fixed/Limited	Large tuning range
Die-Area	Large die-area	Small die-area
Power-Consumption	Zero	Significant: consumes power for generating active inductance, resulting to high Q that may offsets the power consumptions
Linearity	Good Linearity	Poor Linearity: driven under large-signal condition, causing shift in operating point, distortions, and impedance fluctuations
Noise	Superior: good phase noise performance	Poor : poor phase noise performance
EMI	Significant: Due to EM coupling in spiral inductors	EMI insensitive
Floor-Planning	Poor: large die- area makes difficult floor-planning	Not required

Figure 104: *Comparison of Passive and Active Inductors*

➢ INTRODUCTION: ACTIVE INDUCTOR OSCILLATOR

Figure shows the typical Active Inductor Oscillator (AIO), includes a stable active inductor within a conventional integrated LC oscillator
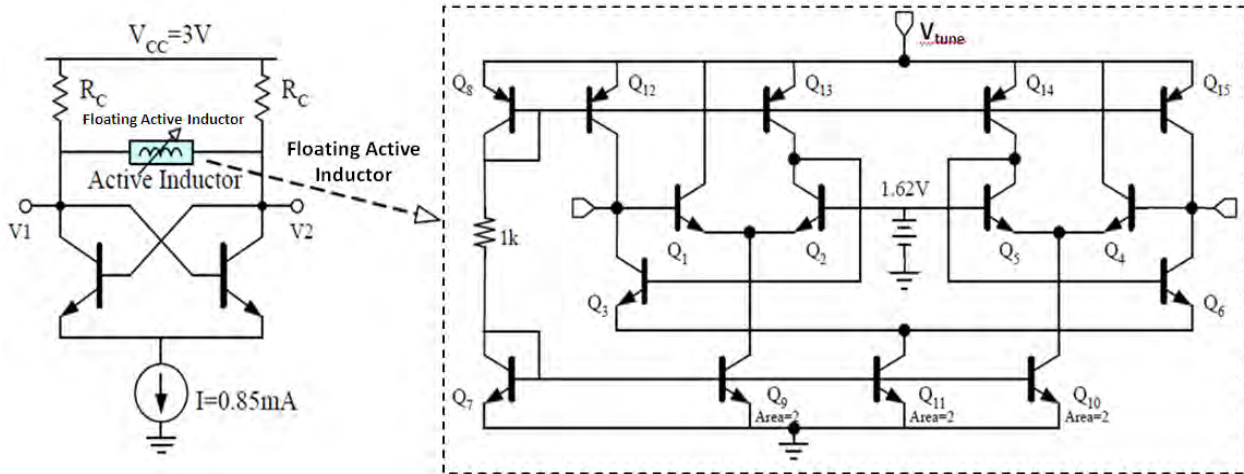
Figure 105: *Typical Active Inductor Oscillator (AIO), includes a stable active inductor within a conventional integrated LC oscillator*

➢ OSCILLATOR PHASE NOISE BASED ON ACTIVE INDUCTOR
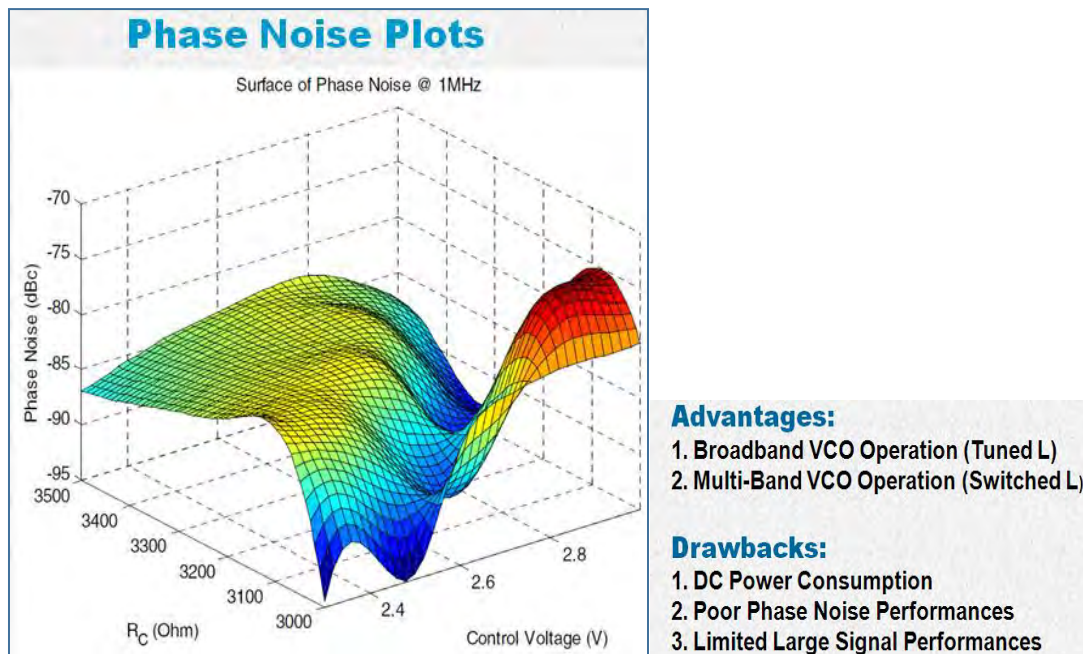
Figure 106: *3-D plots of the Phase Noise of the TAI based oscillator*

➢ SYNTHESIZED INDUCTOR CIRCUITS

SIMULATED TUNBALE INDUCTOR USING SiGe HBT DEVICE
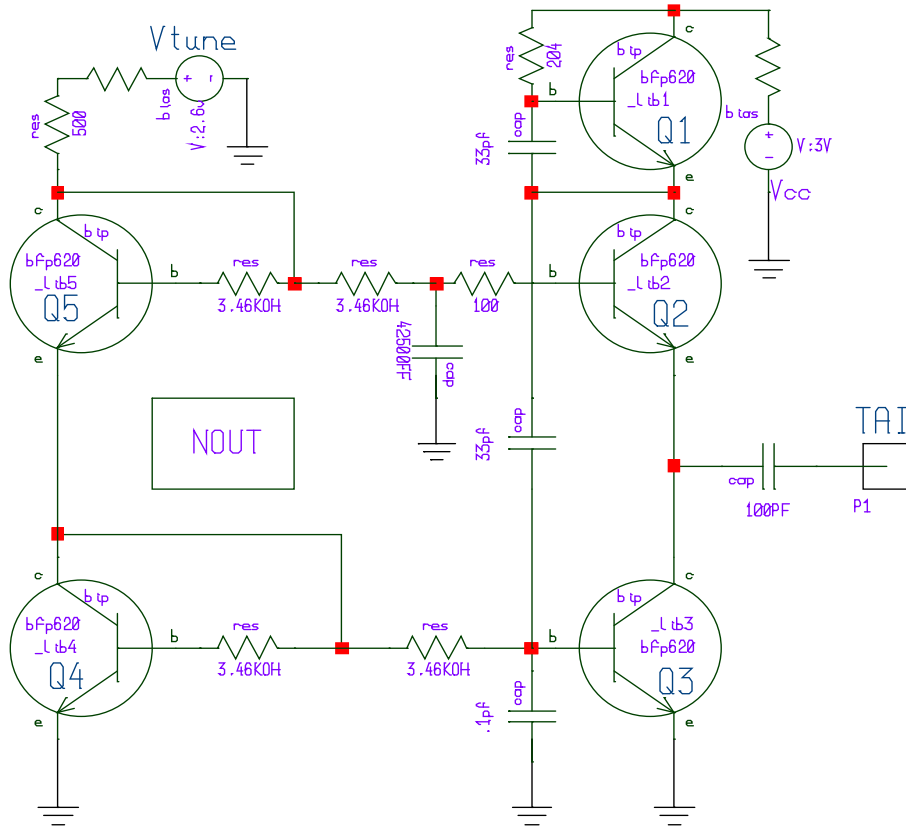
Figure 107: *Schematic of a transistorized inductor using SiGe HBT (BFP 620) from Infineon*

This Figure shows a schematic of a transistorized inductor using SiGe HBT (BFP 620) from Infineon. The reason for using a high cut-off frequency (f_t=75 GHz) SiGe HBT transistor is to minimize the package parasitic effects and allow comparative evaluations of the 1.9 GHz varactor-tuned and synthesized inductor-tuned LC oscillator using discrete components for experimental validations!

The plot in the Figure-108 below shows the typical plot of reactance and equivalent loss resistance of the synthesized inductor using high cut-off frequency (f_t=75 GHz) SiGe HBTs.
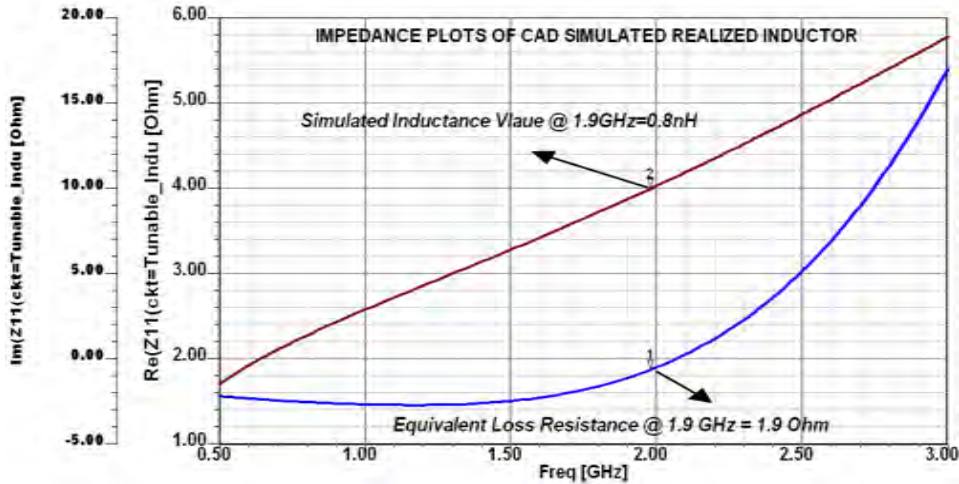
Figure 108: *Impedance plots of the CAD simulated realized inductor*

As shown in Figure 108 the value of the realized inductance and associated equivalent loss resistance are 0.8nH and 1.9Ω at 1.9 GHz for the operating DC bias condition (3V, 1.8mA) and V_{tune} (2.5V). The operating DC bias and V_{tune} are adjusted in such a way that the realized equivalent noise resistance must be positive to avoid the multi-mode oscillations caused by the regenerative effect (if the simulated loss resistance associated with realized inductor has a negative value).

SIMULATED OSCILLATOR PHASE NOISE PLOTS
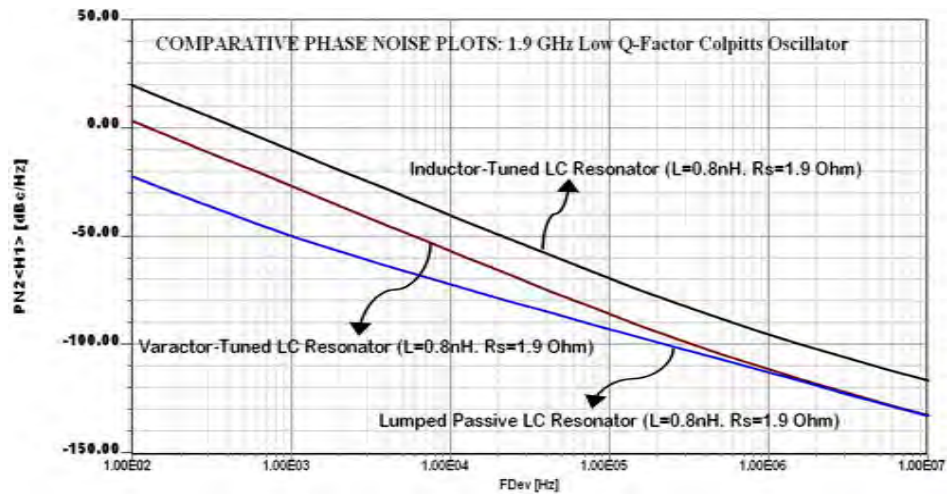
Figure 109: *This plot shows the comparative phase noise plots for the LC Colpitts oscillator using the lumped LC resonator, the varactor-tuned lumped LC resonator and the synthesized inductor-tuned resonator network for identical inductance value and loss resistance (0.8 nH with series loss resistance 1.9Ω).*

106

ACTIVE INDUCTOR NOISE

Circuit that transforms a capacitor into an inductor and identifies the noise
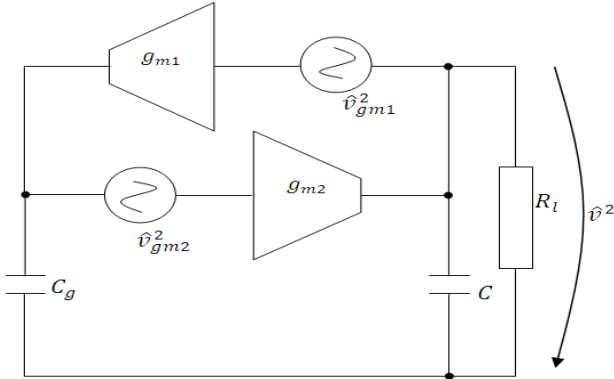
A simplified circuit of active inductor resonator with noise
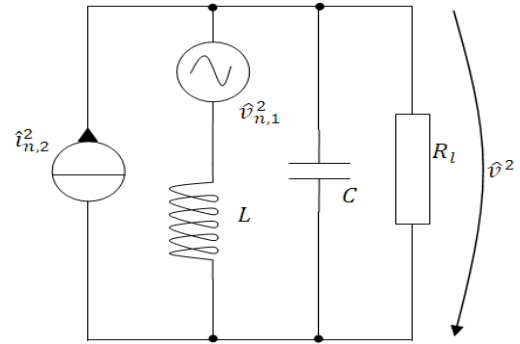
$$\hat{v}_{n,1}^2 = \hat{v}_{gm1}^2 \cong \frac{4kT\lambda}{g_m}$$

$$\hat{i}_{n,2}^2 = \hat{g}_{gm2}^2 \hat{v}_{gm2}^2 = 4kT\lambda g_m$$

V_{gm1} and V_{gm2} are the equivalent noise voltages generated by the transconductances of the Gyrators

Figure 110: *Circuit transforming a capacitor into an inductor, and considering the noise*
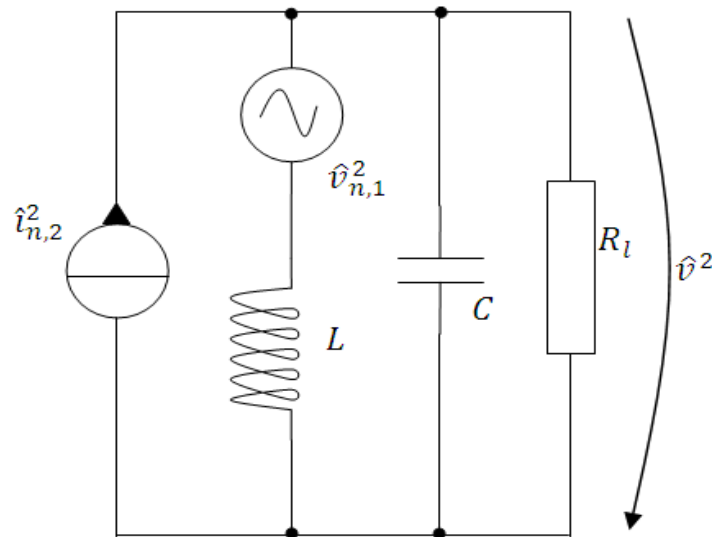
Figure 111: *Final equivalent circuit of the active inductor*

Since the following applies,

$$\hat{v}_n^2 \cong 4kTr_n|R|, \quad \hat{i}_n^2 \cong 4kTg_n|G|$$

where R and G are the negative resistance and conductance values, and the coefficients r_n and g_n are frequency dependent relative noise resistance and conductance (these give a comparative value of how much noise the active negative resistor produces compared to a passive resistor of the same value).

The total noise spectral density in voltage squared, of the active inductor resonator is

$$\hat{v}^2 = \frac{\hat{v}_{gm1}^2 + \hat{v}_{gm2}^2 g_{m2}^2 \omega^2 L^2}{\omega^2 L^2 G_l^2 + (\omega^2 LC - 1)^2} \Longrightarrow \hat{v}^2|_{\omega \to \omega_0} = Q_l^2 \left(\hat{v}_{gm1}^2 + g_{m2}^2 \hat{v}_{gm2}^2 \omega^2 L^2 \right) = 4kT\lambda Q_l^2 \left(\frac{1}{g_{m1}} + \frac{g_{m2}}{\omega_0^2 C^2} \right)$$

The time average Q-factor of active inductor is

$$\frac{\omega_0(1 + r_n, g_n)}{\lambda g_{m2} \left(\frac{1}{C} + \frac{1}{C_g} \right)}$$

The time average normalized noise power of an active inductor resonator can be determined by

$$\overline{v^2} = \int_0^\infty \hat{v}^2 df = \frac{\hat{v}_{gm1}^2}{2\pi} \omega_o \int_0^\infty \frac{d\omega}{[(\omega^2 LC - 1)^2 + \omega^2 L^2 G_l^2]} + \frac{\hat{g}_{gm2}^2 \hat{v}_{gm2}^2}{2\pi} \int_0^\infty \frac{\omega^2 L^2 d\omega}{[(\omega^2 LC - 1)^2 + \omega^2 L^2 G_l^2]}$$

$$\overline{v^2} \approx \frac{kT\lambda}{C} Q_l \left(\frac{g_{m2}}{g_{m1}} \right)^{1/2} \left[\left(\frac{C_g}{C} \right)^{1/2} + \left(\frac{C}{C_g} \right)^{1/2} \right] = \frac{kT\lambda}{C} Q_l \frac{\omega_o}{g_{m1}} (C + C_g)$$
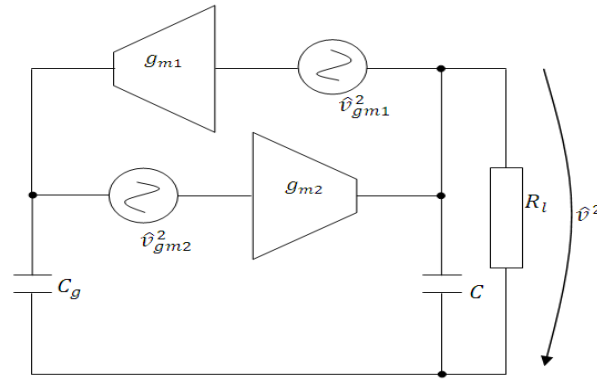
Figure 112: *Equivalent circuit of the oscillator using an active inductor*

➢ PHASE NOISE CONTRIBUTION OF THE VARIOUS PARTS OF THE OSCILLATOR USING AN ACTIVE INDUCTOR
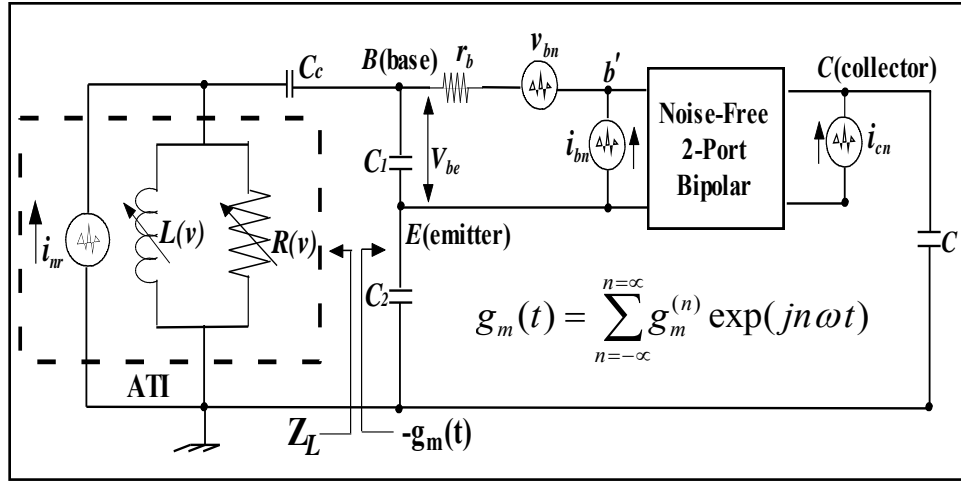
Figure 113: *Noise contributions of the active inductor*

The total noise voltage power within 1 Hz bandwidth can be described by

$$\left|\overline{e_n^2(\omega)}\right|_{\omega=\omega_0} = \overline{[e_n^2(\omega_0)]}_{-gm1} + \overline{[e_n^2(\omega_0)]}_{-gm2}$$

The first term is related to the active inductor noise due to the active inductor and the second term is related to negative resistance generative active device.

After some lengthy calculations and minimal approximations, adding shot noise, flicker noise and the loss resistor, the equivalent expression of the phase noise turns out to be

$$\left|\overline{e_{gm2}^2(\omega)}\right|_{\omega=\omega_0} = [4kTR] + \left[\frac{4qI_{c0}g_{m2}^2 + \dfrac{4K_f I_b^{AF}}{\omega}g_{m2}^2}{\omega_0^2 C_1^2[\omega_0^2(\beta^+)^2 C_2^2 + g_{m2}^2\dfrac{C_2^2}{C_1^2}]}\right]$$

$$g_{m2} = [Y_{21}^+]\left[\frac{C_1}{C_2}\right]^q$$

$$\beta^+ = \left[\frac{Y_{21}^+}{Y_{11}^+}\right]\left[\frac{C_1}{C_2}\right]^p$$

[4kTR] is the thermal noise of the resonator.

$$g_m(t) = \sum_{n=-\infty}^{n=\infty} g_m^{(n)} \exp(jn\omega t)$$

$$L(\omega) = 10 \times \log\left[\left[k_0 + \left(\frac{k^3 k_1 \left[\dfrac{Y_{21}^+}{Y_{11}^+}\right]^2 [y]^{2p}}{[Y_{21}^+]^3 [y]^{3q}}\right)\left(\frac{1}{(y^2+k)}\right)\right]\left[\frac{[1+y]^2}{y^2}\right]\right]$$

109

$$k_0 = \frac{kTR}{\omega^2 \, \omega_0^2 C_2^2 L_{active-inductor}^2 V_{cc}^2}$$

$$k_1 = \frac{qI_c g_{m2}^2 + \frac{K_f I_b^{AF}}{4\omega} g_{m2}^2}{\omega^2 \, \omega_0^4 L_{active-inductor}^2 V_{cc}^2}$$

$$k_2 = \omega_0^4 (\beta^+)^2$$

$$k_3 = \omega_0^2 g_{m2}^2$$

$$k = \frac{k_3}{k_2 C_2^2}$$

$$L_{active-inductor} = \frac{C_1 C_2}{[C_1 + C_2] g_{m1}^2}$$

$$g_m(t) = \sum_{n=-\infty}^{n=\infty} g_m^{(n)} \exp(jn\omega t)$$

$$g_{m2} = [Y_{21}^+] \left[\frac{C_1}{C_2}\right]^q$$

$$\beta^+ = \left[\frac{Y_{21}^+}{Y_{11}^+}\right] \left[\frac{C_1}{C_2}\right]^p$$

$$y = \frac{C_1}{C_2}$$

The values of p and q depend upon the drive level.

Figure 114: *Schematic of self-injection-locked inductor-tuned Colpitts oscillator realized by incorporating phase shifter network in the feedback path*

This Figure 114, shows the schematic of self-injection-locked inductor-tuned Colpitts oscillator realized by incorporating phase shifter network in the feedback path, which improves the $1/f$ noise, including linearization of the large signal drive-level characteristics of the synthesized inductor circuits. Injection locked oscillators are frequently used to reduce the wideband noise. The oscillator's tuned-circuit based

on its Q reduces the far out noise, while up-multiplication makes the noise worse. A variation of the injection locked oscillator is the self-injection, which improves the phase noise further.

CAD simulated phase noise plot:
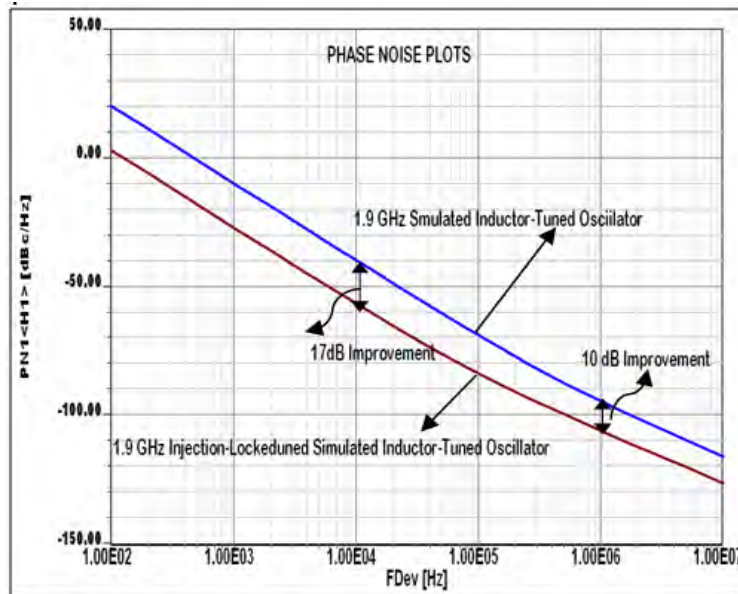
Figure 115: *CAD simulated phase noise (WITH AND WITHOUT INJECTION LOCKING)*

Figure shows the CAD simulated (WITH AND WITHOUT INJECTION LOCKING)

The figure above shows the noise improvement simulation based on injection locking which close-in has a 17dB improvement, while further out at 1MHz offset, shows 10dB improvement, and below is the measured phase noise plot of injection locked 1.9 GHz Tunable Active Inductor (TAI). As shown in Figure XX, injection-locking improves the phase noise performance by 8-10 dB, including the locking range**.**

Measured phase noise plot (Injection-Locked)
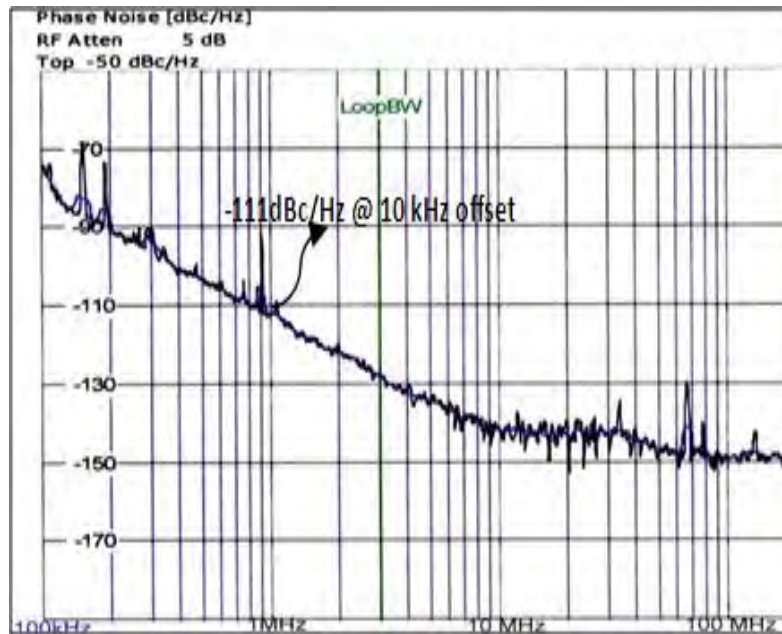
Figure 116: *Measured Phase Noise of the …..*

➢ SUMMARY – Tunable Active Inductors

This research work demonstrates the state-of-the-art in designing the novel tunable inductor based VCO (voltage controlled oscillator) circuits presented in my dissertation to obtain the Habilitation Status of "Dr.-Ing. habil." presented to the Faculty 3: Mechanical engineering, Electrical engineering and industrial engineering, Brandenburg University of Technology Cottbus, Germany

- ✓ Use of TAI (Tunable Active Inductor) resonator is relatively new and its application to replace tuning diodes in VCO (voltage controlled oscillator) have recently begun to be explored
- ✓ Closed form noise models for TAI VCOs involved complex mathematical treatment due to the convergence problems at large drive-level
- ✓ Limitation in the dynamic range may restricts the applications in high performance tunable filters, nevertheless by incorporating my novel techniques one can improve the dynamic range up to an accepted limit
- ✓ The behavior of the TAI (Tunable Active Inductor) oscillator was studied and verified with practical examples.

- ✓ Intensive studies were conducted to find the optimum configuration for the improvement in the phase noise over the tuning range, and a US Patent application was filed.

- ✓ The extension of the research work is to increase the tuning range and dynamic range by employing injection mode coupling and noise cancellation techniques in monolithic IC technology.

- ✓ I expect to see continued research in this field and the use of TAI (Tunable Active Inductor) components as a cost-effective alternative of tuning diodes (Varactor) as a tuning element in filter, resonator, antenna matching network and phase shifter for the applications in concurrent and configurable RF & MW modules/systems.

➢ The Modern Time-Domain Behavior of an Oscillator

The following is a detailed mathematical analysis of the time-domain behavior of oscillators, intended as a stand-alone mathematical derivation. It was developed between Prof. Rizzoli and team from the University of Bologna, Rowan Gilmore and Prof. Fred Rosenbaum from the University of Washington, St. Louise, and my team at Compact Software, where we introduced the world's first harmonic balance mathematics based simulator, that could handle nonlinear noise in amplifiers, frequency doublers, mixers and finally oscillators.

The semiconductor noise contribution for the various devices was fairly challenging, and validated.

The large-signal transfer characteristic affecting the current and voltage of an active device in an oscillator circuit is nonlinear. It limits the amplitude of the oscillation and produces harmonic content in the output signal. The resonant circuit and resulting phase shift sets the oscillation frequency. The nonlinear, exponential relationship between the voltage and current of a bipolar transistor is given as

$$i(t) = I_s e^{\frac{qv(t)}{kT}}$$

(6-82)

I_s is device saturation current, $v(t)$ is the voltage drive applied across the junction, k is Boltzman's constant, q is the electronic charge, and T is the temperature of the device in Kelvins. The bipolar case is mathematically more complex than the FET case. For the FET a similar set of equations exist which can be derived. Since most RFIC's now use SiGe bipolar transistors, the bipolar case has been selected.

The voltage $v(t)$ across the base-emitter junction consists of a DC component and a driven signal voltage $V_1 \cos(wt)$. It can be expressed as

$$v(t) = V_{dc} + V_1 \cos(wt) \qquad\qquad (6\text{-}83)$$

As the driven voltage $V_1 \cos(wt)$ increases and develops enough amplitude across the base-emitter junction, the resulting current is a periodic series of pulses whose amplitude depends on the nonlinear characteristics of the device and is given as

$$i_e(t) = I_s e^{\frac{qv(t)}{kT}} \qquad\qquad (6\text{-}84)$$

$$i_e(t) = I_s e^{\frac{qV_{dc}}{kT}} e^{\frac{qV_1 \cos(wt)}{kT}} \qquad\qquad (6\text{-}85)$$

$$i_e(t) = I_s e^{\frac{qV_{dc}}{kT}} e^{x\cos(wt)} \qquad\qquad (6\text{-}86)$$

assuming $I_c \approx I_e$ ($\beta > 10$)

$$x = \frac{V_1}{(kT/q)} = \frac{qV_1}{kT} \qquad\qquad (6\text{-}87)$$

$i_e(t)$ is the emitter current and x is the drive level which is normalized to kT/q.

From the Fourier series expansion, $e^{x\cos(wt)}$ is expressed as

$$e^{x\cos(wt)} = \sum_n a_n(x)\cos(nwt) \qquad\qquad (6\text{-}88)$$

$a_n(x)$ is a Fourier coefficient and given as

$$a_0(x)\big|_{n=0} = \frac{1}{2\pi} \int_0^{2\pi} e^{x\cos(wt)} d(wt) = I_0(x)$$

(6-89)

$$a_n(x)\big|_{n>0} = \frac{1}{2\pi} \int_0^{2\pi} e^{x\cos(wt)} \cos(nwt) d(wt) = I_n(x)$$

(6-90)

$$e^{x\cos(wt)} = \sum_n a_n(x)\cos(nwt) = I_0(x) + \sum_1^{\infty} I_n(x)\cos(nwt)$$

(6-91)

$I_n(x)$ is the modified Bessel function.

$$\text{As } x \to 0 \Rightarrow I_n(x) \to \frac{(x/2)^n}{n!}$$

(6-92)

$I_0(x)$ are monotonic functions having positive values for $x \geq 0$ and $n \geq 0$; $I_0(0)$ is unity, whereas all higher order functions start at zero.

The short current pulses are generated from the growing large-signal drive level across the base-emitter junction, which leads to strong harmonic generation. The emitter current represented above can be expressed in terms of harmonics as

$$i_e(t) = I_s e^{\frac{qV_{dc}}{kT}} I_0(x) \left[1 + 2\sum_1^{\infty} \frac{I_n(x)}{I_0(x)} \cos(nwt) \right]$$

(6-93)

$$I_{dc} = I_s e^{\frac{qV_{dc}}{kT}} I_0(x) \qquad\qquad (6\text{-}94)$$

$$V_{dc} = \frac{kT}{q} \ln\left[\frac{I_{dc}}{I_s I_0(x)}\right] \Rightarrow \frac{kT}{q} \ln\left[\frac{I_{dc}}{I_s}\right] + \frac{kT}{q} \ln\left[\frac{1}{I_0(x)}\right] \qquad\qquad (6\text{-}95)$$

I_s = collector saturation current

$$V_{dc} = V_{dcQ} - \frac{kT}{q} \ln I_0(x) \qquad\qquad (6\text{-}96)$$

$$i_e(t) = I_{dc}\left[1 + 2\sum_1^\infty \frac{I_n(x)}{I_0(x)} \cos(nwt)\right] \qquad\qquad (6\text{-}97)$$

V_{dcQ} and I_{dc} are the operating DC bias voltage and the DC value of the emitter current. Furthermore, the Fourier transform of $i_e(t)$, a current pulse or series of pulses in the time domain yields a number of frequency harmonics common in oscillator circuit designs using nonlinear devices.

The peak amplitude of the output current, the harmonic content defined as $\left[\dfrac{I_N(x)}{I_1(x)}\right]$, and the DC offset voltage are calculated analytically in terms of the drive level, as shown in Table 6-1. It gives good insight of the nonlinearities involved in the oscillator design.

Table 6-1 For T=300 K, data are generated at a different drive–level.

Drive level [x]	Drive-Voltage $\frac{kT}{q}$*x] mV	Offset-Coefficient ln[I₀(x)]	DC-Offset $\frac{kT}{q}[\ln I_0(x)]$ mV	Fundamental Current 2[I₁(x)/I₀(x)]	Second-Harmonic [I₂(x)/I₁(x)]
0.00	0.000	0.000	0.000	0.000	0.000
0.50	13.00	0.062	1.612	0.485	0.124
1.00	26.00	0.236	6.136	0.893	0.240
2.00	52.00	0.823	21.398	1.396	0.433
3.00	78.00	1.585	41.210	1.620	0.568
4.00	104.00	2.425	63.050	1.737	0.658
5.00	130.00	3.305	85.800	1.787	0.719
6.00	156.00	4.208	206.180	1.825	0.762
7.00	182.00	5.127	330.980	1.851	0.794
8.00	208.00	6.058	459.600	1.870	0.819
9.00	234.00	6.997	181.922	1.885	0.835
10.00	260.00	7.943	206.518	1.897	0.854
15.00	390.00	12.736	331.136	1.932	0.902
20.00	520.00	17.590	457.340	1.949	0.926

From the table above, the peak current 2[I₁(x)/I₀(x)] in column 5 approaches 1.897I$_{dc}$ for a drive level ratio x=10.

for T=300K, $\frac{kT}{q} = 26mV$ (6-98)

and $V_1 = 260mV$ for x=10   (6-99)

The second harmonic-distortion [63] $\dfrac{I_2(x)}{I_1(x)}$ is 85% for a normalized drive level of x=10 and the

corresponding DC offset is 205.518mV. When referring to the amplitude, x is always meant as

normalized to $\dfrac{kT}{q}$. Figure 6-10 is generated with the help of Math-CAD, and shows the plot of the

normalized fundamental and second harmonic current with respect to the drive level.
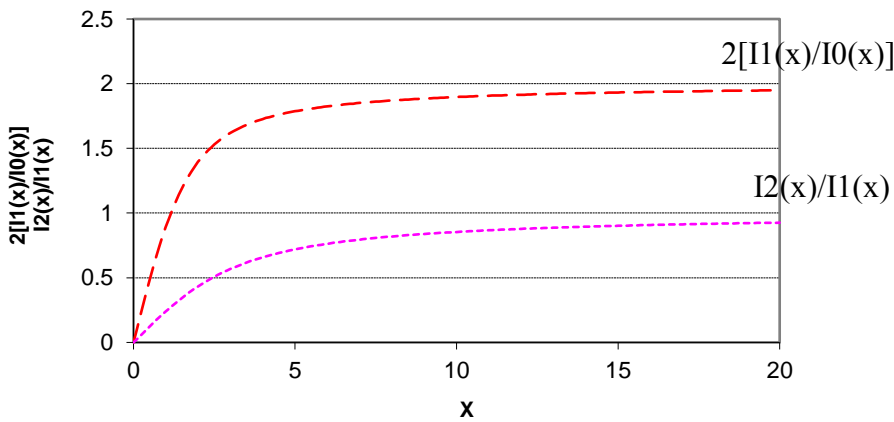
Figure 117: *Figure 6-10   Plot of the normalized fundamental current 2I₁(x)/I₀(x) and second harmonic I₂(x)/I₁(x) with respect to the drive level x.*

One can notice that as the drive level x increases, the fundamental 2I₁(x)/I₀(x) and harmonic I₂(x)/I₁(x)

increases monotonically. Figure 6-11 shows the plot of the coefficient of offset $[\ln I_0(x)]$ with respect to

drive level x so that the DC offset voltage can be calculated at different temperatures by simply

multiplying the factor $\dfrac{kT}{q}$ [61].
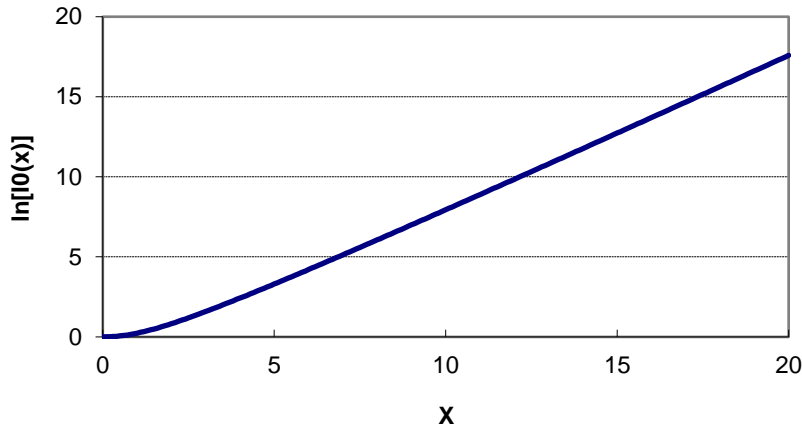
Figure 118: **Figure 6-11 Plot of** $[\ln I_0(x)]$ **Vs drive level X.**

At T= 300K the DC voltage shift is $-26[\ln I_0(x)]mV$

for x=10   (6-100)

$$V_{dc} = V_{dcQ} - \frac{kT}{q}\ln I_0(x)$$

$$V_{dc-offset} = \frac{kT}{q}\ln I_0(x) = 206mV \qquad (6\text{-}102)$$

V_{dcQ} and $V_{dc-offset}$ are the operating bias points and DC offsets due to an increase in the drive level. The DC voltage shift at x=10 is 206mV. Figure 6-12 shows the shape of the output current with respect to the drive level and demonstrates that as the drive level increases, the output current pulse width becomes shorter and the peak current amplitude becomes greater.

$i_e(t)\big|_{x=10} \to 0$, For conduction angle $\geq 60^0$ (6-103)

$i_e(t)\big|_{x=5} \to 0$, For conduction angle $\geq 90^0$ (6-104)

$i_e(t)\big|_{x=2} \to 0$, For conduction angle $>180^0$ (6-105)

The harmonic content trade-off is an important consideration in reducing the noise content by using shorter current pulses [64-67].
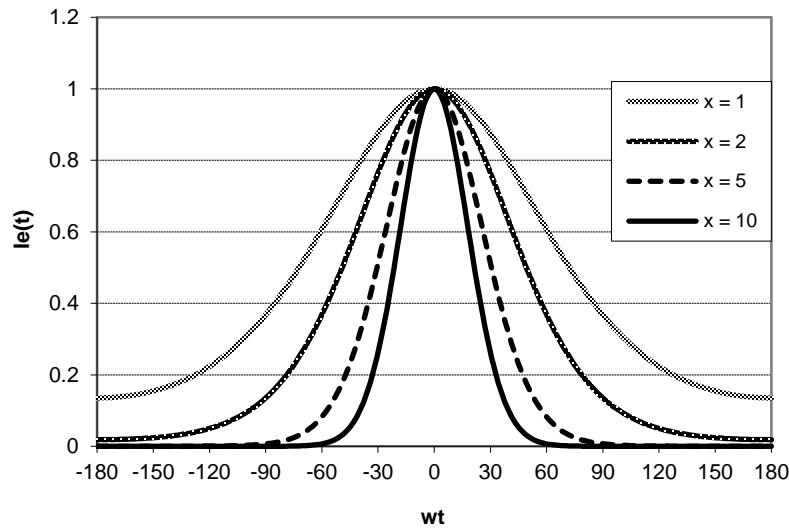
Figure 119: *Figure 6-12 Plot of current with respect to conduction angle- (wt) and drive level X.*

The bipolar transistor is represented by a current source and an input conductance at the emitter for easier analysis of the reactance transformation. For easier calculation of the capacitive transformation factor n, the oscillator circuit is rearranged as shown in Figure 6-15 [68].
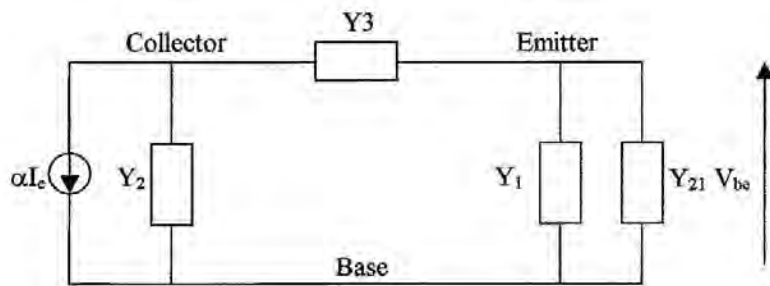
Figure 120: *Figure 6-15 Equivalent oscillator circuit for the analysis of the transformed conductance seen by the current source.*

αI_e and Y_{21} are the current source and large-signal transconductance of the device given by the ratio of the fundamental-frequency component of the current to the fundamental-frequency of the drive voltage.

$$Y_{21} = \frac{I_{1\,peak}}{V_{1\,peak}}\bigg|_{fundamental-frequency} \tag{6-112}$$

$$I_1\big|_{n=1} = I_{dc}\left[1 + 2\sum_1^\infty \frac{I_1(x)}{I_0(x)}\cos(wt)\right] \Rightarrow I_{1\,peak} = 2I_{dc}\frac{I_1(x)}{I_0(x)} \tag{6-113}$$

x = normalized drive level from (6-87)

$$V_1\big|_{peak} = \frac{kT}{q}x \tag{6-114}$$

$$Y_{21}\big|_{l\,arg\,e-signal} = G_m(x) \tag{6-115}$$

$$Y_{21}\big|_{small-signal} = \frac{I_{dc}}{kT/q}\bigg| = g_m \tag{6-116}$$

$$Y_{21}\big|_{l\,arg\,e-signal} = G_m(x) = \frac{qI_{dc}}{kTx}\left[\frac{2I_1(x)}{I_0(x)}\right]_{n=1} = \frac{g_m}{x}\left[\frac{2I_1(x)}{I_0(x)}\right]_{n=1} \tag{6-117}$$

$$\frac{[Y_{21}\big|_{l\,arg\,e-signal}]_{n=1}}{[Y_{21}\big|_{small-signal}]_{n=1}} = \frac{G_m(x)}{g_m} \Rightarrow \frac{2I_1(x)}{xI_0(x)} \tag{6-118}$$

$$|Y_{21}|_{small-signal} > |Y_{21}|_{l\,arg\,e-signal} \Rightarrow g_m > G_m(x)$$

Connected from collector to base, will see a total conductance G_{total}. The oscillator circuit with passive component parameters is shown in Figure 6-17.
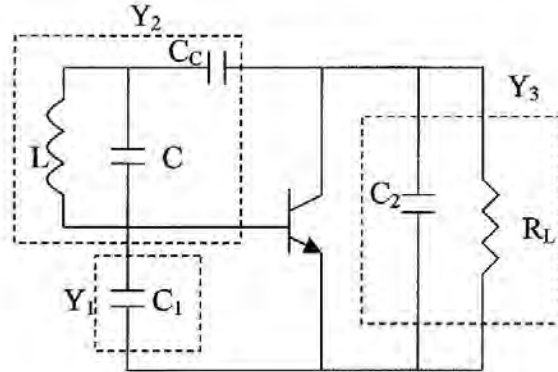
Figure 121: *Figure 6-17   Oscillator circuit with the passive components Y_1, Y_2, and Y_3. The equivalent circuit is shown in Figure 8-12.*

where

$$Y_1 = G_1 + jB_1 \Rightarrow j\omega C_1 \text{ For } G_1 = 0 \tag{6-120}$$

$$Y_2 = G_2 + jB_2 \Rightarrow G_2 + j\left[\frac{(\omega^2 LC - 1)\omega C_c}{\omega^2 L(C_c + C) - 1}\right];$$

G_2 = loss parameter/load conductance of the resonator connected parallel to the resonator component C_1, C_2 and L, respectively.

$$Y_3 = G_3 + jB_3 \Rightarrow G_3 + j\omega C_2;$$

G_3 = conductance of the bias resistor placed across C_2, $1/R_L$ in Figure 6-17.

The large-signal transconductances Y_{21} and G_1 are transformed to the current source through the voltage divider $\dfrac{V_{eb}}{V_{cb}}$. The voltage V_{eb} must be added to V_{ce} to calculate the transformation ratio, which can be written as

$$\frac{V_{eb}}{V_{cb}} = \frac{C_2}{C_1 + C_2} = \frac{1}{n} \qquad\qquad (6\text{-}121)$$

and

$$\frac{V_{ce}}{V_{cb}} = \frac{C_1}{C_1 + C_2} = \frac{n-1}{n} \qquad\qquad (6\text{-}122)$$

The conductance G_2 is already in parallel with the current source so it remains unchanged. The factor n represents the ratio of the collector-base voltage to the emitter-base voltage at the oscillator resonance frequency.

$$G_1 \to \frac{G_1}{n^2} \qquad\qquad (6\text{-}123)$$

$$Y_{21} \to \frac{Y_{21}}{n^2} \Rightarrow \frac{G_m}{n^2} \qquad\qquad (6\text{-}124)$$

$$G_3 \to \left[\frac{n-1}{n}\right]^2 G_3 \qquad\qquad (6\text{-}125)$$

G_2 remains constant

The transformed conductance is proportional to the square of the voltage ratios given in Equations (6-121) and (6-122), producing a total conductance as seen by the current source at resonance as

$$G_{total} = G_2 + \frac{G_m + G_1}{n^2} + \left[\frac{n-1}{n}\right]^2 G_3 \qquad (6\text{-}126)$$

For sustained oscillation, the closed loop gain at resonance is given as

$$\left[\frac{\left(\dfrac{V_{be}Y_{21}\alpha}{nG_{total}}\right)}{V_{be}}\right] = 1 \Rightarrow nG_{total} = Y_{21}\alpha \qquad (6\text{-}127)$$

$$\frac{Y_{21}}{nG_{total}} = \frac{1}{\alpha} \Rightarrow \frac{Y_{21}}{nG_{total}} > 1 \qquad (6\text{-}128)$$

α is assumed to be 0.98 and variation in the value of α, does not influence the expression above greatly. Rearranging the device conductance and circuit conductance, the general oscillator equation, after multiplying (6-126) with n on both sides, is written as

$$nG_{total} = n\left[G_2 + \frac{Y_{21} + G_1}{n^2} + \left(\frac{n-1}{n}\right)^2 G_3\right] \qquad (6\text{-}129)$$

$$Y_{21}\alpha = n\left[G_2 + \frac{Y_{21} + G_1}{n^2} + \left(\frac{n-1}{n}\right)^2 G_3\right] \Rightarrow \left[\frac{-(1-n\alpha)}{n^2}\right]Y_{21} = \left[G_2 + \frac{G_1}{n^2} + \left(\frac{n-1}{n}\right)^2 G_3\right] \qquad (6\text{-}130)$$

$$n^2(G_2 + G_3) - n(2G_3 + Y_{21}\alpha) + (G_1 + G_3 + Y_{21}) = 0 \qquad (6\text{-}131)$$

$$n = \frac{(2G_3 + Y_{21}\alpha) \pm \sqrt{(2G_3 + Y_{21}\alpha)^2 - 4(G_2 + G_3)(G_1 + G_3 + Y_{21})}}{2(G_2 + G_3)} \qquad (6\text{-}132)$$

$$n_1 = \frac{(2G_3 + Y_{21}\alpha)}{2(G_2 + G_3)} + \frac{\sqrt{(2G_3 + Y_{21}\alpha)^2 - 4(G_2 + G_3)(G_1 + G_3 + Y_{21})}}{2(G_2 + G_3)}$$

(6-133)

$$n_2 = \frac{(2G_3 + Y_{21}\alpha)}{2(G_2 + G_3)} - \frac{\sqrt{(2G_3 + Y_{21}\alpha)^2 - 4(G_2 + G_3)(G_1 + G_3 + Y_{21})}}{2(G_2 + G_3)}$$

(6-134)

From the quadratic equation above, the value of the factor n can be calculated, and thereby, an estimation of the capacitance can be done a priori. To ensure higher loop gain, n_1 is selected from $n[n_1, n_2]$.

Once the value of n is fixed, then the ratio of the capacitance is calculated as

$$\frac{C_2}{C_1 + C_2} = \frac{1}{n}$$

(6-135)

$$C_2 = \frac{C_1}{n-1} \Rightarrow \frac{C_1}{C_2} = n-1$$

(6-136)

If G_3 and G_1 are zero then the above quadratic equation is reduced to

$$n^2 G_2 - nY_{21}\alpha + Y_{21} = 0$$

(6-137)

$$Y_{21} \cong \frac{n^2}{1-n} G_2 \Rightarrow Y_{21} = \left[\frac{n^2}{1-n}\right]\frac{1}{R_P}$$

(6-138)

$$\frac{Y_{21}R_P}{n} = \frac{n}{1-n}$$

(6-139)

$$R_P = \frac{1}{G_2}$$

$$\frac{Y_{21}R_P}{n} \to Loop\,Gain \qquad\qquad (6\text{-}140)$$

$$Loop\,Gain \;\; \frac{Y_{21}R_P}{n} \to 1 \qquad\qquad (6\text{-}141)$$

From equation (6-135) and (6-138)

$$Y_{21} \Rightarrow G_m(x) = \frac{1}{R_P}\frac{[C_1 + C_2]^2}{C_1 C_2} \qquad\qquad (6\text{-}142)$$

For a relatively optimum phase noise, the drive level has to be adjusted in such a way that the output current pulse is conducting for a short period without appreciably increasing the harmonic content. Chapter 8 will show the absolute best phase noise operating point.

From equation (6-117) follows

$$Y_{21}\big|_{l\,arg\,e-signal} = G_m(x) = \frac{qI_{dc}}{kTx}\left[\frac{2I_1(x)}{I_0(x)}\right]_{n=1} = \frac{g_m}{x}\left[\frac{2I_1(x)}{I_0(x)}\right]_{n=1} \qquad\qquad (6\text{-}143)$$

From equation (6-142)

$$G_m(x) = \frac{1}{R_P}\frac{[C_1 + C_2]^2}{C_1 C_2} \qquad\qquad (6\text{-}144)$$

From equation (6-143) and   (6-144)

$$\frac{g_m}{x}\left[\frac{2I_1(x)}{I_0(x)}\right]_{n=1} = \frac{1}{R_P}\frac{[C_1+C_2]^2}{C_1C_2} = \frac{1}{R_P}\frac{C_1}{C_2}\left[1+\frac{C_2}{C_1}\right]^2 \tag{6-145}$$

$$\frac{C_1}{C_2}\left[1+\frac{C_2}{C_1}\right]^2 = \frac{R_P g_m}{x}\left[\frac{2I_1(x)}{I_0(x)}\right]_{n=1} \tag{6-146}$$

From equation (6-119)

$$\frac{R_P g_m}{x}\left[\frac{2I_1(x)}{I_0(x)}\right]_{n=1} \leq \frac{C_1}{C_2}\left[1+\frac{C_2}{C_1}\right]^2 \leq R_P g_m \tag{6-147}$$

$$x = \frac{g_m\left[\dfrac{2I_1(x)}{I_0(x)}\right]_{n=1}}{\left(\dfrac{1}{R_P}\dfrac{C_1}{C_2}\right)\left(1+\dfrac{C_2}{C_1}\right)^2} \tag{6-148}$$

The value of $\left[\dfrac{2I_1(x)}{I_0(x)}\right]_{n=1}$ increases monotonically as the drive level x increases, and for large values of x and $C_2 < C_1$, $n>1$, the dependency of x can be expressed as

$$x = \frac{R_P G_m C_2}{C_1} \tag{6-149}$$

For large drive level, $x \propto C_2$ and the corresponding conduction angle of output current is given as

$$\varphi = \cos^{-1}\left[1+\frac{\ln(0.05)}{x}\right] \Rightarrow \varphi \approx \cos^{-1}\left[1-\frac{3}{x}\right] \tag{6-150}$$

127

$$\varphi = \cos^{-1}\left[1 - \frac{C_1}{3R_P G_m C_2}\right] \qquad (6\text{-}151)$$

$$\varphi \propto \frac{1}{C_2} \qquad (6\text{-}152)$$

$$x \propto C_2 \qquad (6\text{-}153)$$

Normally, the value of C_1 is kept fixed to avoid loading by the transistor. By increasing the value of C_2, the conduction angle can be reduced, thereby, shortening the output current pulse. Any change in designed frequency, due to the variation of C_2, can be compensated by changing the value of the resonator inductance without much change of the value of the drive level x.

➢ **Test Case: Design Example of a 100MHz crystal oscillator**

Figure 5-33a: Scaled to 100 MHz based on the 10 MHz HP10811A circuit [17]

Figure 122: *Scaled to 100MHz based on the 10 MHz HP10811A circuit [9]*
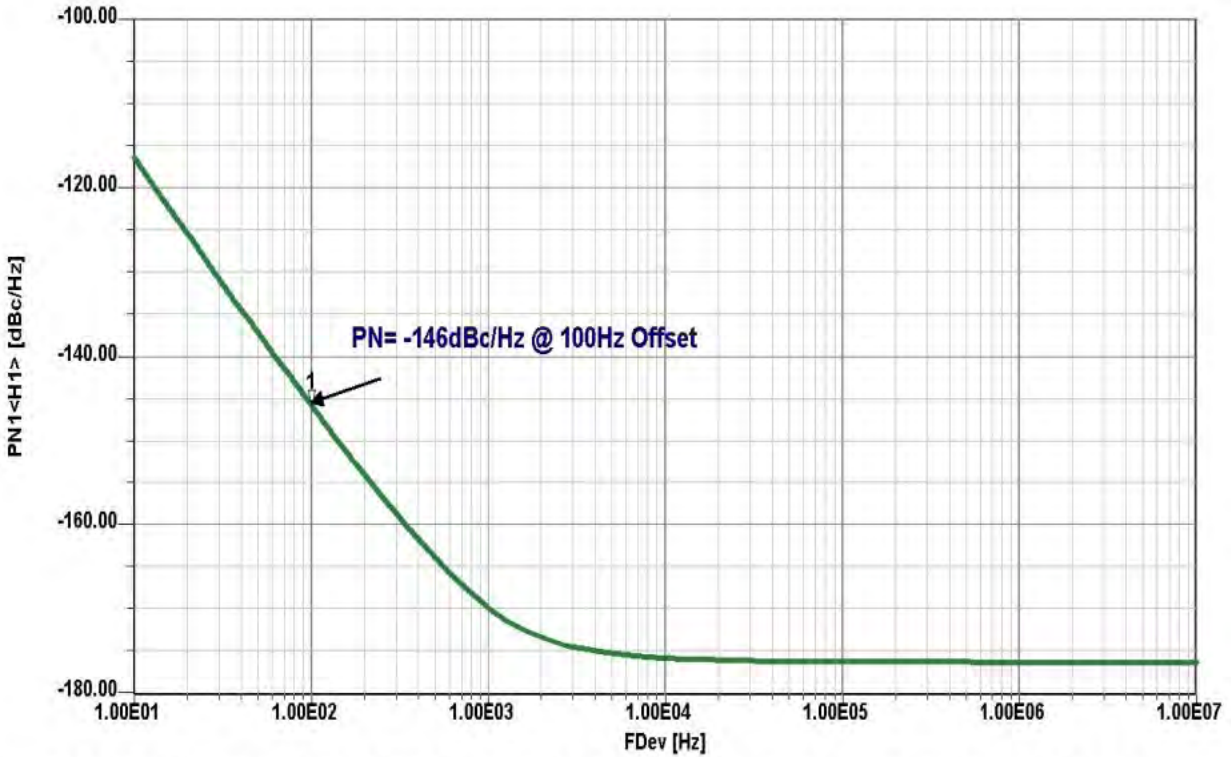
Figure 6-16: CAD simulated Phase Noise Plot of 100 MHz Crystal Oscillator with Buffer Stage [63, Fig 4.16]

Figure 123: *Cad simulated phase noise plot of 100MHz crystal oscillator with buffer stage [9]*
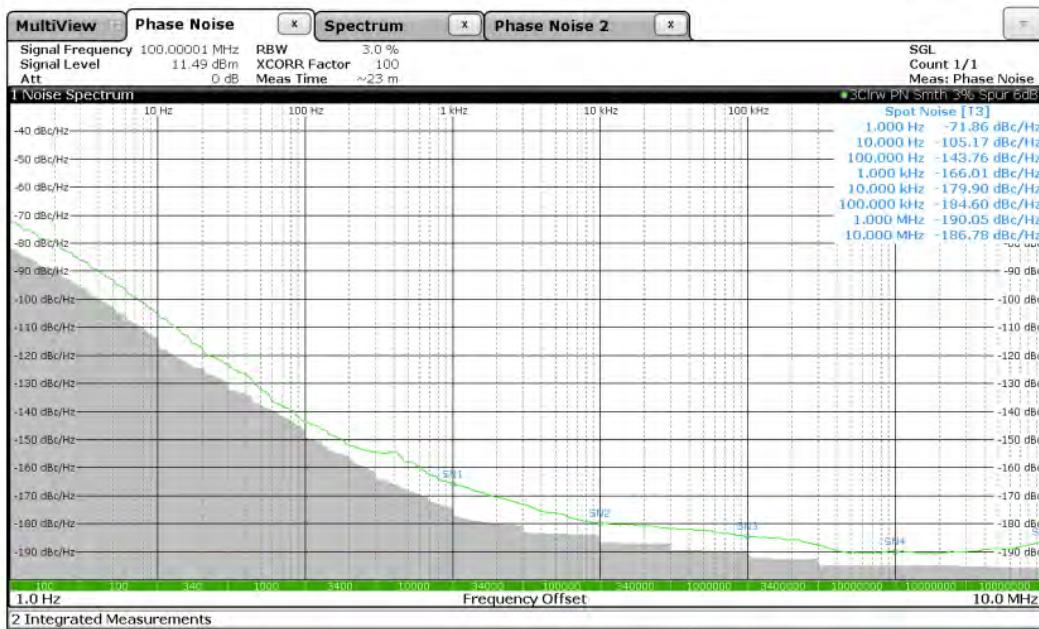
Figure 5-49: Measured phase noise of the 100 MHz crystal oscillator

Figure 124: *Measured phase noise of the 100 MHz Crystal Oscillator [9]*

➢ 100 MHz Crystal Oscillator

$C1 := 15.6\text{pF}$ $C2 := 12.5\text{pF}$ $kT := 4.143 \cdot 10^{-21} \cdot J$ $R := 0.2 \cdot \Omega$

$qcharge := 1.602 \cdot 10^{-19} \cdot coul$ $Ic := 8.2 \cdot mA$ $Ib = 220 \cdot \mu A$

$y11 := (0.000884 - 0.0000158j \cdot mho$

$y21 := (0.0105 - 0.00084j) \cdot mho$

$L := 6.4949 \cdot 10^{-3} \cdot henry$ $af := 2$ $kf := 1 \cdot 10^{-10}$ $y := \dfrac{C1}{C2}$

$Vcc := 10V$ $i := 0..7$ $p := 1.45$ $q := 1.05$

$Q := 25000$ $Q0 := 180000$ $nfdB := 4.747$ $PoutdB := 13$

$fc := 100\ MHz$ $wc := 2\pi \cdot fc$ $gm := |y21| \cdot y^q$

$fo_i := 10^i \cdot Hz$ $wo_i := 2\pi \cdot fo_i$ $B1i := (wo_i)^2 \cdot L^2 \cdot Vcc^2$

$kconstant := \dfrac{KT \cdot R}{wc^2 \cdot C2^2}$ $k0_i := \dfrac{kconstant}{B1_i}$ $b := \dfrac{|y21| \cdot y^p}{|y11|}$

$k1constant_i := qcharge \cdot Ic \cdot gm^2 + \dfrac{kf \cdot Ib^{af} \cdot gm^2}{wo_i}$

$k1_i := \dfrac{k1constant_i}{wc^2 \cdot B1_i}$ $k3_i := wc^2 \cdot gm^2$ $k2_i := wc^4 \cdot b^2$ $k_i := \dfrac{k3_i}{k2_i \cdot C2^2}$

$t2_i := k0_i \dfrac{(1+y)^2}{y^2}$ $t1_i := \left[\left(\dfrac{b^2}{gm^3} \right)^2 \cdot \dfrac{k_i{}^3 \cdot k1_i \cdot (wc)^2}{y^2 + k_i} \right] \cdot \dfrac{(1+y)^2}{y^2}$ $1_i := t1_i + t2_i$

$m_i := 10 \cdot \log \left[1_i \cdot (kg^{-2} \cdot m^{-4} \cdot s^5 \cdot A^2) \cdot \dfrac{Q0^2}{Q^2} \right]$

$L_i := if[m_i < (-177 + Pout(dBm) - nfdB)), (-(177 + PoutdB - nfdB)), m_i$
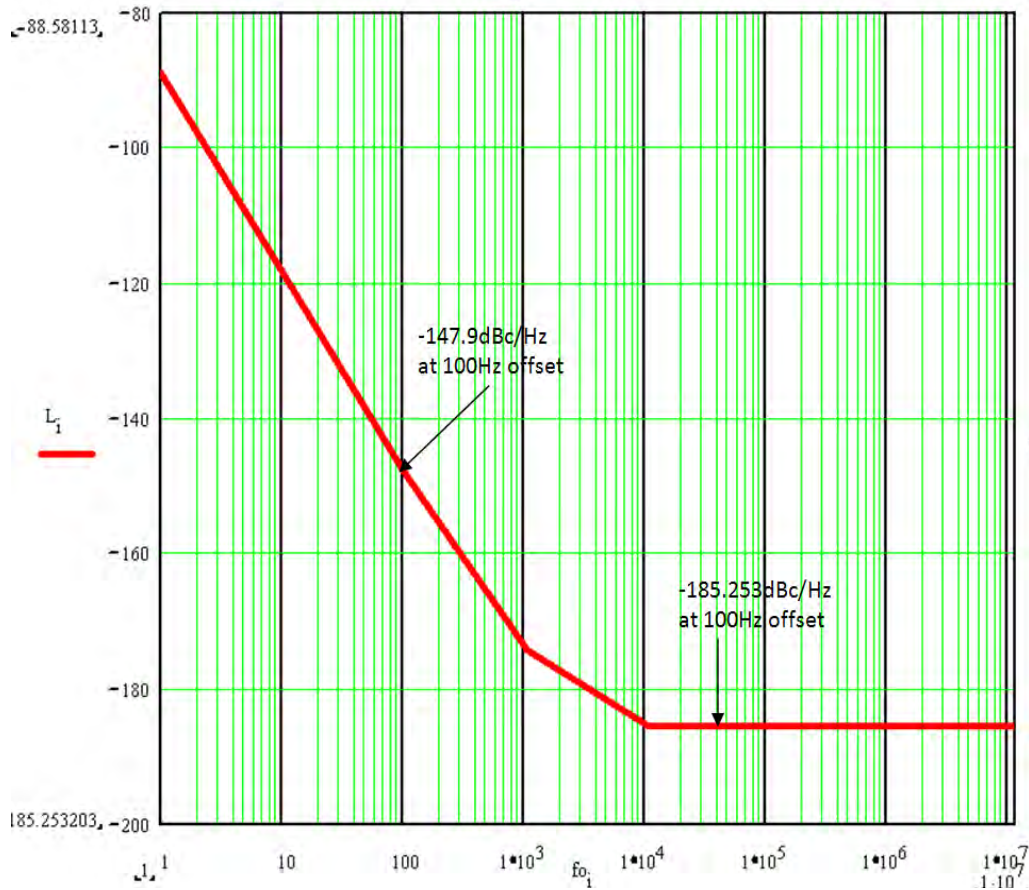
Figure 125: *Calculated Phase Noise of the 100MHz Crystal Oscillator*

Appended:

While the oscillator above war really optimized for best performance, now here is a less optimized circuit to show some design problems.

Analysis of a BFP620 based 100 MHz Oscillator showing AM and FM Noise
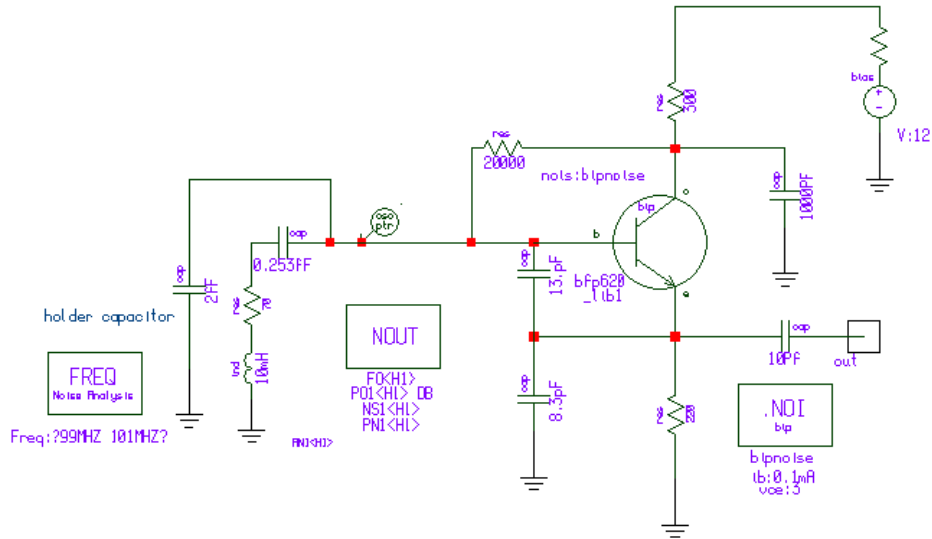
Figure 126: *Schematic circuit of a very noisy crystal oscillator (Poor design)*

The left part is the equivalent of a 100 overtone crystal and the right side is the typical Colpitts arrangement. The DC bias is achieved via the collector 300 Ohm transistor and the 20 K Ohm feedback collector to Base resistor. The emitter resistor is 220 ohm.

Oscillator Design Aid

Analysis Status

Status: The Analysis is Complete.

Frequency: 101.006 MHz   Resonant Frequency: 100.088 MHz

Sweep Number: 100 of 100   Test Current: Re: -1.124 uA
                                              Im: 2.872 uA
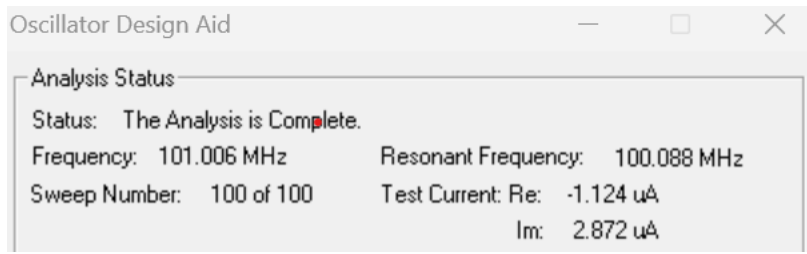
Bias Point Values

Voltage	Current
Vp() = 4.64362 V	Ip() = 0 A
Vbe(_lib1) = 0.859816 V	Ib(_lib1) = 0.109956 mA
Vce(_lib1) = 3.02303 V	Ic(_lib1) = 17.0524 mA
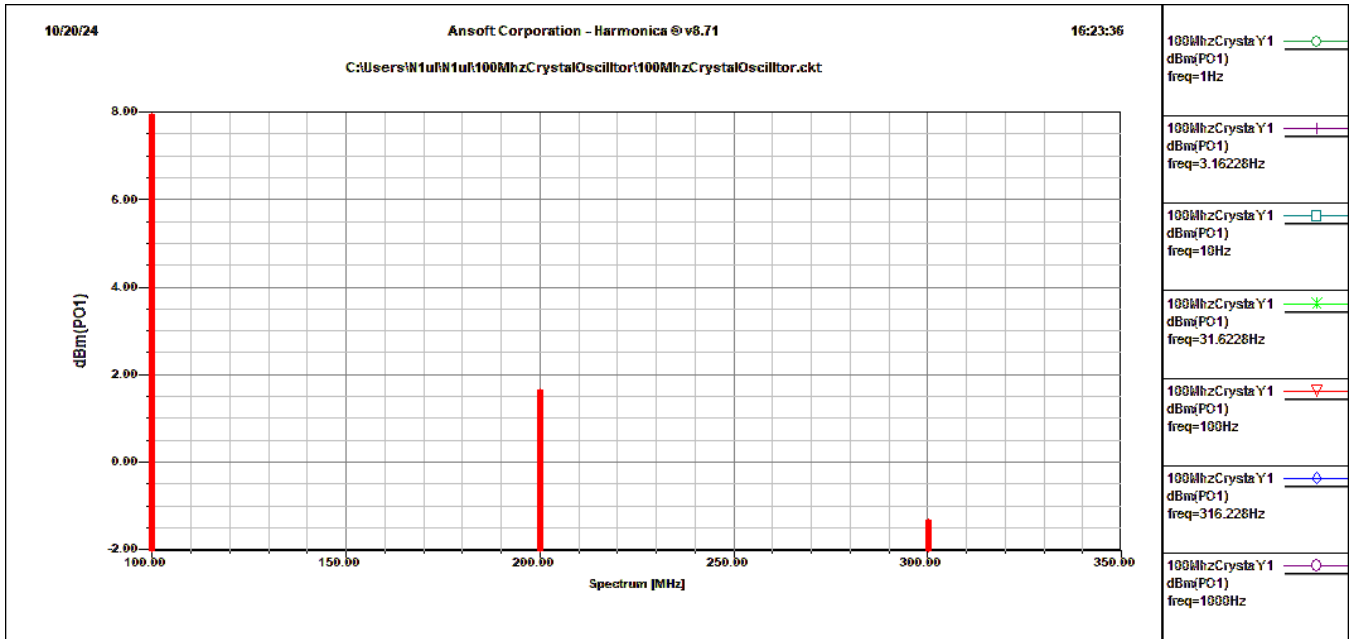
Figure 127: *The output power spectrum of the noisy crystal oscillator*

The output power spectrum looks "normal" But the phase noise result is surprising.
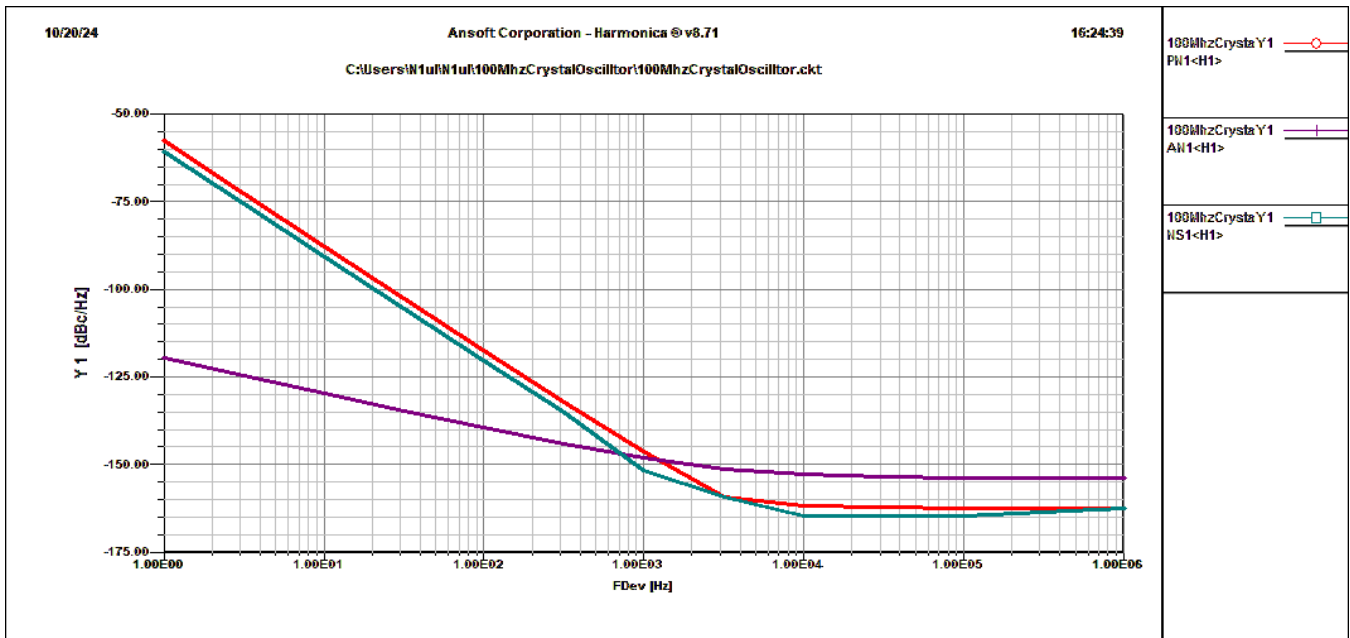
Figure 128: *Simulated phase noise of the noisy crystal oscillator*

The general phase noise is unimpressive, the difference between FM and Spectral density shows some deviation from "normal", but the AM noise also above 1 Khz is poor. The fact that such phenomena can occur are not (well) covered in the literature.

➢ Phase Noise Analysis Based on the Negative Resistance Model

The following noise analysis for the oscillator, while based on the approach of Kurokawa [82], is an attempt to introduce the concept of a "noisy" negative resistance, which is time dependent. Kurokawa, addressing the question of synchronized oscillators, provided insight in the general case of a series oscillator. The method introduced here is specific for a real oscillator and real noise sources.

I now take the basic Colpitts oscillator circuit and develop:
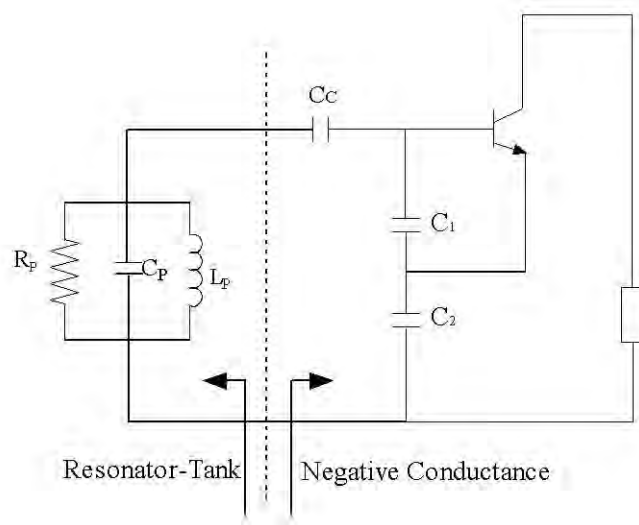
Figure 129: *Figure 8-2 Colpitts Oscillator configuration for the intrinsic case, no parasitics assumed, and an ideal transistor considered.*

The following two circuits show the transition from a series tuned circuit connected with the series time-dependent negative resistance as outlined in Equation (6-1) and the resulting input capacitance marked C_{IN}. Translated, the resulting configuration consists of a series circuit with inductance L and the resulting

135

capacitance C'. The noise voltage e_N(t) describes a small perturbation, which is the noise resulting from R_L and $-R_N$(t).

Figure 8-3 shows the equivalent representation of the oscillator circuit in the presence of noise.
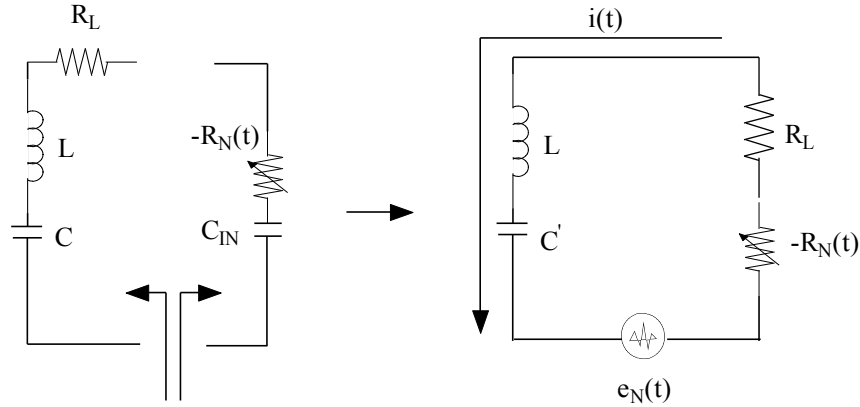
Figure 130: *Figure 8-3   Equivalent representation of the oscillator circuit in presence of noise.*

The circuit equation of the oscillator circuit of Figure 8-3 can be given as

$$L\frac{di(t)}{dt} + (R_L - R_N(t))i(t) + \frac{1}{C'}\int i(t)dt = e_N(t)$$

(8-11)

where i(t) is the time varying resultant current. Due to the noise voltage e_N(t), Equation (8-11) is a nonhomogeneous differential equation. If the noise voltage is zero, it translates into a homogeneous differential equation.

For a noiseless oscillator, the noise signal $e_N(t)$ is zero and the expression of the free-running oscillator current $i(t)$ can be assumed to be a periodic function of time and can be given as

$$i(t) = I_1\cos(\omega t + \varphi_1) + I_2\cos(2\omega t + \varphi_2) + I_3\cos(3\omega t + \varphi_3) + ...I_n\cos(n\omega t + \varphi_n) \quad (8\text{-}12)$$

where $I_1, I_2 .....I_n$ are peak harmonic amplitudes of the current and $\varphi_1, \varphi_2.....\varphi_n$ are time invariant phases.

136

In the presence of the noise perturbation $e_N(t)$, the current $i(t)$ may no longer be a periodic function of time and can be expressed as

$$i(t) = I_1(t)\cos[\omega t + \varphi_1(t)] + I_2(t)\cos[2\omega t + \varphi_2(t)] + I_3(t)\cos[3\omega t + \varphi_3(t)] +$$
$$....I_{n-2}(t)\cos[(n-2)\omega t + \varphi_{n-2}(t)] + I_{n-1}(t)\cos[(n-1)\omega t + \varphi_{n-1}(t)] + I_n(t)\cos[n\omega t + \varphi_n(t)]$$

(8-13)

where $I_1(t)$, $I_2(t)$…..$I_n(t)$ are time variant amplitudes of the current and $\varphi_1(t)$, $\varphi_2(t)$…..$\varphi_n(t)$ are time variant phases.

Considering that $I_n(t)$ and $\varphi_n(t)$ do not change much over the period of $2\pi/n\omega$, each corresponding harmonic over one period of oscillation cycle remains small and more or less variant. The solution of the differential equation becomes easy since the harmonics are suppressed due to a $Q > 10$, which prevents $i(t)$ to flow for the higher terms.

After the substitution of the value of $\dfrac{di}{dt}$ and $\int i(t)dt$, the complete oscillator circuit equation, as given in Equation (8-11), can be rewritten as

$$L\{-I_1(t)(\omega + \frac{d\varphi_1(t)}{dt})\sin[\omega t + \varphi_1(t)] + \frac{dI_1(t)}{dt}\cos[\omega t + \varphi_1(t)] +$$

$$-I_2(t)(2\omega + \frac{d\varphi_2(t)}{dt})\sin[2\omega t + \varphi_2(t)] + \frac{dI_2(t)}{dt}\cos[2\omega t + \varphi_2(t)] +$$

$$-I_3(t)(3\omega + \frac{d\varphi_3(t)}{dt})\sin[3\omega t + \varphi_3(t)] + \frac{dI_3(t)}{dt}\cos[3\omega t + \varphi_3(t)] + ...$$

$$-I_n(t)(n\omega + \frac{d\varphi_n(t)}{dt})\sin[n\omega t + \varphi_n(t)] + \frac{dI_n(t)}{dt}\cos[n\omega t + \varphi_n(t)]\} +$$

$$[(R_L - R_N(t))i(t)] +$$

$$\frac{1}{C'}\left\{\left[\frac{I_1(t)}{\omega} - \frac{I_1(t)}{\omega^2}\left(\frac{d\varphi_1(t)}{dt}\right)\right]\sin[\omega t + \varphi_1(t)] + \frac{1}{\omega^2}\left(\frac{dI_1(t)}{dt}\right)\cos[\omega t + \varphi_1(t)]\right\} +$$

$$\frac{1}{C'}\left\{\left[\frac{I_2(t)}{2\omega} - \frac{I_2(t)}{4\omega^2}\left(\frac{d\varphi_2(t)}{dt}\right)\right]\sin(2\omega t + \varphi_2(t) + \frac{1}{4\omega^2}\left(\frac{dI_2(t)}{dt}\right)\cos(2\omega t + \varphi_2(t))\right\} +$$

$$\frac{1}{C'}\left\{\left[\frac{I_3(t)}{3\omega} - \frac{I_3(t)}{9\omega^2}\left(\frac{d\varphi_3(t)}{dt}\right)\right]\sin[3\omega t + \varphi_3(t)] + \frac{1}{9\omega^2}\left(\frac{dI_3(t)}{dt}\right)\cos[3\omega t + \varphi_3(t)]\right\} + ...$$

$$\frac{1}{C'}\left\{\left[\frac{I_n(t)}{n\omega} - \frac{I_n(t)}{n^2\omega^2}\left(\frac{d\varphi_n(t)}{dt}\right)\right]\sin[n\omega t + \varphi_n(t)] + \frac{1}{n^2\omega^2}\left(\frac{dI_n(t)}{dt}\right)\cos[n\omega t + \varphi_n(t)]\right\} = e_N(t)$$

$$(8\text{-}14)$$

Because Q > 10 we approximate:

$$\frac{di(t)}{dt} = -I_1(t)(\omega + \frac{d\varphi_1(t)}{dt})\sin[\omega t + \varphi_1(t)] + \frac{dI_1(t)}{dt}\cos[\omega t + \varphi_1(t)] + \text{(slowly varying function at higher}$$

order harmonics of a very small amount)

$$\int i(t)dt = \left[\frac{I_1(t)}{\omega} - \frac{I_1(t)}{\omega^2}\left(\frac{d\varphi_1(t)}{dt}\right)\right]\sin[\omega t + \varphi_1(t)] + \frac{1}{\omega^2}\left(\frac{dI_1(t)}{dt}\right)\cos[\omega t + \varphi_1(t)] + \quad \text{(slowly varying}$$

function at higher order harmonics of a very small amount)

After the substitution of the value of $\dfrac{di}{dt}$ and $\int i(t)dt$, the oscillator circuit Equation (8-14) can be rewritten as

$$L\left[-I_1(t)(\omega + \frac{d\varphi_1(t)}{dt})\sin[\omega t + \varphi_1(t)] + \frac{dI_1(t)}{dt}\cos[\omega t + \varphi_1(t)]\right] + [(R_L - R_N(t))I(t)] +$$

$$\frac{1}{C}\left\{\left[\frac{I_1(t)}{\omega} - \frac{I_1(t)}{\omega^2}\left(\frac{d\varphi_1(t)}{dt}\right)\right]\sin[\omega t + \varphi_1(t)] + \frac{1}{\omega^2}\left(\frac{dI_1(t)}{dt}\right)\cos[\omega t + \varphi_1(t)]\right\} = e_N(t) \qquad (8\text{-}15)$$

Following [82], and for simplification purposes, the equations above are multiplied with $\sin[\omega t + \varphi_1(t)]$ or $\cos[\omega t + \varphi_1(t)]$ and integrated over one period of the oscillation cycle, which will give an approximate differential equation for phase $\varphi(t)$ and amplitude $i(t)$ as

$$\left[\frac{2}{IT_0}\right]\int_{t-T_0}^{t} e_N(t)\sin[\omega t + \varphi(t)]dt = -\frac{d\varphi}{dt}\left[L + \frac{1}{\omega^2 C'}\right] + \left[-\omega L + \frac{1}{\omega C'}\right] \qquad (8\text{-}16)$$

$$\left[\frac{2}{T_0}\right]\int_{t-T_0}^{t} e_N(t)\cos[\omega t + \varphi(t)]dt = \frac{dI(t)}{dt}\left[L + \frac{1}{\omega^2 C'}\right] + \left[R_L - \overline{R_N(t)}\right]I(t) \qquad (8\text{-}17)$$

where $\overline{R_N(t)}$ is the average negative resistance under large signal condition.

$$\overline{R_N(t)} = \left[\frac{2}{T_0 I}\right]\int_{t-T_0}^{t} R_N(t)I(t)\cos^2[\omega t + \varphi)]dt \qquad (8\text{-}18)$$

Since magnitude of the higher harmonics are not significant, the subscript of $\varphi(t)$ and $I(t)$ are dropped. Based on [82], we now determine the negative resistance.

139

➢ Calculation of the Region of the Nonlinear Negative Resistance

Under steady-state free running oscillation condition,

$$\frac{dI(t)}{dt} \to 0$$

implies steady current, and

$$e_N(t) \to 0$$

with I = fundamental RF current. Solving the now homogeneous differential equation for $R_L - R_N(t)$ and inserting the two terms into 8-17, we obtain

$$\left[\frac{2}{T_0}\right]\int_{t-T_0}^{t} e_N(t)\cos[\omega t + \varphi(t)]dt = \frac{dI}{dt}\left[L + \frac{1}{\omega^2 C'}\right] + \left[R_L - \overline{R_N(t)}\right]I(t) \tag{8-19}$$

$$\text{term} \to 0$$

now we introduce γ; $\gamma = \dfrac{\Delta R}{\Delta I}$; for $\Delta \to 0$, $\gamma \to 0$ and

$$[R_L - \overline{R_N(t)}] = \gamma\ \Delta I,\ \gamma \to 0 \Rightarrow [R_L - \overline{R_N(t)}]I(t) \to 0 \tag{8-20}$$

$$R_L - \overline{R_N(t)} = R_{Load} - \left[\frac{2}{T_0}\right]\int_{t-T_0}^{t} R_N(t)\cos^2[\omega t + \varphi(t)]dt \to 0 \tag{8-21}$$

140

$[R_L - \overline{R_N(t)}]I(t) \to 0$ gives the intersection of $[\overline{R_N(t)}]$ and $[R_L]$. This value is defined as I_0 which is the minimum value of the current needed for the steady-state sustained oscillation condition.

Figure 8-4 shows the plot of the nonlinear negative resistance, which is a function of the amplitude of the RF current. As the RF amplitude gets larger the conducting angle becomes more narrow.
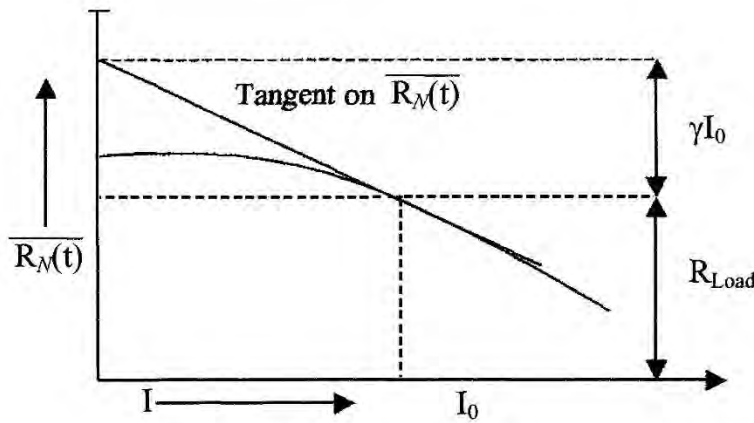
Figure 131: **Figure 8-4 Plot of negative resistance of $[\overline{R_N(t)}]$ vs. amplitude of current I.**

For a small variation of the current ΔI from I_0, the relation above is expressed as

$$[R_L - \overline{R_N(t)}] = \gamma \ \Delta I \tag{8-22}$$

$\gamma \Delta I$ can be found from the intersection on the vertical axis by drawing the tangential line on $[\overline{R_N(t)}]$ at $I = I_0$. $|\Delta I|$ decreases exponentially with time for $\gamma > 0$.

Hence, I_0 represents the stable operating point. On the other hand, if $[\overline{R_N(t)}]$ intersects $[R_L]$ from the other side for $\gamma < 0$ then $|\Delta I|$ grows indefinitely with time. Such an operating point does not support stable operation].

Summary Results

After a really long set of mathematical manipulations, see

The Design of modern Microwave Oscillators for Wireless Applications ,Ulrich L. Rohde , Ajay K. Poddar, Georg Boeck 2005 Wiley, Chapter 8.

The analysis of the oscillator in the time domain has given us a design criteria to find the optimum value of $y = \dfrac{C_1}{C_2}$ with values for $y + 1$ or n ranging from 1.5 to 4. For values above 3.5, the output power is reduced significantly.

Consistent with the previous chapters, we note

$$C_1 = C_1^* \pm X(C_P \, or \, L_P) \qquad (8\text{-}118)$$

$$X(C_{be} \, or \, L_b) \rightarrow C_P \, or \, L_P \qquad (8\text{-}119)$$

In the case of a large value of C_P ($C_P > C_1$), X_1 has to be inductive to compensate extra contributions of the device package capacitance to meet the desired value of C_1!

The following is a set of design guides to calculate the parameters of the oscillator.

$$\omega = \sqrt{\dfrac{1}{L\left[\dfrac{C_1 C_2}{C_1 + C_2} + C\right]}} \qquad (8\text{-}120)$$

$$\left|R_n(L_P = 0)\right| = \dfrac{Y_{21}}{w^2 C_1 C_2} \qquad (8\text{-}121)$$

$$C_1 = \frac{1}{\omega_0} \sqrt{\frac{Y_{11}}{K}} \tag{8-122}$$

C_2 is best be determined graphically from the noise plot.

$$C_C > \left\{ \frac{(\omega^2 C_1 C_2)(1 + \omega^2 Y_{21}^2 L_P^2)}{[Y_{21}^2 C_2 - \omega^2 C_1 C_2)(1 + \omega^2 Y_{21}^2 L_P^2)(C_1 + C_P + C_2)]} \right\} \tag{8-123}$$

$$\frac{C}{10} \geq [C_C]_{L_P=0} > \left[\frac{(\omega^2 C_1 C_2)}{[Y_{21}^2 C_2 - \omega^2 C_1 C_2)(C_1 + C_P + C_2)]} \right] \tag{8-124}$$

The phase noise in dBc/Hz is shown as

$$\pounds(\omega) = 10 \times \log \left| \left[k_0 + \left(\frac{k^3 k_1 \left[\frac{Y_{21}^+}{Y_{11}^+} \right]^2 [y]^{2p}}{[Y_{21}^+]^3 [y]^{3q}} \right) \left(\frac{1}{(y^2 + k)} \right) \right] \left[\frac{[1 + y]^2}{y^2} \right] \right| \tag{8-125}$$

The phase noise improves with the square of the loaded Q_L! 10% higher $Q \to 20\%$ better phase noise!

$$\mathsf{L}\ (\omega) \propto \frac{1}{C_{IN}^2} \tag{8-126}$$

The loaded Q of the resonator determines the minimum possible level of the oscillator phase noise for given bias voltage and oscillator frequency.

To achieve close to this minimum phase noise level set by the loaded Q_L of the resonator, the optimum (rather, how large the value of the C_{IN} can be) value of C_{IN} is to be fixed.

To achieve the best possible phase noise level, the feedback capacitors C_1 and C_2 should be made as large as possible, but still generate sufficient negative resistance for sustaining steady-state oscillation.

$$[-R_N]_{negative\,resis\tan ce} \propto \frac{1}{\omega_0^2} \frac{1}{C_1 C_2}, \text{ (no parasitics)} \qquad (8\text{-}127)$$

The negative resistance of the oscillator circuit is inversely proportional to the feedback capacitors. Therefore, the limit of the feedback capacitor value is determined by the minimum negative resistance for a loop gain greater than unity.

From the phase noise equation discussed, the feedback capacitor C_2 has more influence compared to C_1. The drive level and conduction angle of the Colpitts oscillator circuit is a strong function of C_2.

The time domain approach has provided us with the design guide for the key components of the oscillator; however, it did not include all the noise sources of the transistor. By using the starting parameters, such as C_1 and C_2 and the bias point, as well as the information about the resonator and the transistor, a complete noise model/analysis will follow

This section describes a design example based on the Phase Noise Analysis of the Feedback Model. Up to here we have calculated both the large-signal drive condition, as well as the optimum choice of the feedback capacitance. Now, we are going to consider the oscillator as a feedback loop with a noisy transistor, looking at all typical noise contributions. Based on a fixed set of values of C_1 and C_2, we can

now calculate the accurate phase-noise behavior of the oscillator and analyze the various noise contributions.

First, the noisy bipolar transistor will be introduced. Figure 19 shows the familiar hybrid-π transistor circuit and Figure 20 shows the equivalent circuit with the relevant noise sources included.
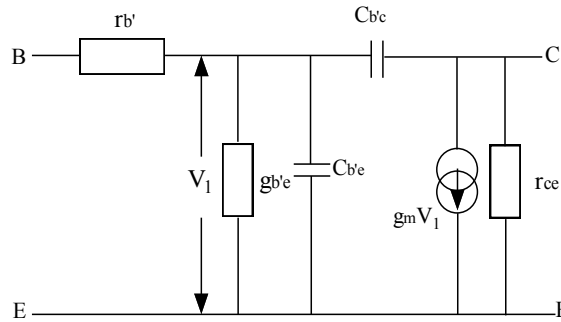
Figure 132: *Figure 19: Grounded emitter bipolar transistor [5]*
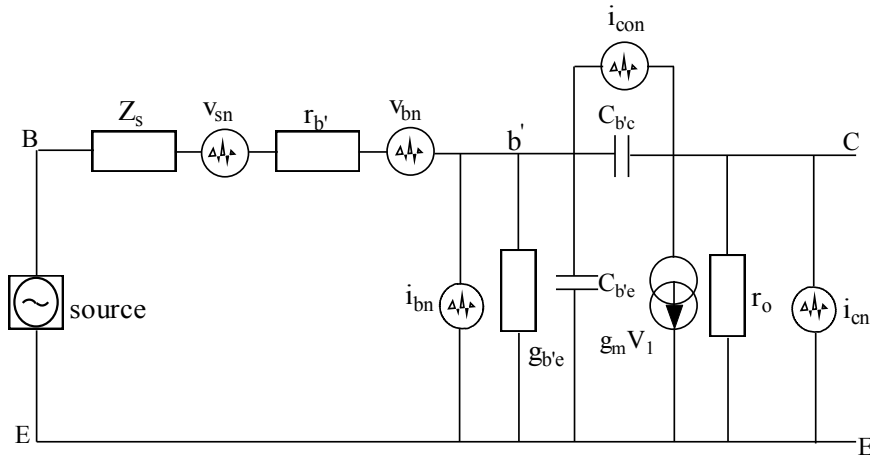
Figure 133: *Figure 20: Hybrid-π configuration of the grounded bipolar transistor with noise sources [5]*

The mean square value of the noise generators in Figure 20, in a narrow frequency offset Δf, are given by

$$\overline{i_{bn}^2} = 2qI_b\Delta f \quad (67)$$

$$\overline{i_{cn}^2} = 2qI_c\Delta f \quad (68)$$

$$\overline{i_{con}^2} = 2qI_{cob}\Delta f \quad (69)$$

$$\overline{v_{bn}^2} = 4kTR_b\Delta f \quad (70)$$

145

$$\overline{v_{sn}^2} = 4kTR_S\Delta f \qquad (71)$$

where I_b, I_c, and I_{cob} are average DC currents over the Δf noise bandwidth.

The noise power spectral densities due to these noise sources are

$$S(i_{cn}) = \frac{\overline{i_{cn}^2}}{\Delta f} = 2qI_c = 2KTg_m \qquad (72)$$

$$S(i_{bn}) = \frac{\overline{i_{bn}^2}}{\Delta f} = 2qI_b = \frac{2KTg_m}{\beta} \qquad (73)$$

$$S(i_{fn}) = \frac{K_f I_b^{AF}}{f} \qquad (74)$$

$$S(v_{bn}) = \frac{\overline{v_{bn}^2}}{\Delta f} = 4KTr_b' \qquad (75)$$

$$S(v_{sn}) = \frac{\overline{v_{sn}^2}}{\Delta f} = 4KTR_s \qquad (76)$$

where r_b' and R_s are base and source resistance, and Z_s is the complex source impedance.

Figure 21 shows the feedback arrangement for the Colpitts oscillator with the noise sources.

2-Port representation of bipolar transistor

2-port representation of feedback-Network
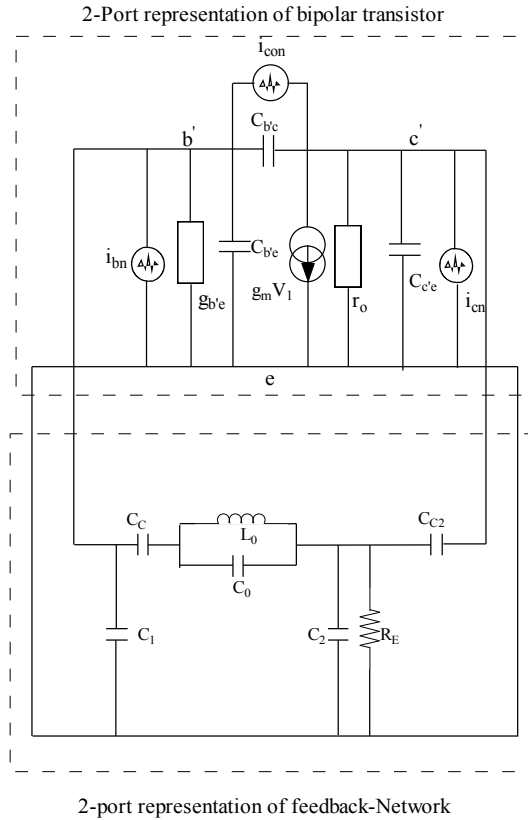
Figure 134: *Figure 21: Feedback arrangement for the Colpitts oscillator with the noise sources [5]*

The transistor is acting like a gain block. The feedback network includes the load conductance and a small part of the output signal goes to the input of the bipolar transistor through the resonant circuit. The ABCD chain matrix will be used for the analysis.

Figure 22 shows the linear representation of the Colpitts oscillator with the input white noise source $i_n(\omega)$.
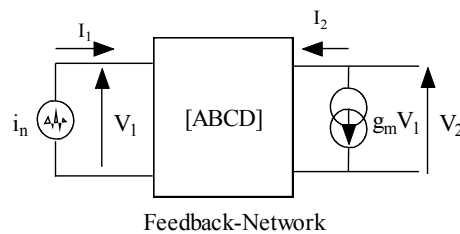
Feedback-Network

Figure 135: *Figure 22: Linear representation of feedback Colpitts oscillator with input white noise source $i_n(\omega)$ [5]*

This is not consistent with Figure 21, but useful because all non-active components are now in the feedback network.

The input noise power spectral density can be given as

$$S_{in} = \frac{\left|\overline{i_n^2}\right|}{\Delta f}$$ (77)

Where:

$$\left|\overline{i_n^2}\right| = \sum_{i=1}^{i=N}\left|\overline{i_{ni}^2}\right| = \left|\overline{i_{n1}^2}\right| + \left|\overline{i_{n2}^2}\right| + \left|\overline{i_{n3}^2}\right| \ldots\ldots + 2C_{ii}[i_{ni}i_{n(i+1)}^{\bullet}]$$ (78)

C_{ii} = the noise correlation coefficient

The [ABCD] matrix of the above oscillator circuit can be given as

$$[A] = 1 + \left[\left(\frac{1}{j\omega C_c} + \frac{j\omega L_0}{1 - \omega^2 L_0 C_0}\right)\left(j\omega C_2 + \frac{1}{R_E}\right)\right]$$

$$[B] = \frac{1}{j\omega Cc_2} + \left(\frac{1}{j\omega C_c} + \frac{j\omega L_0}{1 - \omega^2 L_0 C_0}\right)\left[1 + \left(j\omega C_2 + \frac{1}{R_E}\right)\left(\frac{1}{j\omega Cc_2}\right)\right]$$

$$[C] = j\omega C_1 + \left(j\omega C_2 + \frac{1}{R_E}\right)\left[1 + j\omega C_1\left(\frac{1}{j\omega C_c} + \frac{j\omega L_0}{1 - \omega^2 L_0 C_0}\right)\right]$$

$$[D] = \frac{C_1}{Cc_2} + \left[\left(1 + j\omega C_1\left(\frac{1}{j\omega C_c} + \frac{j\omega L_0}{1 - \omega^2 L_0 C_0}\right)\right)\left(1 + \left(j\omega C_2 + \frac{1}{R_E}\right)\left(\frac{1}{j\omega Cc_2}\right)\right)\right]$$ (79)

$$\begin{bmatrix} V_1 \\ I_1 \end{bmatrix} = \begin{bmatrix} A & B \\ C & D \end{bmatrix} = \begin{bmatrix} V_2 \\ -I_2 \end{bmatrix}$$ (80)

$$V_1 = AV_2 - BI_2$$ (81)

$$I_1 = CV_2 - DI_2$$ (82)

$$Z_{in} = \left[\frac{V_1}{I_1}\right]_{I_{2=0}} = \frac{A}{C}$$ (83)

Where:

$$I_1 = i_n$$ (84)

$$I_2 = -g_m V_1$$ (85)

The equivalent input noise voltage due to the input noise current, $I_1 = i_n$, is

$$v_n(\omega) = I_1 Z_{in} = I_1 \left[\frac{V_1}{I_1} \right]_{I_{2}=0} = I_1 \left[\frac{A(\omega)}{C(\omega)} \right] = i_n \left[\frac{A(\omega)}{C(\omega)} \right] \qquad (86)$$

The input noise voltage $v_n(\omega)$ will produce two narrowband (1 Hz) uncorrelated components in the frequency domain located at $\omega - \omega_0$ and $\omega + \omega_0$ as $[v_n(\omega)]_{\omega=\omega_0-\Delta\omega}$ and $[v_n(\omega)]_{\omega=\omega_0+\Delta\omega}$.

In presence of the two uncorrelated components of the input noise voltage, $[v_n(\omega)]_{\omega=\omega_0-\Delta\omega}$ and $[v_n(\omega)]_{\omega=\omega_0+\Delta\omega}$, the peak carrier signal of amplitude V_c at frequency $\omega = \omega_0$ is modulated with an input phase noise signal $S_{\Delta\phi_{in}}(\omega)$.

The input phase noise spectral density at an offset of $\Delta\omega$ is

$$S_{\Delta\phi_{in}}(\Delta\omega) = \frac{\left| [v_n(\omega)]^2_{\omega=\omega_0-\Delta\omega} \right| + \left| [v_n(\omega)]^2_{\omega=\omega_0+\Delta\omega} \right|}{\left| V_c^2(\omega) \right|} \qquad (87)$$

$$S_{\Delta\phi_{in}}(\Delta\omega) \cong \frac{2\left| \overline{[v_n(\omega)]^2} \right|}{\left| V_c^2(\omega) \right|} \qquad (88)$$

$$S_{\Delta\phi_{in}}(\Delta\omega) = \frac{2\left| \overline{[v_n(\omega)]^2} \right|}{\left| V_c^2(\omega) \right|} = 2 \frac{\left| \overline{[i_n(\omega)]^2} \right|}{\left| V_c^2(\omega) \right|} \frac{\left| \overline{A^2(\omega)} \right|}{\left| C^2(\omega) \right|} \qquad (89)$$

$$\left| \overline{i_n^2} \right| = S_{in}\Delta f \qquad (90)$$

$$\left| \overline{i_n^2} \right|_{\Delta f=1Hz} = S_{in} \qquad (91)$$

$$S_{\Delta\phi_{in}}(\Delta\omega) = 2 \frac{S_{in}}{\left| V_c^2(\omega) \right|} \frac{\left| \overline{A^2(\omega)} \right|}{\left| C^2(\omega) \right|} \qquad (92)$$

where S_{in} and $S_{\Delta\phi_{in}}$ are the input noise power and phase noise spectral density.

Based on [33, 34],

149

$$S_{\Delta\phi_{out}}(\omega) = S_{\Delta\phi_{in}}(\omega)\left[1 + \frac{1}{(\omega^2)}\left(\frac{\omega_0}{2Q_L}\right)^2\right] \tag{93}$$

$$Q_L(\omega = \omega_0) = \frac{\omega_0}{2}\left|\frac{d\phi}{d\omega}\right|_{\omega=\omega_0} \tag{94}$$

The open loop gain is

$$G_{open}(\omega = \omega_0) = -\left[\frac{g_m}{C(\omega_0)}\right] \tag{95}$$

For sustained oscillation $G_{open}(\omega = \omega_0) = 1 ... -\left[\dfrac{g_m}{C(\omega_0)}\right] = 1 \Rightarrow C(\omega)_{\omega=\omega_0}$ is real and negative.

$$C(\omega_0) = C_{Real}(\omega_0) + jC_{Imag}(\omega_0) \tag{96}$$

$$C_{Imag}(\omega_0) = 0 \tag{97}$$

$$C_{Real}(\omega_0) = -g_m \tag{98}$$

$$\left[\frac{d\phi}{d\omega}\right]_{\omega=\omega_0} \approx -\frac{1}{C_{Real}(\omega_0)}\left[\frac{dC_{Imag}(\omega)}{d\omega}\right]_{\omega=\omega_0} \tag{99}$$

$$Q_L(\omega = \omega_0) = \frac{\omega_0}{2}\left|\frac{d\phi}{d\omega}\right|_{\omega=\omega_0} \tag{100}$$

$$Q_L(\omega = \omega_0) = \frac{\omega_0}{2}\left|\frac{1}{C_{Real}(\omega_0)}\left[\frac{dC_{Imag}(\omega)}{d\omega}\right]\right|_{\omega=\omega_0} \tag{101}$$

$$S_{\Delta\phi_{out}}(\Delta\omega) = S_{\Delta\phi_{in}}(\Delta\omega)\left[1 + \frac{1}{(\Delta\omega^2)}\left[\frac{C_{Real}(\omega_0)}{\left(\dfrac{dC_{Imag}(\omega)}{d\omega}\right)}\right]^2_{\omega=\omega_0}\right] \tag{102}$$

$$S_{\Delta\phi_{in}}(\Delta\omega) = 2\frac{S_{in}}{\left|V_c^2(\omega)\right|}\frac{\left|A^2(\omega)\right|}{\left|C^2(\omega)\right|} \tag{103}$$

$$S_{\Delta\phi_{out}}(\Delta\omega) = 2\frac{S_{in}}{\left|V_c^2(\omega_0)\right|}\frac{\left|\overline{A^2(\omega_0)}\right|}{\left|C^2(\omega_0)\right|}\left[1+\frac{1}{(\Delta\omega^2)}\left[\frac{C_{Real}(\omega_0)}{\left(\frac{dC_{Imag}(\omega)}{d\omega}\right)}\right]_{\omega=\omega_0}\right]^2 \quad (104)$$

We now perform the noise analysis of the Colpitts oscillator.

Individual Contribution of all Four Noise Sources

The following contribute to the noise of the oscillator:

- Thermal noise associated with the loss resistance of the resonator,

- Thermal noise associated with the base resistance of the transistor,

- Shot noise associated with the base bias current, and

- Shot noise associated with the collector bias current.

If we now use the oscillator circuit with a noisy resonator, we can calculate the total noise of the oscillator as shown in Figure 23.
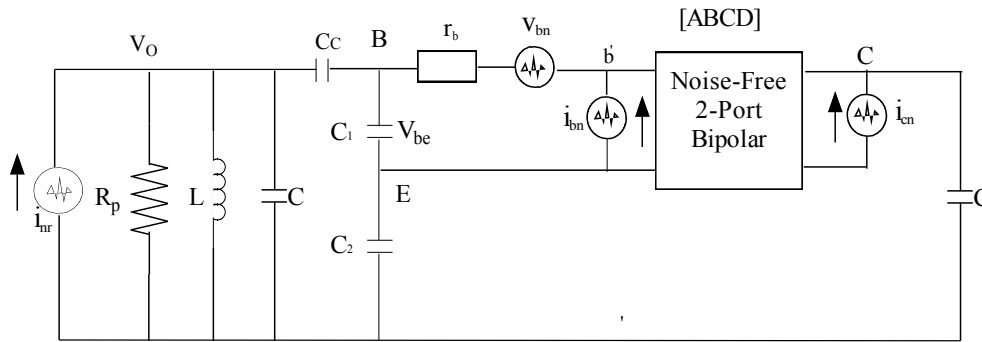
Figure 136: *Figure 23: The oscillator circuit with 2-port [ABCD] matrix, consistent with the approach of Figure 20*

Noise Shaping Function of the Resonator

For phase noise analysis, the oscillator is considered as a feedback system and a noise source is present in the input as shown in the Figure 24.

X(jw)
Noise
H₁(jw)
Y₁(jw)
H₂(jw)
Y(jw) Non-unity gain feedback oscillator

X(jw)
Noise
H(jw)
Y(jw)
Unity gain feedback oscillator
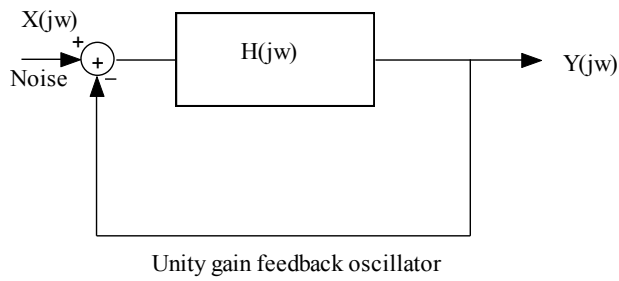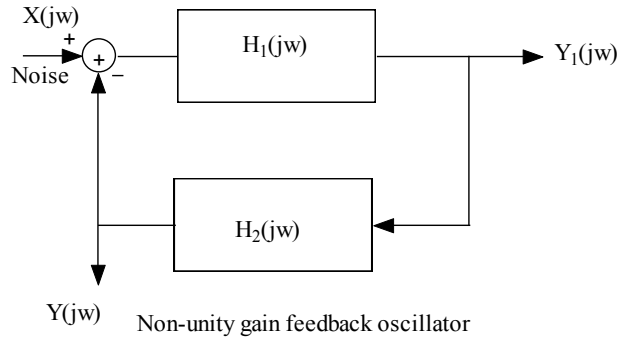
Figure 137: *Figure 24: Feedback oscillator with noise source*

Oscillator output phase noise is a function of

The amount of the source noise present at the input of the oscillator circuit, and

The amount the feedback system rejects or amplifies various noise components.

The unity-gain system closed loop transfer function is

$$\left[TF(j\omega)\right]_{\text{closed-loop}} = \frac{Y(j\omega)}{X(j\omega)} = \frac{H(j\omega)}{1+H(j\omega)} \qquad (105)$$

$$\left[H(j\omega)\right]_{\omega=\omega_0} = -1 \qquad (106)$$

For frequencies close to $\omega = \Delta\omega + \omega$ the open loop transfer function is

$$\left[H(j\omega)\right]_{\omega=\omega_0+\Delta\omega} \approx \left[H(j\omega_0)+\Delta\omega\frac{dH(j\omega)}{d\omega}\right] \qquad (107)$$

The noise transfer function is

$$\left[\frac{Y(j\omega+j\Delta\omega)}{X(j\omega+j\Delta\omega)}\right] = \left[\frac{H(j\omega_0)+\Delta\omega\dfrac{dH(j\omega)}{d\omega}}{1+H(j\omega_0)+\Delta\omega\dfrac{dH(j\omega)}{d\omega}}\right] \qquad (108)$$

152

Since $H(j\omega_0) = -1$ and for most practical case $\Delta\omega \dfrac{dH(j\omega)}{d\omega} \ll 1$, we can write

$$\left[\frac{Y(j\omega + j\Delta\omega)}{X(j\omega + j\Delta\omega)}\right] \approx \left|\frac{-1}{\Delta\omega \dfrac{dH(j\omega)}{d\omega}}\right| \quad (109)$$

From the noise transfer function it appears that the noise component at $\omega = \Delta\omega + \omega_0$ is multiplied by the term

$$\left|\frac{-1}{\Delta\omega \dfrac{dH(j\omega)}{d\omega}}\right|,$$

relative to the output.

The broadband white noise is shaped by the resonator as seen in Figure 3.25.
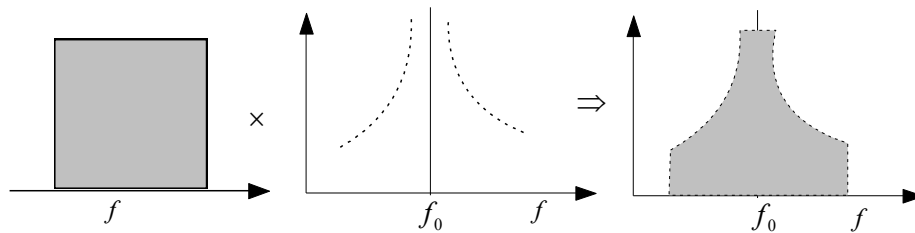
Figure 138: *Figure 25: Noise shaping in the oscillator*

Therefore, the noise power spectral density can be explained as

$$\left|\frac{Y(j\omega + j\Delta\omega)}{X(j\omega + j\Delta\omega)}\right|^2 = \left|\frac{-1}{\Delta\omega \dfrac{dH(j\omega)}{d\omega}}\right|^2 \quad (110)$$

for $H(j\omega) = A(j\omega)\exp[j\varphi(j\omega)]$ (111)

$$\frac{dH(j\omega)}{d\omega} = \left[\frac{dA(j\omega)}{d\omega} + jA(j\omega)\frac{d\varphi(j\omega)}{d\omega}\right]\exp[j\varphi(j\omega)] \quad (112)$$

Assume $\omega = \Delta\omega + \omega_0$, $\omega \to \omega_0$, and $|A(j\omega_0)| \to 1$ then the above equation is reduced to

$$\left|\frac{Y(j\omega+j\Delta\omega)}{X(j\omega+j\Delta\omega)}\right|^2 = \left|\frac{1}{(\Delta\omega)^2\left\{\left[\frac{dA(j\omega)}{d\omega}\right]^2+\left[\frac{d\varphi(j\omega)}{d\omega}\right]^2\right\}}\right|_{\omega=\Delta\omega+\omega_0} \quad (113)$$

The open loop Q_L becomes

$$Q_L = \frac{\omega_0}{2}\sqrt{\left[\frac{dA(j\omega)}{d\omega}\right]^2+\left[\frac{d\varphi(j\omega)}{d\omega}\right]^2} \quad (114)$$

and

$$\left|\frac{Y(j\omega+j\Delta\omega)}{X(j\omega+j\Delta\omega)}\right|^2 = \left|\frac{1}{(\Delta\omega)^2\left\{\left[\frac{dA(j\omega)}{d\omega}\right]^2+\left[\frac{d\varphi(j\omega)}{d\omega}\right]^2\right\}}\right|_{\omega=\Delta\omega+\omega_0} = \frac{1}{4Q_L^2}\left[\frac{\omega_0}{\Delta\omega}\right]^2 \quad (115)$$

For the LC resonator $\left[\dfrac{dA(j\omega)}{d\omega}\right]$ at resonance $(\omega\to\omega_0)$ becomes zero and $Q_L = \dfrac{\omega_0}{2}\dfrac{d\phi}{d\omega}$.

- Non-Unity Gain

For the non-unity gain feedback case where $H(j\omega)=H_1(j\omega)H_2(j\omega)$ it follows that

$$\left[\frac{Y(j\omega+j\Delta\omega)}{X(j\omega+j\Delta\omega)}\right]_{\omega=\Delta\omega+\omega_0} \approx \left|\frac{-1}{\Delta\omega\dfrac{dH(j\omega)}{d\omega}}\right| \quad (116)$$

and

$$\frac{Y_1(j\omega)}{X(j\omega)} = \frac{H_1(j\omega_0)}{1+H(j\omega_0)} \quad (117)$$

then the noise power is shaped by the transfer function as

$$\left|\frac{Y_1(j\omega+j\Delta\omega)}{X(j\omega+j\Delta\omega)}\right|^2 = \frac{|H_1(j\omega)|^2}{(\Delta\omega)^2\left|\dfrac{dH(j\omega)}{d\omega}\right|^2} \quad (118)$$

For the lossy RLC resonator see Figure 26.
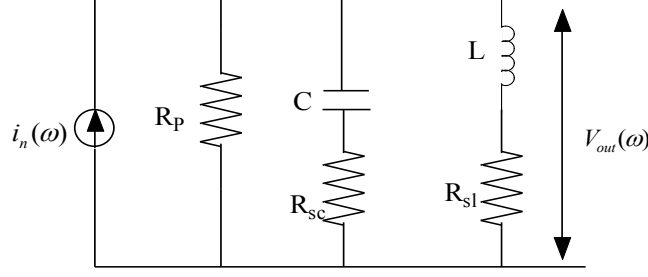
Noise Response to the RLC-Resonator
Figure 139: *Figure 26: Noise response of the RLC resonator*

Then,

$$H(\omega_0 + \Delta\omega) = \left[\frac{V_{out}(\omega_0 + \Delta\omega)}{i_n(\omega_0 + \Delta\omega)}\right]_{\omega = \Delta\omega + \omega_0} = \left[\frac{1}{g_{resonator}}\right]\left[\frac{\omega_0}{\Delta\omega}\right]\left[\frac{1}{2Q_L}\right]$$
(119)

$$g_{resonator} = \frac{1}{R_P}$$, (120)

where R_P is the equivalent loss resistance of the resonator.

- Noise Transfer Function and Spectral Densities

The noise transfer function for the relevant sources is described in this section.

Noise transfer function of the thermal loss resistance of the resonator:

$$NFT_{inr}(\omega_0) = \frac{1}{2}\left[\frac{1}{2\omega_0 C_{eff}}\right]\left[\frac{\omega_0}{\Delta\omega}\right] \rightarrow (121)$$

Noise transfer function of the transistor's base resistance noise:

$$NFT_{V_{bn}}(\omega_0) = \frac{1}{2}\left[\frac{C_1 + C_2}{C_2}\right]\left[\frac{1}{2Q}\right]\left[\frac{\omega_0}{\Delta\omega}\right] \rightarrow (122)$$

Noise transfer function of the transistor's base current flicker noise:

$$NFT_{i_{in}}(\omega_0) = \frac{1}{2}\left[\frac{C_2}{C_1 + C_2}\right]\left[\frac{1}{2\omega_0 Q C_{eff}}\right]\left[\frac{\omega_0}{\Delta\omega}\right] \rightarrow \quad (123)$$

Noise transfer function of the transistor's flicker noise:

$$NFT_{ifn}(\omega_0) = \frac{1}{2}\left[\frac{C_2}{C_1 + C_2}\right]\left[\frac{1}{2\omega_0 Q C_{eff}}\right]\left[\frac{\omega_0}{\Delta\omega}\right] \rightarrow \quad (124)$$

155

Noise transfer function of the collector current shot noise:

$$NFT_{i_{C_{Cn}}}(\omega_0) = \frac{1}{2}\left[\frac{C_1}{C_1+C_2}\right]\left[\frac{1}{2\omega_0 Q C_{eff}}\right]\left[\frac{\omega_0}{\Delta\omega}\right] \rightarrow \quad (125)$$

Where:

$$C_{eff} = C + \frac{C_1 C_2}{C_1 + C_2} \quad (126)$$

$$V_o(\omega_0) = n V_{be}(\omega_0) \quad (127)$$

$NFT_{in}(\omega_0)$, $NFT_{V_{bn}}(\omega_0)$, $NFT_{i_{bn}}(\omega_0)$ and $NFT_{i_{Cn}}(\omega_0)$ are the noise transfer functions as explained.

The various noise sources of the oscillator circuit whereby the flicker noise current is added to the base

current and their noise spectral density is $\dfrac{K_f I_b^{AF}}{f_m}$.

$$[NSD]_{inr} = \frac{4KT}{R_P} \rightarrow$$ noise spectral density of the thermal noise current from the loss resistance of the

resonator

$$[NSD]_{Vbn} = 4KT r_b \rightarrow$$ noise spectral density of the thermal noise voltage from the base resistance

$$[NSD]_{ibn} = 2q I_b \rightarrow$$ noise spectral density of the shot noise current from the base current

$$[NSD]_{ifn} = \frac{K_f I_b^{AF}}{f_m} \rightarrow$$ Noise spectral density due to 1/f- flicker noise

$$[NSD]_{icn} = 2q I_c \rightarrow$$ noise spectral density of the shot noise current from the collector current

The phase noise contribution now is:

$$PN(\omega_0 + \Delta\omega) = [NSD]_{\text{noise-source}}\left[NFT_{\text{noise-source}}(\omega_0)\right]^2 \quad (128)$$

$$PN_{inr}(\omega_0 + \Delta\omega) = \frac{4KT}{R_P}\left[NF_{inr}(\omega_0)\right]^2 \quad (129)$$

$$PN_{Vbn}(\omega_0 + \Delta\omega) = 4KT r_b\left[NF_{Vbn}(\omega_0)\right]^2 \quad (130)$$

$$PN_{ibn}(\omega_0 + \Delta\omega) = 2q I_B\left[NF_{ibn}(\omega_0)\right]^2 \quad (131)$$

$$PN_{ifn}(\omega_0 + \Delta\omega) = \frac{K_f I_b^{AF}}{f_m} \left[NF_{ibn}(\omega_0) \right]^2 \tag{132}$$

$$PN_{icn}(\omega_0 + \Delta\omega) = 2qI_c \left[NF_{icn}(\omega_0) \right]^2 \tag{133}$$

where $PN(\omega_0 + \Delta\omega)$ is the phase noise at the offset frequency $\Delta\omega$ from the carrier frequency ω_0 and $[NSD]_{noise-source}$ is the noise spectral density of the noise sources. The phase noise contribution is

$$PN_{inr}(\omega_0 + \Delta\omega) = \frac{4KT}{R_P} [NFT_{inr}(\omega_0)]^2 = \frac{4KT}{R_P} \left\{ \frac{1}{2} \left[\frac{1}{2\omega_0 C_{eff}} \right] \left[\frac{\omega_0}{\Delta\omega} \right] \right\}^2 \rightarrow$$ Phase noise contribution from the resonator tank.

$$PN_{Vbn}(\omega_0 + \Delta\omega) = 4KTr_b [NFT_{Vbn}(\omega_0)]^2 = 4KTr_b \left\{ \frac{1}{2} \left[\frac{C_1 + C_2}{C_2} \right] \left[\frac{1}{2Q} \right] \left[\frac{\omega_0}{\Delta\omega} \right] \right\}^2 \rightarrow$$ Phase noise contribution from the base resistance.

$$PN_{ibn}(\omega_0 + \Delta\omega) = 2qI_b [NFT_{ibn}(\omega_0)]^2 = 2qI_b \left\{ \frac{1}{2} \left[\frac{C_2}{C_1 + C_2} \right] \left[\frac{1}{\omega_0 Q C_{eff}} \right] \left[\frac{\omega_0}{\Delta\omega} \right] \right\}^2 \rightarrow$$ Phase noise contribution from the base current.

$$PN_{ifn}(\omega_0 + \Delta\omega) = \left(\frac{K_f I_b^{AF}}{f_m} \right) [NF_{ibn}(\omega_0)]^2 = \frac{K_f I_b^{AF}}{f_m} \left\{ \frac{1}{2} \left[\frac{C_2}{C_1 + C_2} \right] \left[\frac{1}{2\omega_0 Q C_{eff}} \right] \left[\frac{\omega_0}{\Delta\omega} \right] \right\}^2 \rightarrow$$ Phase noise contribution from the flicker noise of the transistor.

$$PN_{icn}(\omega_0 + \Delta\omega) = 2qI_c [NFT_{icn}(\omega_0)]^2 = 2qI_c \left\{ \frac{1}{2} \left[\frac{C_1}{C_1 + C_2} \right] \left[\frac{1}{2\omega_0 Q C_{eff}} \right] \left[\frac{\omega_0}{\Delta\omega} \right] \right\}^2 \rightarrow\rightarrow$$ Phase noise contribution from the collector current.

The total effect of all the four noise sources can be expressed as
$$PN(\omega_0 + \Delta\omega) = [PN_{inr}(\omega_0 + \omega)] + [PN_{Vbn}(\omega_0 + \omega)] + [PN_{ibn}(\omega_0 + \omega)] + [PN_{icn}(\omega_0 + \omega)]$$

$$PN(\omega_0 + \Delta\omega) = \frac{4KT}{R_P} \left\{ \frac{1}{2} \left[\frac{1}{2\omega_0 C_{eff}} \right] \left[\frac{\omega_0}{\Delta\omega} \right] \right\}^2 + 4KTr_b \left\{ \frac{1}{2} \left[\frac{C_1 + C_2}{C_2} \right] \left[\frac{1}{2Q} \right] \left[\frac{\omega_0}{\Delta\omega} \right] \right\}^2 + \left[2qI_b + \right.$$

$$\left. \frac{2\pi K_f I_b^{AF}}{\Delta\omega} \right] \left\{ \frac{1}{2} \left[\frac{C_2}{C_1 + C_2} \right] \left[\frac{1}{2Q\omega_0 C_{eff}} \right] \left[\frac{\omega_0}{\Delta\omega} \right] \right\}^2 + 2qI_c \left\{ \frac{1}{2} \left[\frac{C_1}{C_1 + C_2} \right] \left[\frac{1}{2\omega_0 Q C_{eff}} \right] \left[\frac{\omega_0}{\Delta\omega} \right] \right\}^2$$

Where:

K_f = flicker noise constant

AF = flicker noise exponent

$$C_{eff} = C + \frac{C_1 C_2}{C_1 + C_2} \tag{136}$$

Note: The effect of the loading of the Q of the resonator is calculated by the noise transfer function multiplied with the noise sources.

The phase noise contribution from the different noise sources for the parallel tuned Colpitts oscillator circuit at $\Delta\omega = 10\,\text{kHz}\,2\pi$ from the oscillator frequency $\omega_0 = 100\,\text{MHz}\,2\pi$ will next be computed. Circuit parameters are as follows:

Base resistance of transistor r_b = 6.14 ohm.

Parallel loss resistance of the resonator R_P = 7.54E11 ohm

Q of the resonator = 60,000

Resonator inductance = 15 mH

Resonator capacitance = 2.7 pF

Collector current of the transistor I_c = 13 mA

Base current of the transistor I_b = 130 μA.

Flicker noise exponent AF = 2

Flicker noise constant K_f = 1E-11

Feedback factor n = 6

Comparing phase noise at 100 Hz and phase noise at 10 kHz,

$$PN_{inr}\left(\omega_0 + 100\,\text{Hz}\right) = -162 \text{ dBc/Hz} \qquad PN_{inr}\left(\omega_0 + 10\,\text{kHz}\right) = -202\,\text{dBc/Hz}$$

$$PN_{Vbn}\left(\omega_0 + 100\,\text{Hz}\right) = -176\,\text{dBc/Hz} \qquad PN_{Vbn}\left(\omega_0 + 10\,\text{kHz}\right) = -216\text{ dBc/Hz}$$

$$PN_{(ibn+ifn)}\left(\omega_0 + 100\,\text{Hz}\right) = -140 \text{ dBc/Hz} \qquad PN_{(ibn+ifn)}\left(\omega_0 + 10\,\text{kHz}\right) = -200 \text{ dBc/Hz}$$

$$PN_{(icn)}\left(\omega_0 + 100\,\text{Hz}\right) = -148\text{ dBc/Hz} \qquad PN_{(icn)}\left(\omega_0 + 10\,\text{kHz}\right) = -189\text{ dBc/Hz}$$

Note: The noise contribution from the resonator at this offset is the same as the flicker noise contribution from the transistor.

It appears that the flicker noise and the noise from the resonator are the limiting factors for the overall phase noise performance of the oscillator circuit.

The dependence of the phase noise performance due to different noise sources present in the oscillator circuits are

$$PN_{imr}(\omega_0 + \Delta\omega) \propto \frac{1}{R_P} \quad (137)$$

$$PN_{Vbn}(\omega_0 + \Delta\omega) \propto = r_b \left\{ \frac{1}{Q} \left[1 + \frac{C_1}{C_2} \right] \right\}^2 \quad (138)$$

$$PN_{ibn}(\omega_0 + \Delta\omega) \propto I_b \left\{ \frac{1}{QC_{eff}} \left[\frac{C_2}{C_1 + C_2} \right] \right\}^2 \quad (139)$$

$$PN_{icn}(\omega_0 + \Delta\omega) \propto = I_c \left\{ \frac{1}{QC_{eff}} \left[\frac{C_1}{C_1 + C_2} \right] \right\}^2 \quad (140)$$

Once the resonator Q is known (parallel loss resistance is fixed) then the only option left is to select a device having a low flicker noise. The base resistance, current, and collector current add little to the performance! Finally, optimization of the phase noise can be done by proper selection of the feedback capacitor under the constraints of the loop gain so that it maintains oscillation.

The value of 'n' is defined as $(1 + C1/C2)$. Table 3 shows the resulting phase noise of a 100 MHz crystal oscillator.

Table 3 Phase Noise as a Function of Feedback Factor n

$n = (1 + C1/C2)$	Resulting PN at 100 Hz	Resulting PN at 10kHz
2	−130 dBc/Hz	−190 dBc/Hz
3	−136 dBc/Hz	−193.4 dBc/Hz
4	−140 dBc/Hz	−193.4 dBc/Hz
5	−142 dBc/Hz	−193.4 dBc/Hz
6	−144 dBc/Hz	−193.4 dBc/Hz
7	−146 dBc/Hz	−193.4 dBc/Hz

Interesting enough, the far out noise is not affected, but the close-in noise is. The reason for this is that the larger the $C1$ becomes, the more it short-circuits the transistor noise, to the point where the feedback

is no longer is large enough for oscillation. There is a limit for how large '*n*' can be made as one has to consider tolerances in the components and also the temperature-dependence; 7, seems to be a reasonable value, for this particular transistor. The value of *n* would have to be recalculated for different transistor and frequency of oscillation.

Figure 27 illustrates the negative impedance calculation. The capacitance ratio based on an open loop gain of 6 and calculations of Y_{21} (0.225) and the DC (100 mV) offset based on the Bessel function is 6.
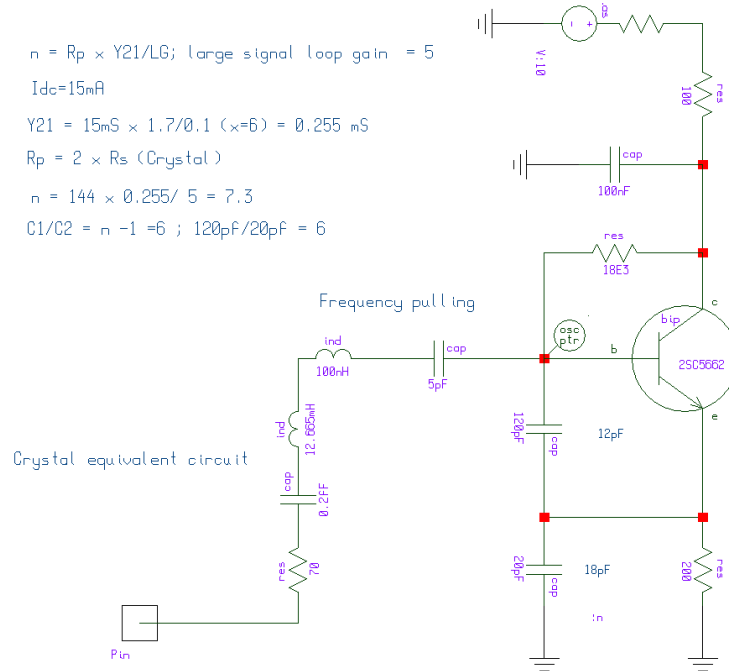
Figure 140: *Figure 27: Negative impedance calculation*

The simulation confirms that oscillation occurs at the correct frequency and the phase noise, as shown in Figure 28 and Figure 29, is attractive.
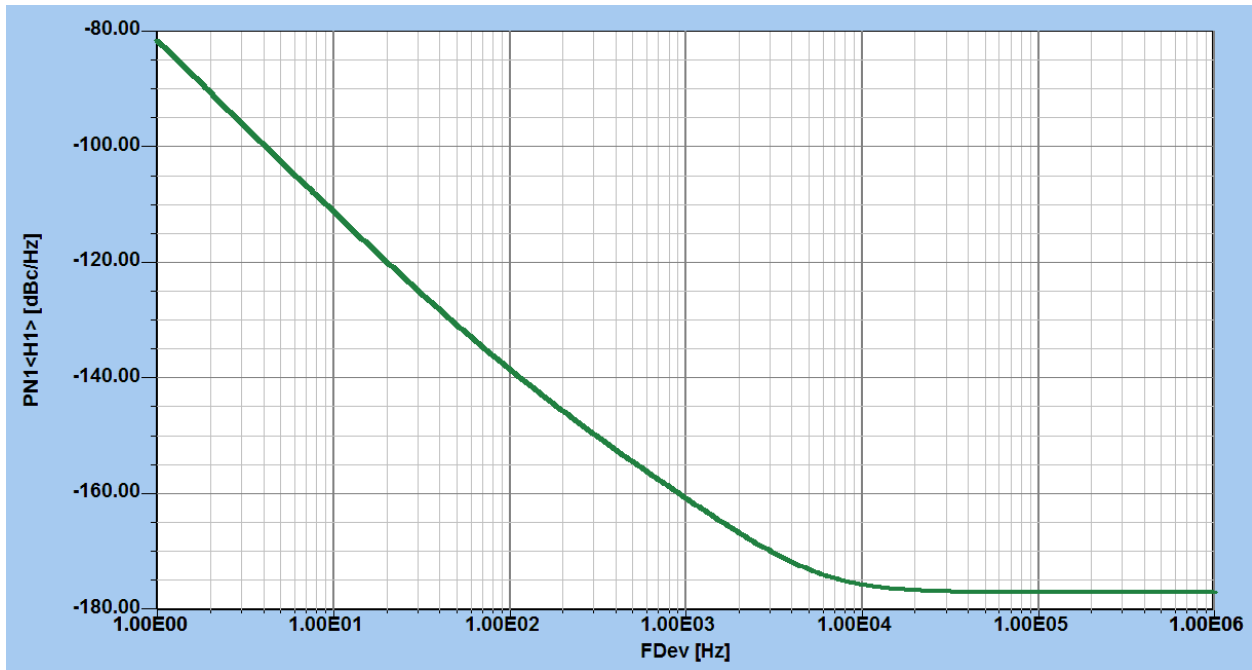
Figure 141: *Figure 28: Simulated phase noise plot of the circuit in Figure 27*
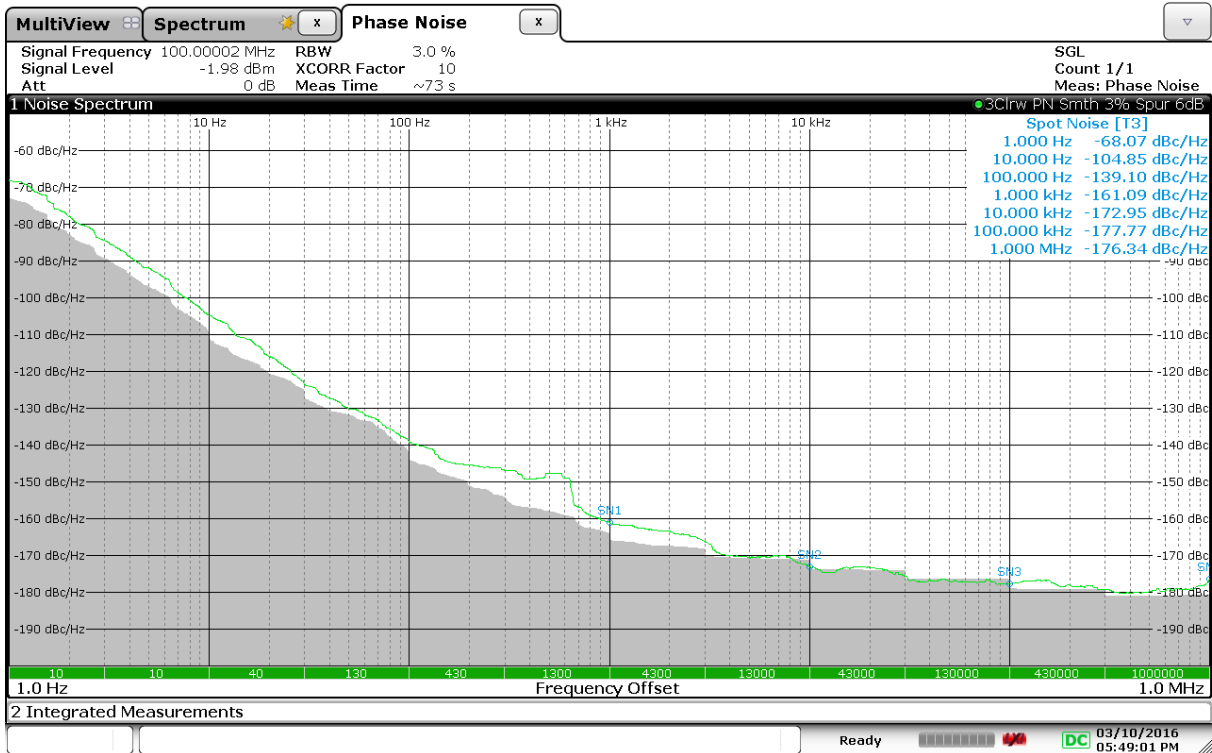
Figure 142: *Figure 29: Measured phase noise plot of a 100 MHz crystal oscillator*

Now a numerical example

➢ Design Example of an Oscillator for Best Phase Noise and Good Output Power
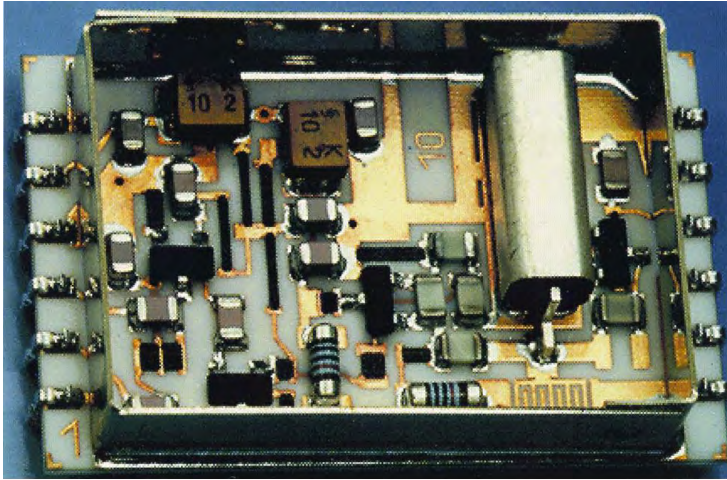
Figure 143: *Figure C-1 shows the parallel-tuned Colpitts oscillator circuit, which has to be designed with the following specifications. The unit was also built and measured. It uses a ceramic resonator and its equivalent circuit is shown.*

Requirements:

- output power requirement: 13 dBm

- operating frequency: 1000 MHz

- load: 50 Ω

- phase noise –124 dBc/Hz @10KHz

Design Steps

Step 1:

Calculation of the operating point for a fixed, normalized drive of x = 20 (high output power), see Table 6-1.

Based on output power requirement, the following is calculated.

The oscillator output voltage at the fundamental frequency is

$$V_{out}(\omega_0) = \sqrt{P_{out}(\omega_0)*2R_L} = \sqrt{20E - 3*2*50} \approx 1.414V \qquad \text{(C-1)}$$

The fundamental current is

$$I_{out}(\omega_0) = \frac{V_{out}(\omega_0)}{50} = \frac{1.414}{50} = 28.3mA \qquad \text{(C-2)}$$

The DC operating point is calculated based on the normalized drive level x = 20. The expression for the emitter dc current can be given in terms of the Bessel function with respect to the drive level is

$$[I_E(\omega_0)] = 2I_{DC}\left[\frac{I_1(x)}{I_0(x)}\right]_{x=Normalized-Drive-Level} \qquad \text{(C-3)}$$

1000MHz_Parallel-Tuned_Resonator_Oscillator

Figure 144: *Figure C-1   Schematic of the 1000 MHz oscillator.*
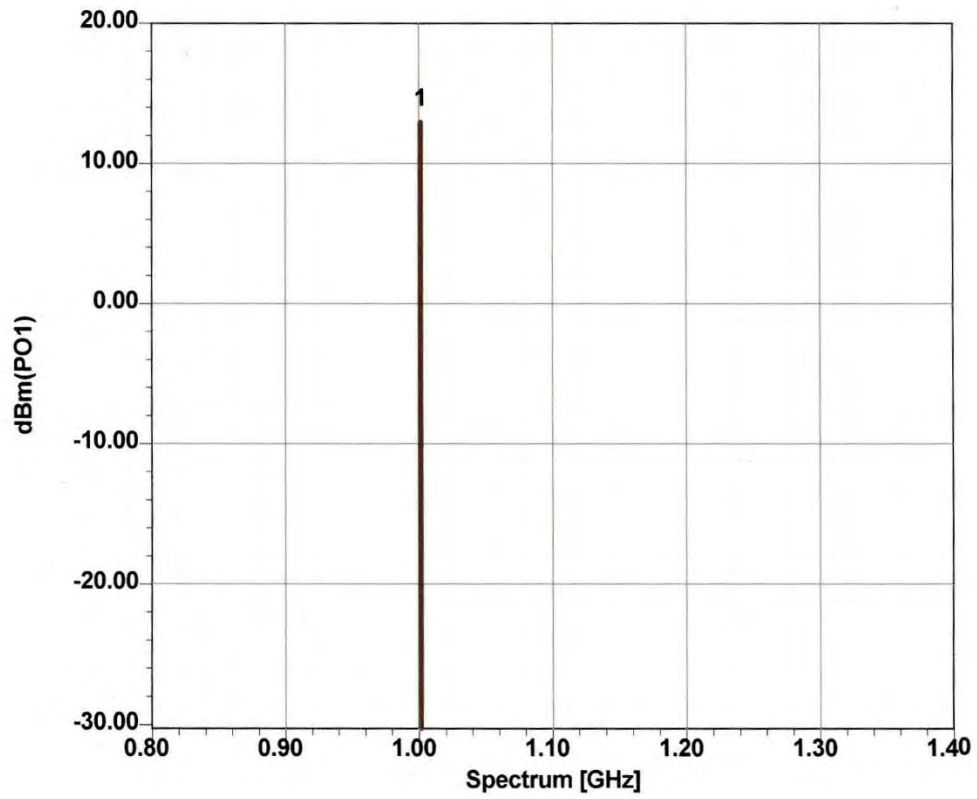
X1= 1.00GHz
Y1= 12.96

Figure 145: *Figure C-2   Predicted output power of the oscillator.*
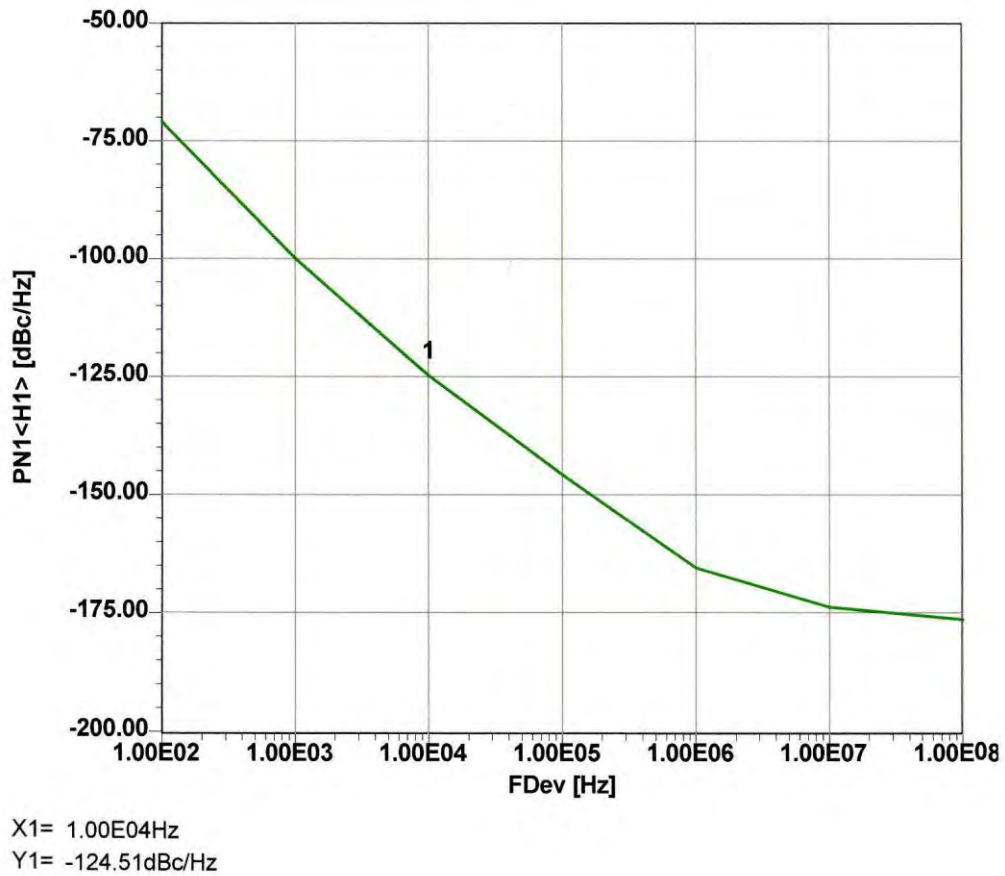
Figure 146: *Figure C-3   Predicted phase noise of the oscillator.*

For the normalized drive level x = 20, the output emitter current at the fundamental frequency can be given as

$$[I_E(\omega_0)]_{x=20} = [I_{E1}(\omega_0)]_{x=20} + [I_{E2}(\omega_0)]_{x=20} = 2I_{DC}\left[\frac{I_1(x)}{I_0(x)}\right]_{x=20} \approx 56mA \qquad \text{(C-4)}$$

$$[I_{E1}(\omega_0)]_{x=20} = I_{out}(\omega_0) = 28.3mA \text{ (output current to the load)} \qquad \text{(C-5)}$$

Figure C-4 shows the oscillator circuit configuration in which DC and RF current distribution is shown and divided into its components.
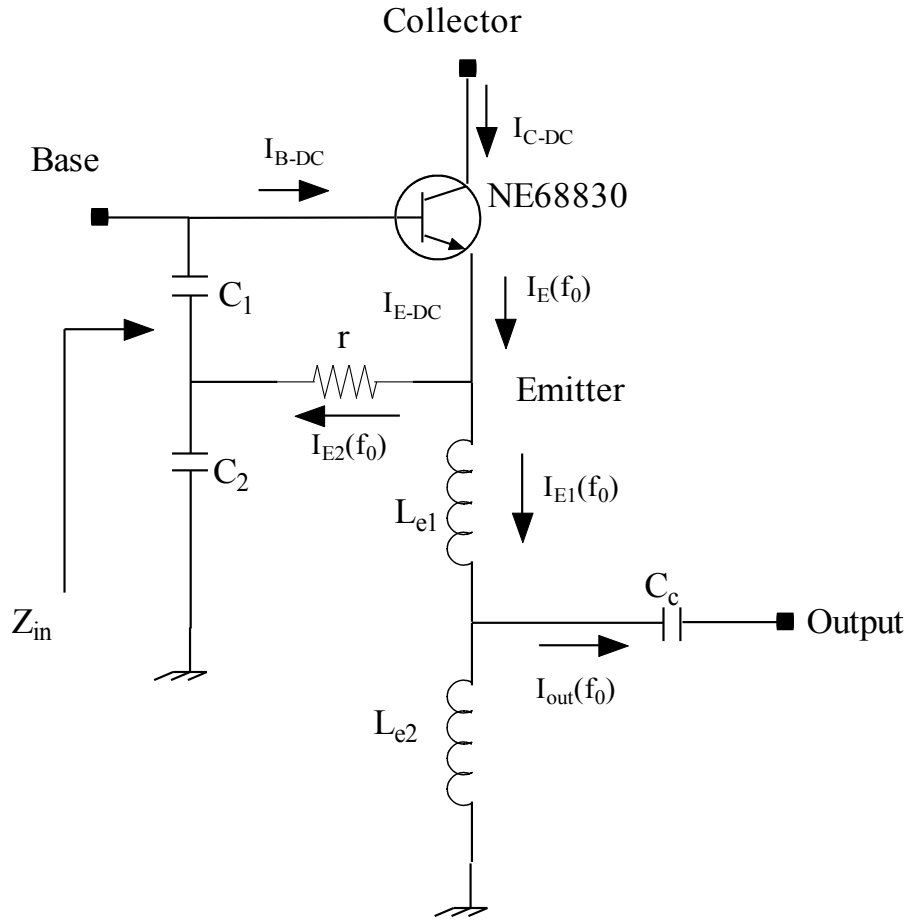
Figure 147: *Figure C-4 Current distribution in the oscillator circuit.*

$$[I_{E2}(\omega_0)]_{x=20} = [I_E(\omega_0)]_{x=20} - [I_{E1}(\omega_0)]_{x=20} = 27.3mA \qquad \text{(C-6)}$$

$$I_{E-DC} = \frac{[I_E(\omega_0)]_{x=20}}{2\left[\dfrac{I_1(x)}{I_0(x)}\right]_{x=20}} = 28.3mA \qquad \text{(C-7)}$$

For this application, the NE68830 was selected.

Step 2:

Biasing circuit

For the best phase noise close-in, a DC/AC feedback circuit is incorporated, which provides the desired operating DC condition [84]:

I_E=28.3mA

V_{CE}=5.5V, Supply Voltage V_{cc}=8V

β=120

I_B≈0.23mA

Step 3:

Calculation of the large-signal transconductance.

$$Y_{21}\big|_{l\arg e-signal} = G_m(x) = \frac{qI_{dc}}{kTx}\left[\frac{2I_1(x)}{I_0(x)}\right]_{fundamentd} \tag{C-8}$$

$$\left[Y_{21}\right]_{\omega=\omega_0} = \left[\frac{1.949I_{E-DC}}{520mV}\right] = 0.107 \tag{C-9}$$

Step 4:

Loop Gain.

The loop gain is

$$Loop-Gain=[LG]_{sustained-condition}=\left[\frac{R_P Y_{21}(x)}{n}\right]=\left[\frac{R_P g_m}{x}\right]\left[\frac{2I_1(x)}{I_0(x)}\right]\left[\frac{1}{n}\right]>1 \tag{C-10}$$

$$R_{PEQ}(f_0)=R_P \parallel Bias-circuit \Rightarrow 50.73\Omega \tag{C-11}$$

As earlier derived, the loop gain should be 2.1 to have good starting conditions!

$$n=\left[\frac{R_{PEQ}Y_{21}(x)}{2.1}\right]=\frac{0.107*50.73}{2.1}\approx 2.523 \tag{C-12}$$

Step 5:

Calculation of the feedback capacitor ratio.

$$n=1+\left[\frac{C_1}{C_2}\right]=2.523 \Rightarrow \left[\frac{C_1}{C_2}\right]_{x=20}=1.523\ (2.523-1) \tag{C-13}$$

Step 6:

Calculation of absolute values of feedback capacitor.

The expression of Z_{in} (Looking in to the base of the transistor) can be given as

$$Z_{in}\cong -\left[\left(\frac{Y_{21}}{\omega^2(C_1^*+C_P)C_2}\right)\left(\frac{1}{(1+\omega^2 Y_{21}^2 L_P^2)}\right)\right]-j\left[\left(\frac{(C_1^*+C_P+C_2)}{\omega(C_1^*+C_P)C_2}\right)-\left(\frac{\omega Y_{21}L_P}{(1+\omega^2 Y_{21}^2 L_P^2)}\right)\left(\frac{Y_{21}}{\omega(C_1^*+C_P)C_2}\right)\right]$$

169

(C-14)

where

$C_P = (C_{BEPKG} + \text{contribution from layout}) = 1.1\text{pF}$

$L_P = (L_B + L_{BX} + \text{contribution from layout}) = 2.2\text{nH}.$

The expression for the negative resistance R_n is

$$R_{neq} = \frac{R_n}{(1+\omega^2 Y_{21}^2 L_P^2)} = \frac{R_n}{[1+(2\pi *1E9)^2 *(0.107)^2 *(2.2nH)^2]} \qquad \text{(C-15)}$$

$$R_{neq} \approx \frac{R_n}{3.65} \qquad \text{(C-16)}$$

$$R_n = -\left[\frac{Y_{21}^+}{\omega^2 C_1 C_2}\right]_{x=20} = \frac{0.107}{(2\pi *1E9)^2 C_1 C_2} \qquad \text{(C-17)}$$

R_n is the negative resistance without parasitics (C_P, L_P).

For sustained oscillation $\rightarrow R_{neq} \geq 2R_{PEQ} \cong 101.4\ \text{Ohm}$

$$R_n = 3.65 * 101.4 \approx 371 Ohm \qquad \text{(C-18)}$$

$$C_1 C_2 = \left[\frac{1}{\omega^2}\right]\left[\frac{0.107}{371}\right] \approx 7.26 \qquad \text{(C-19)}$$

$$\left[\frac{C_1}{C_2}\right]_{x=20} \approx 1.52 \qquad\qquad\qquad \text{(C-20)}$$

$$C_1 = 3.3\,pF \qquad\qquad\qquad\qquad \text{(C-21)}$$

$$C_2 = 2.2\,pF \qquad\qquad\qquad\qquad \text{(C-22)}$$

Step 7:

Calculation of the coupling capacitor r_e.

The expression for the coupling capacitor is

$$\frac{C}{10} > C_C > \left\{ \frac{(\omega^2 C_1 C_2)(1+\omega^2 Y_{21}^2 L_P^2)}{[Y_{21}^2 C_2 - \omega^2 C_1 C_2)(1+\omega^2 Y_{21}^2 L_P^2)(C_1 + C_P + C_2)]} \right\} \qquad\qquad \text{(C-23)}$$

$$C_c \rightarrow 0.4\,pF \qquad\qquad\qquad\qquad \text{(C-24)}$$

Figure C-5 shows the transistor in the package parameters for the calculation of the oscillator frequency and loop gain.
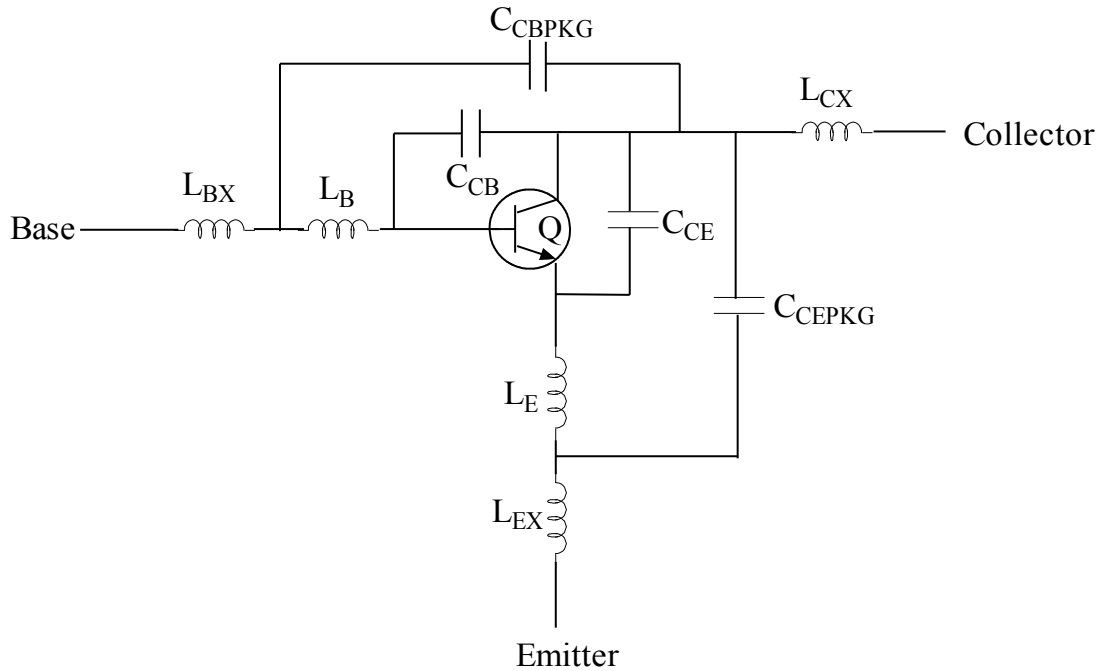
Figure 148: *Figure C-5 NE68830 with package parasitics. Q is the intrinsic bipolar transistor*

Tables C-1 and C-2 show NE68830 nonlinear parameters and package parameters which were taken from the NEC data sheets.

 Table C-1 Nonlinear parameters

Parameters	Q	Parameters	Q
IS	3.8E-16	MJC	0.48
BF	135.7	XCJC	0.56
NF	1	CJS	0
VAF	28	VJS	0.75
IKF	0.6	MJS	0
NE	1.49	TF	11E-12
BR	12.3	XTF	0.36
NR	1.1	VTF	0.65
VAR	3.5	ITF	0.61

IKR	0.06	PTF	50
ISC	3.5E-16	TR	32E-12
NC	1.62	EG	1.11
RE	0.4	XTB	0
RB	6.14	XTI	3
RBM	3.5	KF	0
IRB	0.001	AF	1
RC	4.2	VJE	0.71
CJE	0.79E-12	MJE	0.38
CJC	0.549E-12	VJC	0.65

Table C-2 Package parameters of NE68830

Parameters	NE68830
C_{CB}	0.24E-12
C_{CE}	0.27E-12
L_B	0.5E-9
L_E	0.86E-9
C_{CBPKG}	0.08E-12
C_{CEPKG}	0.04E-12
C_{BEPKG}	0.04E-12
L_{BX}	0.2E-9
L_{CX}	0.1E-9
L_{EX}	0.2E-9

Design Calculations

1.   Frequency of Oscillation

Frequency of the oscillation is

$$\omega_0 = \sqrt{\dfrac{1}{L\left[\dfrac{\left[\dfrac{(C_1^*+C_P)C_2 C_c}{(C_1^*+C_P+C_2)}\right]}{\left[\dfrac{(C_1^*+C_P)C_2}{(C_1^*+C_P+C_2)}+C_c\right]}+C\right]}} \approx 1000 MHz$$

(C-25)

with

L = 5nH (Inductance of the parallel resonator circuit)

$C_1^* = 2.2pF$

$C_1 = C_1^* + C_P$

$C_P = 1.1Pf$ (C_{BEPKG} + Contribution from layout)

$C_2 = 2.2pF$

$C_c = 0.4pF$

C =4.7pF

$R_P = 12000$ (Measured)

$$Q_{unloaded} = \left[\dfrac{R_P}{\omega L}\right] = 380$$
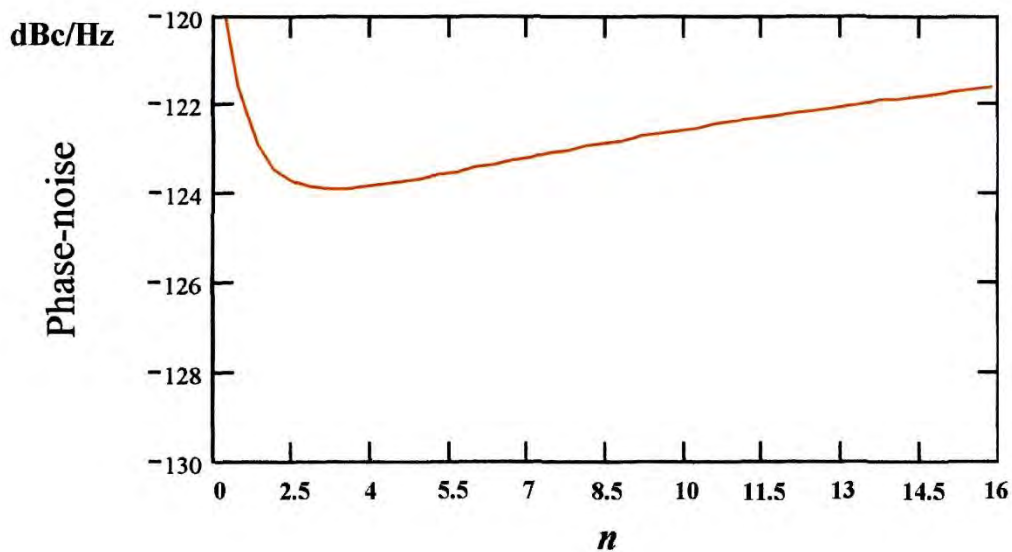
Figure 149: *Figure C-6   The phase noise contribution of the lossy resonator at 10 KHz offset.*

The calculated phase noise at 10 kHz off the carrier is –124 dBc/Hz, which agrees with the measurements within 1 dB. The other values are –140 dBc/Hz at 100 kHz offset and –160 dBc/Hz at 1 MHz offset.

 The actual measured phase noise is shown next.

 Considering that Equation (8-109) only contains shot and flicker noise, as well as resonator noise, it has been proven that this by itself is a very accurate formula for practical use. Figure 9-5 has been generated from using Ansoft Designer, which includes all noise sources and is based on the harmonic balance principle.

The important conclusion found in Chapter 8 is that for the first time we have a complete mathematical synthesis procedure for best phase noise that covers both flicker noise and white noise for the oscillator. In the past, most publications have referenced an oscillator built with many shortcuts and then the author found that the measured results agree with the expectations. A complete synthesis approach has not appeared previously.

$$(A-21)$$

The important message that can be derived from this calculation is the fact that the parasitics now dominate the design. The negative resistance which used to be proportional to $1/\omega^2$ now is $1/\omega^4$. The rule of thumb is to use a large device for lower frequencies and operate it at medium DC currents. This in the millimeter wave area would be fatal. The large device would have excessive parasitic elements such as inductors and capacitors and the optimum design is no longer possible since the parasitics would be larger than the values required for optimum performance. These parasitics are the major reason why at millimeter wave and wide tuning ranges the phase noise is not as good as what a narrowband Colpitts oscillator would provide.

2000 MHz GaAs FET-Based Oscillator

Low cost applications are frequently implemented as an RFIC. For further validation, a GaAs FET-based 2000 MHz Colpitts oscillator was designed and built. Figure 9-11 shows the circuit diagram of the oscillator. It uses a combination of transmission lines and rectangular inductors as resonators. The inductor in the middle of the schematic in Figure 9-11, connected to a via hole, is needed as a DC return. If a tuning diode is connected to the capacitor on the left of the schematic in Figure 9-11, then a DC control voltage can be applied, and the center inductor becomes an RF choke. The output is taken from the source. An additional external DC decoupling capacitor will be needed because of the DC coupling. The transistor and the circuit were constructed using the TriQuint GaAs Foundry and the transistor was optimized for the DC current. Figure 9-12 shows the predicted phase noise of this oscillator.

Figure 150: *Figure 9-11   Circuit schematic the 2 GHz GaAs FET oscillator built on GaAs substrate with very fine resolution of the components*

X1= 1.00E05Hz   X2= 1.00E06Hz   X3= 1.00E07Hz
Y1= -98.04dBc/Hz   Y2= -122.22dBc/Hz Y3= -142.68dBc/Hz
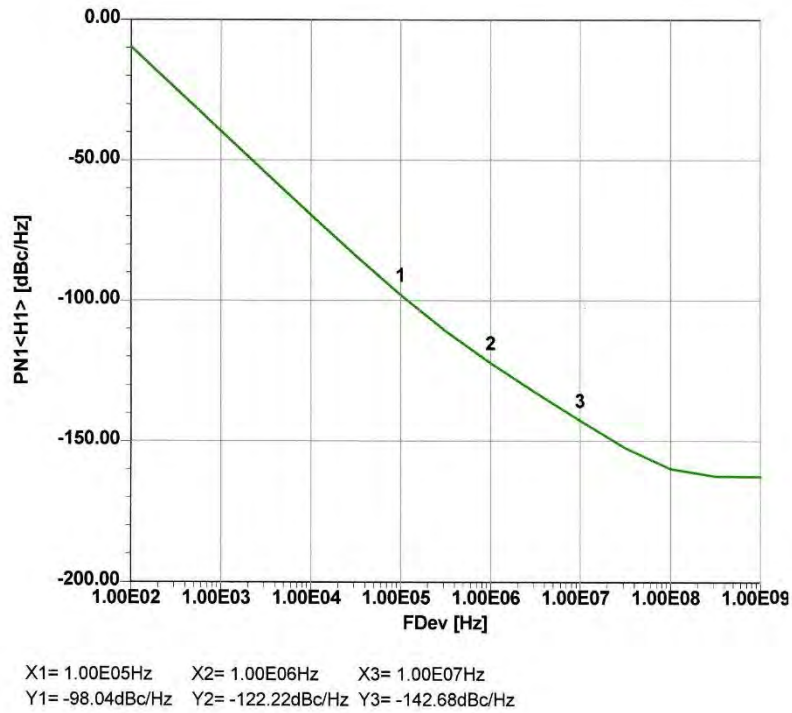
Figure 151: *Figure 9-12   Predicted phase noise of the oscillator shown in Figure 9-11.   The measured values were 100 dBc/Hz at 100 kHz and 120 dBc/Hz at 1 MHz. There is a deviation of about 2 dB compared to simulation.*

It is interesting to examine the load line of this oscillator, which is shown in Figure 9-13. This circuit is operated in a fairly linear range.
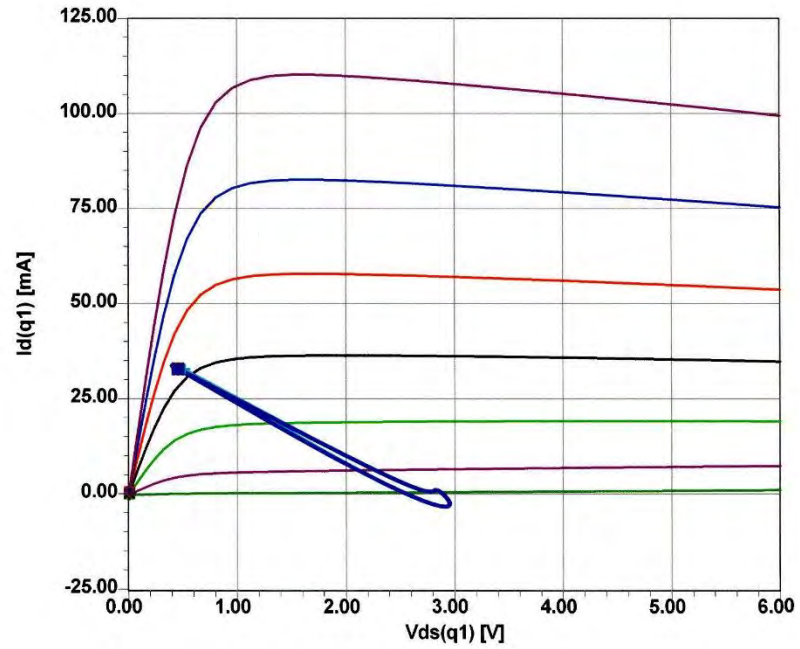
Figure 152: *Figure 9-13   Shows the DC-IV and the load line for the GaAs FET oscillator.*

Figure 9-14 shows the layout of the 2 GHz GaAs FET oscillator. Its output power is 1.8 dBm.
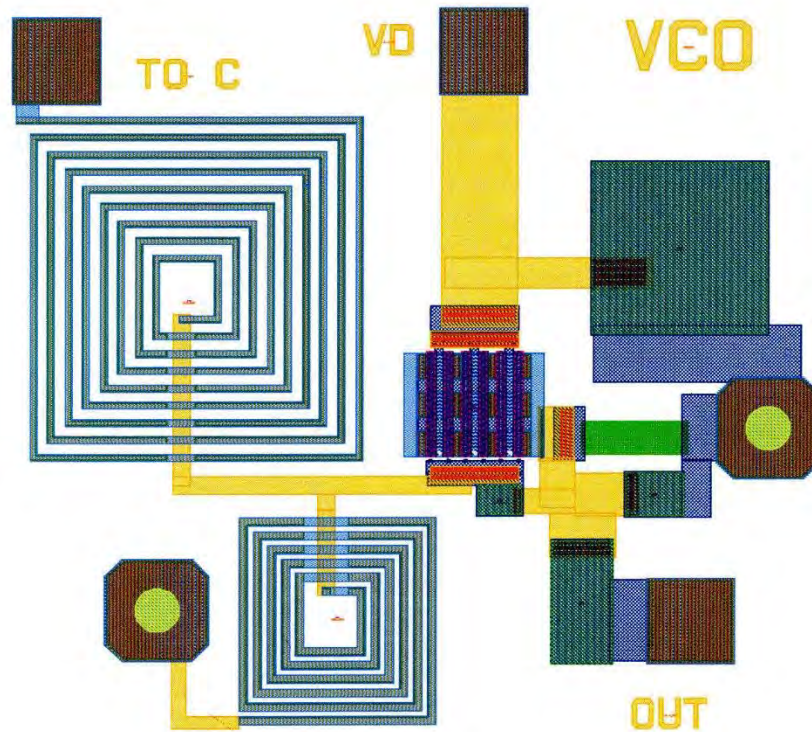
Figure 153: *Figure 9-14   Layout of the 2 GHz GaAs FET oscillator*

Now a detailed GaAs FET Oscillator Analysis

An FET Published Example

Figure D-5 shows a 950MHz MESFET oscillator circuit configuration based on the publication:

K. Cheng, K. Chan, "Power Optimization of High-Efficiency Microwave MESFET Oscillators," IEEE Transactions on Microwave Theory and Techniques, Vol. 48, No. 5, pp. 787 –790, May 2000.

And the analytical approach used there for optimum operating conditions for maximum oscillator output power. The analysis is based on a quasi-linear approach and is experimentally supported with the conversion efficiency of 54%, which is the maximum conversion efficiency published for this topology. However, the publication does not give any emphasis on the optimum phase noise, which is the key parameter for the oscillator design.

The main point of this section is to show a very thorough design procedure for the MES FET including optimization of the parameters for best performance. This is particular of interest as the author supplied measured data and not just simulation, and can show the amount of optimization.

Power optimization of the GaAs-950MHz-MESFET oscillator:
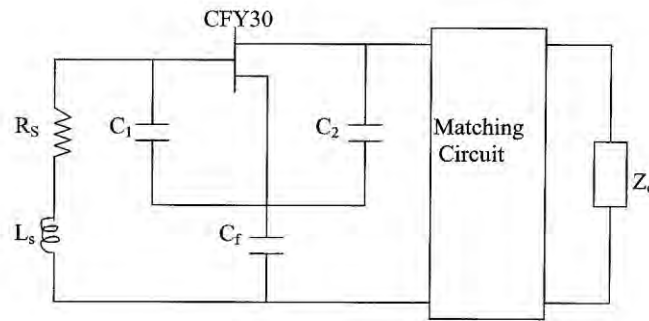
Figure 154: *Figure D-5   A 950MHz MESFET oscillator circuit configuration*

The derivation of the analytical expressions are based on the open loop model of the oscillator. Figure D-6 shows an equivalent circuit of the oscillator shown in Figure 6-46.

Here are the SPICE parameters:

```
.MODEL CFY30 FET (
+    IDSS=  .4425E-01  VP0 = -.1413E+01  GAMA= -.7250E-01  E   =  .1581E+01
+    KE  = -.1169E-01  SL  =  .1399E+00  KG  =  .3045E+00  MGS =  .5000E+00
+    MGD =  .5000E+00  FCC =  .8000E+00  T   =  .5234E-11  SS  =  .4856E-03
+    IG0 =  .9350E-12  AFAG=  .1790E+02  IB0 =  .1270E-06  AFAB=  .1120E+01
+    VBC =  .9000E+01  R10 =  .1229E+02  KR  = -.9807E-01  C10 =  .3583E-12
+    K1  =  .8877E+00  C1S =  .0000E+00  CF0 =  .2034E-13  KF  =  .5000E+00
+    RG  =  .6887E+01  RD  =  .8653E+01  RS  =  .4053E+00  LG  =  .8197E-09
+    LD  =  .8812E-09  LS  =  .7181E-10  CDS =  .1129E-12  CDSD=  .1000E-04
+    RDSD=  .2967E+03  CGE =  .2257E-13  CDE =  .4703E-13  CGSP=  .5359E-13
+    CDSP=  .2827E-13  ZGT =  .5000E+02  LGT =  .2317E-02  ZDT =  .5000E+02
+    LDT =  .2389E-02  CGDP=  .8908E-17  ZST =  .5000E+02  LST =  .2606E-03
+    CGDE=  .2987E-13  VDMX=10)
! Siemens's GaAs FET in SOT-143 Package
```
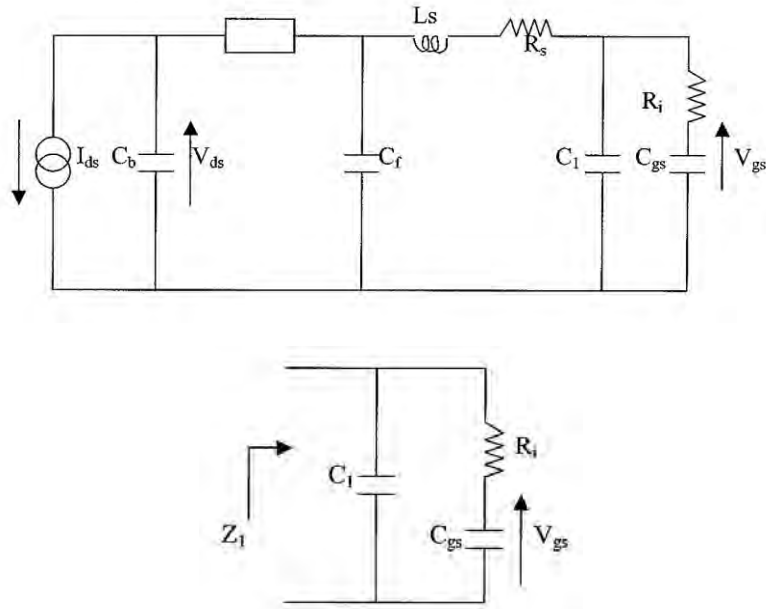
Figure 155: *Figure D-6   An equivalent circuit of the open model MESFET oscillator.*

Z_1 can be expressed as

$$Z_1 = \frac{\left[R_i + \dfrac{1}{j\omega C_{gs}}\right]\dfrac{1}{j\omega C_1}}{\left[R_i + \dfrac{1}{j\omega C_{gs}} + \dfrac{1}{j\omega C_1}\right]} = \frac{-\left[\dfrac{jR_i}{\omega C_1} + \dfrac{1}{\omega^2 C_{gs}C_1}\right]}{\left[R_i - j\left(\dfrac{1}{\omega C_{gs}} + \dfrac{1}{\omega C_1}\right)\right]}$$

(D-138)

Multiplying the numerator and the denominator by the conjugate yields:

$$Z_1 = \frac{\left[\dfrac{-jR_i^2}{\omega C_1} - \dfrac{R_i}{\omega^2 C_{gs}C_1}\right] + \dfrac{R_i}{\omega^2 C_1}\left[\dfrac{1}{C_1} + \dfrac{1}{C_{gs}}\right] - \dfrac{j}{\omega^3 C_{gs}C_1}\left[\dfrac{1}{C_1} + \dfrac{1}{C_{gs}}\right]}{\left[R_i^2 + \left(\dfrac{1}{\omega C_{gs}} + \dfrac{1}{\omega C_1}\right)^2\right]}$$

(D-139)

The following assumptions are made for simplification purposes.

$$\frac{R_i}{\omega^2 C_{gs} C_1} << \frac{R_i}{\omega^2 C_1}\left[\frac{1}{C_1} + \frac{1}{C_{gs}}\right] \tag{D-140}$$

$$\frac{jR_i^2}{\omega C_1} << \frac{j}{\omega^3 C_{gs} C_1}\left[\frac{1}{C_1} + \frac{1}{C_{gs}}\right] \tag{D-141}$$

$$R_i << \left|\frac{1}{\omega C_{gs}} + \frac{1}{\omega C_1}\right| \tag{D-142}$$

then modified Z_1 can be represented as

$$Z_1 = \left|\frac{\dfrac{R_i}{\varpi^2 C_1}\left(\dfrac{1}{C_1} + \dfrac{1}{C_{gs}}\right) - \dfrac{j}{\omega^3 C_{gs} C_1}\left(\dfrac{1}{C_1} + \dfrac{1}{C_{gs}}\right)}{\left(\dfrac{1}{\omega C_{gs}} + \dfrac{1}{\omega C_1}\right)^2}\right| \tag{D-143}$$

$$Z_1 = \left|\frac{\left(\dfrac{R_i}{C_1}\right)}{\left(\dfrac{1}{C_1} + \dfrac{1}{C_{gs}}\right)} - \left(\dfrac{j}{\omega[C_1 + C_{gs}]}\right)\right| \tag{D-144}$$

defining the three new variables as

$$C_a = C_1 + C_{gs} \tag{D-145}$$

183

$$C_b = C_2 + C_{ds} \qquad\qquad\qquad \text{(D-146)}$$

$$R_a = R_s + \frac{C_{gs}^2}{C_a^2} R_i \qquad\qquad\qquad \text{(D-147)}$$

$$X_a = \omega L_s - \frac{1}{\omega C_a} \qquad\qquad\qquad \text{(D-148)}$$

$$\omega(X_a = 0) = \frac{1}{\sqrt{L_s C_a}} \qquad\qquad\qquad \text{(D-149)}$$

Figure D-7 shows a simplified open loop model of the oscillator for easy analysis. In this open loop model, the parasitic elements of the device are absorbed into the corresponding embedding impedances.
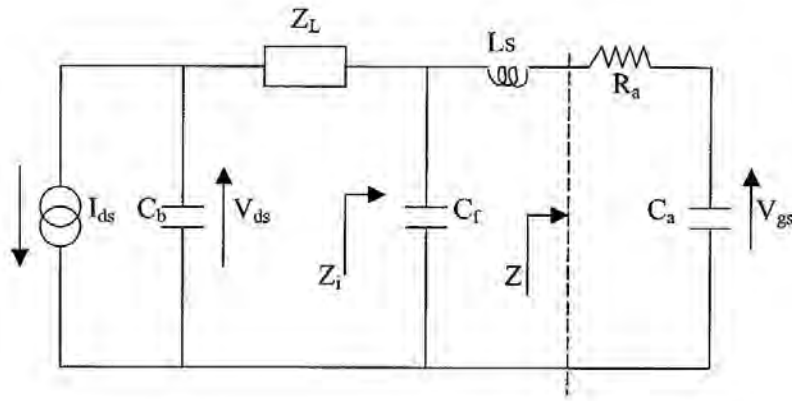
Figure 156: *Figure D-7 A simplified loop model of the oscillator.*

$$Z = R_a + \frac{1}{j\omega C_a} \Rightarrow R_s + \frac{C_{gs}^2}{C_a^2} R_i - \frac{j}{\omega C_a} \qquad\qquad \text{(D-150)}$$

$$Z + j\omega L_s = R_s + \frac{C_{gs}^2}{C_a^2} R_i - \frac{j}{\omega C_a} + j\omega L_s \Rightarrow \left[R_s + \frac{C_{gs}^2}{C_a^2} R_i \right] + j\left[\omega L_s - \frac{1}{\omega C_a} \right]$$
$$\qquad\qquad\qquad\qquad\qquad\qquad\qquad\qquad\qquad \text{(D-151)}$$

184

$$Z_a = Z + j\omega L_s \Rightarrow R_a + jX_a \qquad\qquad\qquad\text{(D-152)}$$

$$R_a = R_s + \frac{C_{gs}^2}{C_a^2} R_i \qquad\qquad\qquad\text{(D-153)}$$

$$X_a = \omega L_s - \frac{1}{\omega C_a} \qquad\qquad\qquad\text{(D-154)}$$

$$Z_i = Z_a \parallel C_f \Rightarrow [Z + j\omega L_s] \parallel C_f \qquad\qquad\qquad\text{(D-155)}$$

$$Z_i = \frac{-j\left[\dfrac{R_a + jX_a}{\omega C_f}\right]}{\left[R_a + jX_a - \dfrac{j}{\omega C_f}\right]} \Rightarrow \frac{[R_a + jX_a]}{[1 + jR_a\omega C_f - \omega C_f X_a]} = \frac{[R_a + jX_a]}{1 + j\omega C_f[R_a + jX_a]}$$

$$\text{(D-156)}$$

The circuit model of the oscillator is shown in Figure D-8, in which the output current through Z_L is given as

$$I = \frac{I_{ds}}{1 + j\omega C_b[Z_i + Z_L]} \qquad\qquad\qquad\text{(D-157)}$$
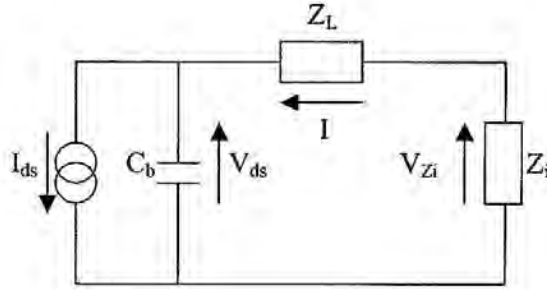
Figure 157: *Figure D-8   A circuit model of an oscillator.*

The voltage across Z_i is given as:

$$V_{zi} = IZ_i = -I_{ds}\left[\frac{[R_a + jX_a]}{1 + j\omega C_f[R_a + jX_a]}\right]\left[\frac{1}{1 + j\omega C_b[Z_i + Z_L]}\right] \qquad \text{(D-158)}$$

Applying the voltage divider in Figure D-8, V_{gs} can be expressed as

$$V_{gs} = -I_{ds}\left[\frac{1}{j\omega C_b[R_a + jX_a]}\right]\left[\frac{Z_i}{1 + j\omega C_b[Z_i + Z_L]}\right] \qquad \text{(D-159)}$$

Steady-state oscillation occurs when $I_{ds}(t)=I_1$ and $V_{gs}=V_p$. Consequently, the equation above can be written as

$$1 + j\omega C_b[Z_i + Z_L] = -\frac{I_{ds}}{V_{gs}}\frac{Z_i}{j\omega C_a(R_a + jX_a)} \qquad \text{(D-160)}$$

$$1 + j\omega C_b[Z_i + Z_L] = \frac{-g_{mc}Z_i}{j\omega C_a(R_a + jX_a)} \Rightarrow \frac{-g_{mc}[R_a + jX_a]}{j\omega C_a(R_a + jX_a)[1 + j\omega C_f(R_a + jX_a)]} \qquad \text{(D-161)}$$

$$1 + j\omega C_b [Z_i + Z_L] = \frac{-g_{mc}}{j\omega C_a [1 + jwC_f(R_a + jX_a)]} = \frac{g_{mc}}{\omega^2 C_f C_a - j[\omega C_a - \omega^2 C_f C_a X_a]}$$

(D-162)

$$Z_L = Z_i \frac{g_{mc}}{\omega^2 C_b C_a [R_a + jX_a]} - Z_i - \frac{1}{j\omega C_b}$$

(D-163)

$$Z_L = \frac{g_{mc}(R_a + jX_a)}{[1 + j\omega C_f(R_a + jX_a)][\omega^2 C_b C_a(R_a + jX_a)]} - \frac{(R_a + jX_a)}{[1 + j\omega C_f(R_a + jX_a)]} - \frac{1}{j\omega C_b}$$

(D-164)

$$Z_L = \frac{g_{mc}}{\omega^2 C_b C_a [1 + j\omega C_f(R_a + jX_a)]} - \frac{(R_a + jX_a)}{[1 + j\omega C_f(R_a + jX_a)]} - \frac{1}{j\omega C_b}$$

(D-165)

where

$$g_{mc} = \frac{I_1}{V_p} = \frac{I_{max}}{2V_p}$$

(D-166)

In addition, V_{ds} can be determined by calculating $I_{cb,}$ the current through C_b with the help of Figure D-8.

$$I_{cb} = I_{ds} \frac{[Z_L + Z_i]}{Z_L + Z_i + 1/j\omega C_b}$$

(D-167)

Based on the last result we can conclude that

$$V_{ds} = I_{cb} \frac{j}{\omega C_b} = \frac{[Z_L + Z_i]}{Z_L + Z_i + 1/j\omega C_b} I_1$$

(D-168)

or in square magnitude form

$$V_{ds}^2 = \frac{[Z_L + Z_i]^2}{[1 + j\omega C_b(Z_L + Z_i)]^2} I_1^2$$
(D-169)

Also, Re[Z_L] can be defined as follows

$$\text{Re}[Z_L] = \frac{g_{mc}[1 - \omega C_f X_a - j\omega C_f R_a]}{\omega^2 C_b C_a[(1 - \omega C_f X_a)^2 + \omega^2 C_f^2 R_a^2]} - \frac{(R_a + jX_a)[1 - \omega C_f X_a - j\omega C_f R_a]}{[(1 - \omega C_f X_a)^2 + \omega^2 C_f^2 R_a^2]}$$
(D-170)

$$\text{Re}[Z_L] = \frac{g_{mc}[1 - \omega C_f X_a - j\omega C_f R_a] - \omega^2 C_b C_a(R_a + jX_a)[1 - \omega C_f X_a - j\omega C_f R_a]}{\omega^2 C_b C_a[(1 - \omega C_f X_a)^2 + \omega^2 C_f^2 R_a^2]}$$
(D-171)

$$\text{Re}[Z_L] = \frac{g_{mc}[1 - \omega C_f X_a] - \omega^2 C_b C_a R_a + \omega^3 C_b C_a C_f X_a - \omega^3 C_b C_a C_f R_a)}{\omega^2 C_b C_a[(1 - \omega C_f X_a)^2 + \omega^2 C_f^2 R_a^2]}$$
(D-172)

The power delivered to the load Z_L and the magnitude of V_{ds} can be determined by

$$P_{out} = \frac{1}{2} I^2 \text{Re}[Z_L]$$
(D-173)

$$P_{out} = \frac{1}{2} I_1^2 \frac{\text{Re}[Z_L]}{[1 + j\omega C_b(Z_L + Z_i)]^2}$$
(D-174)

$$V_{ds}^2 = \frac{[Z_L + Z_i]^2}{[1 + j\omega C_b(Z_L + Z_i)]^2} I_1^2$$
(D-175)

$$[1 + j\omega C_b(Z_i + Z_L)]^2 = \frac{g_{mc}^2}{[\omega^2 C_f C_a R_a - j(\omega C_a - \omega^2 C_f C_a X_a)][\omega^2 C_f C_a R_a + j(\omega C_a - \omega^2 C_f C_a X_a)]}$$

(D-176)

188

$$1 + j\omega C_b(Z_i + Z_L)]^2 = \frac{g_{mc}^2}{(\omega^2 C_f C_a R_a)^2 + (\omega C_a - \omega^2 C_f C_a X_a)^2} = \frac{g_{mc}^2}{\omega^2 C_a^2[(1 - \omega^2 C_f C_a X_a)^2 + (\omega^2 C_f C_a R_a)^2}$$

(D-177)

Based on the equations above, the output power can be estimated as

$$P_{out} = \frac{1}{2} I^2 \, \mathrm{Re}[Z_L]$$

(D-178)

$$P_{out} = \frac{1}{2} I_1^2 \frac{\mathrm{Re}[Z_L]}{[1 + j\omega C_b(Z_L + Z_i)]^2}$$

(D-179)

$$P_{out} = \frac{1}{2} I_1^2 \frac{\left\{ \dfrac{g_{mc}[1 - \omega C_f X_a] - \omega^2 C_b C_a R_a + \omega^3 C_b C_a C_f X_a - \omega^3 C_b C_a C_f R_a)}{\omega^2 C_b C_a[(1 - \omega C_f X_a)^2 + \omega^2 C_f^2 R_a^2]} \right\}}{\left\{ \dfrac{g_{mc}^2}{\omega^2 C_a^2[(1 - \omega^2 C_f C_a X_a)^2 + (\omega^2 C_f C_a R_a)^2]} \right\}}$$

(D-180)

$$P_{out} = \frac{1}{2} I_1^2 C_a \frac{[1 - \omega C_f X_a] - \omega^2 C_b C_a R_a + \omega^3 C_b C_a C_f X_a - \omega^3 C_b C_a C_f R_a)}{g_{mc} C_b}$$

(D-181)

Below 5 GHz, it is valid to ignore some of the terms by assuming that

$$\omega^2 C_b C_a R_a \gg \omega^3 C_b C_a C_f X_a$$

(D-182)

$$\omega^2 C_b C_a R_a \gg \omega^3 C_b C_a C_f R_a$$

(D-183)

The power output is now expressed as

$$P_{out} = \frac{1}{2}I_1^2 C_a \frac{g_{mc}[1-\omega C_f X_a]-\omega^2 C_b C_a C_f R_a)}{g_{mc}^2 C_b}$$
(D-184)

$$P_{out} = \frac{1}{2}I_1^2\left[C_a w\frac{[1-\omega C_f X_a]}{\omega C_b} - \frac{\omega^2 C_a^2 R_a}{g_{mc}^2} \right]$$
(D-185)

$$P_{out} = \frac{1}{2}I_1^2\left[\alpha \frac{[1-\omega C_f X_a]}{\omega C_b} - \alpha^2 R_a \right]$$
(D-186)

$$\alpha = \frac{\omega C_a}{g_{mc}}$$
(D-187)

In a similar manner, V_{ds} is given by

$$V_{ds}^2 = I_1^2\left[\frac{\alpha^2[1-\omega C_f X_a]^2 + [1-\omega C_f R_a]^2}{\omega^2 C_b^2} \right]$$
(D-188)

Both the output power and V_{ds} depend on C_b if the other parameters are fixed.

This is a limitation for the maximum value. However, a maximum value of the current and the voltage a transistor can take before burn-out. Therefore, by setting $|V_{ds}| = V_{dsm}$ give an optimal condition according to the author is given by

$$\frac{|V_{ds}|^2}{I_1^2} = \frac{|V_{dsm}|^2}{I_1^2} = \frac{\alpha^2[1-\omega C_f X_a]^2 + [1-\omega C_f R_a]^2}{\omega^2 C_b^2}$$
(D-189)

The optimum load impedance that the device needs to see to deliver the highest power is defined as

$$\frac{|V_{ds}|}{I_1} = \frac{2|V_{dsm}|}{I_{max}} = R_{opt} \tag{D-190}$$

leading to the following definition

$$\omega C_b R_{opt} = \sqrt{\alpha^2 [1 - \omega C_f X_a]^2 + [1 - \omega C_f R_a]^2} \tag{D-191}$$

Using the result above, the optimum P_{out} is, therefore, given by

$$P_{out} = \frac{V_{dsm} I_{dsm}}{4} \alpha \frac{[1 - \omega C_f X_a]}{\sqrt{\alpha^2 [1 - \omega C_f X_a]^2 + [1 - \omega C_f R_a]^2}} - (\omega C_a V_p)^2 \frac{R_a}{2} \tag{D-192}$$

The first term is the power available from the current source and the second term is the power absorbed by R_a. This also indicates that a high Q inductor minimizes the absorbed power, increasing the power available from the current source. P_{out} simplifies further at the oscillation frequency since $X_a \approx 0$.

$$P_{out} = \frac{V_{dsm} I_{dsm}}{4} \alpha \frac{1}{\sqrt{\alpha^2 + [1 - \alpha \omega C_f R_a]^2}} - (\omega C_a V_p)^2 \frac{R_a}{2} \tag{D-193}$$

The above analytical analysis gives the following important results:

1) Maximum output power is attained if we set

$$C_f = \frac{1}{\alpha \omega R_a} \tag{D-194}$$

and

$$P_{out}(\text{max}) = \frac{V_{dsm} I_{max}}{4} \left[1 - \frac{1}{G}\right] \tag{D-195}$$

$$\frac{1}{G} = \frac{P_f}{P_{av}} = \omega^2 C_a^2 R_a \frac{2V_p^2}{V_{dsm} I_{max}} \tag{D-196}$$

Accordingly, the DC/RF conversion efficiency is calculated by

$$P_{dc} = \frac{V_{DS} I_{max}}{\pi} \tag{D-197}$$

$$\eta_{max} = \frac{P_{out}(\text{max})}{P_{dc}} \tag{D-198}$$

$$\eta_{max} = \left[1 - \frac{1}{G}\right] \frac{V_{dsm}}{V_{DS}} \tag{D-199}$$

In order to maximize the oscillator output power and efficiency, the loss resistance R_a of the input circuit has to be reduced (increasing G), and an optimal biasing condition V_{DS} has to be selected.

2)
$$C_b = \frac{[1 - \omega C_f R_a] C_a}{g_{mc} R_{opt}} \tag{D-200}$$

$$C_b(C_f = 0) = \frac{C_a}{g_{mc} R_{opt}} \tag{D-201}$$

3) Combining the above equation leads to expressions for Z_L in terms of

$$Z_L = \frac{1 + j\alpha}{1 + \alpha^2} R_{opt} \qquad\qquad\qquad \text{(D-202)}$$

From these analytical calculations, the following results were achieved. The circuit simulation of the oscillator done was using a nonlinear Materka model.
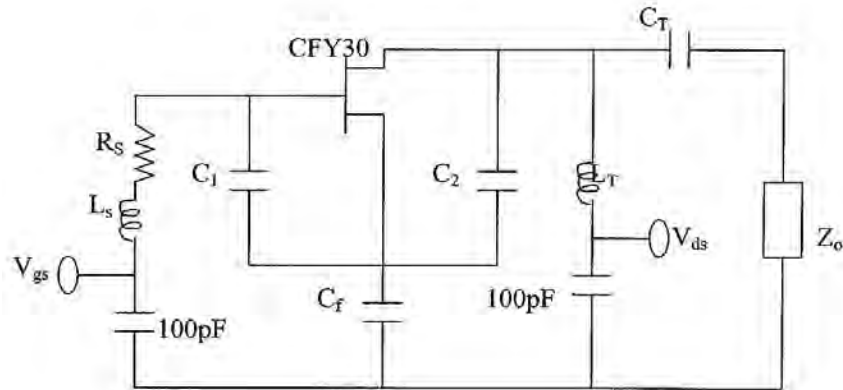
Figure 158: *Figure D-9 Schematic diagram of the oscillator operating at 950 MHz as published in [108].*

Figure D-9 above shows the schematic diagram of a practical oscillator operating at 950 MHz. A simple high-pass filter consisting of L_T and C_T is used to transfer the $Z_0/50\Omega$ load to the required Z_L value.

From above expression all the effective components of oscillator can be given as:

1.   Bias condition:

$$V_{DS} = 5V$$

$$I_{DS} = 18mA$$

2.   Device Parameters:

$I_{max} = 45mA$

$V_P = 1.25V$

$V_K (knee-voltage) = 0.5V$

3.　　Device Parasitic:

$C_{gs} = 0.5pF$

$C_{ds} = 0.2pF$

$C_{gd} = 0.0089pF$

4.　　Oscillator Parameters:

$$\omega = \frac{1}{\sqrt{L_s C_a}} \Rightarrow f = 950MHz$$

$C_1 = 6pf$

$C_2 = 1.5pf$

$C_f = 20pF$

$L_s = 3.9nH$

$$C_a = C_1 + C_{gs} = 6.5\,pF$$

$$C_b = C_2 + C_{ds} = 1.7\,pF$$

$$L'_f = 18nH$$

$$C'_f = 15\,pF$$

$$R_a = R_s + \frac{C_{gs}^2}{C_a^2}R_i = 4\Omega$$

5.   Output matching circuit:

$$L_d(pacakge) = 0.7nH$$

$$L_T = 8.9nH$$

$$L'_T = 8.9nH - L_d = 8.7nH$$

$$C_T = 1.91\,pF$$

6.   Calculation of R_{opt}:

$$I_{dc} = \frac{I_{max}}{\pi}$$

$$I_1 = \frac{I_{max}}{2} = 22.5mA$$

$$R_{opt} = \frac{V_{dsm}}{I_1} = \frac{V_{DS} - V_K}{I_1} = \frac{5V - 0.5V}{22.5mA} = 200\Omega$$

7.   Calculation of Z_L:

$$Z_L = \frac{1 + j\alpha}{1 + \alpha^2} R_{opt}$$

$$g_{mc} = \frac{I_1}{V_p} = \frac{I_{max}}{2V_p} = \frac{45mA}{2*1.25} = 18.8mS$$

$$\alpha = \frac{w_0 C_a}{g_{mc}} = \frac{2*\pi*950E+6*6.5E-12}{0.0188} = 2.0$$

$$Z_L = \frac{1 + j\alpha}{1 + \alpha^2} R_{opt} = \frac{1 + j2}{1 + 4} * 200 = 40 + j80\Omega$$

8.   Output power:

$$P_{out}(\text{max}) = \frac{V_{dsm} I_{max}}{4} \left[1 - \frac{1}{G}\right] = 16.6dBm$$

$$\frac{1}{G} = \frac{P_f}{P_{av}} = \omega^2 C_a^2 R_a \frac{2V_p^2}{V_{dsm} I_{max}}$$

9.   DC-RF conversion efficiency:

$$P_{dc} = \frac{V_{DS} I_{max}}{\pi} = \frac{5 * 45mA}{\pi} = 71.62mW$$

$$\eta_{max} = \frac{P_{out}(\text{max})}{P_{dc}} = \frac{45.7mW}{71.62mW} = 0.64$$

$$\eta_{max} = 64\%$$

Simulated Results

Figures D-10, D-11, D-12, D-13, D-14, and D-15 show the oscillator test circuit and its simulated results. After the oscillator circuit is analyzed in the harmonic-balance program, the oscillator frequency is found to be 1.08 GHz, and some tuning is required to bring the oscillator frequency back to the required value by changing L_s from 3.9nH to 4.45nH. The slight shift in the oscillator frequency may be due to the device parasitic. The simulated power output is 17.04 dBm, which is about the same as the measured value by [108]. The DC to RF conversion efficiency at the fundamental frequency is 55%. The calculation in [108], as well as the calculation here, assumes an ideal transistor. By finding a better value between C_1 and C_2, the efficiency was increased to 64%, compared to the published result of 55%. This means that the circuit in [108] has not been properly optimized.
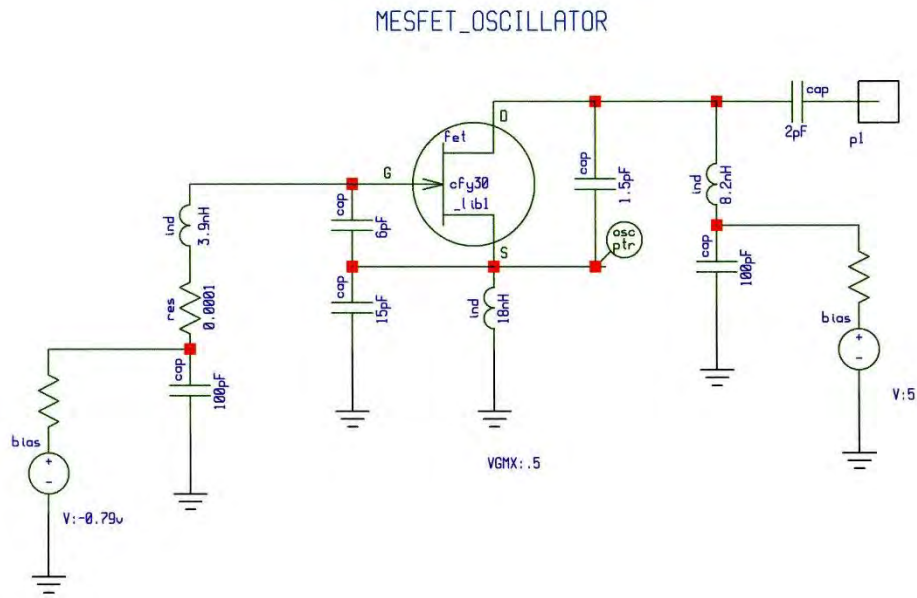
Figure 159: *Figure D-10   Schematic of the test oscillator based on [108].*
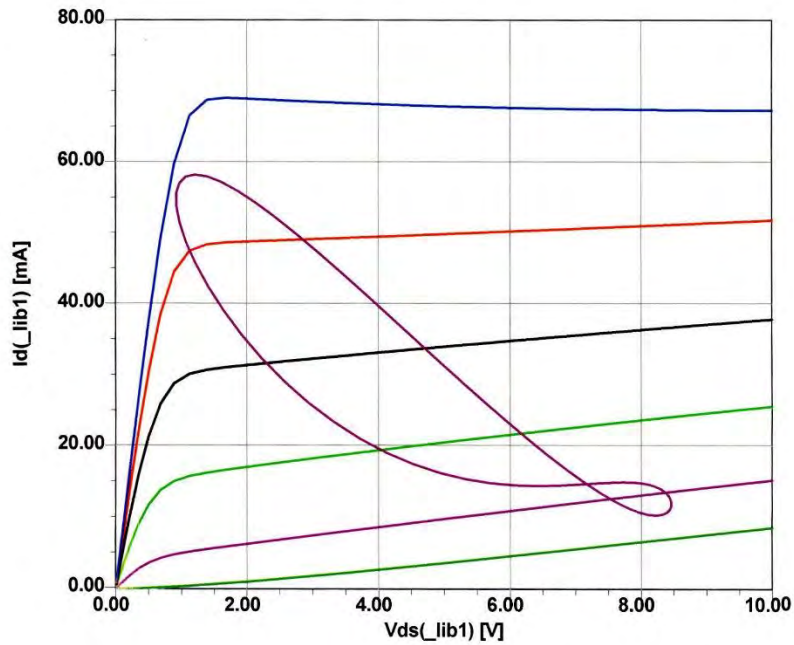
Figure 160: *Figure D-11   Load line of the oscillator shown in Figure D-10. Because the load is a tuned circuit, the "load line" is a curve and not a straight line.*

198
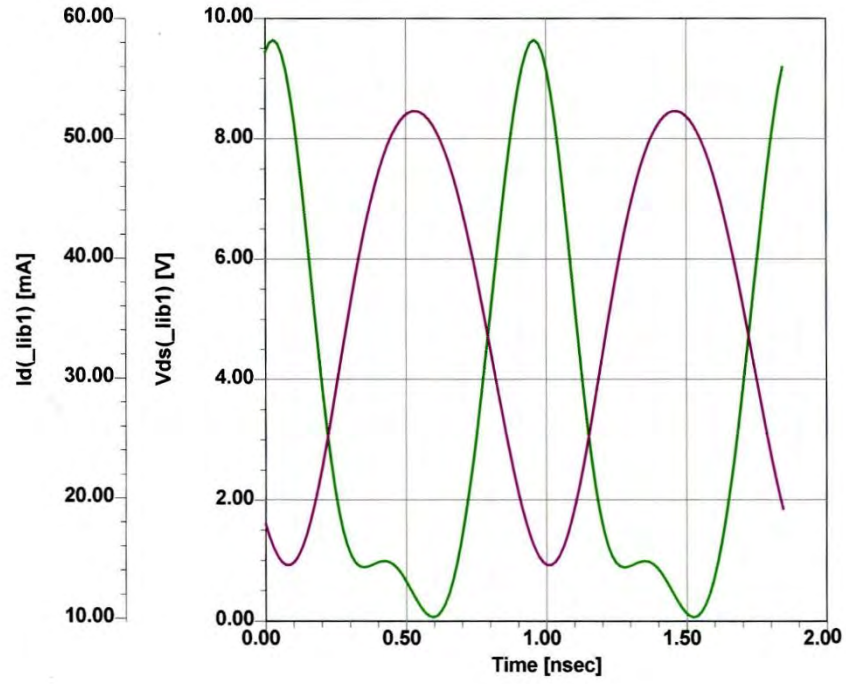
Figure 161: *Figure D-12   Plot of drain current and drain source voltage as a function of time.*
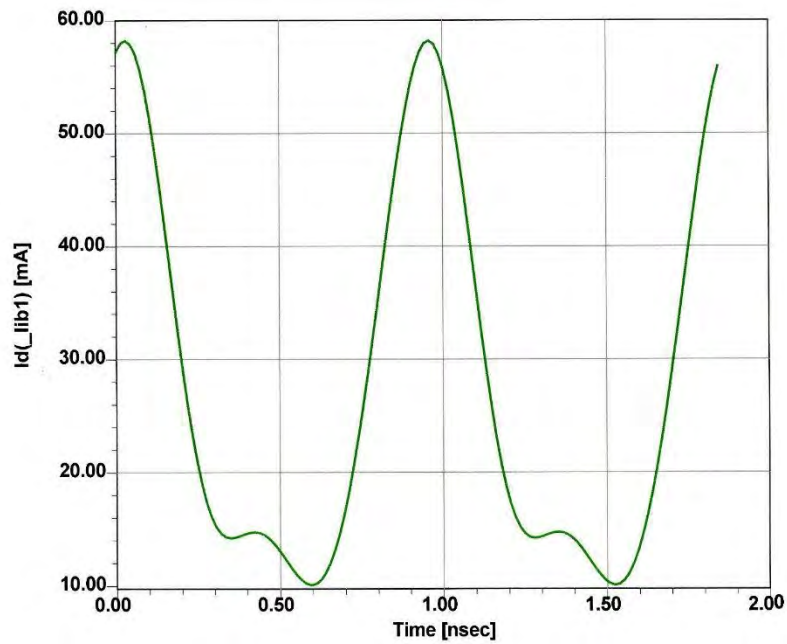
Figure 162: *Figure D-13   AC drain current simulated for Figure D-10.*

199
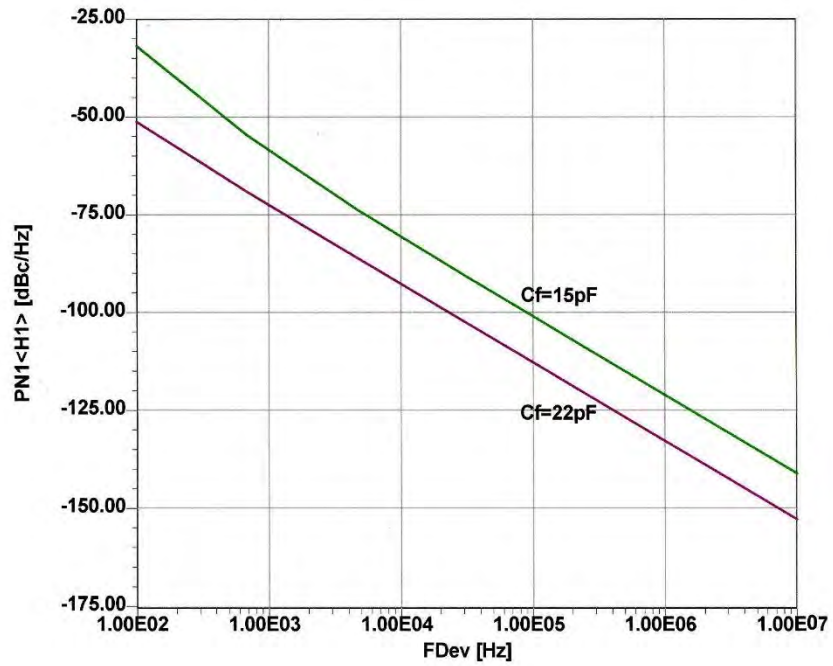
Figure 163: *Figure D-14 Simulated noise figure of the circuit shown in Figure D-10. An increase of the feedback capacitor from 15 to 22pF improves the phase noise.*
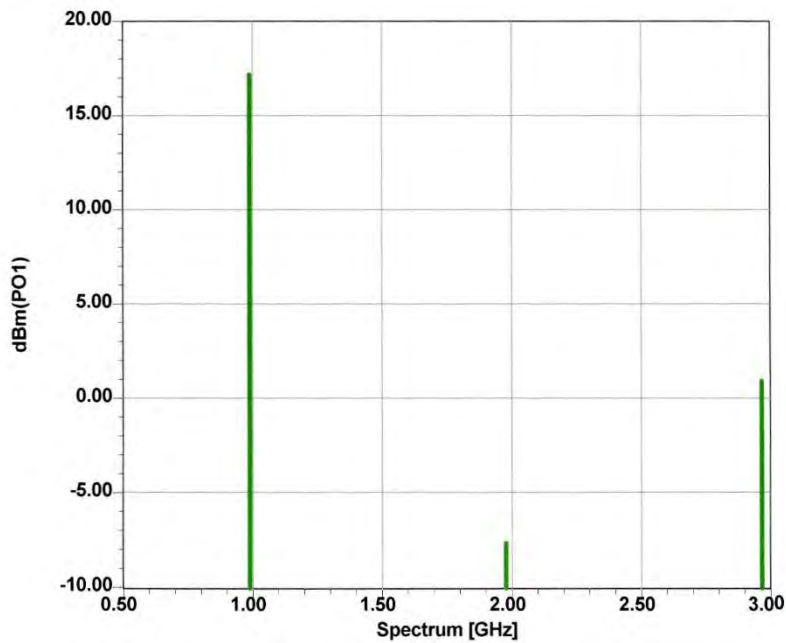
Figure 164: *Figure D-15 Simulated output power of the oscillator shown in Figure D-10.*

Taking the published experimental results into consideration, the analytical expression gives excellent insight into the performance of the oscillator circuit.

The maximum achievable output power and efficiency for a given active device can be predicted through the closed-form expressions without the need of a large-signal device characterization and an HB-simulation. This publication for has not addressed the power optimization and best phase noise, which is a very important requirement for the oscillator. By proper selection of the feedback ratio at the optimum drive level, the noise is improved by 8 dB, keeping the output power approximately the same. In Chapter 8 we discuss fixing the optimum feedback ratio and the absolute values of the feedback capacitor, with consideration for the best possible phase noise.

The design of the cross coupled oscillator

Phase Noise in CMOS Differential LC Oscillators

Ali Hajimiri Thomas H. Lee

Stanford University, Stanford, CA 94305

Figure 165: *A symmetric LC Oscillator*

201

2400 MHz MOSFET-Based Push-Pull Oscillator
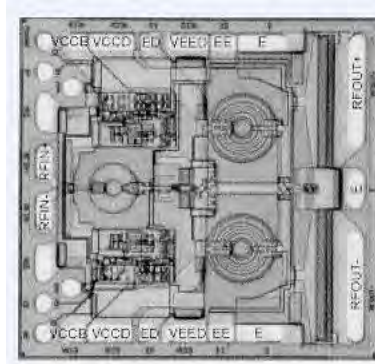
Figure 166: *Push-Pull Oscillator*
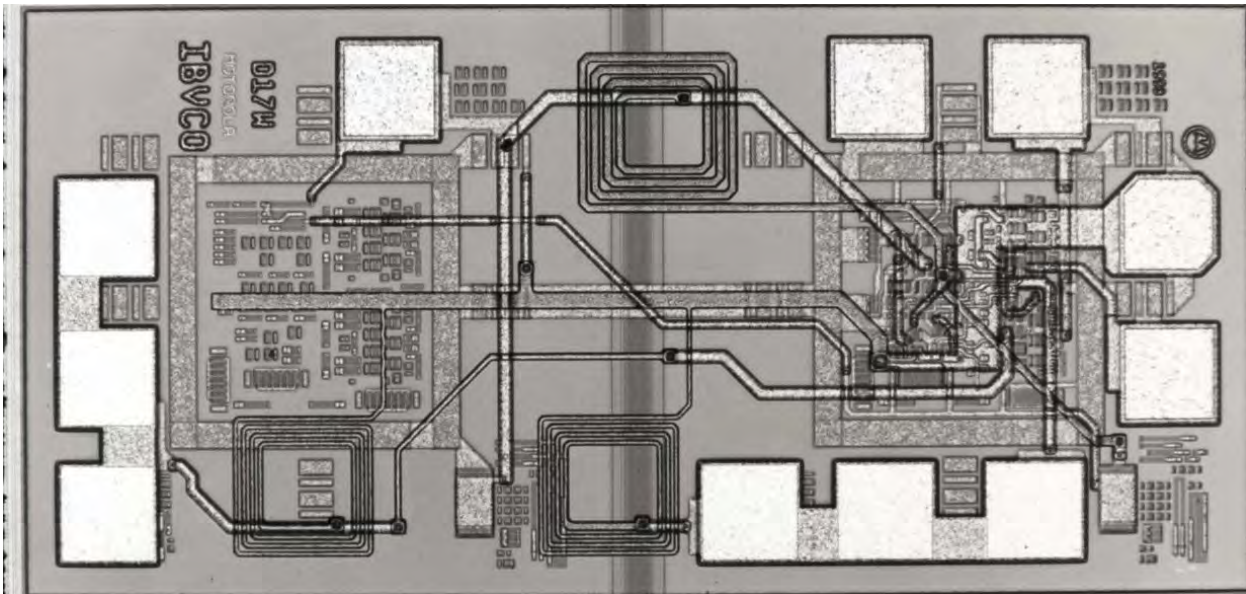
Figure 167: *Another example of a Push-Pull Oscillator*

Wireless applications are extremely cost sensitive, and when implemented as an RFIC, they are designed using silicon technology. Most mixers in RFIC's are built on the principle of differential amplifiers (Gilbert cell) and require a phase and out of phase signal (symmetrical drive). For these symmetrical requirements, this is best achieved using a push-pull technology with two outputs. The design choices are SiGe transistors or BiCMOS transistors. As will be seen, the critical phase noise is determined by the Q of the inductor and other elements of the resonator and by the flicker noise from the device. Here is some relevant literature

Systematic characterization for RF small-signal parameter extraction of 28 nm FDSOI MOSFETs up to 110 GHz

https://www.sciencedirect.com/science/article/abs/pii/S0026269223001751?via%3Dihub

Figure 8-23 shows the circuit of the 2400 MHz integrated CMOS oscillator 0.35um in cross-coupled (push-pull) configuration, the 0.35umsize was used for the numerical example and doesn't not represent the state of the art!
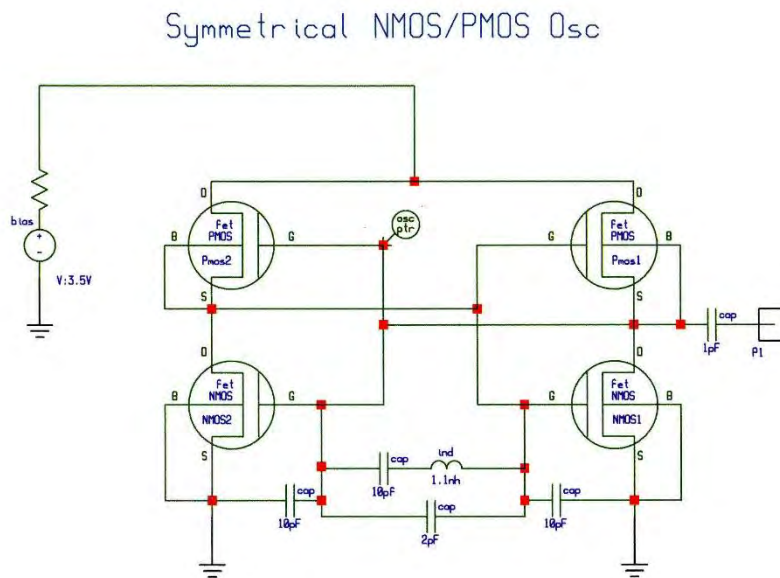
Figure 168: *Figure 8-23 Circuit of the 2400 MHz integrated CMOS oscillator.*

The circuit above uses a cross-coupled CMOS-NMOS pair as an oscillator. The advantage compared to an all NMOS structure is that it generates a large symmetrical signal swing and balances out the pull-up and pull-down signals, resulting in a better noise. This type of topology rejects the common mode noise and substrate noise.

Figure 8-24 shows the starting condition which requires a negative resistance and a cancellation of the reactances at the frequency of oscillation. The currents shown in Figure 8-25 indication that this condition is met.
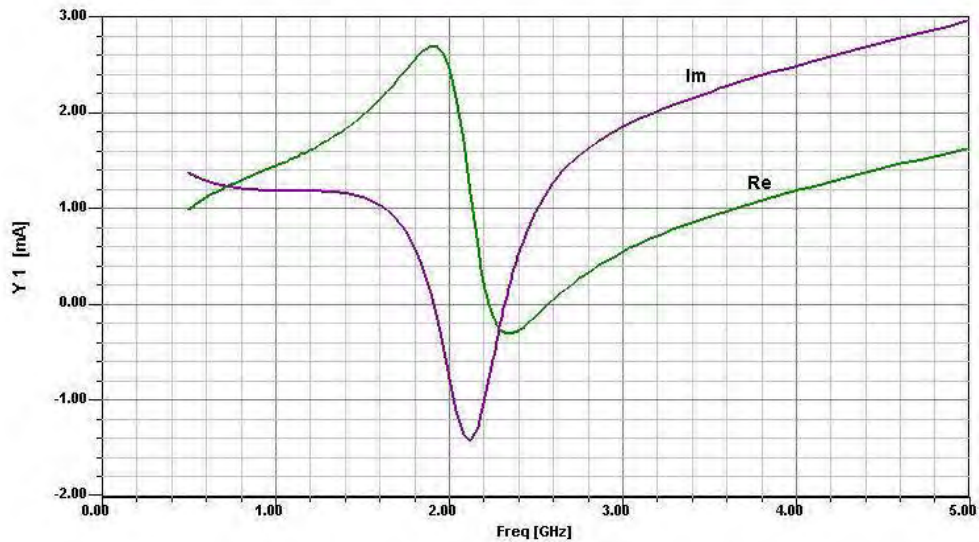
Figure 169: *Figure 8-24 The real and imaginary currents which causes the negative resistance for oscillation.*

It is important to notice that the condition of zero reactance does not quite occur at the point of most negative current. Since the circuit is totally symmetrical, only the condition $C_1 = C_2$ can be met (Section 8.2). C_1 and C_2 refer to the gate source capacitance of the field-effect transistors. As outlined previously, this is not necessarily the best condition for phase noise. While the oscillator phase noise simulation was performed, the mathematically solution to determine the noise will follow

Figures 8-25 and 8-26 show the predicted phase and RF output power, including harmonic contents.
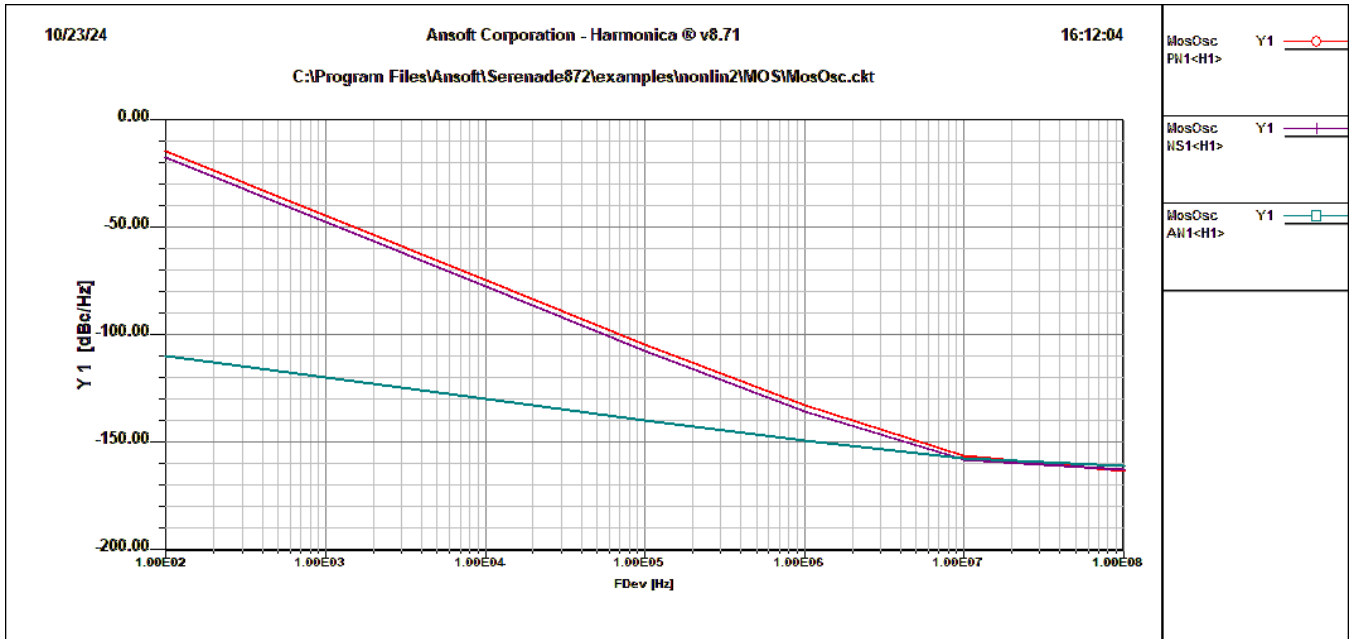
Figure 170: *Figure 8-25 Simulated phase, spectral density and AM noise of the 2400 MHz of the MOSFET Oscillator.*
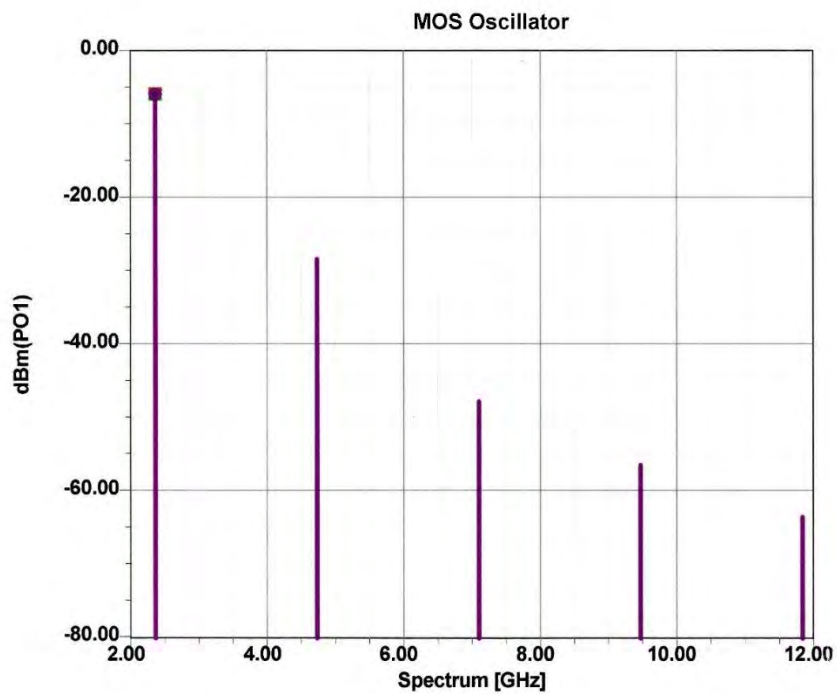
Figure 171: *Figure 8-26 Predicted output spectrum of the 2400 MOSFET oscillator.*

Design Equations

1.   The transconductance.

Figure 8-27 shows a cross-coupled PMOS and a cross-coupled NMOS pair using CMOS devices.

According to the literature, PMOS transistors offer lower 1/f and thermal noise while NMOS transistors exhibit a higher f_T and a higher transconductance for the same operating point.
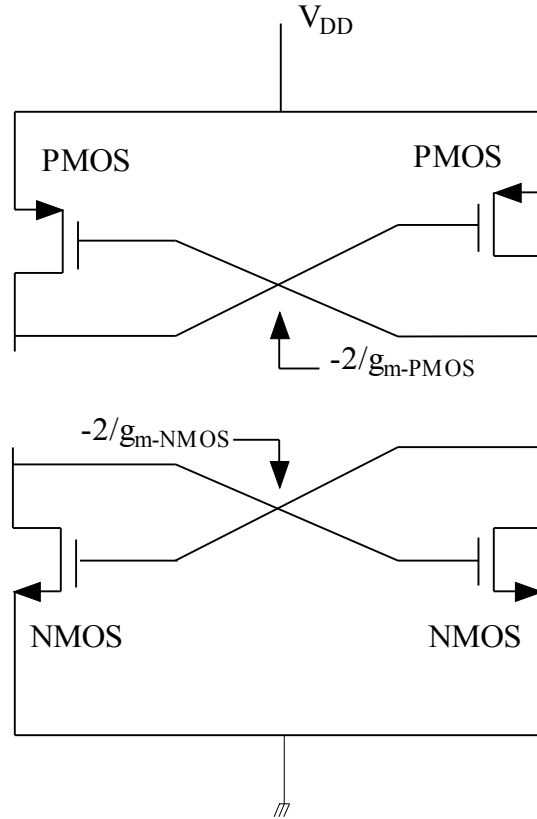
Figure 172: *Figure 8-27Determining the transconductance of the differential circuit of the cross-coupled PMOS and NMOS pair.*

The total transconductance is

$$[g_m]_{l\,\arg e-signal} = -\frac{[g_m]_{PMOS} + [g_m]_{NMOS}}{2}$$ (8-202)

$$[g_m]_{l\,\arg e-signal} = \frac{\partial I_{ds}}{\partial V_{gs}}$$ (8-203)

$$[g_m]_{NMOS} = \sqrt{2I_{ds}\mu_{nmos}C_{ox-nmos}\left[\frac{w}{L}\right]_{nmos}}$$ (8-204)

$$[g_m]_{PMOS} = \sqrt{2I_{ds}\mu_{pmos}C_{ox-nmos}\left[\frac{w}{L}\right]_{pmos}}$$ (8-205)

$$\frac{\partial I_{ds}}{\partial V_{gs}} = K_p \frac{w}{L}(V_{gs}-V_{th})$$ (8-206)

$$[g_m]_{l\,\arg e-signal} = \sqrt{\frac{2wK_pI_{ds}}{L}}$$ (8-207)

with

K_p = transconductance parameter

μ_{pmos} = carrier mobility of the PMOS device

μ_{nmos} = carrier mobility of the NMOS device

C_{ox} = unit capacitance of the gate oxide

2.   The transconductance parameter.

The transconductance parameter is defined as

$$K_p = \mu \, C_{ox} \qquad\qquad (8\text{-}208)$$

where μ is the carrier mobility and C_{ox} is the unit capacitance of the gate oxide.

3.   The Gate-oxide capacitance of the device.

The unit capacitance of the gate oxide C_{ox} is given as

$$C_{ox} = \varepsilon_{ox} \left[\frac{w_i l_i}{t_{ox}} \right] \qquad\qquad (8\text{-}209)$$

with

ε_{ox} = permitivity of the oxide

t_{ox} = thickness of the oxide layer between spiral and substrate

w_i = width of the spiral line

l_i = length of the spiral line.

4.   The drain current.

The drain current is

$$I_{ds} = \frac{1}{2}\left[K_p \frac{w}{L}(V_{gs}-V_{th})^2\right] \qquad\qquad (8\text{-}210)$$

$$I_{ds} = \frac{g_m}{2}(V_{gs}-V_{th}) \qquad\qquad (8\text{-}211)$$

where $(V_{gs}-V_{th})$ is defined as

$$(V_{gs}-V_{th}) = \sqrt{\frac{2I_{ds}L}{K_p w}} \qquad\qquad (8\text{-}212)$$

5.   The size of the device.

The size of the device determines the transconductance of the transistor and the large signal transconductance needs to be large enough to sustain oscillation and compensate the losses of the resonator.

The expression of the ratio of the channel width (gate) and channel length (gate) is

$$\frac{w}{L} = \frac{(2SG_P)^2}{2K_p I_{ds}} \rightarrow \frac{(g_m)^2}{2K_p I_{ds}} \qquad\qquad (8\text{-}213)$$

where w is the width of the channel (gate) and L is the length of the channel (gate) of the device.

6.   The total equivalent resistance at resonant frequency.

Figure 8-28a and b show the equivalent cross-coupled oscillator resonant circuit and the corresponding equivalent resistances at resonance condition.
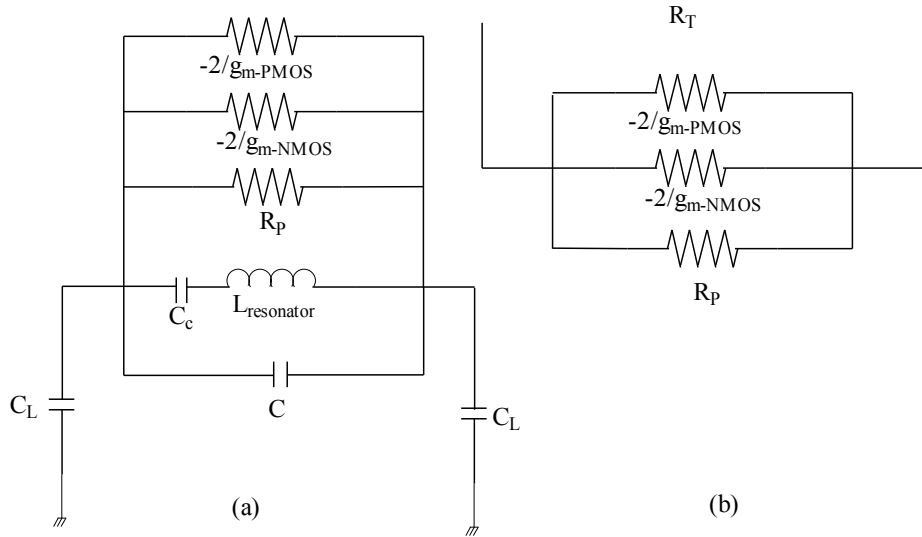
Figure 173: *Figure 8-28 a) The equivalent cross-coupled oscillator resonator circuit and b) the equivalent resistances at resonance condition.*

The total equivalent parallel resistor at resonance frequency is

$$R_T = \frac{2R_P}{2 - R_P(g_{m-NMOS} + g_{m-PMOS})} \qquad (8\text{-}214)$$

$$Q_L = \frac{R_P}{\omega L} \qquad (8\text{-}215)$$

where g_{m-NMOS} and g_{m-PMOS} are the corresponding large signal transconductances of the NMOS and PMOS device.

For a symmetrical output signal, the large signal transconductance of the NMOS and PMOS transistors have to be ideally equal as $g_{m-NMOS}=g_{m-PMOS}=g_m$ and the equivalent resistance at resonance condition is

$$R_T = \cfrac{1}{\left[\cfrac{1}{R_P}-g_m\right]} \qquad (8\text{-}216)$$

The differential negative resistance generated by the cross-coupled NMOS and PMOS transistors-pair compensates the parallel loss resistance R_P of the resonator circuit.

7.   Start-up Conditions

For the start-up condition and guaranteed sustained oscillation condition, the value of R_T must be negative and

$$R_T = \cfrac{1}{\left[\cfrac{1}{R_P}-g_m\right]} < 0 \Rightarrow g_m > \frac{1}{R_P} \qquad (8\text{-}217)$$

From the loop gain criteria using a stability factor of 2 (loop gain=2, the gain is adjusted to 1 by self-adjusting the conducting angle of the circuit), the start-up condition is

$$\frac{g_m}{SG_p} \rightarrow 2 \qquad (8\text{-}218)$$

where

$$G_P = \frac{1}{R_P} \qquad\qquad (8\text{-}219)$$

S = stability factor

R_P = Equivalent parallel loss resistance of the resonator.

Design Calculations

Parallel Loss Resistance of the Resonator

The equivalent parallel loss resistance of the resonator is given as

$$R_P = (1 + Q^2)R_s \Rightarrow 101R_s \quad for \ (Q = 10) \qquad\qquad (8\text{-}220)$$

where R_s is series loss-resistance.

$$[R_P]_{f=2400MHz} = Q\omega L_{ind} = 190\Omega \qquad\qquad (8\text{-}221)$$

Where $Q=10$, $L_{ind}=1.1nH$ and $G_P = \dfrac{1}{R_P} \Rightarrow 6.577mS$

Large Signal Transconductance

$$[g_m]_{laurge-signal} = \sqrt{\frac{2wK_p I_{ds}}{L}} = \sqrt{\frac{2*(250E-6)*(35.6E-6)*(14.8E-3)}{0.35E-6}} = 27.435mS \quad (8\text{-}222)$$

Size of the Device

The width of the CMOS is given as

$$\frac{w}{L} = \frac{(2SG_P)^2}{2K_p I_{ds}} \rightarrow \frac{(g_m)^2}{2K_p I_{ds}} \tag{8-223}$$

$$\frac{w}{L} = \frac{(2SG_P)^2}{2K_p I_{ds}} = 714.3\mu\ m \tag{8-224}$$

For $L = 0.35\mu\ m$; $w = 250\mu\ m$

where

$K_p = 35.6E - 6$

$I_{ds} = 14.8mA$

$G_P = 6.577mS$

$S = 2$

Oscillation Frequency

The frequency of the oscillation is given as

$$f_0 = \frac{1}{2\pi \sqrt{L_{resonator-\tan k} C_{resonator-\tan k}}} \tag{8-225}$$

$$C_{resonator-\tan k} = \frac{1}{2}\left[C_{NMOS} + C_{PMOS} + C_L + C\right] \tag{8-226}$$

where

$$C_{NMOS} = 4C_{gd-nmos} + C_{gs-nmos} + C_{db-nmos} \tag{8-227}$$

$$C_{PMOS} = 4C_{gd-pmos} + C_{gs-pmos} + C_{db-pmos} \tag{8-228}$$

For the cross-coupled configuration $C_{NMOS-Pair}$ is the series combination of the two C_{NMOS} and is given as

$$C_{NMOS-Pair} = 2C_{gd-nmos} + \frac{1}{2}C_{gs-nmos} + \frac{1}{2}C_{db-nmos} \tag{8-229}$$

Similarly, $C_{PMOS-Pair}$ is the series combination of the two C_{PMOS} and is given as

$$C_{PMOS-Pair} = 2C_{gd-pmos} + \frac{1}{2}C_{gs-pmos} + \frac{1}{2}C_{db-pmos} \tag{8-230}$$

The capacitance of the resonator is given as

$$C_{resonator-\tan k} = \frac{1}{2}\left[C_{NMOS} + C_{PMOS} + C_L + C\right] \tag{8-231}$$

where

C_L =10pF (Load capacitance)

C= ½-Resonator- parallel capacitance

$$f_0 = \frac{1}{2\pi\sqrt{L_{resonator-\tan k}C_{resonator-\tan k}}} = \frac{1}{2\pi\sqrt{1.1E-9*3.3E-12}} = 2400MHz$$

<div align="right">(8-232)</div>

where

$L_{resonator-\tan k} = 1.1\text{nH}$

$C_{resonator-\tan k} = 3.3pF$

➢ Phase Noise of the integrated CMOS oscillator

The phase noise of CMOS oscillators has been subject to endless discussions. The main contributors still are the resonant circuit with a low Q and the flicker frequency contribution from the device. From Chapter 8 we take the following equations and adapt them to the CMOS device.

The phase noise of CMOS oscillators has been subject to endless discussions. The main contributors still are the resonant circuit with a low Q and the flicker frequency contribution from the device.
From [2,3],

$$PN_{imf}(\omega_0 + \omega) = \frac{4KT}{R_P}[NFT_{brr}(\omega_0)]^2 = \frac{4KT}{R_P}\left\{\frac{1}{2}\left[\frac{1}{2\omega_0 C_{eft}}\right]\left[\frac{\omega_0}{\omega}\right]\right\}^2$$

→ phase noise contribution from the resonator.

$$PN_{V_{gn}}(\omega_0 + \omega) = 4KT_g\left[NFT_{V_{gm}}(\omega_0)\right]^2 = 4KTr_g\left\{\frac{1}{2}\left[\frac{C_1 + C_2}{C_2}\right]\left[\frac{1}{2Q_0}\right]\frac{\omega_0}{\omega}\right\}^2$$

→ phase noise contribution from the gate resistance.

$$PN_{bgr}(\omega_0 + \omega) = 2qI_g\left[NFT_{kg}(\omega_0)\right]^2 = 2qI_R\left\{\frac{1}{2}\left[\frac{C_2}{C_1 + C_2}\right]\left[\frac{1}{\omega_0 C_{cft}}\right]\left[\frac{\omega_0}{\omega}\right]\right\}^2$$

→ phase noise contribution from the gate current.

$$PN_{sm}(\omega_0 + \omega)$$

$$= \left(\frac{8kTgm}{3} + \frac{K_f I_z^{*F}}{f_m^F}\right)\left|NF_{y_k}(\omega_0)\right|^2 = \left(\frac{8kTgm}{3} + \frac{K_f I_\varepsilon^{NF}}{\omega}\right)\left\{\frac{1}{2}\left[\frac{C_2}{C_1 + C_2}\right]\left[\frac{1}{2\omega_0 Q_0 C_{es}}\right]\left[\frac{\omega_0}{\omega}\right]\right\}^2$$

→ phase noise contribution from the flicker noise of the transistor.

$$PN_{btn}(\omega_0 + \omega) = 2qI_d\left[NFT_{kn}(\omega_0)\right]^2 = 2qI_d\left\{\frac{1}{2}\left[\frac{C_1}{C_1 + C_2}\right]\left[\frac{1}{2\omega_0 C_{\Delta f}}\right]\left[\frac{\omega_0}{\omega}\right]\right\}^2$$

→ phase noise contribution from the drain current.

The total effect of all the four noise sources can be expressed as

$$PN(\omega_0 + \omega) = \left[PN_{inr}(\omega_0 + \omega)\right] + \left[PN_{Vgn}(\omega_0 + \omega)\right] + \left[PN_{tgn}(\omega_0 + \omega)\right] + \left[PN_{tjn}(\omega_0 + \omega) + \left[PN_{tdn}(\omega_0 + \omega)\right]\right.$$

$$PN(\omega_0 + \omega) = \frac{4KT}{R_F}\left\{\frac{1}{2}\left[\frac{1}{2\omega_0 C_{ef}}\right]\left[\frac{\omega_0}{\omega}\right]\right\}^2 + 4KT_g\left\{\frac{1}{2}\left[\frac{C_1 + C_2}{C_2}\right]\left[\frac{1}{2Q}\right]\frac{\omega_0}{\omega}\right\}^2$$

$$+ \left[2qI_g + \frac{8kTgm}{3} + \frac{2\pi K_f I_g^{AF}}{\omega}\right]\left\{\frac{1}{2}\left[\frac{C_2}{C_1 + C_2}\right]\left[\frac{1}{2Q\omega_0 C_{eff}}\right]\left[\frac{\omega_0}{\omega}\right]\right\}^2 \qquad (20)$$

$$+ 2qI_d\left\{\frac{1}{2}\left[\frac{C_3}{C_1 + C_2}\right]\left[\frac{1}{2\omega_0 QC_{v\sigma}}\right]\left[\frac{\omega_0}{\omega}\right]\right\}^2$$

where

K_f = Flicker noise constant, AF = Flicker noise exponent.

$$C_{eff} = C + \frac{C_1 C_2}{C_1 + C_2}$$

The following values were used for the calculation of the phase noise.

$R_p = 190\Omega$

$f_0 = 2.4$ GHz

$L = 1.1$nH

$C_O = 2$pF

$C_1 = C_2 = 0.2$pF

$n = 2$

$I_g = 100\mu A$

$I_d = 14$mA

$AF = 2$

$KF = 5E\text{-}5$

$q = 1.6E\text{-}19$

$T = 290°$ K

and the following contributions were obtained at 1 MHz offset

PN1 = -117.78 dBc/Hz

PN2 = -146.37 dBc/Hz

PN3 = -123.4 dBc/Hz

PN4 = -140.9 dBc/Hz

These calculations show that the phase noise contribution from the tuned circuit dominates and sets the value at −117.78 dBc/Hz.

The circuit was then analyzed using Microwave Harmonica/Ansoft Designer, using a lossy circuit with a Q_0 of 10 and using the SPICE-type parameters which were obtained from the manufacturer.

The output power measured single-ended was −7 dBm. Figure 8-29 shows the simulated output power and harmonic contents. The accuracy of the prediction is within 1 dB.
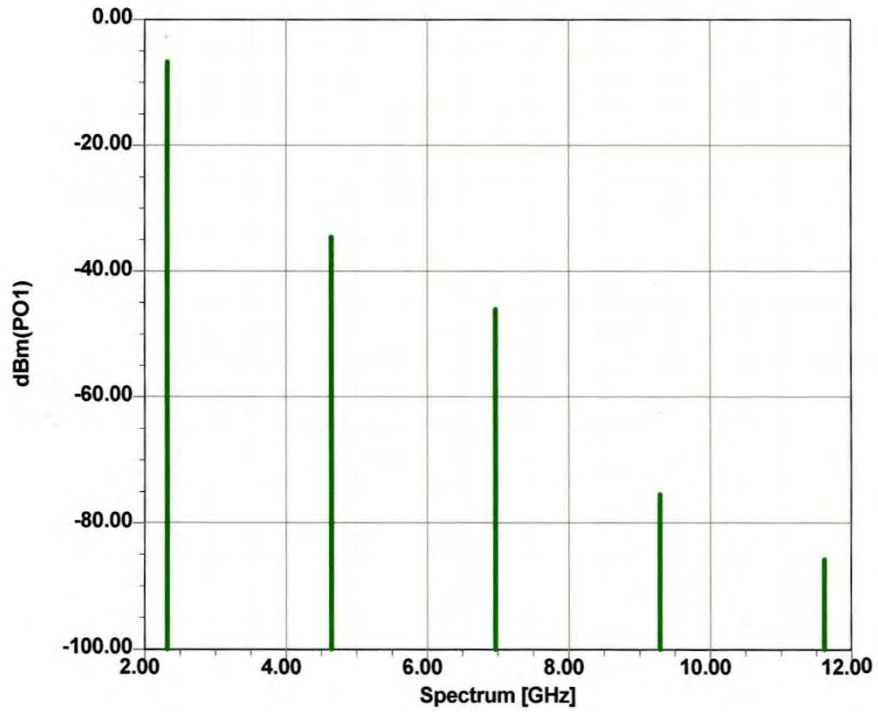
Figure 174: *Figure 8-29 The predicted output spectrum of the CMOS oscillator.*
Figure 175:

Besides the cross coupled oscillator the Colpitts oscillator is always a good reference.
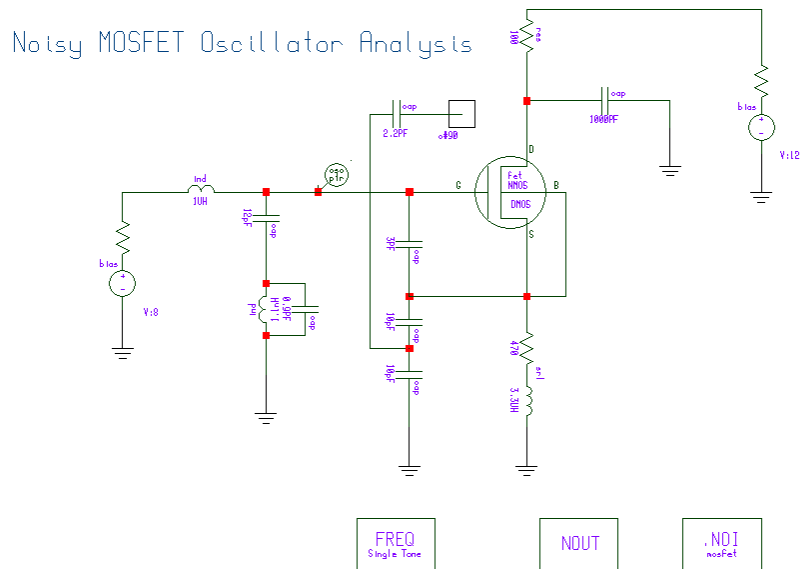
Figure 176: *A typical lossy NMOS based design*

This is a typical lossy NMOS based design.

Analysis Status

Status: The Analysis is Complete.

Frequency: 4.561 GHz   Resonant Frequency: 3.027 GHz

Sweep Number: 129 of 129   Test Current: Re: -5.368 uA
                                            Im: 454.165 uA

Voltage	Current
Vp() = 8 V	Ip() = 0 A
Vgs(DMOS) = 3.56269 V	Ig(DMOS) = 0 A
Vds(DMOS) = 6.5719 V	Id(DMOS) = 9.4361 mA
Vbs(DMOS) = -2.35902 mV	Ib(DMOS) = -15.5405 pA
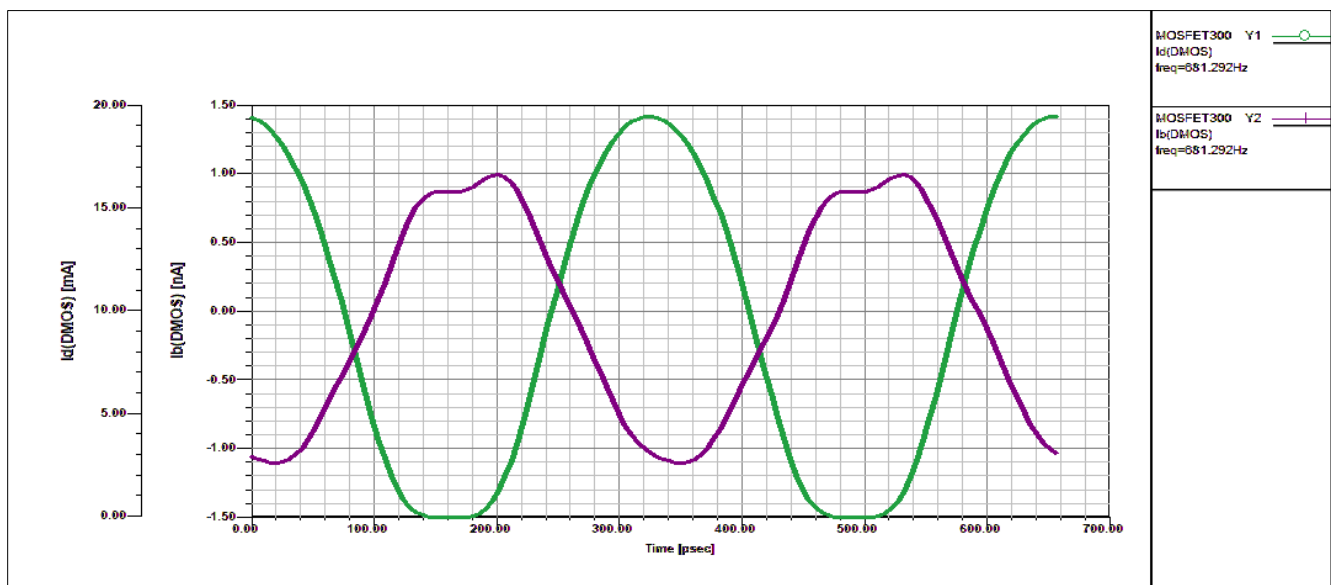
Figure 177: *Gate and Drain currents as a function of time*

The drain current is in slight saturation.
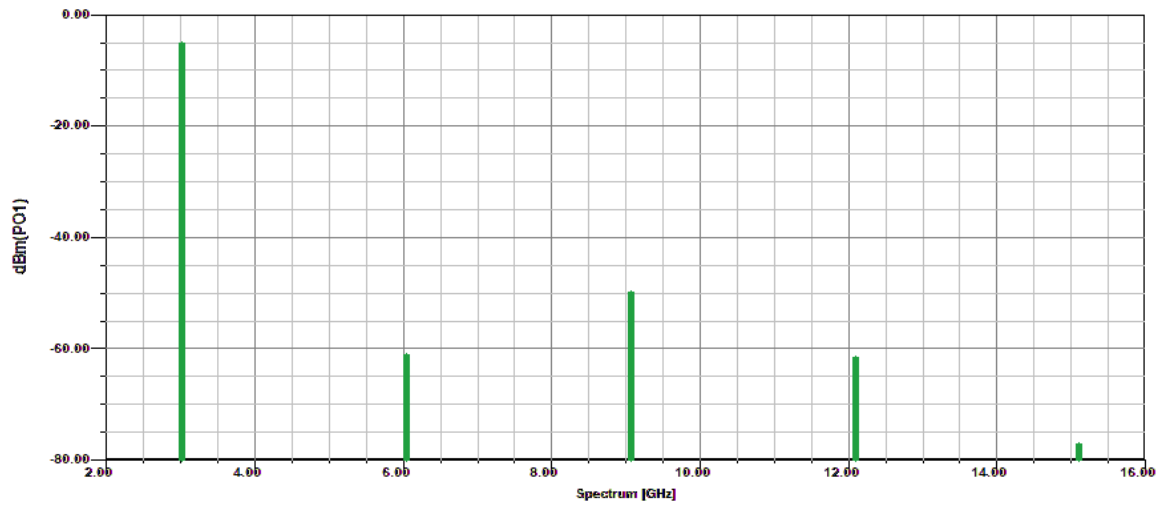
Figure 178: *Simulated output power of the CMOS oscillator*
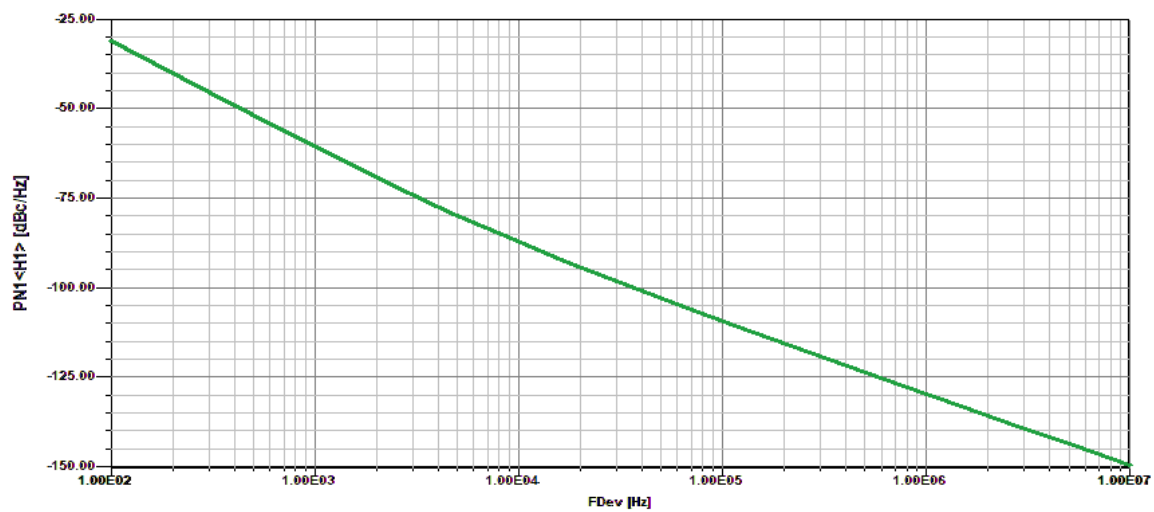
Figure 179: *Simulated phase noise of the CMOS oscillator*
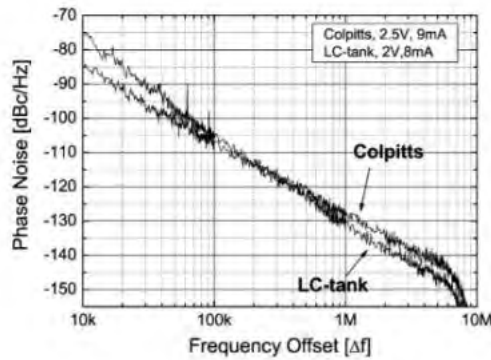
Figure 67c: Measured phase noise of a CMOS LC and Colpitts

Oscillator at 2.9 Ghz.

A study of phase noise in colpitts and LC-tank CMOS oscillators

Andreani, Pietro; Wang, Xiaoyan; Vandi, Luca; Fard, A.

Published in:

I E E E Journal of Solid State Circuits

Figure 180: *Measured phase noise of the CMOS LC oscillator and Colpitts single transistor versions*

Figure 8-30 shows the predicted phase noise from Designer and the phase noise prediction from the set of equations shown above. It should be pointed out that close-in the flicker noise contribution dominates, in the medium range, the resonator Q dominates and for high currents, the drain current adds significant noise.
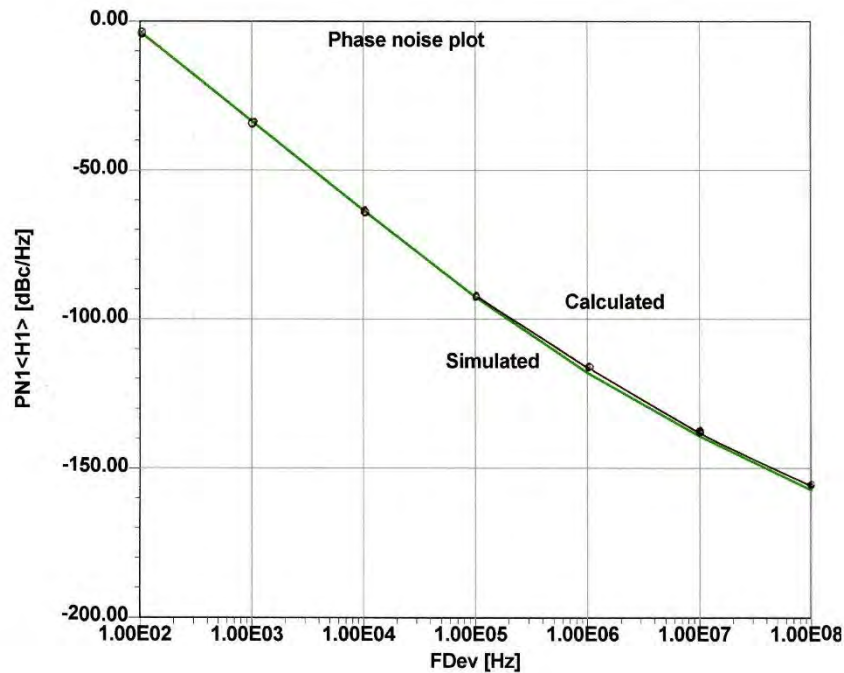
Figure 181: *Figure 8-30 - The predicted phase noise from Ansoft Designer.*

This approach has shown a very good agreement between the simulations and calculations as demonstrated. The following table shows a list of oscillators implemented in various technologies. It is apparent from the list that this design is state-of-the-art. The publications, which cover this topic, have analyzed various other contributions, both from the transistor and the tuning mechanism. When FETs are used as varactors, the average Q is in the vicinity of 30, which means that the low Q inductor still is responsible for the overall phase noise. The three areas of improvement are the power supply voltage, the Q, and the device selection. So far, the power supply voltage has not been addressed, however, latest designs operating at 1.5V show a poorer noise performance. Their distinct trade-offs and the application dictates if such degradation is allowable.

This equation is extremely significant because it covers most of the causes of phase noise in oscillators. [AM-to-PM conversion must be added; see (5-56).] To minimize the phase noise, the following design rules apply:

1. Maximize the unloaded Q.

2. Maximize the reactive energy by means of a high RF voltage across the resonator and obtain a low LC ratio. The limits are set by breakdown voltages of the active devices and the tuning diodes, and the forward-bias condition of the tuning diodes. If L becomes too high, the circuit degenerates into a squegging oscillator. Using lower L allows larger capacitance, which allows us to swamp the oscillating device's internal, nonlinear capacitance with external, linear capacitance, reducing the phase-noise degradation caused by the nonlinear capacitance. The ceramic-resonator oscillator best illustrates this approach, which may be hard to accomplish in discrete circuits because high-Q inductors with values above 1 nH cannot be built unless high-Q transmission lines or resonators are used.

3. Avoid saturation at all cost, and try to either have limiting or automatic gain control (AGC) without degradation of Q. Isolate the tuned circuit from the limiter or AGC circuit. Use tuning diodes in antiseries configurations to avoid forward bias.

4. Choose an active device with the lowest possible noise figure and flicker corner frequency. The noise figure of interest is the noise figure obtained with the actual impedance at which the device is operated. Using FETs rather than BJTs, it is preferable to deal with the equivalent noise voltage and noise currents rather than with the noise figure, since they are independent of source impedance. The noise figure improves as the ratio between source impedance and equivalent noise resistance increases. In addition, in a tuned circuit, the source impedance changes drastically as a function of the offset frequency, and this effect has to be considered. For low phase-noise operation, use a medium-power transistor. If you need your output power to be achieved at 6 - 9 mA, select a transistor with an I_{Cmax} of 60 - 90 mA. Also avoid an f_T greater than 3 - 5× the operating frequency. To make transistors that are stable across their full frequency ranges, manufacturers add circuitry that makes the flicker corner frequency higher as f_T increases.

➢ Appendix

➢ A Solution for Calculating Phase Noise in Oscillators

The following appendix address various important calculation issues on noise. The mathematical solution (Compact Software) paid for, was developed between Prof. Rizzoli and team from the University of Bologna, Prof. Fred Rosenbaum, and Rowan Gilmore from the University of Washington, St. Louise, and my team at Compact Software, where we introduced the world's first harmonic balance mathematics based simulator, that could handle nonlinear noise generated by semiconductors in amplifiers, frequency doublers, mixers and finally oscillators. It didn't take a long time until Keysight (at the time Hewlett Packard) and others followed. The drawback of a University Professor is that one has to publish many of the findings which invites these findings to be copied.

The noise and oscillators has already been discussed, but since many publications, which have been referenced, omitted a lot of important steps, it is difficult to follow the noise concept. The noise discussion has two aspects. One is a physics-based aspect and one is a mathematic-based aspect. Previously the noise has been explained from a physics point of view, while all the necessary mathematical tools are now presented here. The mechanism that adds the noise, both close-in noise and far-out noise, to the carrier will be mathematically described here. The resulting noise figure, under large signal condition, is an important issue. When modeling the transistors, typically the noise correlation is incomplete. This portion, which deals with the inner transistor, was already shown,

There are two important linear noise models which are necessary to understand the SSB noise. One is the Leeson phase noise equation and the other is based on the Lee and Hajimiri noise model. The noise theory can be divided into modulation noise and conversion noise. All of this will be explained in detail.

General Analysis of Noise Due to Modulation and Conversion in Oscillators

The equations E-1 to E-93 are from the book, The Design of modern Microwave Oscillators for Wireless Applications, Ulrich L. Rohde, Ajay K. Poddar, and Georg Boeck 2005

The degree to which an oscillator generates constant frequency throughout a specified period of time is defined as the frequency stability of the oscillator. The cause of frequency instability is due to the presence of noise in the oscillator circuit that effectively modulates the signal, causing a change in frequency spectrum commonly known as phase noise.

The unmodulated carrier signal is represented as

$$f(t) = A\cos(2\pi f_c t + \theta_0) \qquad\qquad \text{(E-1)}$$

$$\theta = 2\pi f_c t + \theta_0 \qquad\qquad \text{(E-2)}$$

$$f_c = \frac{1}{2\pi}\left(\frac{d\theta}{dt}\right) \qquad\qquad \text{(E-3)}$$

For the case of an unmodulated signal, f_c is constant and is expressed by the time derivative of the phase (angle-θ), but in general, this derivative is not constant and can be represented as an instantaneous frequency, which can vary with time and is expressed as $f_i = \frac{1}{2\pi}\left(\frac{d\theta_i}{dt}\right)$ and the corresponding phase is determined as $\theta_i(t) = \int 2\pi f_i dt$. For the unmodulated-carrier $\theta_i(t) = (2\pi f_c t + \theta_0)$, where $\theta_0 = \theta_i(t)\big|_{t=0}$.

The phase/angle of the carrier can be varied linearly by the modulating signal m(t), which results into phase modulation as $\theta_i(t)$.

$$\theta_i(t) = 2\pi f_c t + k_p m(t) \qquad\qquad \text{(E-4)}$$

k_p is defined as phase sensitivity and its dimension is given as radians per units of the modulating signal and the instantaneous frequency ω_i of the carrier is modified by modulation with the modulating signal as

$$\omega_i = \frac{d\theta_i}{dt} \Rightarrow \omega_i = \omega_c + k_p \frac{dm}{dt}$$

$$(\text{E-5})$$

The phase-modulated signal can be expressed in time domain as

$$s(t) = A_c \cos[2\pi f_c t + k_p m(t)]$$

$$(\text{E-6})$$

Modulation by a Sinusoidal Signal

Consider a sinusoidal modulating signal given by $m(t) = A_m \cos(2\pi f_m t)$ and the instantaneous frequency of the modulated signal is given as

$$f_i(t) = f_c + k_f A_m \cos(2\pi f_m t)$$

$$(\text{E-7})$$

$$f_i(t) = f_c + \Delta f \cos(2\pi f_m t)$$

$$(\text{E-8})$$

$$\Delta f = k_f A_m$$

$$(\text{E-9})$$

Δf is defined as the frequency deviation corresponding to the maximum variation of the instantaneous frequency of the modulated signal from the carrier frequency. The angle of the modulated signal is determined by integration as

$$\theta_i(t) = 2\pi \int_0^t f_i(t)dt$$

$$(\text{E-10})$$

$$\theta_i(t) = 2\pi f_c + \frac{\Delta f}{f_m} \sin(2\pi f_m t)$$

$$(\text{E-11})$$

The coefficient of the sine term is called the modulation index of the modulating signal, and is denoted by $\beta = \dfrac{\Delta f}{f_m}$. The expression for the angle of the modulated signal can be written as

$\theta_i(t) = 2\pi f_c + \dfrac{\Delta f}{f_m}\sin(2\pi f_m t)$ and the time representation of the modulated signal can be expressed as

$$s(t) = A_c \cos[\theta_i(t)] = A_c \cos[2\pi f_c t + \beta \sin(2\pi f_m t)] \qquad \text{(E-12)}$$

$$s(t) = \text{Re}[A_c e^{j[2\pi f_c t + \beta \sin(2\pi f_m t)]}] \qquad \text{(E-13)}$$

$$s(t) = \text{Re}[\sigma(t) A_c e^{j2\pi f_c t}] \qquad \text{(E-14)}$$

$\sigma(t)$ is the complex envelope of the frequency modulated signal and can be given as $\sigma(t) = A_{c\,n} e^{j\beta \sin(2\pi f_m t)}$ and it is a periodic function of time with a fundamental frequency equal to the modulating frequency f_m, and can be expressed as

$$\sigma(t) = \sum_{n=-\infty}^{\infty} C_n e^{j2\pi f_m t} \qquad \text{(E-15)}$$

C_n is Fourier coefficient given as

$$C_n = f_m \int_{-\frac{1}{2\pi f_m}}^{\frac{1}{2\pi f_m}} \sigma(t) e^{-j2\pi f_m t}\, dt \qquad \text{(E-16)}$$

227

$$C_n = A_c f_m \int_{-\frac{1}{2\pi f_m}}^{\frac{1}{2\pi f_m}} e^{j[\beta \sin(2\pi f_m t) - j2\pi f_m t]} dt$$

(E-17)

$$C_n = A_c f_m \int_{-\frac{1}{2\pi f_m}}^{\frac{1}{2\pi f_m}} e^{j(\beta \sin x - nx)} dt$$

(E-18)

$x = 2\pi f_m t$, and the expression of coefficients may be rewritten as $C_n = \dfrac{A_c}{2\pi} \int_{-\pi}^{\pi} e^{j(\beta \sin x - nx)} dx$, and this

equation is called n^{th} order Bessel function of the first kind with the argument β.

The expression for $\sigma(t)$ and $s(t)$ is given as

$$\sigma(t) = \sum_{n=-\infty}^{\infty} C_n e^{j2\pi f_m t} = A_c \sum_{n=-\infty}^{\infty} J_n(\beta) e^{j2\pi f_m t}$$

(E-19)

$$s(t) = A_c \, \mathrm{Re} \left[\sum_{n=-\infty}^{\infty} J_n(\beta) e^{j2\pi(f_c + nf_m)t} \right] = A_c \sum_{n=-\infty}^{\infty} J_n(\beta) \cos[2\pi(f_c + nf_m)t]$$

(E-20)

Applying a Fourier transform to the time domain signal $s(t)$ results in an expression for the discrete

frequency spectrum of $s(t)$ as

$$s(f) = \frac{A_c}{2} \sum_{n=-\infty}^{\infty} J_n(\beta)[\delta(f - f_c - nf_m) + (f + f_c + nf_m)]$$

(E-21)

$$\sum_{n=-\infty}^{\infty} J_n(\beta)^2 = 1$$

(E-22)

The spectrum of the frequency-modulated signal has an infinite number of symmetrically located sideband components spaced at frequencies of f_m, $2f_m$, $3f_m$..nf_m around the carrier frequency. The amplitude of the carrier component and the sideband components are the products of the carrier amplitude and a Bessel function.

Modulation by a Noise Signal

Considering a noise signal defined as $n(t) = r_n(t)\cos[2\pi f_c t + \theta + \Phi_n(t)]$ introduced to an oscillator circuit in a random fashion and the desired oscillator output signal is represented by $f(t) = A\cos(2\pi f_c t + \theta)$. $r_n(t)$ is the coefficient of the noise signal having a Rayleigh distribution and functions of a noise signal. The phase $\Phi_n(t)$ is linearly distributed and a distribution function of a noise signal. The output of the oscillator circuit is given as the superposition of the combined signal, which is expressed as

$$g(t) = f(t) + n(t) \qquad \text{(E-23)}$$

$$g(t) = A\cos[(2\pi f_c t + \theta)] + r_n(t)\cos[2\pi f_c t + \theta + \Phi_n(t)] \qquad \text{(E-24)}$$

$$g(t) = A\cos[(2\pi f_c t + \theta)] + r_n(t)\cos[\Phi_n(t)]\cos[2\pi f_c t + \theta] - r_n(t)\sin[\Phi_n(t)]\sin[2\pi f_c t + \theta] \qquad \text{(E-25)}$$

$$g(t) = \cos[(2\pi f_c t + \theta)]\{A + r_n(t)\cos[\Phi_n(t)]\} - r_n(t)\sin[\Phi_n(t)]\sin[2\pi f_c t + \theta] \qquad \text{(E-26)}$$

$$g(t) = \sqrt{C_1^2 + C_2^2}\left[\frac{C_1}{\sqrt{C_1^2 + C_2^2}}\cos\Phi_e(t) - \frac{C_2}{\sqrt{C_1^2 + C_2^2}}\sin\Phi_e(t)\right] \qquad \text{(E-27)}$$

$$g(t) = [\sqrt{C_1^2 + C_2^2}]\cos[\psi + \Phi_e(t)] \qquad \text{(E-28)}$$

where

$$\sin[\Phi_e(t)] = \frac{C_2}{\sqrt{C_1^2 + C_2^2}}$$

(E-29)

$$\cos[\Phi_e(t)] = \frac{C_1}{\sqrt{C_1^2 + C_2^2}}$$

(E-30)

$$R(t) = \sqrt{C_1^2 + C_2^2}$$

(E-31)

$$g(t) = C_1 \cos\psi - C_2 \sin\psi$$

(E-32)

$$C_1 = A + r_n(t)\cos[\Phi_n(t)]$$

(E-33)

$$C_2 = r_n(t)\sin[\Phi_n(t)]$$

(E-34)

$$\psi = 2\pi f_c t + \theta$$

(E-35)

The phase term $\Phi_e(t)$ is a time-variant function and can be represented as

$$\Phi_e(t) = \tan^{-1}\left[\frac{C_2}{C_1}\right] = \tan^{-1}\left[\frac{r_n(t)\sin[\Phi_n(t)]}{A + r_n(t)\cos[\Phi_n(t)]}\right]$$

(E-36)

For large signal to noise ratio (SNR), $\Phi_e(t)$ can be approximated as

$$\Phi_n(t) = \frac{r_n(t)}{A} \sin[\Phi_n(t)] \qquad\qquad\qquad\qquad\text{(E-37)}$$

and the oscillator output signal can be expressed as

$$g(t) = f(t) + n(t) \Rightarrow g(t) = R(t)\cos[2\pi f_c t + \theta + \Phi_e(t)] \qquad\qquad\text{(E-38)}$$

$$R(t) = \sqrt{C_1^2 + C_2^2} = \left\{[A + r_n(t)\cos[\Phi_n(t)]]^2 + r_n(t)\sin[\Phi_n(t)]^2\right\} \qquad\text{(E-39)}$$

which is phase modulated due to the noise signal n(t), and the resultant oscillator output signal contains modulation sidebands due to noise present in the circuit, which is called phase noise.

The amplitude of a phase modulation sideband is given by the product of the carrier amplitude and a Bessel function of the first kind and can be expressed as

$$A_{SSB} = \frac{1}{2} A_c [J_n(\beta)]_{n=1} \qquad\qquad\qquad\qquad\text{(E-40)}$$

$$\frac{A_{SSB}}{A_c} = \frac{1}{2}[J_1(\beta)] \qquad\qquad\qquad\qquad\text{(E-41)}$$

$$\frac{A_{SSB}}{A_c} = \frac{P_{SSB}}{P_c} \qquad\qquad\qquad\qquad\text{(E-42)}$$

$$L(f) = 10\log\left[\frac{P_{SSB}}{P_c}\right] - 10\log[BW_n] \qquad\qquad\text{(E-43)}$$

$L(f)$ is phase noise due to noise modulation, A_{SSB} is the sideband amplitude of the phase modulation at offset Δf from the carrier and BW_n is the noise bandwidth in hertz.

➢ Oscillator Noise Models

At present, two separate, but closely related models, of the oscillator phase noise exists. The first is proposed by Leeson (1966), referred to as Leeson's model and the noise prediction using Leeson's model is based on time-invariant properties of the oscillator such as resonator Q, feedback gain, output power, and noise figure. This was shown in Chapter 7.

Leeson has introduced a linear approach for calculation of oscillator phase noise and his noise formulae was extended by Rohde by adding $\dfrac{2kTRK_0^2}{f_m^2}$ [75].

Modified Leeson's Phase-Noise Equation

$$L\ (f_m) = 10\log\left\{\left[1+\frac{f_0^2}{(2f_mQ_L)^2(1-\frac{Q_L}{Q_0})^2}\right]\left(1+\frac{f_c}{f_m}\right)\frac{FkT}{2P_{sav}}+\frac{2kTRK_0^2}{f_m^2}\right\} \qquad\qquad \text{(E-44)}$$

$L\ (f_m)$ = SSB noise power spectral density defined as ratio of sideband power in 1-Hz bandwidth at f_m to total power in dB, unit is dBc/Hz.

f_m = frequency offset

f_0 = center frequency

f_c = flicker frequency- region between $1/f^3$-$1/f^2$

Q_L = loaded Q of the tuned circuit

Q_0 = unloaded Q of the tuned circuit

F = noise figure of the oscillator

kT = 4.1 × 10^{-21} at 300 K_0 (room temperature)

P_{sav} = average power at oscillator output

R=equivalent noise resistance of tuning diode

K_0= oscillator voltage gain

232

The last term of the Leeson's phase-noise equation is responsible for the modulation noise.

Shortcomings of the Modified Leeson Noise Equation

F is empirical, apriori, and difficult to calculate due to Linear Time Variant (LTV) characteristics of the noise.

Phase noise in $1/f^3$ region is an empirical expression with fitting parameters.

Lee and Hajimiri Noise Model

The second noise model was proposed by Lee and Hajimiri, which is based on the time-varying properties of the oscillator current waveform [64] [T. Lee…. Must reference].

This very nice model, unfortunately gives no insight in the contribution of the semiconductor used and only the flicker noise is discussed, as shown below. All the other noise sources for either the bipolar transistor or the variation of the FET are not considered.

The phase noise equation for the $1/f^3$ region can be expressed as

$$L\ (f_m) = 10\log\left[\frac{C_0^{\ 2}}{q_{max}^2} * \frac{i_n^{\ 2}/\Delta f}{8f_m^2} * \frac{w_{1/f}}{f_m}\right] \qquad \text{(E-45)}$$

and the phase noise equation for the $1/f^2$ region can be expressed as

$$L\ (f_m) = 10\log\left[\frac{\Gamma_{rms}^{\ 2}}{q_{max}^2} * \frac{i_n^{\ 2}/\Delta f}{4f_m^2}\right] \qquad \text{(E-46)}$$

where

C_0 : coefficient of Fourier series, 0th order of the ISF.

i_n : the noise current magnitude.

233

Δf: noise bandwidth.

$\omega_{1/f}$: 1/f noise corner frequency of the device/transistor.

q_{max}: maximum charge on the capacitors in the resonator.

$\Gamma(rms)$: is the rms value of the ISF.

Shortcomings of the Lee and Hajimiri Noise Model

ISF function is tedious to obtain and depends upon topology of the oscillator.

Mathematical, yet lacks practicality.

1/f noise-conversion is not clearly specified.

Modulation and Conversion Noise

Modulation noise is defined as the noise that is generated by actually modulating the oscillator due to tuning diode. The noise associated with the series loss resistance in the tuning diode will introduce frequency modulation, which is further translated into the oscillator phase noise and this portion of the noise is responsible for the near-carrier noise. There is an additional phenomenon called conversion noise, which produces noise in a manner similar to the mixing process.

The Nonlinear Approach for the Computation of the Noise Analysis of Oscillator Circuits

The mechanism of noise generation in autonomous circuits and oscillators combines the equivalent of modulation and frequency conversion (mixing) with the effect of AM to PM conversion [70, 109].

Traditional approaches relying on frequency conversion analysis are not sufficient to describe the complex physical behavior of a noisy oscillator. The accuracy of this nonlinear approach is based on the dynamic range of the harmonic-balance simulator and the quality of the parameter extraction for the active device.

Figure E-1 shows a general noisy nonlinear network, which is subdivided into linear and nonlinear sub-networks and noise-free multi-ports. Noise generation is accounted for by connecting a set of noise voltage and noise current sources at the ports of the linear and nonlinear sub-network. It is assumed that the circuit is forced by DC source and a set of sinusoidal sources located at the carrier harmonics $k\omega_0$ and at the sideband $\omega + k\omega_0$.

The electrical regime under this condition of the autonomous circuit will be quasi-periodic, and the nonlinear system to be solved is formulated in terms of the harmonic balance error vector E, defined as the difference between linear and nonlinear current harmonics at the common ports of the circuits.
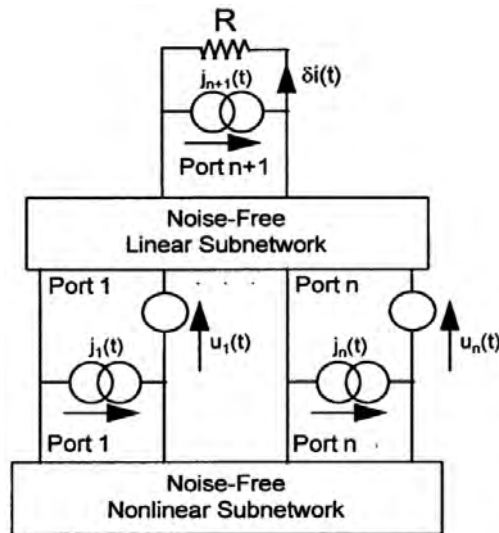
Figure 182: *Figure E-1 shows a general noisy nonlinear network.*

The solution of this nonlinear algebraic system can be expressed in the form as

$$E(X_B, X_H) = F \qquad \text{(E-47)}$$

$$E(X_B, X_H) \Rightarrow E_B, E_H \qquad \text{(E-48)}$$

where

F= Forcing term comprises of DC, harmonics and sideband-excitations

X_B= State-variable vectors (SV) consists components at sideband

X_H= State-variable vectors (SV) consists components at carrier harmonics

E=Vector of real and imaginary parts of all HE-errors

E_B=Error sub-vector due to sideband

E_H=Error sub-vector due to carrier harmonics

Under autonomous (noiseless) steady state conditions, the forcing term F contains only DC excitations and the possible solution for nonlinear algebraic system $E(X_B, X_H) = F$ will have the form as

$$X_B = 0 \qquad \text{(E-49)}$$

$$X_H = X_H^{ss} \rightarrow steady-state \qquad \text{(E-50)}$$

Since the system is operating under autonomous conditions, the phase of the steady state will be arbitrary, and the carrier frequency ω_0 represents one of the unknowns of the nonlinear algebraic system above $E(X_B, X_H) = F$; so that one of the harmonics of the vector X_H is replaced by ω_0.

Now, let us assume that the steady state condition of the autonomous (noiseless) circuit is perturbed by set of small-signal noise sources generated inside the linear/nonlinear sub-network ports of the circuit; this situation can be described by introducing a noise voltage and a noise current source at every interconnecting port, as shown in Figure E-1.

Under small noise perturbations, the noise-induced deviation $[\partial X_B, \partial X_H]$ of the system state from the autonomous (noiseless) steady state $[0, X_H^{SS}]$ can be quantitatively expressed by perturbing expression $E(X_B, X_H) = F$ in the neighborhood of the steady state as

$$\left[\frac{\partial E_B}{\partial X_B}\right]_{ss} \partial X_B + \left[\frac{\partial E_B}{\partial X_H}\right]_{ss} \partial X_H = J_B(\omega) \Rightarrow M_{BB}\partial X_B + M_{BH}\partial X_H = J_B(\omega) \tag{E-51}$$

$$\left[\frac{\partial E_H}{\partial X_B}\right]_{ss} \partial X_B + \left[\frac{\partial E_H}{\partial X_H}\right]_{ss} \partial X_H = J_H(\omega) \Rightarrow M_{HB}\partial X_B + M_{HH}\partial X_H = J_H(\omega) \tag{E-52}$$

where

$$M_{BB} = \left[\frac{\partial E_B}{\partial X_B}\right]_{ss} \tag{E-53}$$

$$M_{BH} = \left[\frac{\partial E_B}{\partial X_H}\right]_{ss} \tag{E-54}$$

$$M_{HB} = \left[\frac{\partial E_H}{\partial X_B} \right]_{ss} \qquad \text{(E-55)}$$

$$M_{HH} = \left[\frac{\partial E_H}{\partial X_H} \right]_{ss} \qquad \text{(E-56)}$$

and M is the Jacobian matrix of the HB errors and can be expressed as

$$M = \begin{bmatrix} \left.\frac{\partial E_B}{\partial X_B}\right|_{ss} & \left.\frac{\partial E_B}{\partial X_H}\right|_{ss} \\ \left.\frac{\partial E_H}{\partial X_B}\right|_{ss} & \left.\frac{\partial E_H}{\partial X_H}\right|_{ss} \end{bmatrix} \qquad \text{(E-57)}$$

At a steady state condition, $X_B = 0 \Rightarrow M_{BH}$ and $M_{HB} = 0$ and the system of equations will be reduced to a set of uncoupled equations as

$$\left[\frac{\partial E_B}{\partial X_B} \right]_{ss} \partial X_B = J_B(\omega) \Rightarrow M_{BB} \partial X_B = J_B(\omega) \qquad \text{(E-58)}$$

$$\left[\frac{\partial E_H}{\partial X_H} \right]_{ss} \partial X_H = J_H(\omega) \Rightarrow M_{HH} \partial X_H = J_H(\omega) \qquad \text{(E-59)}$$

In the equation above, $M_{BB} \partial X_B = J_B(\omega)$ is responsible for the mechanism of the conversion noise, which is being generated by the exchange of the power between the sidebands of the unperturbed large-signal steady state through the frequency conversion in the nonlinear sub-network/devices. Equation $M_{HH} \partial X_H = J_H(\omega)$ is responsible for mechanism of modulation noise, which is being described as a jitter of the oscillatory steady state.

➢ Noise Generation in Oscillators

The physical effects of random fluctuations taking place in the circuit are different depending on their spectral allocation with respect to the carrier.

Noise components at low frequency deviations result in frequency modulation of the carrier through mean-square frequency fluctuation proportional to the available noise power.

Noise components at high frequency deviations result in phase modulation of the carrier through mean-square phase fluctuation proportional to the available noise power.

Frequency Conversion Approach

The circuit has a large-signal time-periodic steady state of fundamental angular frequency ω_0 (carrier). Noise signals are small perturbations superimposed on the steady state, represented by families of pseudo-sinusoids located as the sidebands of the carrier harmonics. The noise sources are modeled as pseudo-sinusoids having random amplitudes, phases, and deterministic frequencies corresponding to the noise sidebands.

Therefore, the noise performance of the circuit is determined by the exchange of the power between the sidebands of the unperturbed steady state through frequency conversion in the nonlinear subnetwork. From the expression $M_{BB}\partial X_B = J_B(\omega)$, it can be seen that the oscillator noise is essentially an additive noise that is superimposed on each harmonic of a lower and upper sideband at the same frequency offset.

Conversion Noise Analysis

Consider a set of noise currents and voltage sources connected to the linear/nonlinear sub-network ports as shown in Figure E-1. The vectors of the sideband phasor of such sources at the pth noise sideband $\omega + p\omega_0$ are represented by $J_p(\omega)$ and $U_p(\omega)$, respectively, where ω is the frequency offset from the carrier $(0 \leq \omega \leq \omega_0)$. Due to the perturbative assumption, the nonlinear subnetwork can be replaced with multi-

frequency linear multi-port described by a conversion matrix. The flow of noise signals can be computed by the conventional linear circuit techniques.

Assuming that the noise perturbations are small, the kth sideband phasor of the noise current through a load resistance R may be expressed through frequency-conversion analysis by the linear relationship as

$$\partial I_k(\omega) = \sum_{p=-nH}^{nH} T_{k,p}^J(\omega) J_p(\omega) = \sum_{p=-nH}^{nH} T_{k,p}^U(\omega) U_p(\omega) \qquad \text{(E-60)}$$

For k=0, upper and lower sideband noise is $\partial I_0(\omega)$ and $\partial I_0(-\omega) = \partial I_0^{\otimes}(\omega)$.

$T_{k,p}^J(\omega)$ and $T_{k,p}^U(\omega)$ are the conversion matrices and n_H is the number of the carrier harmonics taken into account in the analysis. From the equation above, the correlation coefficient of the kth and r^{th} sidebands of the noise delivered to the load can be given as

$$C_{k,r}(\omega) = R\langle \partial I_k(\omega) \partial I_r^*(\omega) \rangle \qquad \text{(E-61)}$$

$$C_{k,r}(\omega) = R \sum_{p,q=-nH}^{nH} \{[T_{k,p}^J(\omega)\langle J_p(\omega) J_q^{\otimes}(\omega)\rangle T_{r,q}^{J\otimes}(\omega)] \qquad \text{(E-62)}$$

$$+[T_{k,p}^U(\omega)\langle U_p(\omega) U_q^{\otimes}(\omega)\rangle T_{r,q}^{U\otimes}(\omega)] \qquad \text{(E-63)}$$

$$+[T_{k,p}^J(\omega)\langle J_p(\omega) U_q^{\otimes}(\omega)\rangle T_{r,q}^{U\otimes}(\omega)] \qquad \text{(E-64)}$$

$$+[T_{k,p}^U(\omega)\langle U_p(\omega) J_q^{\otimes}(\omega)\rangle TJ_{r,q}^{J\otimes}(\omega)]\} \qquad \text{(E-65)}$$

where ' * ' denotes the complex conjugate, ' $\otimes$ 'denotes the conjugate transposed and $\langle \bullet \rangle$ denotes the ensemble average. $J_p(\omega)$ and $U_p(\omega)$ are the side-band noise sources.

From the above expression of correlation coefficient of the kth and rth sidebands $C_{k,r}(\omega)$, the power available from the noise sources is redistributed among the all sidebands through frequency conversion, and this complex mechanism of inter-frequency power flow is described by the family of the sideband-sideband conversion matrices $T_{k \cdot p}^{J}(\omega)$ and $T_{k \cdot p}^{U}(\omega)$.

The noise power spectral density delivered to the load at $\omega+k\omega_0$ can be given as

$$N_k(\omega) = R\left\langle \left| \partial I_k(\omega) \right|^2 \right\rangle = C_{k,k}(\omega)$$

(E-66)

The Noise Performance Index Due to Frequency Conversion

The PM noise due to frequency conversion, the AM noise to carrier ratio due to frequency conversion, and the PM-AM correlation coefficient due to frequency conversion can be expressed in terms of simple algebraic combination of the equations above.

The PM Noise for the kth harmonic can be expressed as

$$\left\langle \left| \delta\varphi_{ck}(\omega) \right|^2 \right\rangle = \left[\frac{[N_k(\omega) - N_{-k}(\omega)] - 2\,\mathrm{Re}[C_{k,-k}^{\bullet}(\omega)\exp(j2\varphi_k^{ss})]}{R\left| I_k^{ss} \right|^2} \right]$$

(E-67)

where

$\left\langle \left| \delta\varphi_{ck}(\omega) \right|^2 \right\rangle$ = PM noise at k^{th} harmonic, subscript 'c' in $\varphi_{ck}(\omega)$ stands for frequency-conversion.

$N_k(\omega), N_{-k}(\omega)$ = noise power spectral densities at the upper and lower sidebands of the kth harmonics.

$C_{k,-k}^{\bullet}(\omega)$ = Correlation coefficient of the upper and lower sidebands of the kth carrier harmonics.

$\left| I_k^{SS} \right| \exp(j2\varphi_k^{ss})$ = k^{th} harmonic of the steady-state current through the load.

R = load resistance

$\langle \bullet \rangle$ = Represents the ensemble average

AM noise for the kth harmonic can be given as

$$\left\langle \left| \delta A_{ck}(\omega) \right|^2 \right\rangle = 2\left[\frac{[N_k(\omega) - N_{-k}(\omega)] + 2\,\mathrm{Re}[C_{k,-k}^{\bullet}(\omega)\exp(j2\varphi_k^{ss})]}{R\left| I_k^{SS} \right|^2} \right] \qquad \text{(E-68)}$$

where

$\left\langle \left| \delta A_{ck}(\omega) \right|^2 \right\rangle$ = AM noise to carrier ratio at k^{th} harmonic, subscript 'c' in $A_{ck}(\omega)$ stands for frequency-conversion.

$N_k(\omega), N_{-k}(\omega)$ = noise power spectral densities at the upper and lower sidebands of the kth harmonic.

$C_{k,-k}^{\bullet}(\omega)$ = correlation coefficient of the upper and lower sidebands of the kth carrier harmonic.

$\left| I_k^{SS} \right| \exp(j2\varphi_k^{ss}) = k^{\text{th}}$ harmonic of the steady-state current through the load.

$R = $ load resistance.

$\langle \bullet \rangle = $ Represents the ensemble average.

For k = 0, expression for $\partial I_k(\omega)$ can be given as

$$\partial I_k(\omega) = \sum_{p=-nH}^{nH} T_{k,p}^J(\omega) J_p(\omega) = \sum_{p=-nH}^{nH} T_{k,p}^U(\omega) U_p(\omega)$$

(E-69)

$$\partial I_k(\omega)\big|_{k=0} = \partial I_0(\omega) \Rightarrow \partial I_0^\otimes(\omega)$$

(E-70)

$$\partial I_{-k}(\omega)\big|_{k=0} \Rightarrow \partial I_0(-\omega) \Rightarrow \partial I_0^\otimes(\omega)$$

(E-71)

$$\varphi_k^{ss}\big|_{k=0} = 0, \pi \Rightarrow \left\langle \left| \delta \Phi_{c0}(\omega) \right|^2 \right\rangle = 0$$

(E-72)

$N_k(\omega)\big|_{k=0} = N_0(\omega) \rightarrow$ which is pure AM noise.

The PM-AM correlation coefficient for the kth harmonic can be given as

$$C_{ck}^{PMAM}(\omega) = \left\langle \delta \Phi_{ck}(\omega) \delta A_k(\omega)^* \right\rangle = -\sqrt{2} \left[\frac{2\,\text{Im}[C_{k,-k}^\bullet(\omega) \exp(j2\varphi_k^{ss})] + j[N_k(\omega) - N_{-k}(\omega)]}{R\left| I_k^{SS} \right|^2} \right]$$

(E-73)

where

$C_{ck}^{PMAM}(\omega)$ = PM-AM noise correlation coefficient for the kth harmonic, subscript 'c' in $C_{ck}^{PMAM}(\omega)$ stands for frequency-conversion.

$N_k(\omega), N_{-k}(\omega)$ = noise power spectral densities at the upper and lower sidebands of the kth harmonic.

$C_{k,-k}^{\bullet}(\omega)$ = correlation coefficient of the upper and lower sidebands of the kth carrier harmonic.

$|I_k^{SS}| \exp(j2\varphi_k^{ss})$ = k^{th} harmonic of the steady-state current through the load.

R = load resistance.

$\langle \bullet \rangle$ = represents the ensemble average.

The frequency conversion approach frequently used has the following limitations.

The frequency-conversion approach is not sufficient to predict the noise performance of an autonomous circuit. The spectral density of the output noise power, and consequently, the PM noise computed by the conversion analysis, is proportional to the available power of the noise sources.

In the presence of both thermal and flicker noise sources, PM noise, due to frequency conversion, raises as ω^{-1} for, and approach a finite limit for $\omega \to \infty$ like kT.

Frequency conversion analysis correctly predicts the far-carrier noise behavior of an oscillator, but the oscillator noise floor does not provide results consistent with the physical observations at low frequency deviations from the carrier.

This inconsistency can be removed by adding the modulation noise analysis.

Modulation Noise Analysis

Equation $\left[\frac{\partial E_H}{\partial X_B}\right]_{ss} \partial X_B + \left[\frac{\partial E_H}{\partial X_H}\right]_{ss} \partial X_H = J_H(\omega)$ describes the noise-induced jitter of the oscillatory-

state, represented by the vector δX_H, and under this approach, the PM noise is the result of direct frequency modulation by the noise sources present in the circuits.

The noise sources under this approach are modeled as modulated sinusoids located at the carrier harmonics with random pseudo-sinusoidal phase and amplitude modulation causing frequency fluctuations with a mean-square value proportional to the available power of the noise sources. The associated mean-square phase fluctuation is proportional to the available noise power divided by ω^2 and this mechanism is referred as modulation noise.

One of the entries of δX_H is $\delta\omega_0$, where $\delta\omega_0(\omega)$ is the phasor of the pseudo-sinusoidal components of the fundamental frequency fluctuations in a 1 Hz band at frequency ω. Frequency jitter with a mean square value proportional to the available noise power is described by $M_{HH}\partial X_H = J_H(\omega)$.

In the presence of both thermal and flicker noise, the PM noise, due to modulation, raises as ω^{-3} for $\omega \to 0$ and tends to go to 0 for $\omega \to \infty$. Modulation noise analysis correctly describes the noise behavior of an oscillator at low deviations from the carrier and does not provide results consistent with physical observations at high deviations from the carrier. The combination of both phenomena explains the noise in the oscillator shown in Figure E-2 where the near-carrier noise dominates below ω_X and far-carrier noise dominates above ω_X.
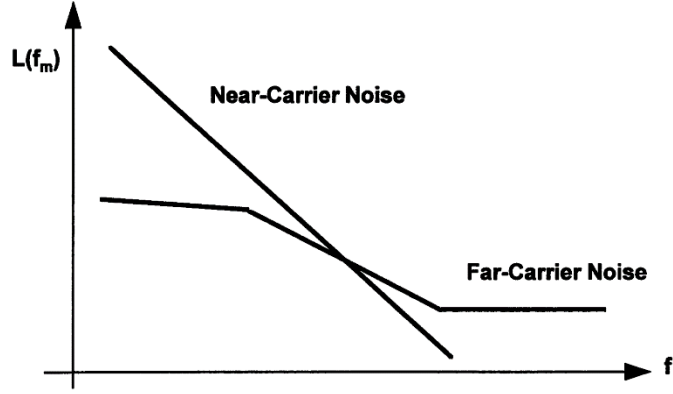
Figure 183: *Figure E-2   Oscillator noise components.*

From a strict harmonic-balance view point, the forcing term $J_H(\omega)$ of the uncoupled equation $M_{HH}\partial X_H = J_H(\omega)$ represents a synchronous perturbation with time-independent spectral components at the carrier harmonics only, and it can be expressed in terms of side-band noise sources $J_p(\omega)$ and $U_p(\omega)$, whose correlation matrices are calculated from following expression:

$$C_{k,r}(\omega) = R\left\langle \partial I_k(\omega)\partial I_r^*(\omega)\right\rangle \qquad\qquad \text{(E-74)}$$

$$C_{k,r}(\omega) = R\sum_{p,q=-nH}^{nH}\{[T_{k,p}^J(\omega)\left\langle J_p(\omega)J_q^{\otimes}(\omega)\right\rangle T_{r,q}^{J\otimes}(\omega)] \qquad\qquad \text{(E-75)}$$

$$+[T_{k,p}^U(\omega)\left\langle U_p(\omega)U_q^{\otimes}(\omega)\right\rangle T_{r,q}^{U\otimes}(\omega)] \qquad\qquad \text{(E-76)}$$

$$+[T_{k,p}^J(\omega)\left\langle J_p(\omega)U_q^{\otimes}(\omega)\right\rangle T_{r,q}^{U\otimes}(\omega)] \qquad\qquad \text{(E-77)}$$

$$+[T_{k,p}^U(\omega)\left\langle U_p(\omega)J_q^{\otimes}(\omega)\right\rangle TJ_{r,q}^{J\otimes}(\omega)]\} \qquad\qquad \text{(E-78)}$$

In a conventional (deterministic) HB analysis, $J_H(\omega)$ would contain real and imaginary parts of the synchronous perturbation phasor at $k\omega_0$. But, in reality, forcing the term $J_H(\omega)$ at the kth harmonic arises due to superposition of the upper and lower sideband noise at $\omega + k\omega_0$, and for noise analysis, the noise source waveforms may be viewed as sinusoidal signal at frequencies $k\omega_0$ slowly modulated in both amplitude and phase at the rate of ω.

In equation $M_{HH}\partial X_H = J_H(\omega)$, the phasor of the deterministic perturbations are replaced by the complex modulations laws, each generated by the superposition of an upper and lower sideband contribution.

Under this quasi-stationary viewpoint, the real part of the constant synchronous perturbation is replaced by the phasor of the amplitude modulation law, and the imaginary part by the phasor of the phase modulation law.

Thus, the expression for the noising forcing term $J_H(\omega)$ can be expressed as

$$J_H(\omega) = \left\{ \left[J_0^T(\omega)...[J_k(\omega) + J_{-k}(\omega)]^T ...[- jJ_K(\omega) + jJ_{-K}(\omega)]^T ....\right]^T \right\} \ (1 \leq k \leq n_H)$$

(E-79)

T denotes the transpose operation and from Figure E-1, the equivalent Norton phasor of the noise source sidebands is given as

$$J_k(\omega) = -\left[J_{Lk}(\omega) + J_{Nk}(\omega) + Y(\omega + k\omega_0)U_{Nk}(\omega)\right]$$

(E-80)

$Y(\omega + k\omega_0)$ is the linear sub-network admittance matrix, $J_{Lk}(\omega)$ and $J_{Nk}(\omega)$ are the forcing terms corresponding to the linear and nonlinear sub-network.

$J_k(\omega)$, $U_k(\omega)$ are the phasor of the pseudo-sinusoids representing the noise components in 1 Hz bandwidth located in the neighborhood of the sidebands $\omega + k\omega_0$.

247

In phasor notation with a rotating vector exp (jωt), the forcing term $J_H(ω)$ can be given as

$$J_H(\omega) = \begin{bmatrix} J_0(\omega) \\ --- \\ J_K(\omega) + J_{-K}(\omega) \\ -jJ_K(\omega) + jJ_{-K}(\omega) \\ --- \end{bmatrix} \quad (1 \le k \le n_H)$$

(E-81)

After replacing the forcing term $J_H(\omega)$ in the earlier given uncoupled equation $M_{HH}\partial X_H = J_H(\omega)$ by $\left[J_0^T(\omega) ... [J_k(\omega) + J_{-k}(\omega)]^T ... [-jJ_K(\omega) + jJ_{-K}(\omega)]^T .... \right]^T$, the entries of the perturbation vector ∂X_H become a complex phasor of the pseudo-sinusoidal fluctuations of the corresponding entries of the state vector δX_H at frequency ω.

The solution of the equation $M_{HH}\partial X_H = J_H(\omega)$ for δX_H and for $\partial \omega_0$ can be given by introducing row matrix S=[000..1..0], where the nonzero element corresponds to the position of the entry $\partial \omega_0$ in the vector δX_H and we obtain

$$\partial \omega_0(\omega) = S[M_{HH}]^{-1} J_H(\omega) = T_F J_H(\omega)$$

(E-82)

$\partial \omega_0(\omega)$ represents the phasor of the pseudo-sinusoidal component of the fundamental-frequency fluctuations in a 1 Hz band at frequency ω and T_F is a row matrix.

Furthermore, a straightforward perturbative analysis of the current of the linear sub-network allows the perturbation on the current through the load resistor R to be linearly related to the perturbation on the state vector, δX_H is obtained from equation $M_{HH}\partial X_H = J_H(\omega)$, and the phasor of the pseudo-sinusoidal component of the load current fluctuations in 1 Hz band at a deviation ω from kω0 can be given as

$$\partial I_k(\omega) = T_{AK}J_H(\omega) \tag{E-83}$$

T_{AK} is a row matrix and $J_H(w)$ is a forcing term of the uncoupled equation.

The Noise Performance Index Due to Contribution of the Modulation Noise

PM noise due to noise modulation, AM noise due to noise modulation, and PM-AM correlation coefficient due to noise modulation can be expressed in terms of a simple algebraic combination of the equations above.

PM noise for the kth harmonic due to contribution of modulation:

$$<\left|\partial\Phi_k(\omega)\right|^2> = \frac{k^2}{\omega^2}\left[T_F\left\langle\left|J_H(\omega)J_H^{\otimes}(\omega)\right|\right\rangle T_F^{\otimes}\right] \tag{E-84}$$

where

$\left\langle\left|\delta\varphi_{mk}(\omega)\right|^2\right\rangle$ =PM noise at k^{th} harmonic, subscript 'm' in $\varphi_{mk}(\omega)$ stands for modulation mechanism.

$\left\langle\left|J_H(\omega)J_H^{\otimes}(\omega)\right|\right\rangle$ = Correlation matrix.

$T_F^{\otimes}$ = Conjugate-transpose.

$J_H(w)$ = Forcing-term.

$\langle \bullet \rangle$ =Represents the ensemble average denotes the ensemble average.

AM noise due to modulation contribution:

The kth harmonic of the steady state current through the load can be expressed as

$$I_k^{SS} = Y_R(k\omega_0)V_k(X_H) \qquad\qquad\qquad (E\text{-}85)$$

where

I_k^{SS} = k^{th} harmonic of the steady state current through the load.

$Y_R(k\omega_0)$ = Trans-admittance matrix.

V_k = Vector representation of the kth harmonics of the voltages at the nonlinear subnetwork ports.

By perturbing I_k^{SS} in the neighborhood of the steady state, the phasor of the pseudo-sinusoidal component of the kth harmonic current fluctuations at frequency ω can be expressed as a linear combination of the elements of the perturbation vector δX_H.

From the equation $\left[\dfrac{\partial E_H}{\partial X_H}\right]_{ss} \partial X_H = J_H(\omega) \Rightarrow M_{HH}\partial X_H = J_H(\omega); \quad \partial I_k(\omega) = T_{AK}J_H(w)$

the modulation contribution for the kth harmonic AM noise to carrier ratio at frequency ω can be expressed as

$$< \partial |A_{mk}(\omega)|^2 > = \frac{2}{|I_k^{SS}|^2}\left[T_{Ak}\langle |J_H(\omega)J_H^{\otimes}(\omega)|\rangle T_{Ak}^{\otimes}\right]$$

$$\qquad\qquad\qquad\qquad\qquad (E\text{-}86)$$

where

$\left\langle \left| \delta A_{mk}(\omega) \right|^2 \right\rangle$ = AM noise to carrier ratio at k^{th} harmonic, subscript 'm' in $A_{mk}(\omega)$ stands for modulation-mechanism.

$\left\langle \left| J_H(\omega) J_H^{\otimes}(\omega) \right| \right\rangle$ = Correlation matrix.

$J_H(w)$ = Forcing-term.

T_{Ak} = Row-matrix.

$T_{Ak}^{\otimes}$ = Conjugate-transpose.

PM-AM Correlation Coefficient

From the equation $\left[\dfrac{\partial E_H}{\partial X_H} \right]_{ss} \partial X_H = J_H(\omega) \Rightarrow M_{HH} \partial X_H = J_H(\omega)$, the information of the RF phase is lost and it is not possible to calculate the phase of the PM-AM correlation coefficient from the expressions above. In order to calculate PM-AM correlation, the first order approximation of the normalized k^{th} harmonic PM-AM normalized correlation coefficient $C_{ck}(\omega)$ computed from frequency conversion analysis is given as

$$C_{ck}(\omega) = \left| \frac{C_{ck}^{PMAM}(\omega)}{\sqrt{\left\langle \left| \delta \Phi_{ck}(\omega) \right|^2 \right\rangle \left\langle \left| \delta A_{ck}(\omega) \right|^2 \right\rangle}} \right| \qquad \text{(E-87)}$$

and can be correctly evaluated from frequency conversion analysis even for $\omega \to 0$

where $C_{ck}(\omega)$ is the normalized PM-AM correlation coefficient, which compensates for the incorrect dependency of $\left\langle \left| \delta\Phi_{ck}(\omega) \right|^2 \right\rangle$ of the frequency at low frequency offsets from the carrier. From the PM-AM correlation coefficient above due to modulation contribution to the kth harmonic can be given as

$$C_{mk}^{PMAM}(\omega) = C_{ck}(\omega)\left[\sqrt{\left\langle \left| \delta\Phi_{mk}(\omega) \right|^2 \right\rangle \left\langle \left| \delta A_{mk}(\omega) \right|^2 \right\rangle} \right] \qquad \text{(E-88)}$$

$$C_{mk}^{PMAM}(\omega) \cong \left\langle \delta\Phi_k(\omega)\delta A_k(\omega)^* \right\rangle = \frac{k\sqrt{2}}{j\omega\left| I_k^{SS} \right|}\left[T_F \left\langle J_H(\omega)J_H^\otimes(\omega) \right\rangle T_{Ak}^\otimes \right] \qquad \text{(E-89)}$$

Now, the near-carrier noise power spectral density $N_k(\omega)$ of oscillator, due to modulation contribution at an offset ω from $k\omega_0$ ($-n_H \le k \le n_H$), can be given as

$$N_k(\omega) = \frac{1}{4}R\left[\frac{k^2}{\omega^2}\left| I_k^{SS} \right|^2 T_F \left\langle J_H(\omega)J_H^\otimes(\omega) \right\rangle T_F^\otimes \right] \qquad \text{(E-90)}$$

$$+\frac{1}{4}R\left[T_{AK}\left[J_H(\omega)J_H^\otimes(\omega) \right]T_{Ak}^\otimes \right] \qquad \text{(E-91)}$$

$$+\frac{kR}{2\omega}\left| I_k^{SS} \right|\text{Re}\left[T_F \left\langle J_H(\omega)J_H^\otimes(\omega) \right\rangle T_{Ak}^\otimes \right] \qquad \text{(E-92)}$$

$$\Rightarrow N_k(\omega) = \frac{1}{4}R\left| I_k^{SS} \right|^2\left[\left\langle \left| \delta\Phi_{mk}(\omega) \right|^2 \right\rangle + \frac{1}{2}\left\langle \left| \delta A_{mk}(\omega) \right|^2 \right\rangle - \frac{k}{|k|}\sqrt{2}\,\text{Im}[C_{mk}^{PMAM}(\omega)] \right] \qquad \text{(E-93)}$$

where

$J_H(\omega)$ = vector of Norton equivalent of the noise sources.

T_F = frequency transfer matrix.

R = load resistance.

I_k^{ss} = kth harmonic of the steady-state current through the load.

➢ Summary

The majority of this work is a result of research done at my company Compact Software and friends and colleagues like Prof. Rizzoli, Prof. Fred Rosenbaum, and my engineers. My contribution was essentially the non-linear semiconductor noise in frequency doublers, mixers and oscillators calculation addition which was tested and validated through the work done by Dr. Ajay Poddar, and my Ph.D. students Dr. Anisha Apte, and Dr. Wolfgang Griebel. An interesting problem was the ability to measure phase noise down to two times kT_0 as only recently the Rohde & Schwarz FSWP had the capability for the required dynamic range. In the case of Griebel's Ph. D, we had to measure 10 seconds instability to a resolution of 1e-14, which was needed for the prediction of accurate landing on planets like Mars with the Voyager system. In general I would like to thank each and every one who made this successful research possible.

➢ Key references:

1. M. Odyniec, Editor, *RF and Microwave Oscillator Design*, Chapter 5: Modern Harmonic-Balance Techniques for Oscillator Analysis and Optimization, by V. Rizzoli, A. Neri, A. Costanzo, F. Mastri, Artech House, 2002.

2. U.L. Rohde, C.R Chang, J. Gerber, "Design and Optimization of Low-Noise Oscillators Using Nonlinear CAD Tools," IEEE Frequency Control Symp. Proc., pp 548-554, 1994.

3. U. L. Rohde, C. R. Chang, J. Gerber, "Parameter Extraction for Large Signal Noise Models and Simulation of Noise in Large Signal Circuits Like Mixers and Oscillators," Proceedings of the 23rd European Microwave conference, Madrid, Spain, Sept. 6-9, 1993.

4. V. Rizzoli, F. Mastri, C. Cecchefti, "Computer-Aided Noise Analysis of MESFET and HEMT Mixers," IEEE Trans. Microwave Theory and Techniques, Vol. MTT-37, pp 1401-1410, Sept. 1989.

5. V. Rizzoli, A. Lippadni, "Computer-Aided Noise Analysis of Linear Multiport Networks of Arbitrary Topology," IEEE Trans. Microwave Theory and Techniques, Vol. MTT-33, pp 1507-1512, Dec. 1985.

6. V. Rizzoli, F. Mastri, D. Masotti, "General-Purpose Noise Analysis of Forced Nonlinear Microwave Circuits," Military Microwave, 1992.

7. W. Anzill, F. X. Kärtner, P. Russer, "Simulation of the Single-Sideband Phase Noise of Oscillators," Second International Workshop of Integrated Nonlinear Microwave and Millimeterwave Circuits, 1992.

8. U. L. Rohde, Matthias Rudolph RF/Microwave Circuit Design for Wireless Applications, Second Edition, Wiley, 2013

9. Anisha M. Apte, "A New Analytical Design Method of Ultra-low-noise Voltage Controlled VHF Crystal Oscillators and it's Validation", Ph.D. Dissertation Brandenburgischen Technischen Universität Cottbus–Senftenberg, February, 2020

10. Fundamentals of RF and Microwave Techniques and Technologies Kindle Edition by Hans L. Hartnagel, Rüdiger Quay, Ulrich L. Rohde, Matthias Rudolph, Springer 2023

11. Microwave Circuit Design Using Linear and Nonlinear Techniques 3rd Edition by George D. Vendelin, Anthony M. Pavio, Ulrich L. Rohde, Matthias Rudolph, Wiley 2021

12. Microwave and Wireless Synthesizers: Theory and Design, 2nd Edition by Ulrich L. Rohde, Enrico Rubiola, Jerry C. Whitaker Wiley, 2021

13. Wolfgang Griebel, " Space Qualified 5MHz Crystal Oscillators with Maximum Stability between 1 and 10 Seconds", Ph. D. dissertation Brandenburgischen Technischen Universität Cottbus–Senftenberg, April, 2021